NOTICE

The quality of this microform is heavily dependent upon the quality of the original thesis submitted for microfilming. Every effort has been made to ensure the highest quality of reproduction possible.

If pages are missing, contact the university which granted the degree.

Some pages may have indistinct print especially if the original pages were typed with a poor typewriter ribbon or if the university sent us an inferior photocopy.

Reproduction in full or in part of this microform is governed by the Canadian Copyright Act, R.S.C. 1970, c. C-30, and subsequent amendments.

AVIS

La qualité de cette microforme dépend grandement de la qualité de la thèse soumise au microfilmage. Nous avons tout fait pour assurer une qualité supérieure de reproduction.

S'il manque des pages, veuillez communiquer avec l'université qui a conféré le grade.

La qualité d'impression de certaines pages peut laisser à désirer, surtout si les pages originales ont été dactylographiées à l'aide d'un ruban usé ou si l'université nous a fait parvenir une photocopie de qualité inférieure.

La reproduction, même partielle, de cette microforme est soumise à la Loi canadienne sur le droit d'auteur, SRC 1970, c. C-30, et ses amendements subséquents.

Canada

ISBN 0-315-83821-3

UNIVERSITÉ D'OTTAWA
UNIVERSITY OF OTTAWA

ACKNOWLEDGMENTS

I would like to thank Professor Christian Detellier, my research supervisor, for his invaluable advice, excellent guidance and encouragement throughout my studies.

I wish to express my gratitude to Dr. T. Matsuura for sharing his membrane expertise with me and providing the opportunity of undertaking gas permeation experiments.

I am indebted to my group-mates, Zhigang Chen, Jim Tunney, Louis Mercier and Laila Raki for the pleasure that they have brought to me during my studies and their invaluable discussion.

I would like to thank John McCaffrey and Ron Conlon for the SEM micrographs and X-Ray diffraction spectrum. Thanks is also given to Professor S. Kaliaguine for his kind providing his laboratory for the BET measurments.

I wish to acknowledge my parents for their constant support throughout my studies. I also wish to thank my uncle, Raymond Leung, for his kind support making possible for my study in Canada.

I would especially like to thank my wife, Thanh Mach, for her constant support, encouragement and patience throughout my studies and it is to her that I wish to dedicate this thesis.

Finally, I would like to thank the Institute of Chemical and Scientific Technology, Natural Sciences and Engineering Research Council of Canada, and the University Research Incentive Fund for their continuous financial support.

ABSTRACT

A series of quaternarized ammonium mono and di-cations, quaternarized amino acid ester mono and di-cations, and quaternarized polyammonium cations were synthesized by methylation reaction. The synthesized quaternarized ammonium derivatives were incorporated into the interlamellar space of the smectites, montmorillonite (SWy-1) and hectorite (SHCa-1). The adsorption of these quaternarized ammonium cations by the smectites were studied by colorimetric and Na-electrode methods. Also the CEC values were determined from the adsorption isotherms and were found to be close to the CECs of the smectites. The intercalation of the quaternarized ammonium cations into the interlamellar space of the smectites were evaluated by X-ray powder diffraction technique and the changes of the interlayer spacings upon intercalation were measured. The adsorption and X-ray results indicated that the quaternarized ammonium cations adopt a parallel orientation arrangement in the interlamellar space of the smectites.

Insight into the micropore structure of the prepared organo-smectites has been obtained with N_2 adsorption and desorption studies. The BET interlayer surface area, external surface area, micropore volume and mesopore volume were calculated from the N_2 adsorption and desorption isotherms. The total BET surface areas of the orgnao-smectites were in the range of 58-224 m^2/g, depending on the size of the intercalated cations. It has been implied that the incorporation of the quaternarized ammonium cations into the interlamellar space of the smectites results in a microporous material with a network of cavities whose height and volume are controlled by the size and the shape of the organic cation.

The gas chromatographic properties of these organo-smectites have been determined with focus on the separation of air, CH_4 and CO_2 as well as the separation of C_1-C_4 and C_5-C_8 hydrocarbons. The organo-smectites have been proven to be a GC adsorbent for gas separations. The separation of methane and carbon dioxide was controlled by the interactions with the clay surface, not by the interaction with the substituents of the alkylammonium chain. The shapes of the microcavities played a role in the separation of gas mixtures. The CO_2 retention time has been found to increase with increasing the free surface area of the organo-smectite. Moreover, it has been shown that the retention time of C_1-C_4 hydrocarbons decreased with increasing the free volume of the organo-smectite.

Furthermore, some microporous organo-smectite materials have been imbedded into the cross-linked polydimethylsiloxane (PDMS) polymers giving composite membranes. The composite membranes have been evaluated by the gas permeation experiments. The pure gas permeation results showed that the gas permeabilities decreased upon filling of the organo-smectites into the PDMS polymers. The pure gas permeability ratios of O_2/N_2 and CO_2/CH_4 were found to be controlled by both the organo-smectite content and the microporosity of the organo-smectites. The maximum pure gas permeability ratio for CO_2/CH_4 achieved was 8.7 as compared to 3.9 which was obtained for organo-smectite free PDMS membranes.

TABLE OF CONTENTS

LIST OF FIGURES AND SCHEMES

Figures:

Schemes:

LIST OF TABLES

SYMBOLS AND ABBREVIATIONS

SWy-1(M)	montmorillonite, from Clay Spur Wyoming USA
SHCa-1(H)	hectorite, from San Bernardino county California USA

Organic cations:

GLY-Et^{+}	trimethylated ammonium derivative of glycine ethyl ester($Me_3N^+CH_2COOCH_2CH_3$)
TPP^{+}	tetraphenyl phosphonium(Ph_4P^+)
TMA^{+}	tetramethyl ammonium(Me_4N^+)
LYS-Me^{2+}	trimethylated ammonium derivative of lysine methylester ($(Me_3N^+(CH_2)_4CH(COOCH_3)N^+Me_3)$
ORN-Me^{2+}	trimethylated ammonium derivative of ornithine methyl ester ($(Me_3N^+(CH_2)_3CH(COOCH_3)N^+Me_3)$
MMDA^{2+}	trimethylated ammonium derivative of methane diamine($Me_3N^+CH_2N^+Me_3$)
MDEA^{2+}	trimethylated ammonium derivative of ethylene diamine($Me_3N^+CH_2CH_2N^+Me_3$)
MTETA^{4+}	trimethylated ammonium derivative of triethylene tetraamine

$(Me_3N^+CH_2CH_2N^+(Me_2)CH_2CH_2N^+(Me_2)CH_2CH_2N^+Me_3$

Organo-Clays:

TMA-M(H)	TMA-montmorillonite (hectorite)
TPP-M(H)	TPP-montmorillonite (hectorite)
GLY-Et-M(H)	GLY-Et-montmorillonite (hectorite)
LYS-Me-M(H)	LYS-Me-montmorillonite (hectorite)
ORN-Me-M(H)	ORN-Me-montmorillonite (hectorite)
MMDA-M(H)	MMDA-montmorillonite(hectorite)
MDEA-M(H)	MDEA-montmorillonite (hectorite)
MTETA-M(H)	MTETA-montmorillonite (hectorite)

Clay filled and Organo-clay polymeric composite membranes:

PDMS	polydimethylsiloxane
Na-M	Sodium-montmorillonite
Na-M-PDMS-20	20% (w/w) of Na-M in PDMS membrane
Na-M-PDMS-33	33% (w/w) of Na-M in PDMS membrane
LYS-Me-M-PDMS-20	20% (w/w) of LYS-Me-M in PDMS membrane
LYS-Me-M-PDMS-33	33% (w/w) of LYS-Me-M in PDMS membrane
LYS-Me-M-PDMS-45	45% (w/w) of LYS-Me-M in PDMS membrane
TPP-M-PDMS-20	20% (w/w) of TPP-M in PDMS membrane
MTETA-M-PDMS-20	20% (w/w) of MTETA-M in PDMS membrane
TMA-M-PDMS-45	45% (w/w) of TMA-M in PDMS membrane
MMDA-M-PDMS-45	45% (w/w) of MMDA-M in PDMS membrane

CEC	cation exchange capacity
K	equilibrium constant for cation adsorption reaction
γ_{Na}, γ_N	activity coefficient of Na^+ and organic cation
E	sodium electrode potential
d001	basal spacing
c	interlayer distance of clays
CPK	Corey-Pauling precision molecular model
SEM	scanning electron microscopy
XRD	x-ray diffraction
n	quantity of gas adsorbed
p/p^0	relative pressure of gas
H	hysteresis
v	surface tension
V_L	molar volume of liquid nitrogen
V	volume of N_2 adsorbed
V_m	monolayer capacity
a_m	average area occupied by a molecule of adsorbate in the monolayer
C	BET constant
t	monolayer thickness
U_0	adsorbent-adsorbate interaction
P_a	adsorbate-adsorbate-adsorbent interaction
ϕ, ϕ^*	potential function

δ	distance between a gas atom and the surface at zero interaction energy
γ	distance from the surface
N_a	number of atoms per unit area of surface
l	distance between the nuclei of two layers
m	mass of an electron
C	velocity of light
α_a, α_A	polarizability
χ_a	magnetic susceptibility
d_a	diameter of an adsorbent
d_A	diameter of adsorbate
ω	mass of nitrogen adsorbed into the pores
ω_∞	maximum amount of nitrogen adsorbed into the pores
γ_m	core radius
γ_p	pore radius
δV_i	volume desorbed
δV_i^K	core volume
$\delta^V i^f$	volume of film on the walls of pores
Q_i	conversion factor
PSA	pressure swing adsorption
EOR	enhanced oil recovery operation
N	theoretical plate number
HETP	height equivalent to a theoretical plate

L	column length
t_R	total retention time
t_m	retention time of mobile phase
t_s	retention time in stationary phase
K	partition coefficient
k'	capacity ratio
α	separation factor
A,B,C	terms in van Deemter equation
μ	interstitial velocity
D_m	molecular diffusivity
τ	axial tortuosity
R_p	particle radius
P_e	peclet number
ϵ	interparticle void volume
k	Henry's constant
μ_{opt}	optimum velocity
b_{AB}	half width
R_{AB}	resolution
P	Permeability
D	diffusion coefficient
S	solution coefficient
Q_i	permeation rate
P_i	gas component permeability

A	cross-sectional area
l	membrane thickness
Δp_i	pressure difference
I	current
V	voltage
R	resistance
R_i	gas transport resistance
n	number of particles
ϕ_i	organo-clay content

Chapter 1

Introduction

1.1 The Chemistry of Clay Minerals

1.1.1 Structure of Clay minerals

Clays are naturally occuring minerals, characterized by a layered structure[1]. The principal building elements of the clay minerals are two-dimensional arrays of silicon-oxygen tetrahedra and two-dimensional arrays of aluminum or magnesium oxygen-hydroxyl octahedra[2]. In most clay minerals, the tetrahedra and octahedra sheets are superimposed in different fashions to form the clay layers. Figure 1.1 schematically illustrates the framework structure of a 2:1 clay. In the silicon-oxygen sheets, the silicon atoms are coordinated with four oxygen atoms and the oxygen atoms are located on the four corners of a regular tetrahedron with the silicon atom in the center. In the aluminum or magnesium oxygen-hydroxyl sheets, the Al or Mg atoms are coordinated with six oxygen atoms or OH groups which are located around the Al or Mg atom with their centers on the six corners of a regular octahedron. The analogous symmetry and the almost identical dimensions in the tetrahedral and the octahedral sheets allow the sharing of oxygen atoms between these sheets. The fourth oxygen atom protruding from the tetrahedral sheet is shared by the octahedral sheet. Clay minerals can be classified according to their layer structure. In general, there are two groups: 1:1 and 2:1 clays. The 1:1 mineral consists of

repeated layers which are made up of one tetrahedral sheet and one octahedral sheet. The 2:1 mineral consists of layers which are made up of two tetrahedral sheets and one on either side of a central octahedral sheet. Montmorillonite and hectorite which will be used in this work are 2:1 smectite clays. Within each layer a certain unit repeats itself in a lateral direction. When the octahedral sheets are made up of Al(III), only 2/3 of the available octahedral positions need to be filled to maintain the electrical neutrality of the layers. This kind of clay minerals is defined as dioctahedral clays. On the other hand, when the octahedral sheets are made up of Mg(II) , one must fill all available octahedral positions to achieve the electrical neutrality of the layers. This clay belongs to the trioctahedral group.

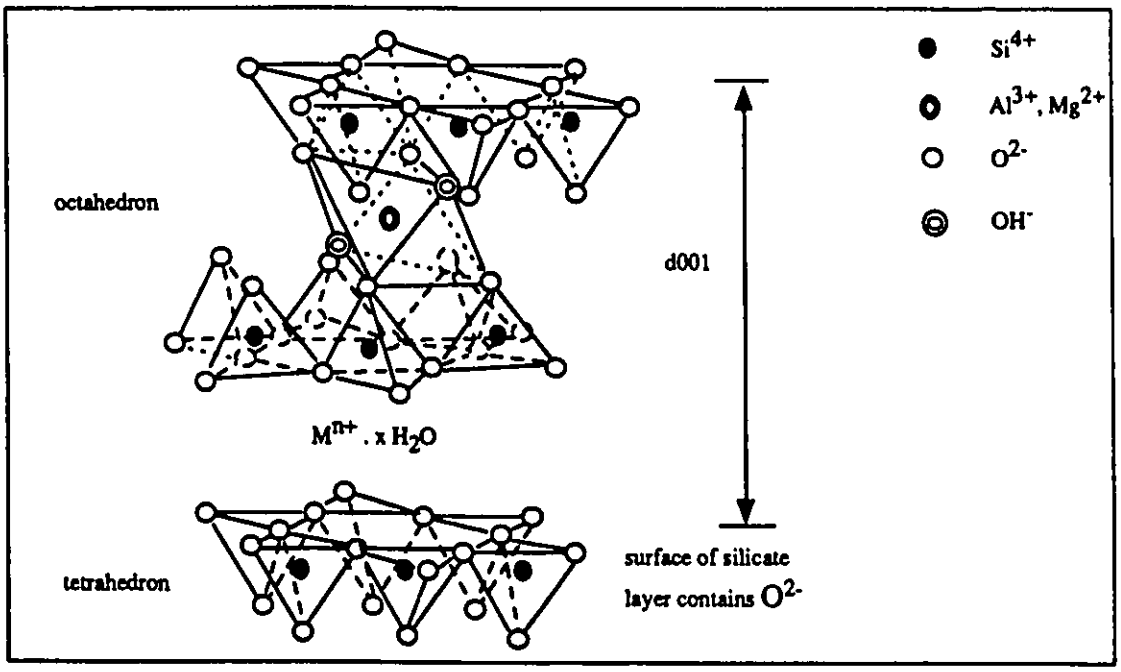

Figure 1.1 Schematic representation of a 2:1 layered clay

The most important property of clay minerals is the existence of a net negative charge on their layers[2]. The neutral 2:1 layer structure is represented by the mineral *pyrophyllite* in which the octahedral sheets are made up of Al(III). If the octahedral sheet contains Mg(II) atoms and all the octahedral positions are filled, the electroneutral structure represents the mineral *talc*. Smectite clays such as montmorillonite and hectorite are derived from the above two neutral minerals by substitution of some of the tetrahedral Si(V) atoms by Al(III) or of some of the octahedral Al(III) or Mg(II) by Mg(II) or Li(I). This substitution by a lower valency atom causes a deficiency of positive charge, resulting in the observed negative layer charge. The negative charge of the clay layer is counter balanced by adsorbed or intercalated exchangeable cations, usually a mixture of alkali and alkaline earths metal cations. These are called exchangeable cations since they can be replaced by other cations from solution. The extent of isomorphous substitution and therefore the magnitude of the layer charge, is determined by the clay cation exchange capacity (CEC), the amount of adsorbed cations needed to neutralize it. The layer charge in octahedrally charged clays is distributed over all oxygens in the framework.

Clay minerals are also characterized by the nature of their interlayer spacings[3]. The distance between two clay layers in a stack is called the interlayer spacing as shown in Figure 1.1. In some clays this distance is not fixed, but expandable. When dispersed in water these clays can swell, intercalating up to four water layers.

Table 1.1 shows a classification of clay minerals, according to the layer structure (1:1 or 2:1 minerals), the occupancy of the octahedral sheet (dioctahedral or trioctahedral) and the nature of the interlayer spacings (stable or expandable).

Table 1.1 Classification of clay minerals.

Type of layer	Type of sheet	Interlayer space	Clay
1 : 1	Dioctahedral	Stable	Kaolinite
		Expandable	Halloysite
	Trioctahedral	Stable	Serpentines
2 : 1	Dioctahedral	Stable	Illites
			Micas
			Pyrophyllites
		Expandable	Beidellite
			Nontronite
			Montmorillonite
	Trioctahedral	Stable	Talc
			Micas
		Expandable	Hectorite
			Stevensite
			Saponite
			Sauconite
			Vermiculite

Smectite clays possess a combination of cation exchange, intercalation, and swelling properties which makes them unique. Their capacity as cation exchangers is fundamental to their intercalation and swelling properties. This distinguishes smectites from the mica and pyrophyllite-talc groups of minerals, which have little or no ion exchange capacity.

1.2 Cation exchange, intercalation and swelling properties of smectite clays

The most important property of smectites is their ability to expand beyond a single molecular layer of intercalant. The extent of interlayer swelling depends on the nature of the swelling agent, the exchange cation, and the layer charge of the clay. The Li^+ and Na^+ exchanged forms of the minerals are particularly susceptible to swelling by water[4]. As the interlayer water content of Na^+-smectites is increased with increasing partial pressure, the interlayer spacing can jump to a value corresponding to two or more intercalated water layers. Under appropriate conditions the silicate layers can be separated by hundreds of angstroms of water. In fact, the silicate layers of Na^+-montmorillonite in dilute aqueous suspension are completely dispersed. As the concentration of the dispersion is increased, gelation occurs. The gelation phenomenon, which occurs at a concentration as low as 2 percent clay by weight, is believed to result from layer edge-to-face interactions which generate a "house-of-cards" structure[2]. The inorganic cations in the interlamellar spaces of the clay may be exchanged when the clay minerals holding them come in contact with a solution rich in other cations. The alkali ions are more easily replaced than the alkaline ions. The stability of the inorganic cations in the clay may be considered as the following sequence[2]:

$$Na^+ < K^+ < Ca^{2+} < Mg^{2+} < NH_4^+$$

Ca^{2+} is generally more stable or more firmly fixed in the interlayer space than is Na^+. However, this series can vary with conditions or type of clay mineral. The cation exchange capacity depends on the structure of the clay and its charge density. For expandable clay minerals, there is a linear increase of the CEC with the layer charge. Table 1.2 shows the structural formulae, the CEC values of pyrophyllite-talc minerals and two smectite clays[5,6]. The positive charge deficiency in the layers of smectites ranges from 0.4 to 1.2 *e* per Si_8O_{20}[7]. In hectorite which typically exhibits a layer charge of 0.66 *e* per Si_8O_{20}, the cation

exchange capacity on an anhydrous basis is 89 milliequivalents per 100 grams. In montmorillonite, the layer charge of 0.68 *e* per Si_8O_{20} is obtained which gives rise to the cation exchange capacity, 87 milliequivalent per 100 grams[6]. With large, complex exchanged cations, the extent of ion replacement may be size-limited. Since the average distance between exchange equivalents in the smectite is about 8.3Å, cations with cross-sectional diameters greater than this value can fully cover the interlamellar surfaces before 100 percent exchange is reached[6]. Although the interlamellar surface is very large, the size of the exchanging ion can be a limiting factor in determining ion loading.

Table 1.2 Formula and CEC values of pyrophyllite-talc minerals and smectite clays

Mineral	Formula	CEC meq / 100g
Pyrophyllite	$[Al_{4.0}](Si_{8.0})O_{20}(OH)_4$	---
Talc	$[Mg_{6.0}](Si_{8.0})O_{20}(OH)_4$	---
Montmorillonite	$[Al_{3.22}Fe^{3+}_{0.26}Mg_{0.40}Fe^{2+}_{0.12}](Si_{7.84}Al_{0.16})O_{20}(OH)_4X^{+}_{0.68}$	0.87
Hectorite	$[Mg_{5.30}Al_{0.44}Li_{0.66}](Si_{8.00})O_{20}(OH)_4X^{+}_{0.66}$	0.89

As shown in Figure 1.2, various types of cations can be intercalated into the interlamellar space of the smectites[8]. The pillaring agent P^+ may be an alkylammonium ion, a bicyclic amine cation, a *tris* metal chelate or a polynuclear hydroxy metal ion. The region between the pillaring cations defines the pores for the adsorption and the possible catalysic reactions of organic molecules. The intercalation of a large cation into the interlamellar

space of smectites can create different sizes of pores which will exhibit molecular sieving properties.

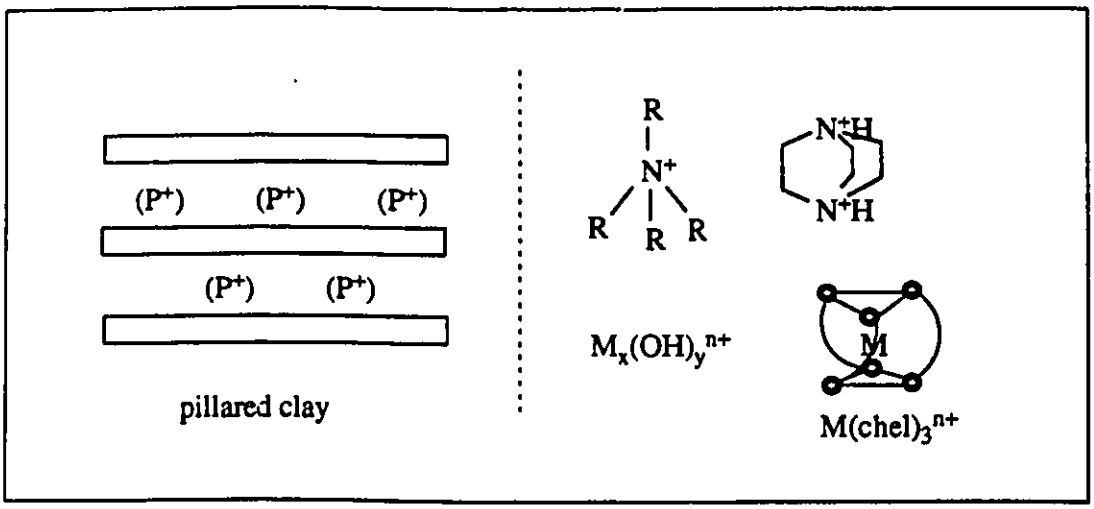

Figure 1.2 A schematic representation of pillared clay

Neutral molecules other than water can also be intercalated between the silicate layers of smectites. Several binding mechanisms may operate in the intercalation processes. For example, the hydrated water molecules in Cu^{2+} exchange forms of smectites can be replaced by pyridine (py)[9]:

$$\underline{\quad\quad}\ [Cu(H_2O)_x]^{2+}\ \underline{\quad\quad} \;+\; py \;\rightarrow\; \underline{\quad\quad}\ [Cu(py)_4]^{2+}\ \underline{\quad\quad} \;+\; x\,H_2O$$

where the horizontal lines symbolize the silicate layers.

1.3 Organo-clays and their environmental applications

A very important property of smectites is its ion exchange capacity. The inorganic cations in the smectites can be replaced by a variety of organic cations. The intercalation of the organic cation into the interlamellar space results in a microporous organo-clay material depending upon the size of the organic cation and the nature of the clay. The study of the microporosity of organo-smectites was pioneered in the 1950s by Barrer[10]. In a series of papers, which he recently reviewed, Barrer, with his co-workers, showed that when the natural interlamellar inorganic cations of montmorillonite and hectorite are replaced by small alkylammonium organic cations, permanent microporosity is created, and sorption of gases and of organic molecules is very favored[10]. The type of exhangeable cations on clays strongly influence their sorptive characteristics[10].

In the past few years, there has been increasing interest in designing recyclable inorganic adsorbents for the efficient removal of organic pollutants from aqueous solutions. The chlorinated phenols represent one of the most challenging classes of priority pollutants to be removed from waste streams and ground waters[11]. The removal of trace levels of priority pollutants from extremely large volumes of wastewater is a microseparation process requiring cost-effective adsorbents[12]. It has been established that modified clay adsorbents are suitable for such applications due to the organophilic properties of the organo-clays[13,14]. Depending on the size of the organic cation, the exchanged organic ions have been shown to form either a microscopic organic phase as in hexadecyltrimethylammonium-smectite[15] or discrete organic-modified surface adsorption sites as in TMA-smectite[16]. The substitution of organic cations reduces the hydration of the clay and decreases the free aluminosilicate mineral surface area. As a result, the surface properties of the clay may change considerably from highly hydrophilic to increasingly organophilic as the inorganic cation is progressively replaced by the organic cation. Therefore the sorption properties to organic compounds

would be very favored. Organic cations possessing long-chain alkyl groups are particularly able to impart hydrophobic quality to the mineral surface. Such clay-organic complexes can sorbe molecules. This process is essentially a non-polar interaction between the organic phase of the clay organic complex and the hydrophobic organic molecule. It has been shown that the uptake of phenol and chlorophenols from water was enhanced by modified clays exchanged with large quaternary alkyl ammonium cations. It has been reported that dry hexadecyltrimethyl ammonium-smectite (HDTMA) acted as a dual sorbent for the sorption of non-ionic organics[15]. The free aluminosilicate mineral surface functioned as a solid adsorbent and the bulky organic moieties of the exchanged HDTMA ions functioned as a partition medium. It has been recently reported that addition of cetyl pyridinium cations to a hydroxy-Al cation exchange form of montmorillonite resulted in an effective adsorbent for removing pentachlorophenol and benzo(a)pyrene from aqueous solution[17]. Moreover, aluminum-pillared clays modified by the addition of the nonionic surfactant have been found to exhibit interesting adsorption properites with regard to chlorinated phenols[18].

1.4 Reactions on clay surfaces

Beside the adsorption properties of the clays, another important property is the presence of Brønsted and Lewis acid sites on the surface of the clays[8]. Many organic reactions can take place in the smectite interlayers involving the activation of the reagents by the acid sites. In those organic reactions, the first step is the protonation of one of the reagents by the Brønsted acid sites of the clay. For example, the dehydration of primary alcohols over Al^{3+}-montmorillonite at 200°C has been shown to yield 1,1'-dialkyl esters in high yields[19]. In this case the reaction is catalyzed by the acid sites of the clay.

$$2\,RCH_2CH_2OH + H^+ \rightarrow RCH_2CH_2\text{-}O\text{-}CH_2CH_2R + H_2O \quad (1\text{-}1)$$

Other types of acid catalyzed reactions found to occur in clays were oxidation reduction processes such as the conversion of 1,1'-diphenylethylene to benzophenone and 1,1'-diphenylethane and hydrogen transfer reactions between 9,10-dihydroanthracene and 1,1-diphenylethylene which took place on synthetic hectorite[20,21].

There are also cases in which the clay was used to adsorb a catalyst in addition to the reagents. An example of a catalyst is the rhodium hydrogenation catalyst RhL_n^+ (L = triphenyl phosphine n=2 or 3) adsorbed in hectorite. In homogeous solution, this complex catalyzed the hydrogenation of both terminal and nonterminal olefins, while in the clay interlayer space terminal olefins were selectively hydrogenated[22]. The higher selectivity to the terminal olefins was attributed to the interlamellar spacing of 7.7Å of the clay upon intercalation of the catalyst. A pillared clay has been proven to be a catalyst for the conversion of cyclohexane to benzene at 550°C[23]. Its activity was found to be substantially higher than that of a commercial chromia catalyst supported on alumina. Similar pillared clays, intercalated with alumina and zirconia were found to be petroleum cracking catalysts having shape selectivity compared to that of commercial zeolite catalysts. The hydroxy zirconium pillar is a Zr_4 oligomer of the type $Zr_4(OH)^{x+}_{16-x}$ and the structure of the pillar for hydroxy aluminum is an Al_{13} oligomer related to the cation $Al_{13}O_4(OH)^{7+}_{24}$. The remarkable thermal stability of the Zr_4 and Al_{13} pillared smectites has been attributed to the formation of metal oxide clusters upon dehydroxylation of the hydroxy cations at elevated temperature[24].

1.5 Membrane gas separation processes in industries

1.5.1 History

Membranes are microporous barriers of polymeric, ceramic or metallic materials that can be used in separation processes. The development of membrane processes for the gas separation has made remarkable progress during the last two decades. Membrane separation of gases has emerged from a technical curiosity in the 1860's to initial commercialization in the 1970's followed by intense research activity and further commercialization in the 1980's[25]. Major applications have been for the recovery of H_2 from purge gas streams, removal of CO_2 from natural gas and the separation of oxygen from nitrogen in air[26]. Operating pressures range from 100 psi for oxygen/nitrogen separation to 1,000 psi and greater for recovery of H_2 from purge gases. While the first modules for gas separation were of hollow fiber design, spiral-wound membrane modules have become more common recently[26]. Membrane separation has become economically competive in these areas because of the development of high-flux asymmetric membranes and the ability to fabricate such membranes in the form of hollow fibers. These membrane processes are competitive with conventional gas separation techniques. The great interest in membrane separation technology is due mainly to the fact that it is potentially energy-efficient. In addition, the required process equipment is simple, compact, and relatively easy to operate and control[26].

Membrane business as a whole is expected to grow at a rate of 10 to 15% per year, with gas separation systems being the main growth area. It has been estimated that the present market for gas separation systems is expected to grow to $1.5 billion by 1995[27].

1.5.2 Membrane Materials

In general, membranes used in industrial gas separation are of polymeric materials. There are many types of membrane materials including glassy (cellulose acetates, polyamides, polysulfone, polyimide) and rubbery polymers (silicone rubbers, nitrile rubbers)[26]. The natural and synthetic rubbery polymers are the most permeable of the polymeric materials to the permeant gases. However, the selectivity in these polymeric materials is low. Glassy polymers tend to have very high selectivities with permeation rates depending on the morphology of the membrane. Asymmetric glassy polymers have both high permeation rates and high selectivities. The main advantage of polymers as a material for membrane preparation is the relative simplicity of thin film formation which enables one to obtain rather high permeability rates. However, polymeric membranes have several limitations such as low selectivity, high temperature instability, swelling and decomposition in organic solvents, and a low ability to be stream sterilized. In petroleum industry, refinery streams can contain many contaminants such as asphaltenes, various organic species, metals, colloidal particles, silica, polymers, tars and others. These streams can foul membranes, leading to substantial reductions in permeation rates and changes in separation efficiencies[28]. These limitations can be overcome by using inorganic and molecular sieve membranes[29,30].

Ceramic and other inorganic membranes have found application in many industries since about 1980. Ceramic and inorganic membrane exhibit several advantages such as thermal stability, ability to withstand prolonged exposure to non-aqueous media, stability to pH and organic solvents[31]. The disadvantages include high cost, low selectivity and their fragility due to brittleness[31]. Much progress has been made in recent years to improve the weakness mentioned above. This remains a new challenge for membrane separation processes.

1.6 The goals of the research

The objective of this work was to design new organo-clays with rigid, large, hydrophobic microcavities whose size, shape and functionalities would be well-controlled for specific recognition. The microporosity of the organo-clays was to be characterized by both XRD and BET adsorption methods. These organo-clays were explored as gas chromatographic adsorbents for the gas separations due to their microporosity. Further approach involved the incorporation of organo-clay materials into polymers to form composite membranes. The efficiency of these composite membranes for gas separation was tested. Scheme 1.1 summarizes the research direction of this thesis.

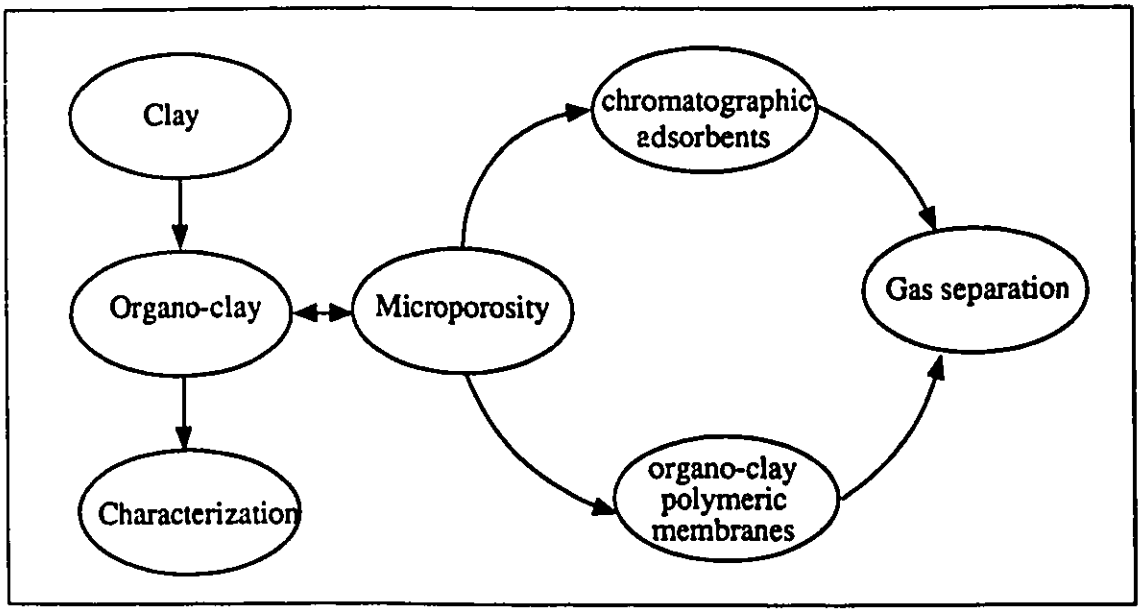

Scheme 1.1 Summary of research direction of this thesis

Chapter 2

Synthesis

2.1 Introduction

As discussed in chapter 1, the natural clays exhibit adsorption properties. The inorganic cations in the clay can be replaced by larger organic cations and therefore the basal spacing of the organo-clay will be increased. This intercalation produces a pore network whose size can be adjusted by changing the size of the intercalated cation. In order to prepare some microporous organo-clay materials, several quaternarized ammonium derivatives with different alkyl chain and functional groups were synthesized. Some quaternary alkylammonium mono-cations such as Et_4N^+, Pr_4N^+, Bu_4N^+, Pe_4N^+, Hex_4N^+, Hep_4N^+ and Oct_4N^+ have been incorporated into the interlamellar space of the clay[32]. Amino acids which have both one or two amino groups and one carboxylic group should also be intercalated into the interlamellar space of the clays upon tri-methylation of the amine functions. Such quaternarized amino acid ester derivatives which have both ester and tri-methylated ammonium functional groups provide good examples for incorporation studies and chromatographic studies. Some polyammonium cations were also be prepared from the corresponding polyamines by methylation reaction, provided quaternarized ammonium cation with higher charge density as compared to the quaternarized amino acid ester derivatives.

2.2 *Synthesis and characterization of methyl quaternarized amino acid ester derivatives*

2.2.1 Esterification

The natural amino acids can be transferred to the corresponding methyl esters by esterification reaction. There are many methods for esterification of carboxylic group in the literature. Esterification of carboxylic acid can be achieved via acid chloride method[33]. Other methods include esterification by pyrolysis of the tetramethylammonium salt[34] , reaction with alkyl halides using hexamethylphosphoramide (HMPA)[35], reaction with dimethyl sulphate[36] and reaction with alkyl halides using cesium salt[37]. However, esterification via dimethyl sulphate has been subject to side reactions involving hydrolysis of the dimethyl sulphate by the basic medium and hydrolysis of the ester once it was formed. With alkyl halides, esterification was found to be generally rapid and quantitative, and allowed the preparation of esters other than the methyl variety. Esterification via cesium salt and alkyl halides has been used for the preparation of esters derived from protected amino acids and peptides under mild conditions. Reaction of suitable protected amino acid or peptide cesium salts with alkyl halides could yield the desired esters readily under neutral conditions at room temperature. No racemization has been observed during this process. Esterification of amino acids by using thionyl chloride is a simple and efficient method. In the case of esterification of amino acids, this last method was adopted for the methylation of the carboxylic group according to the procedures reported by Boisonnas et al[38] using $SOCl_2$ and methanol. Scheme 2.1 represents the esterification reaction of amino acids catalyzed by $SOCl_2$. By this method, lysine and ornithine were effectively transferred to methyl esters with very high yield (>90%).

Other amino acid esters such as GLY-Et, Ala-Et, Val-Et, Leu-Et and Phe-Et have also been synthesized similarly in our laboratory[39].

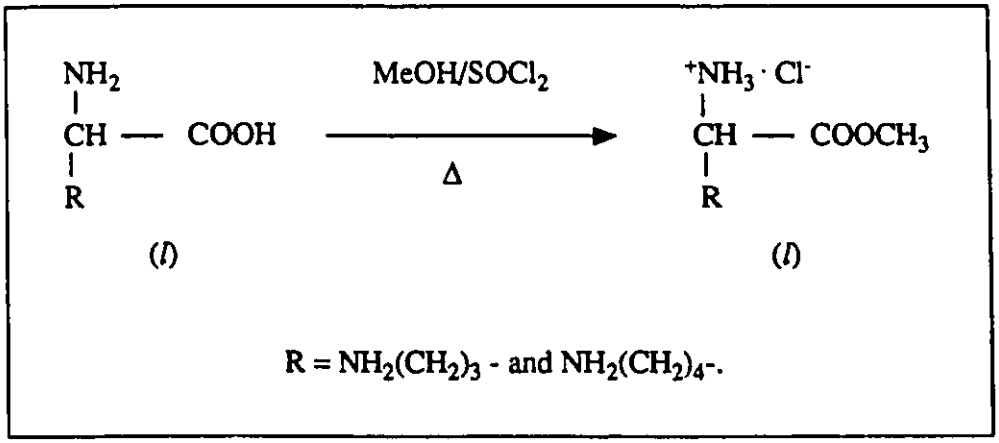

Scheme 2.1 Esterification of *l*-amino acids

2.2.2 Quaternarization

Many methods can be used for methylation of the amine groups. Most methods used for quaternarizing an amino group involved a methylation reagent and a strong base. Prolonged reaction time and heat were often needed[40,41]. These stringent conditions limited the applicability of the method, and could lead to surprizing results during the methylation with dimethyl sulphate[42]. Diazomethane in aqueous solution can also be used but the reaction was very slow. The combination of methyl iodide-potassium bicarbonate-methanol has been proved to be a mild, efficient, reasonably selective, and generally applicable reagent for the quaternarization of amines[43]. By this method, several tri-methylated amino ester derivatives were prepared by N-methylation of the corresponding amino esters using MeI under mild basic conditions. Scheme 2.2 represents the methylation reaction of the amino acid esters. The methylation reagents did not attach the methyl ester group. For the full quaternarization (two amine groups), more methyl iodide and sodium bicarbonate were

added after the α-amino group was completely quaternarized.

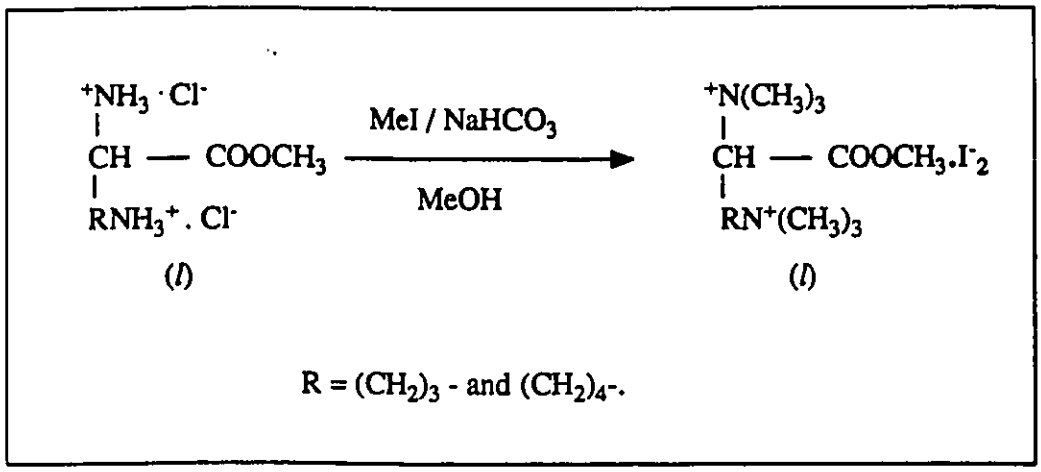

Scheme 2.2 Quaternarization of (*l*)-amino methyl esters

2.2.3 *Synthesis of methylated quaternary polyammonium cations*

Two methylated quaternary diammonium cations ($Me_3N^+CH_2N^+Me_3$, $Me_3N^+CH_2CH_2N^+Me_3$) and one methylated quaternary tetraammonium ($Me_3N^+CH_2CH_2N^+(Me_2)CH_2CH_2N^+(Me_2)CH_2CH_2N^+Me_3$) cation were synthesized from the corresponding diamines and tetraamine. It has been shown that N,N,N',N'-tetramethyl ethylene diamine with zinc borohydride was a good reducing agent for acyl chlorides[44]. 1,1,4,7,10,10-hexamethyltriethylene tetramine has been found to be a good multidentate ligand and the metal complexes of this polyamine has also been employed in carbohydrate epimerization[45]. Keggin-type and Dawson-type heteropolytungstate (HPT, η_5-$R(C_5H_4)TiPW_{11}O_{39}^{4-}$ and η_5-$R(C_5H_4)$-$TiP_2W_{17}O_{61}^{7-}$) ions were of interest as possible soluble models for industrially important metal oxide supported catalysis[46,47] and as small,

highly electron dense labels for the study of biological specimens[48]. The R group represented a chemoselective protein-reactive functional group at the end of an organic spacer arm. One limitation in the use of these polyanionic HPT EM labels is the tendency that they have to form insoluble precipitates with biomolecules bearing positively charged groups[49,50]. This nonspecific electrostatic interaction hampered the intended binding of HPT to specific sites on the biomolecule by way of the protein-reactive functional group at the end of the spacer arm. An organic polycation with the charges appropriately spaced and with additional water-solubilizing groups could well exhibit preferential electrostatic interaction with the HPTs, thereby effectively preventing precipitation with other cations. Simple tetra- and pentaammonium salts and quaternary diamines were all of low aqueous solubility. When methylated quaternary tetraamine was employed, the nonspecific precipitation reaction between polycationic biomolecules and polyanionic heteropolytungstates (HPT's) was prevented[51]. The methylated quaternary polyammonium cations were prepared by the treatment of the corresponding polyamines with MeI in ethanol. The synthesis is summarized in scheme 2.3.

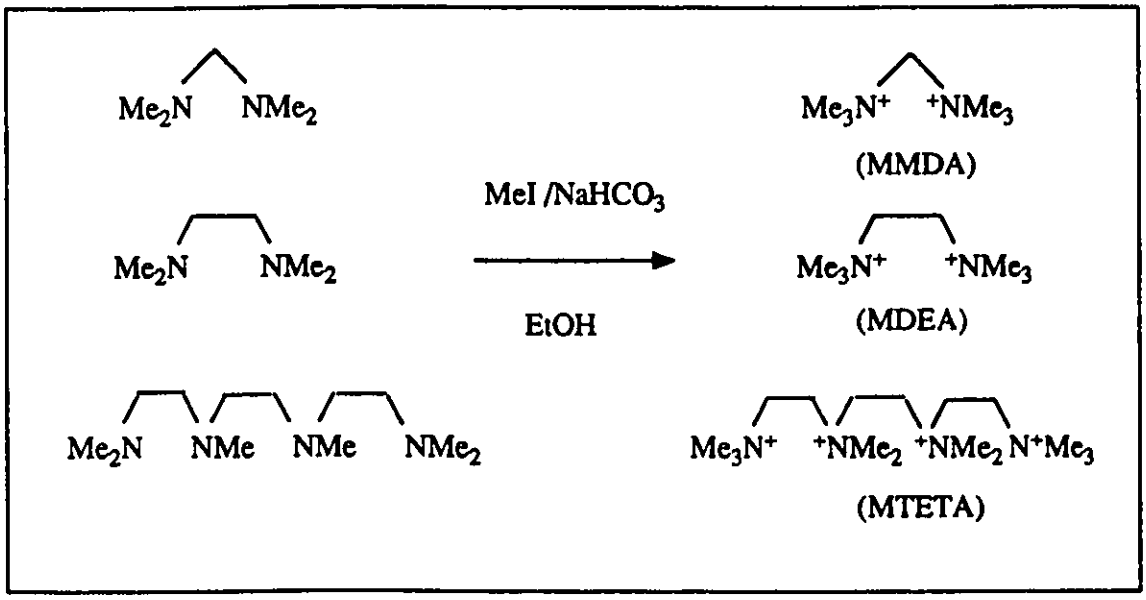

Scheme 2.3 Quaternarization of polyamines

2.2.4 *Characterization of quaternarized amino acid ester and polyamine derivatives*

^1H NMR, ^{13}C NMR, IR and MS were used to characterize the sythesized organic derivatives. In the ^1H NMR spectrum of quaternary methyl lysine ester, two significant signals at 3.07 and 3.20 ppm were observed and assigned to the two different tri-methyl groups (Me_3N^+---N^+Me_3)[52]. Also, the methyl ester group gave a singlet at 3.65 ppm. In the ^{13}C NMR spectrum, two strong signals at 55.8 and 55.3 ppm corresponded to the methylated carbons of the molecules. A $^{14}N^{13}C$ coupling was also observed in the spectra examined and splitting of the signals was observed. IR spectrum of the quaternarized lysine methyl ester gave a significant vibration at 1750 cm^{-1}, indicating the presence of a ester carboxylic group. Elemental analysis also confirmed the structure of this product (see page 198, chapter 8).

In the ^1H NMR spectrum of $MMDA^{2+}I_2^-$, a single peak at 3.56 ppm was assigned to the protons of the methyl groups and a singlet at 4.30 ppm corresponded to the methylene protons. In the ^{13}C NMR spectrum of $MMDA^{2+}I_2^-$, only two signals at 57.3 and 60.8 ppm were observed which were assigned to the methyl carbons and methylene carbon respectively. Typical ^1H and ^{13}C NMR spectra for the quaternarized $MMDA^{2+}.I^-_2$ are shown in Figure 2.1. $MDEA^{2+}$ showed a similar ^1H and ^{13}C NMR spectrum (see page 199). For the quaternarized tetraammonium cation ($MTETA^{4+}I_4^-$), the ^1H and ^{13}C NMR spectrum are more complicated. In the ^1H NMR spectrum of this compound, the ethylene protons were found in the region between 4.2-4.5 ppm with irregular triplet. The two dimethyl groups gave a singlet at 3.51 ppm and the two tri-methyl groups showed a singlet at 3.39 ppm. In the ^{13}C NMR spectrum, two significant signals at 55.3 and 57.5 ppm were observed and corresponded to the two different types of methyl carbons.

MS analysis of $(LYS\text{-}Me)I_2$, $(MMDA)I_2$ and $(MTETA)I_4$ showed the corresponding ion fragments at 245.3, 132.9 and 289.1 for $LYS\text{-}Me^{2+}$, $MMDA^{2+}$ and

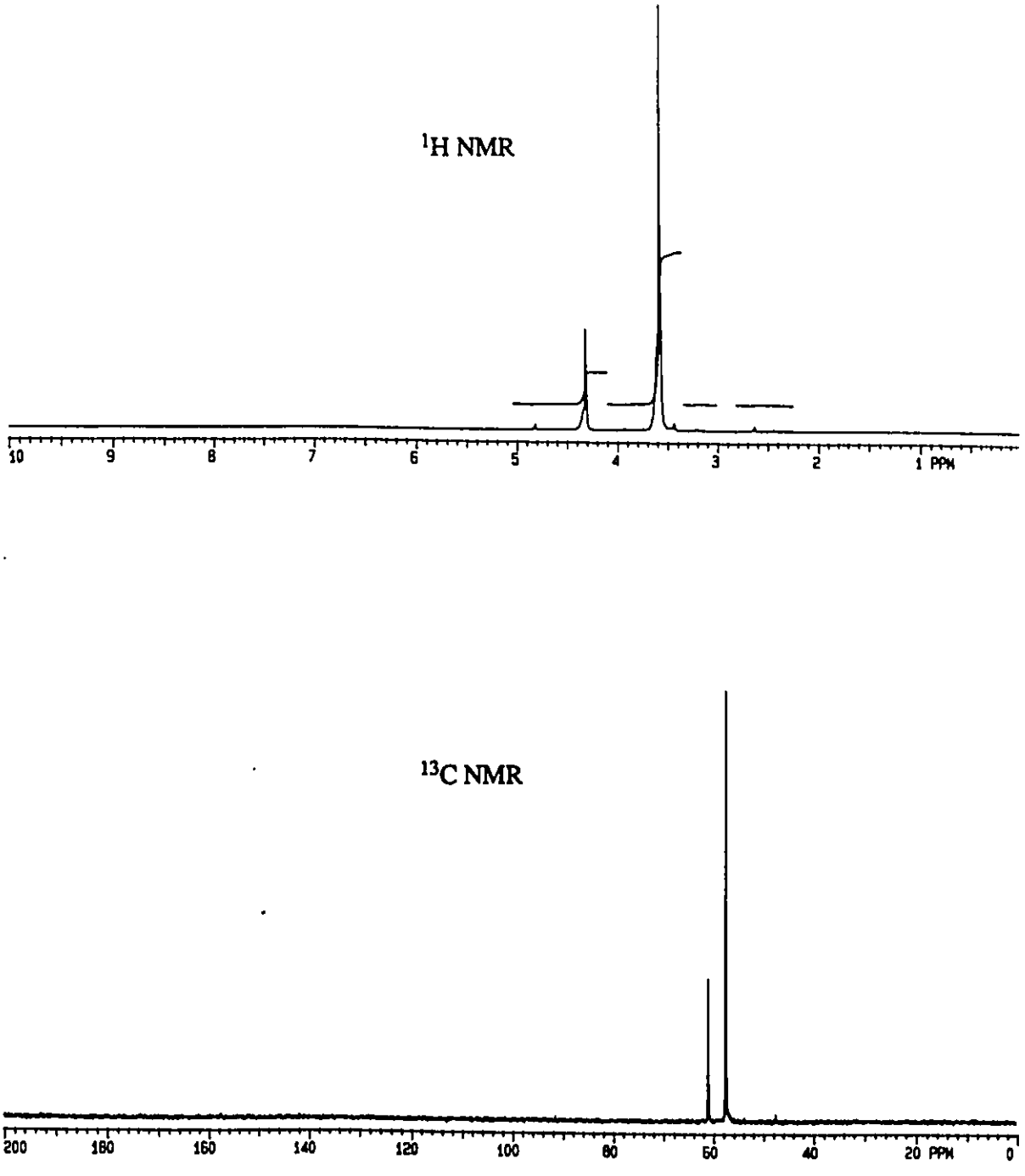

Figure 2.1 ^{1}H and ^{13}C NMR spectrum of quaternarized $MMDA^{2+}I^-_2(D_2O)$.

$MTETA^{4+}$ cations, respectively (see pages 198-200).

2.3 Conclusion

Two different types of quaternarized ammonium cations were synthesized and characterized by ^{1}H NMR, ^{13}C NMR and MS spectroscopy methods.

Chapter 3

Studies of The Incorporation of Organic Cations By Clay Minerals

3.1 Introduction

The layered structure of clay minerals was discussed in chapter 1. Due to isomorphous substitution, clay minerals carry a permanent negative charge in their structural framework. The negative charge of the clay layer is counter balanced by sorption of an equivalent amount of extraneous inorganic cations such as sodium, calcium and potassium. The inorganic cations in the clays can be replaced by organic cation such as alkylammonium and quaternary ammonium cations[53]. The alkylammonium cations have been known to cause considerable modifications in the hydration and swelling properties of the clay[54,55,56]. The large organic cations are more strongly held by the clay than are the inorganic cations. Their presence markedly alters the dispersibility of the clay and practically destroys their ability to swell in water[57]. In fact, the intercalation of alkylammonium cation into the interlamellar space of the clays has been studied extensively[58,59,60]. Quantitative exchange of the interlayer cations of smectites by alkylammonium cations provides the best method for characterization of smectites and determination of their layer charge[61,62]. The intercalation of the pillared cations into the

interlamellar space of the clays leads to the formation of porous networks analogous to those of zeolites. Since pillared clays can have pore sizes similar to larger than those of zeolites, they offer a promising way in modifying the pore size of solid materials for separation purposes. The most obvious manifestation of the introduction of organic molecules into the interlayer space of clay is a modification of the basal spacing of the mineral. The orientation of the intercalated cation depends on the layer charge density of the clay, the charge density of the cation, and the size of the cation. Clays exchanged with long chain alkylammonium ions show long basal spacings related to the length of the carbon chain. Quantitative relationships with the layer charge of the silicate, the shape, the cross-sectional area of the molecules and the resulting basal spacings of the complexes formed can be found in the literature[63]. A larger size of alkylammonium cation would cause a bilayer structure in the interlamellar space of the smectites. The adsorptions of some quaternarized amino acid ester derivatives, phosphonium and polyammonium cations are discussed in this chapter with three different systems to examine the interaction between these organic cations and the smectite clays. Further characterization of the organo-clays by X-ray diffraction method will be discussed in chapter 4.

3.2 Intercalation of quaternary ammonium derivative cations into the interlamellar space of clay minerals

Three types of quaternarized ammonium derivatives or quaternarized phosphonium cations are used in this study including quaternarized ammonium (phosphonium) mono-cations, mono- and di-quaternarized amino acid ester derivative, and poly-quaternarized ammonium cations. All these quaternarized cations could be intercalated into the interlamellar space of the clays. The adsorption isotherms of these organic cations

by the clays are studied and the CECs are calculated from the adsorption isotherms. Two clays are chosen for this study, Na-montmorillonite and Na-hectorite. The first system includes tetramethyl ammonium (TMA^+), trimethyl glycine ethyl ester ($GLY\text{-}Et^+$) and tetraphenylphosphonium (TPP^+) cations. In this system, the exchange process between the alkylammonium (phosphonium) cations (N^+) in the solution and the Na^+ ions in the clay (Z) can be represented by the following equation[8]:

$$Na^+\text{-}Z \quad + \quad N^+ \quad \rightleftharpoons \quad N^+\text{-}Z \quad + \quad Na^+ \qquad (3\text{-}1)$$

The above reaction proceeds until the exchangeable sodium ions are completely or nearly completely replaced. The thermodynamic equilibrium constant K for the above reaction is defined by:

$$K = \gamma_{Na^+}/\gamma_{N^+} \cdot ([Na^+][N^+\text{-}Z])/([Na^+\text{-}Z][N^+]) \qquad (3\text{-}2)$$

where γ_{Na^+}, γ_{N^+} are the activity coefficients of the Na^+ ion and the organic cation in the solution respectively, and $[Na^+]$, $[N^+\text{-}Z]$, $[Na^+\text{-}Z]$, $[N^+]$ are the concentration of the Na^+ ion in the solution, the organic cation adsorbed by the clay, the Na^+ ion in the clay and the free organic cation in the solution, respectively. For a dilute solution, the ratio $\gamma_{Na^+}/\gamma_{N^+}$ is approximately 1[64]. Therefore, equation 3-2 can be rewritten as:

$$K=([Na^+][N^+\text{-}Z])/([N^+][Na^+\text{-}Z]) \qquad (3\text{-}3)$$

In the second system, some di-quaternarized ammonium derivative cations are employed. These include quaternarized lysine methyl ester ($LYS\text{-}Me^{2+}$), quaternarized ornithine methyl ester ($ORN\text{-}Me^{2+}$), quaternarized methane diamine ($MMDA^{2+}$) and quaternarized

ethylene diamine ($MDEA^{2+}$) cations. The exchange equilibrium between these quaternarized ammonium cations and Na^+-saturated montmorillonite or hectorite (Z) may be expressed as:

$$2Na^+\text{-}Z + A^{2+} \rightleftharpoons Z\text{-}A^{2+} + 2Na^+ \quad (3\text{-}4)$$

The K constant is given by:

$$K=([Na^+]^2[Z\text{-}A^{2+}])/([A^{2+}][Na^+\text{-}Z]^2) \quad (3\text{-}5)$$

where $[A^{2+}]$ and $[Z\text{-}A^{2+}]$ are the concentration of the organic cations in solution and on the clay respectively.

The Na^+ ions released is twice as much as the organic cations adsorbed by the clay.

In the third system, a poly-quaternarized ammonium cation ($MTETA^{4+}$) is introduced. The equilibrium equation is expressed as:

$$4Na^+\text{-}Z + B^{4+} \rightleftharpoons B^{4+}\text{-}Z + 4Na^+ \quad (3\text{-}6)$$

where $[B^{4+}]$ and $[B^{4+}\text{-}Z]$ are the concentration of $MTETA^{4+}$in solution and on the clay respectively.

In equations (3-4) and (3-6), the concentration of $[Na^+]$ can be expressed as:

$[Na^+]=2[A^{2+}]$ and $[Na^+]=4[B^{4+}]$ respectively.

To simplify the calculation, the concentration of $[A^{2+}]$ in equation (3-4) and the concentration of $[B^{4+}]$ in equation (3-6) are transferred to the general form $[N^+]$ with the

unit in milliequivalent (meq). Therefore the equilibrium constant in the cases of di- and poly-quaternarized ammonium cations can be rewritten as:

$$K=([Na^+][N^+\text{-}Z])/([N^+][Na^+\text{-}Z]) \qquad (3\text{-}7)$$

In order to determine the CEC of the clays, some assumptions have to made: (a) The CEC is assumed to be equal to the sum of the concentration of Na^+ ions remaining in the clay and the concentration of organic cation adsorbed by the clay; (b) The total concentration of organic cation added $[N^+]_0$shall be equal to the sum of the concentration of organic cation adsorbed by the clay $[N^+\text{-}Z]$ and the concentration of the organic cations remaining in the solution $[N^+]$. That is:

$$[N^+]_0=[N^+]+[N^+\text{-}Z] \qquad (3\text{-}8)$$

Let $x=[N^+]_0$, $y=[N^+\text{-}Z]$

Therefore equation (3-7) becomes:

$$K=\frac{y^2}{(x-y)(CEC-y)} \qquad (3\text{-}9)$$

Solving equation (3-9) gives:

$$y=\frac{K(x+CEC)-(K^2(x+CEC)^2+4(1-K)K\ CEC\ x)^{1/2}}{2(K-1)} \qquad (3\text{-}10)$$

where x, y are the initial moles of organic cation added and the moles of organic cation

adsorbed by the clay respectively. By inserting x, y values to equation (3-9), the K constant and CEC can be calculated using a non-linear fitting procedure. The moles of organic cation adsorbed by the clay (y) can be measured either by colorimetry or Na electrode methods which will be discussed in the following section.

3.3 Adsorption measurements

3.3.1 Colorimetry method

Adsorption isotherm is formed by plotting the molar amount of the organic cation adsorbed by the clay against the molar amount of the organic cation added in the solution. The amount of the cation adsorbed by the clay can be determined by measuring the change in concentration of the supernatant solution after solutions of the quaternarized ammonium salts of different strengths have been shaken with accurately weighed amounts of clay. Although no further increase in the amount adsorbed was observed after stirring the suspension for 2 hours, an overnight stirring in room temperature was adopted in all instances to ensure that equilibrium was attained. The clay suspensions were then centrifuged. There are several methods which can be used for the measurements of the ammonium cation either by elemental analysis or by titration of the ammonium contents. There are also other spectrometric methods which can be used for the measurements. However, in the latter methods, the cations to be measured have to be UV-vis or fluorescent active in order to be detected by UV-vis or fluorescence spectroscopic methods.

In the cases of quaternarized ammonium salts, they are neither UV-vis active nor fluorescent active compounds. Therefore a new method has to be used to determine the concentration of these types of quaternarized ammonium salts. Colorimetric methods are classically used for the quantitative determination of various types of amines. These

methods were developed primarily for the determination of traces of long-chain aliphatic amines in water[65]. Bromo-cresol green (sulphonphthaleins) could react with primary, secondary, tertiary and quaternary amines to form a yellow complex. This complex was extracted from the aqueous solution by shaking with chloroform. The intensity of the yellow colour in the chloroform layer after extraction was proportional to the concentration of amine and was estimated by comparison with Loribond permanent glass colour standards[66]. The structure of Bromo-cresol green is shown as below:

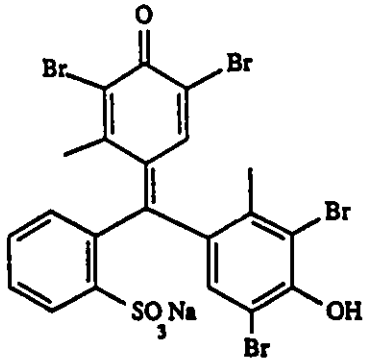

Bromo-cresol green

This method was adopted and modified in this study. Instead of colour determination by comparison of the colour with the standards, the concentration of the quaternarized ammonium salt was determined by UV-vis absorbance at 415nm after the quaternarized ammonium salt reacted with Bromo-cresol green. In all the cases studied here, calibration curves (the relationship between the concentration and the absorbance at 415nm) were made. By this method, the adsorptions of GLY-Et^+, LYS-Me^{2+}, ORN-Me^{2+}, $MMDA^{2+}$ and $MDEA^{2+}$ cations by Na^+-montmorillonite and Na^+-hectorite could be measured. In the cases of TPP^+ and $MTETA^{4+}$, the colorimetric method was no longer

suitable and a Na^+ electrode method was used for the measurements of the adsorption by the clays.

3.3.2 Sodium electrode method

Theoretically, as the quaternarized ammonium cations are adsorbed by the clay, the molar equivalent amounts of organic cations adsorbed are equal to the molar amounts of sodium ions released from the clay. Therefore the adsorption of the cations by the clays can be evaluated by the amounts of sodium ions released upon exchange with the organic cations. The concentration of the sodium ions in the solution can be determined by a sodium selective eletrode[67]. This method has already been applied to the cation adsorption study in our group[39].

The relationship between the Na electrode potential and the Na^+ concentration can be expressed as[67]:

$$E = cte + RT/\mathcal{F} \ln(\gamma_{Na^+} . [Na^+]) \qquad (3\text{-}11)$$

where E is the potential of the Na^+ electrode, *cte* is the potential difference between the reference electrode and the selective electrode, γ_{Na^+} is the activity coefficient of the Na^+ ion and $[Na^+]$ is the Na^+ concentration in solution.

Before the measurements, a series of standard Na^+ solutions were prepared and the potentials for these solutions were measured. Plotting the potential against the $\ln[Na^+]$, a standard curve was obtained. From the slope and the y-intercept of the standard curve, equation 3-11 could be rewritten as:

$$C_{Na^+} = \exp (E - 37.92) / 15.71 \qquad (3\text{-}12)$$

where C_{Na}+ is the concentration of the Na^+ ions released from the clay and E is the potential measured from the Na-electrode. Therefore the quantity of the Na^+ ions exchanged by the organic cations can be determined by measuring the potential value of the solution.

3.3.3 Adsorption isotherms and CECs of Na-montmorillonite and Na-hectorite

The adsorption isotherms for the quaternarized ammonium derivative cations and quaternarized phosphonium cation in solution by Na-montmorillonite and Na-hectorite are shown in Figure 3.1-3.15. The isotherms are plotted as milliequivalent moles of the quaternarized cations adsorbed by the clay against the milliequivalent moles of quaternarized cation added in the solution. The CECs and log K values are calculated from the adsorption isotherms and are given in Table 3.1 and 3.2. The cation exchange capacity of Na-montmorillonite (<0.2μm) and Na-hectorite (<2.0μm) are taken as 87 meq/100g and 89 meq/100g respectively[5,68]. From the adsorption isotherms, one can note that the maximum adsorption amounts are close or in a little excess to the CEC of the clays. This demonstrates that there is only monolayer cation coverage in the interlamellar space of the clay. The monolayer coverage can be confirmed by the X-ray diffraction results given in chapter 4. It has been shown that the adsorption amounts of alkylammonium compounds may exceed the exchange capacity of the mineral[8]. Electroneutrality is maintained by simultaneous adsorption of anions. For small cations, the excess salt accumulated in the interlayer space may be easily desorbed by washing with water or alcohol-water mixture, but for large cations the excess adsorbed will resist washing[8]. If the cations are too large, the area available may become insufficient to accommodate all the cations and therefore the cations may form double layers[57]. If the cations have asymmetric structures with the charge at one end, the cations may also form double layers, each one in contact with one silicate surface or they may stand at large angles to the basal plane[58]. In our cases, the quaternarized ammonium cations adopt monolayer coverage since the sizes of all the cations are smaller

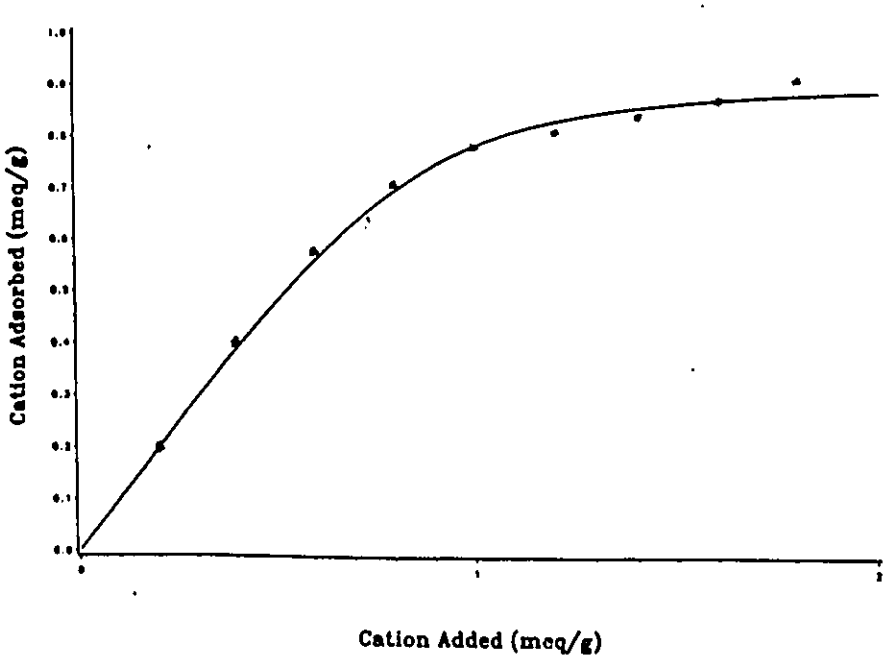

Figure 3.1 Adsorption of GLY^+ by Na-montmorillonite

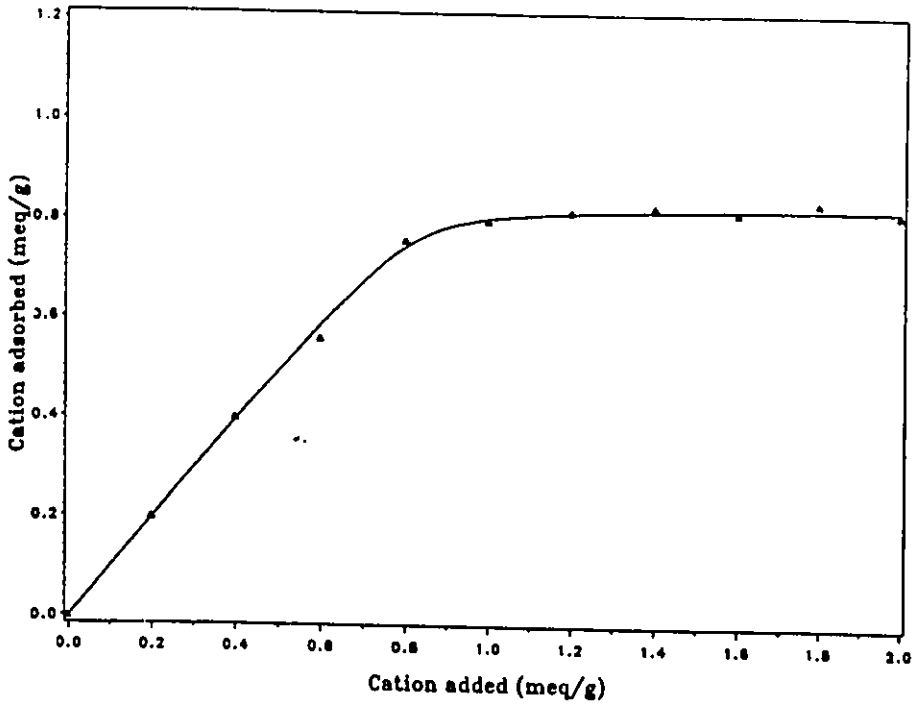

Figure 3.2 Adsorption of TPP^+ by Na-montmorillonite

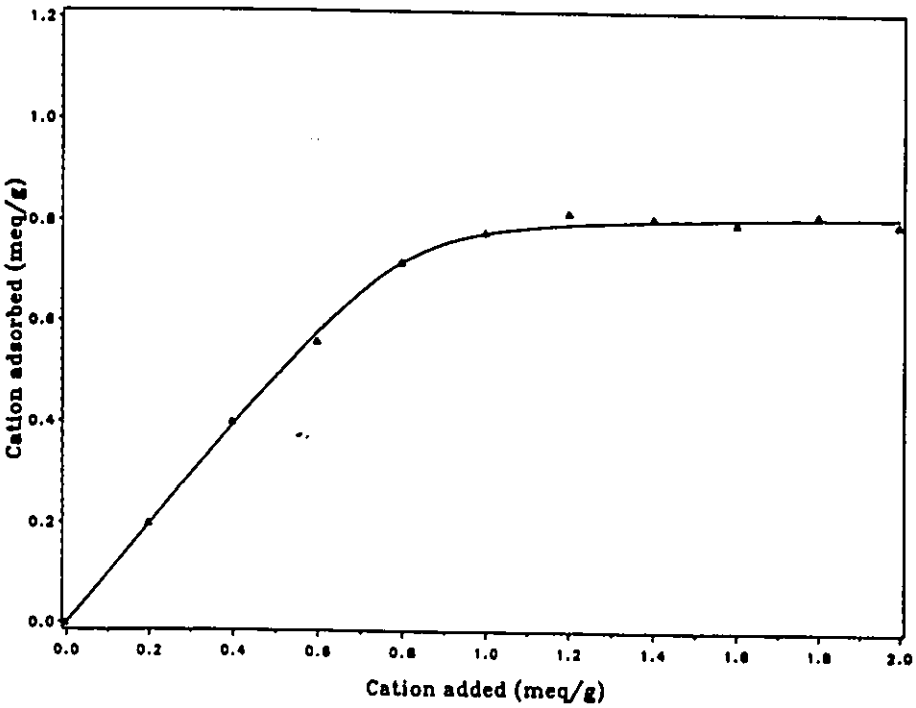

Figure 3.3 Adsorption of TPP^+ by Na-hectorite

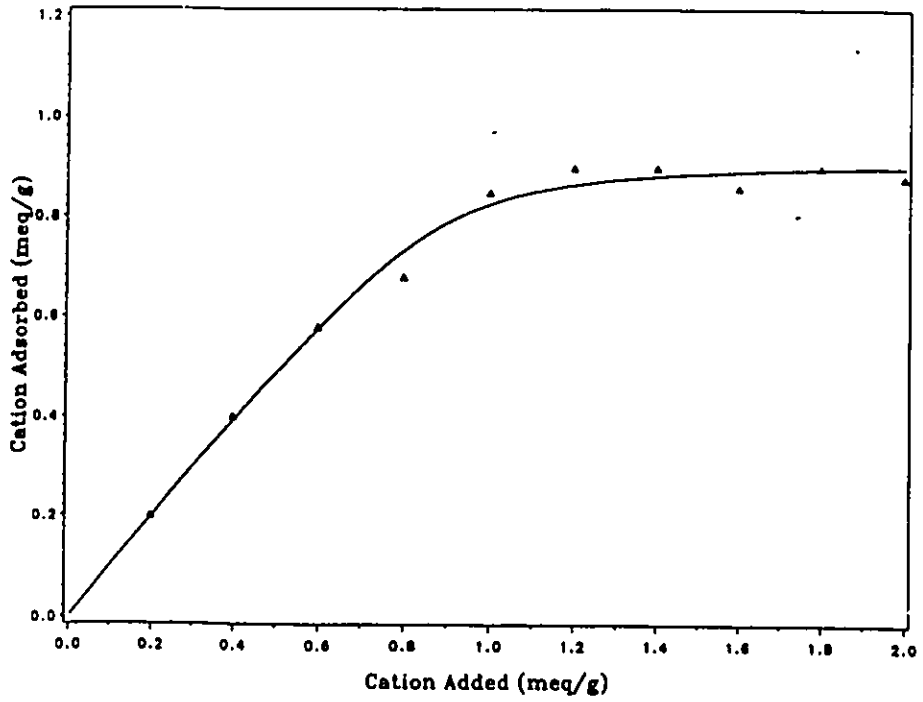

Figure 3.4 Adsorption of TMA^+ by Na-montmorillonite

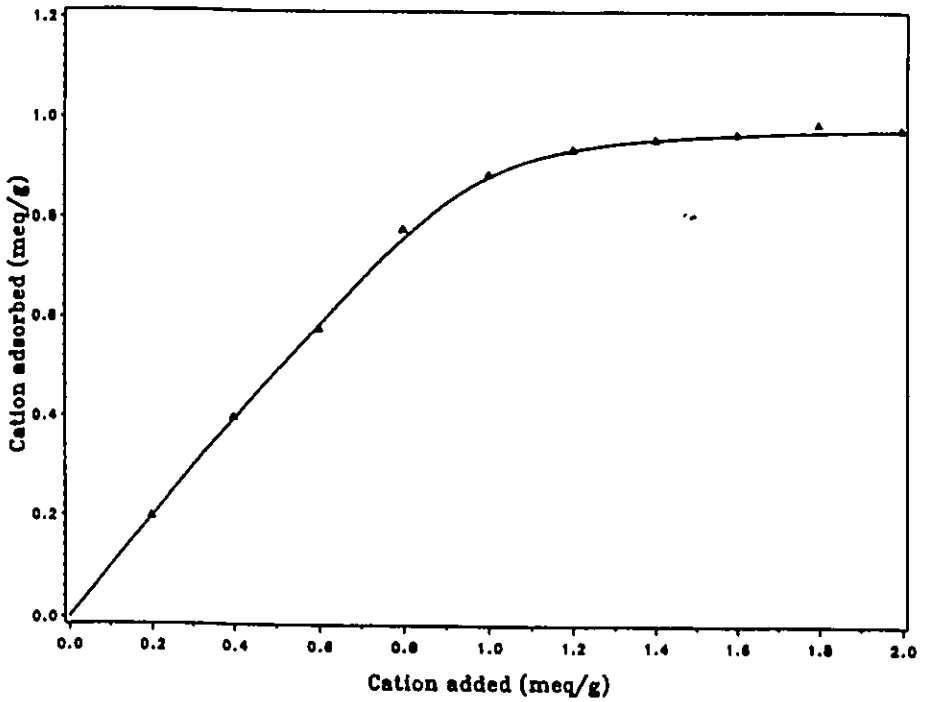

Figure 3.5 Adsorption of TMA^+ by Na-hectorite

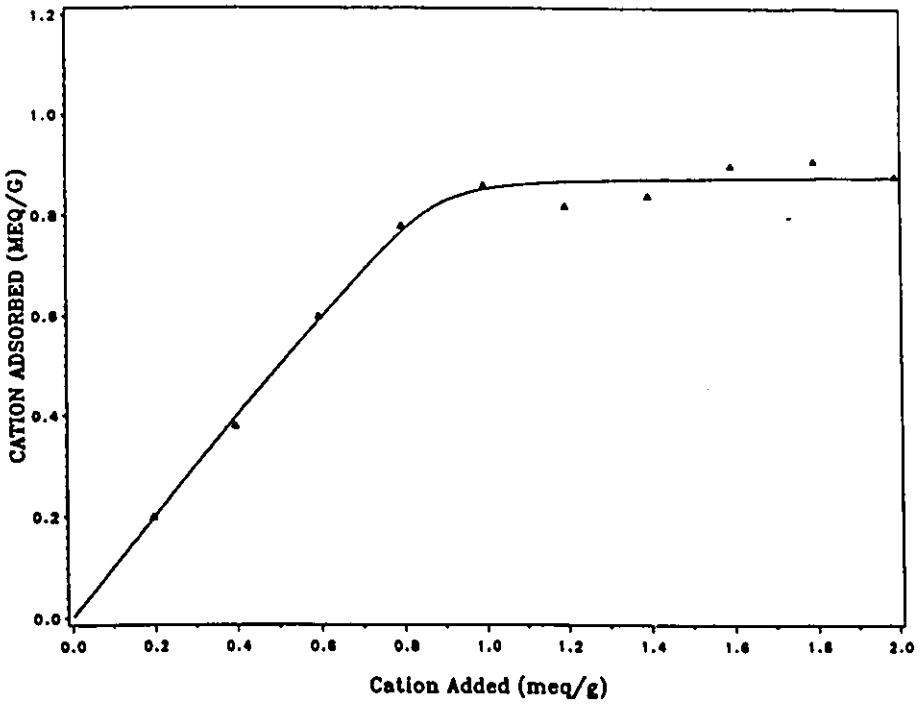

Figure 3.6 Adsorption of LYS-Me^{2+} by Na-montmorillonite

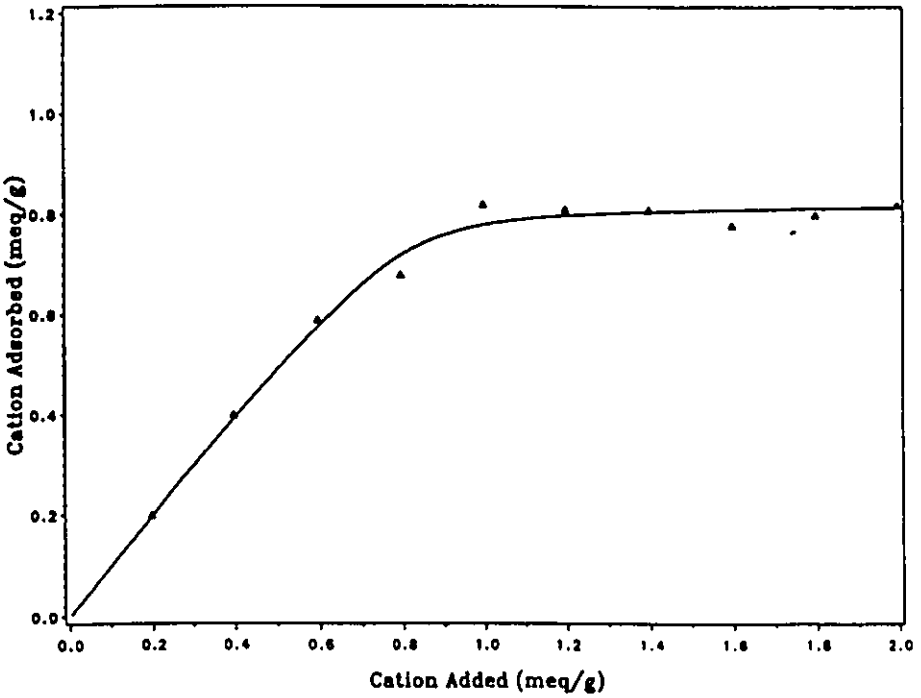

Figure 3.7 Adsorption of LYS-Me^{2+} by Na-hectorite

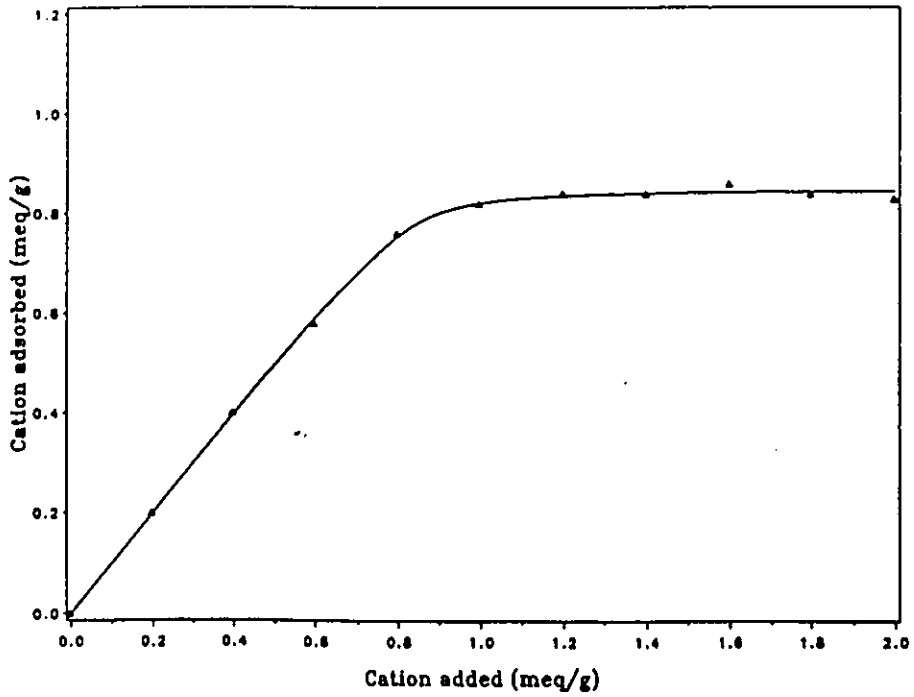

Figure 3.8 Adsorption of ORN-Me^{2+} by Na-montmorillonite

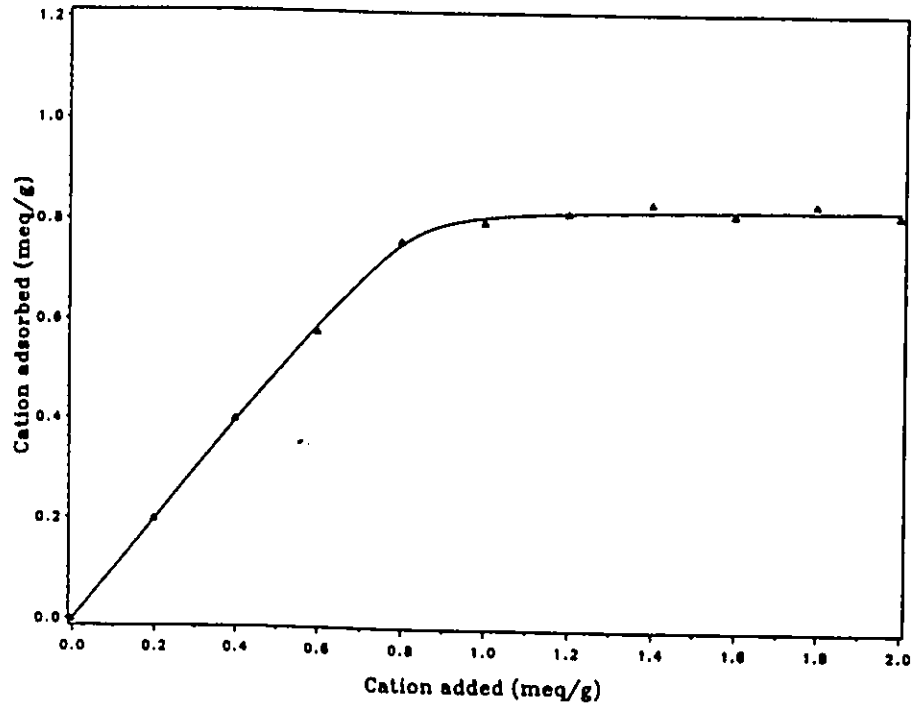

Figure 3.9 Adsorption of ORN-Me^{2+} by Na-hectorite

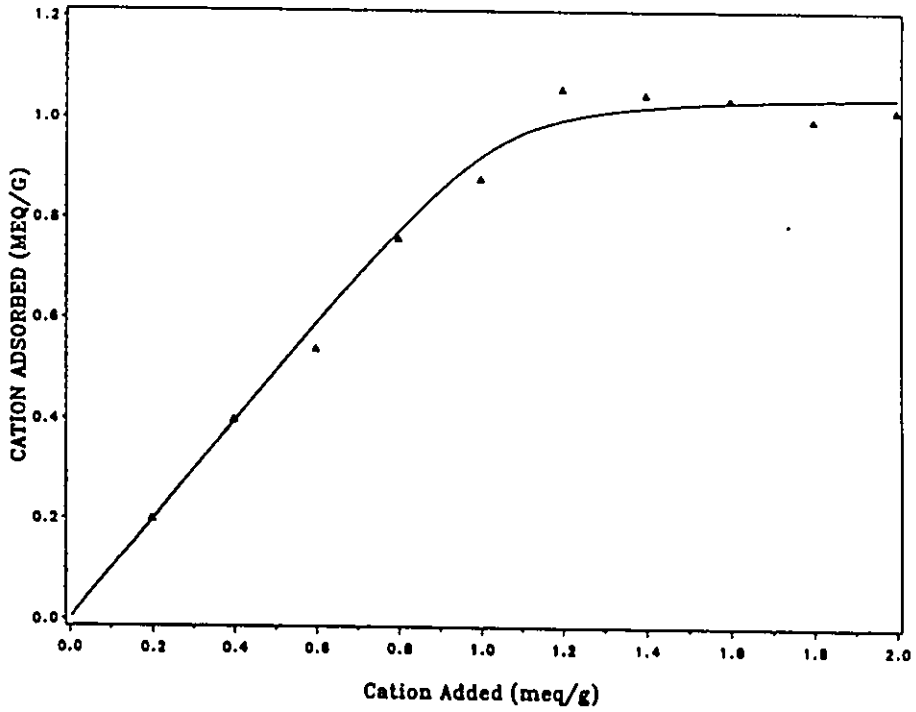

Figure 3.10 Adsorption of $MMDA^{2+}$ by Na-montmorillonite

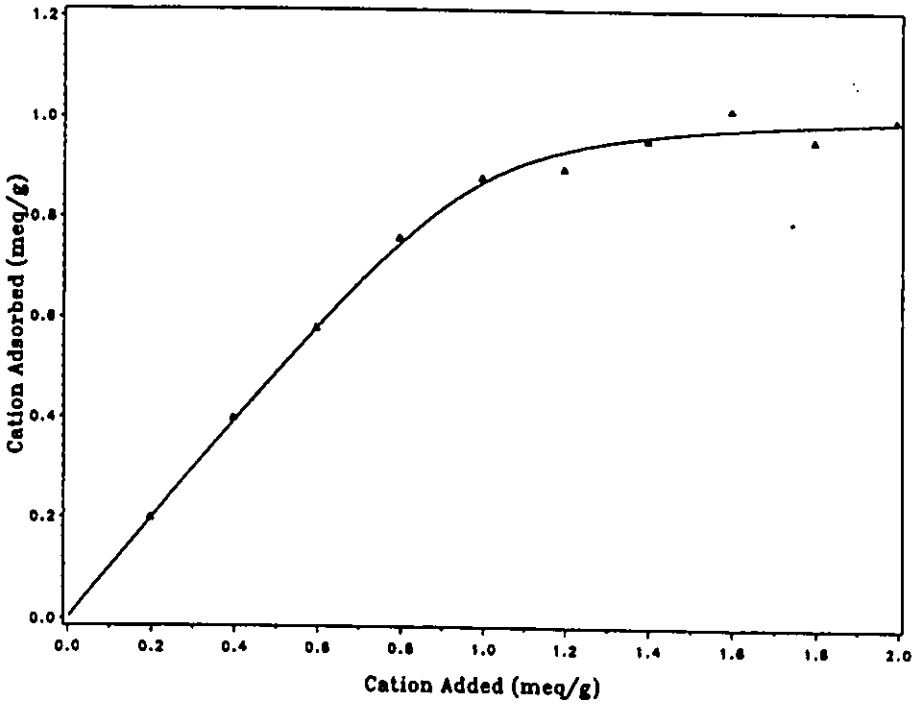

Figure 3.11 Adsorption of $MMDA^{2+}$ by Na-hectorite

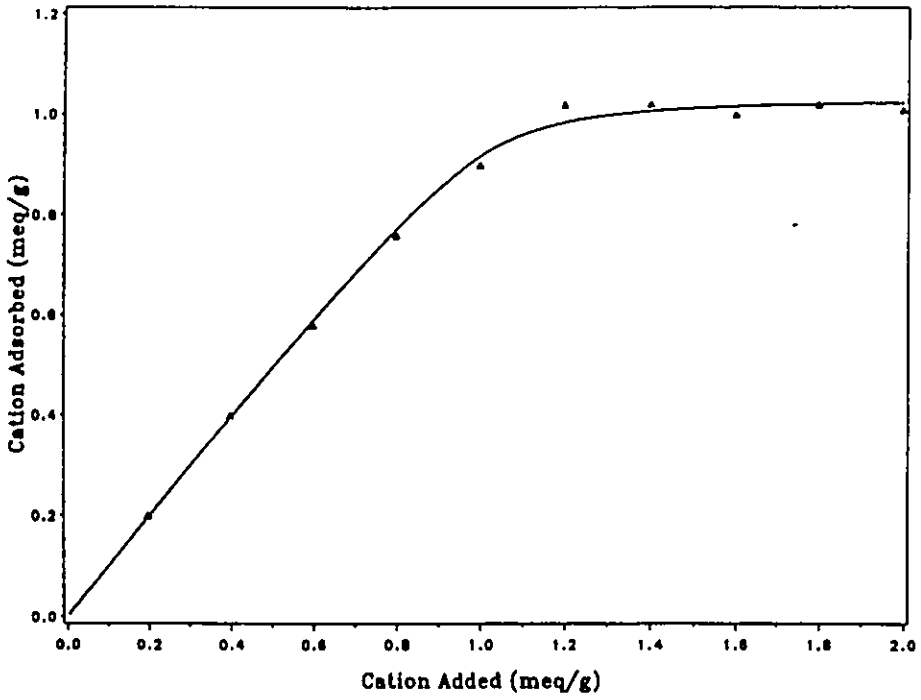

Figure 3.12 Adsorption of $MDEA^{2+}$ by Na-montmorillonite

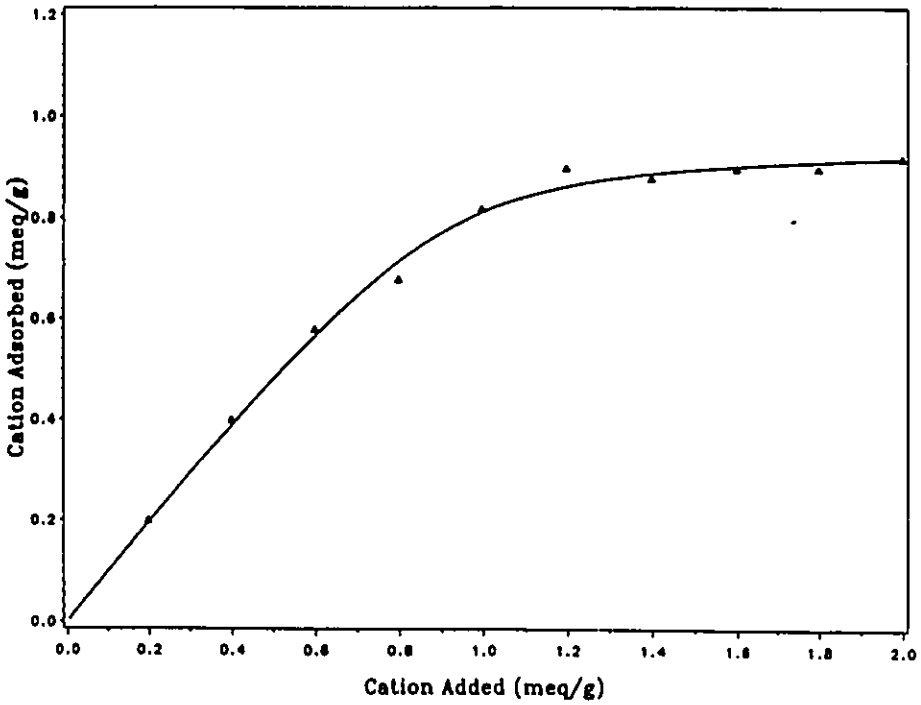

Figure 3.13 Adsorption of $MDEA^{2+}$ by Na-hectorite

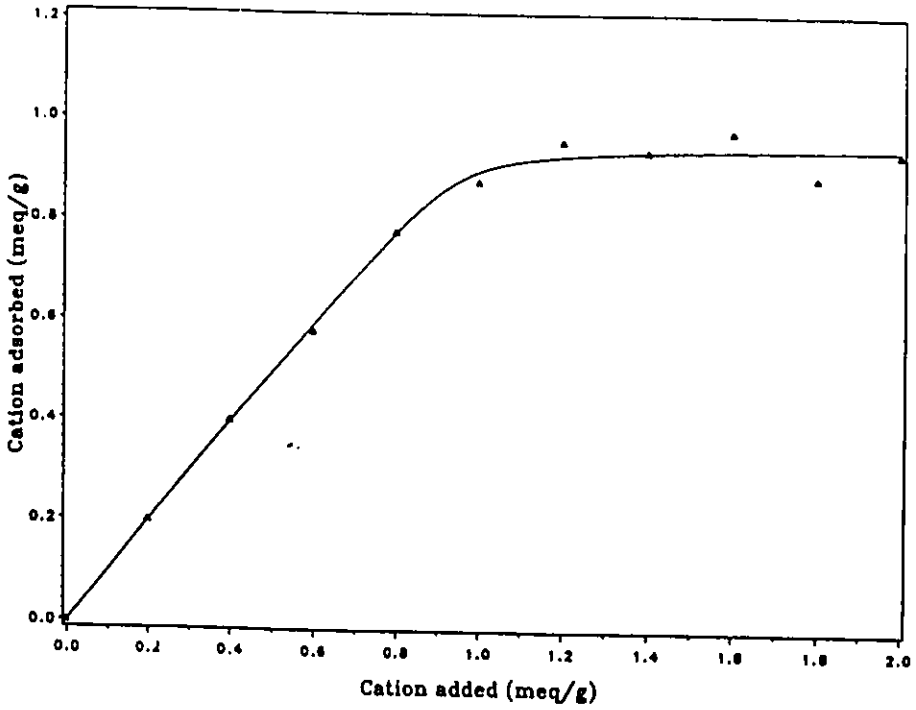

Figure 3.14 Adsorption of $MTETA^{4+}$ by Na-montmorillonite

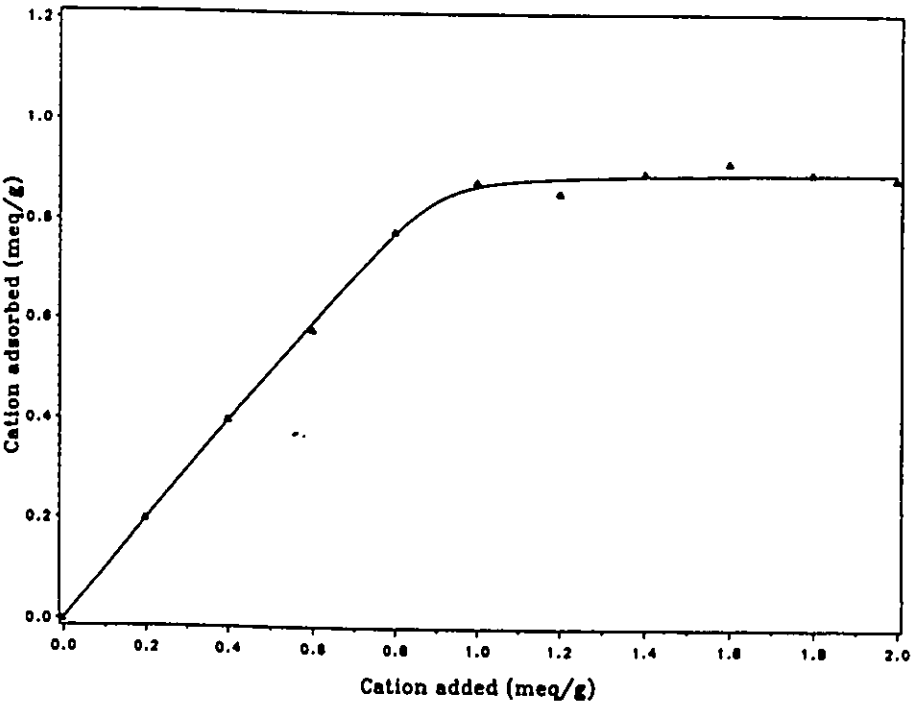

Figure 3.15 Adsorption of $MTETA^{4+}$ by Na-hectorite

than the area of the clay surface per unit charge (see chapter 5).

The adsorption of organic cations by the clays is influenced by both electrostatic (coulombic) and van der Waals attractive forces[69]. The adsorption isotherms on Na-montmorillonite and Na-hectorite show that the slope of the isotherms (log K) rises more steeply for the organic cations with higher molecular weight. This observation is of general applicability to the adsorption of the organic cations by montmorillonite[70,71]. The linkage between the organic cations and the charged silicate surface is fundamentally electrostatic forces. Also, van der Waals attraction between the aliphatic residues and the surface as well as between the adjacent molecules adds to the adsorption forces and becomes progressively significant as the molecular weight increases. For larger cations, van der Waals forces dominate the adsorption process. For a given cation, the initial rise in the slope of the isotherms can be explained in terms of co-operative exchange. The presence of an ammonium cation on the clay will favour adsorption of other cations on adjacent sites[72]. Since van der Waals forces decay rapidly with distance, their contribution to the adsorption energy will be greater for those cations which are in close contact to the surface, as in the cases of TMA^+ and $MMDA^{2+}$. The log Kcap values for these two cations are larger than that of GLY-Et^+ although the molecular weights of TMA^+ and $MMDA^{2+}$ are smaller than that of GLY-Et^+.

Table 3.1 Equilibrium constant K and CEC values for the adsorption of various organic cations on Na-montmorillonite

Cations	Molecular weight	log Kcap	CECs (meq/g)
GLY-Et^{+}	146	1.3 ± 0.1	0.92 ± 0.02
TMA^{+}	74	1.8 ± 0.1	0.91 ± 0.01
LYS-Me^{2+}	246	2.2 ± 0.1	0.88 ± 0.02
ORN-Me^{2+}	232	2.1 ± 0.1	0.85 ± 0.01
MMDA^{2+}	132	1.9 ± 0.1	1.06 ± 0.02
MDEA^{2+}	146	2.1 ± 0.1	1.03 ± 0.02
MTETA^{4+}	290	2.2 ± 0.1	0.95 ± 0.02
TPP^{+}	339	2.1 ± 0.1	0.83 ± 0.01

Table 3.2 Equilibrium constant K and CEC values for the adsorption of various organic cations on Na-hectorite

Cations	Molecular weight	log Kcap	CECs (meq/g)
TMA^{+}	74	1.8 ± 0.1	0.99 ± 0.01
LYS-Me^{2+}	246	2.2 ± 0.1	0.81 ± 0.02
ORN-Me^{2+}	232	2.2 ± 0.1	0.83 ± 0.01
MMDA^{2+}	132	1.6 ± 0.1	1.02 ± 0.02
MDEA^{2+}	146	2.0 ± 0.1	0.91 ± 0.02
MTETA^{4+}	290	2.3 ± 0.1	0.90 ± 0.02
TPP^{+}	339	1.8 ± 0.1	0.82 ± 0.01

3.4 Conclusions

Some quaternarized ammonium cations were intercalated into the interlamellar spaces of smectites. The adsorption studies gave information on the nature of the incorporation of these organic cations in the clays. The cation exchange capacities of the smectites were also determined. Both colorimetry and sodium electrode methods were used for the incorporation measurements.

Chapter 4

Characterization of Organo-Clays by X-Ray Diffraction and Scanning Electron Microscopy

4.1 Introduction

Smectite minerals have dioctahedral or trioctahedral 2:1 layer structure with isomorphous substitution leading to a negative layer charge. The structural units of smectite clays consist of a sandwich of one octahedral sheet between two tetrahedral sheets as discussed in chapter 1. For the studies of the clay layer structure, X-ray diffraction provides knowledge of the type or types of clays present, and the degree of crystalline order[73]. X-ray powder diffraction is undoubtedly the most widely used technique for identification and characterization of clay minerals. X-ray diffraction techniques can yield information about the interlayer spacings of the clay minerals, especially in the cases of modified clay minerals, where the interlayer spacings are variable. In more recent years, electron microscopy and microanalytical techniques have provided very powerful insights into these areas, notably into the details of clay formation and transformation in various environments[74]. Scanning electron microscopy provides direct imaging of particle morphologies at scales down to only a few nanometres and when used in back-scatter mode can be a very sensitive means of identifying different minerals since the brightness of the resulting image depends strongly on mean atomic number. The principles of X-ray

diffractometry and scanning electron microscopy as well as the applications of these techniques to the organo-clay minerals are discussed in this chapter.

4.2 X-ray diffraction analysis of interlayering in clay minerals

4.2.1 X-ray diffraction methods in clay mineralogy

X-rays are electromagnetic radiations characterized by wavelengths between 0.1 and 4.5Å. They are generated when electrons collide with the atoms of an obstacle[73]. The energy lost by the electrons in these collisions is emitted as X-ray photons. The wavelengths of these photons are a function of the amount of energy lost by the electrons during the encounters. This gives rise to a continuous spectrum of X-ray radiation[73]. When the energy of the bombarding electrons is varied to a critical level, which depends on the composition of the target, they have sufficient energy to penetrate to the interior of the atoms and dislodge electrons from the inner most shells. Electrons from higher levels fall in to fill the vacancies, emitting X-ray photons having a characteristic wavelength, which depends on the difference between the energy levels involved in the transition. This gives rise to a characteristic or line spectrum as shown in Figure 4.1[3]. The characteristic spectrum from a Mo target can be seen as superimposed on the white radiation spectrum[74]. In the selection of diffraction beam, a monochromatic (i.e., single wavelength) x-ray beam simiplifies the analysis of structural spacings in clay minerals. However, Figure 4.1(a) shows the characteristic spectrum with two peaks kα and kβ. If one could eliminate the kβ, an essentially monochromatic beam can be obtained. A metal foil is selected to absorb the shorter wavelength kβ radiation of the target metal, but is relatively more transparent to the longer wavelength kα radiation as shown in Figure 4.1(b). The intensity of the continuous spectrum is also reduced. There are several radiation sources available for the clay studies. Table 4.1 shows some characteristics of radiations used in clay studies. The widely used

widely used radiations for clay studies are copper and cobalt. Copper radiation is quite adequate for X-ray analysis of most clay materials.[75]

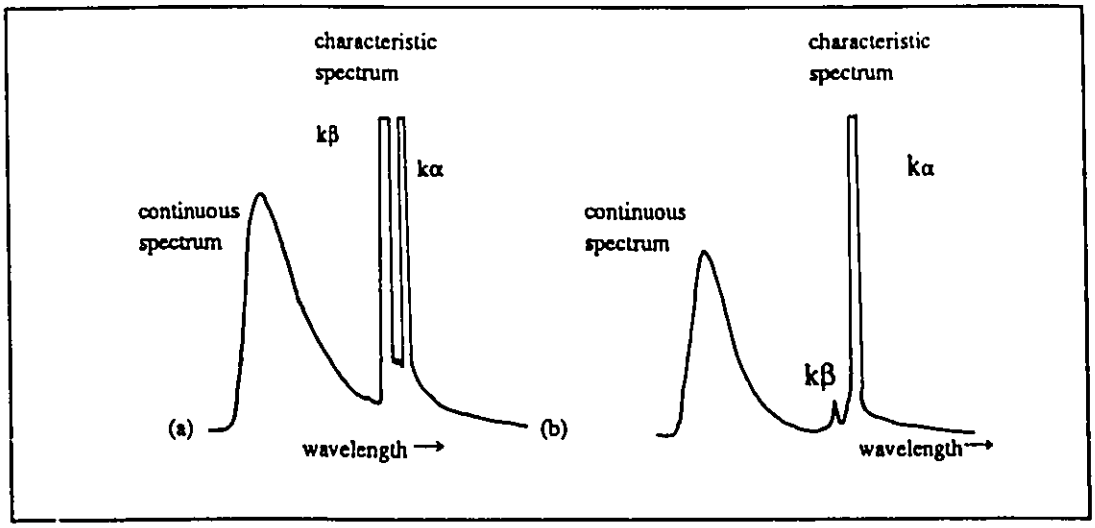

Figure 4.1 The continuous and characteristic spectrum of a metal target (a) without and (b) with an appropriate filter

Table 4.1 Some characteristics of X-radiation used in clay studies

Element	Cu (Å)	Co (Å)	Fe (Å)
Kα	1.5418	1.7903	1.9399
Kβ	1.3922	1.6208	1.7566

When an incident X-ray beam impinges upon an array, scattering occurs such that the scattered waves interfere with and destroy one another. In certain specific directions the

scattered waves are in phase with one another and combine to form new wave-fronts. This constructive interference is known as diffraction. The directions in which diffraction occurs depend upon the size and shape of the unit cell of the crystal, whereas the intensity of diffraction is determined by the actual atomic array or the nature of the crystal structure.

X-ray diffraction can be conveniently visualized as a reflection of the incident beam by parallel, closely spaced planes of atoms within a crystal. The reflected rays combine to form a diffracted beam only if they differ in phase by a whole number of wavelengths, that is, if the path length difference is equal to a multiple of the wavelength of the X-ray used. The condition for reflection is met only when the Bragg's equation is satisfied[3]:

$$n\lambda = 2\,d\sin\theta \qquad (4\text{-}1)$$

where λ is the wavelength of the X-ray, d the spacing between the lattice planes and θ the angle of incidence of the X-ray beam. Figure 4.2 shows a beam of parallel X-rays of wavelength λ falling at angle θ onto the face of a crystal possessing a layer structure of parallel planes of atoms with spacing d[74].

A diffractometer consists of an X-ray generator, a goniometer for measuring diffraction angles and a number of electronic circuits for determining the intensity of diffraction at any angle. The diffractometer is shown schematically in Figure 4.3[74]. The X-ray beam passes through the flat sample in the specimen at an incident angle of θ. The diffracted beam by the sample is then recorded by a counter which is mounted so as to sweep an arc. The sample is rotated about the goniometer axis to sweep all the values of θ. At the same time the counter is moved along the goniometer arc so that the angle between the X-ray generator and the receiver is 2θ. A diffraction peak is detected when the sample passes through a value of θ for which equation 4-1 is satisfied. Measuring the angle θ at

which diffraction occurs allows the calculation of the lattice spacing d, from which the lattice dimension can also be deduced.

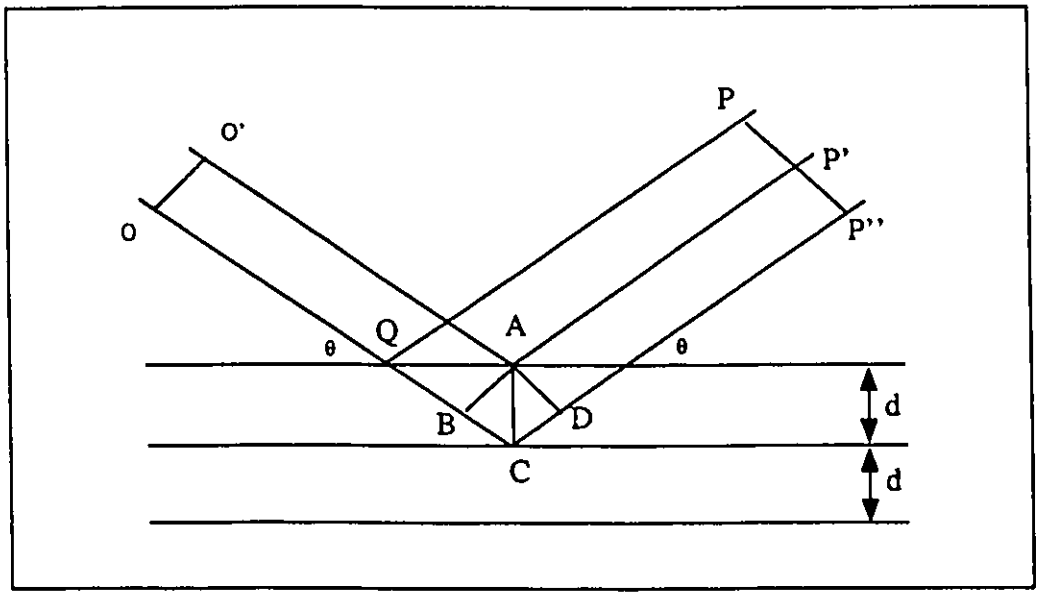

Figure 4.2 X-ray diffraction from a layer structure

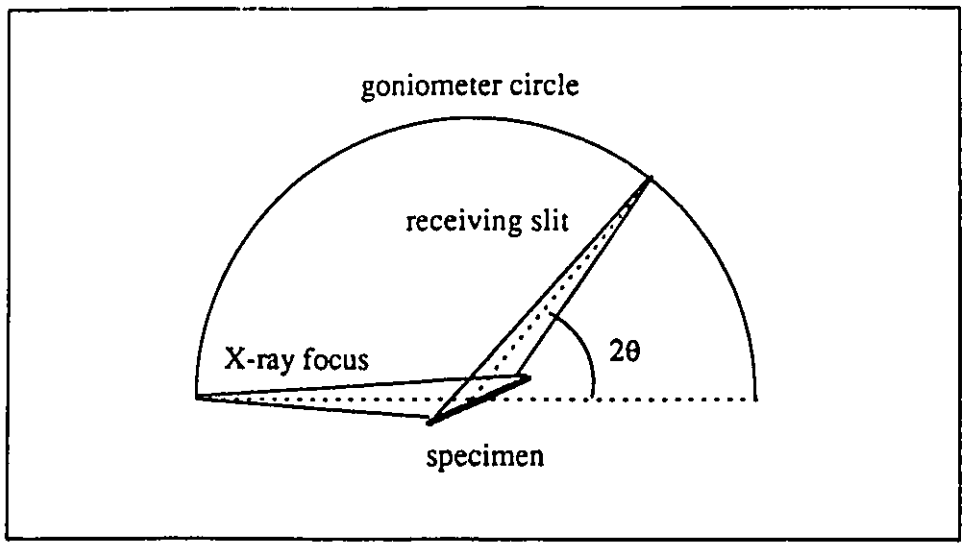

Figure 4.3 Schematic representation of a diffractometer X-ray optical system.

With respect to diffraction from the layer-structured crystal illustrated in Figure 4.2, as the crystal is rotated through an arc, it will pass through positions at which the phase differences are 1,2,3... wavelengths and where there will be a series of reflections deriving from the set of planes of spacing d. In clay mineralogy such reflections derive from the fundamental layer-repeat of clay minerals, they are of great diagnostic significance. X-ray diffraction from one set of planes deriving from a layer-repeat has been considered as basal reflections (00*l*), but diffraction will also occur from many other lattice planes within a layer-structured crystal[74]. For clay minerals these planes may be referred to in a general way as non-basal (*hkl*) planes, as they occur at right angles or are inclined to the basal planes. The complete X-ray powder pattern of a clay mineral, therefore, consists of basal and non-basal reflections and when the mineral is highly crystalline this pattern should be completely diagnostic for identification purposes. Clay minerals are identified by using X-ray diffraction patterns of oriented aggregates that enhance the basal(00l) reflections. The hkl peaks are not very diagnostic because the structures of most clays are very similar

in their X-Y directions. It is the atomic pattern along Z that is the most different from mineral to mineral. In an oriented film, order is found in only one direction, the direction normal to the basal plane (i.e. normal to the plane of the clay layers, the c-axis), the direction that coincides with the stacking sequence of the layers. The observed X-ray diffraction pattern is only due to the lattice plane spacings along that direction. However, one hkl reflection is of particular diagnostic significance and should always be measured whenever possible. This is the 060 or 60 reflection, which occurs at about 1.5Å and is often stronger and sharper than the other hkl reflections[3]. Measurement of this reflection will yield the b parameter in the unit cell of the clay mineral and will indicate whether it belongs to the dioctahedral or trioctahedral subgroups. In general, the 060 reflection of dioctahedral minerals occurs between 1.49 and 1.51Å, whereas for trioctahedral minerals a spacing between 1.53 and 1.55 Å is usually recorded.

The d_{001} diffraction can be calculated from all the d_{00l} diffractions by the following equation[3]:

$$d_{001} = (d_{001} + 2d_{002} + 3d_{003} + 4d_{004} + ...)/n \qquad (4\text{-}1)$$

$$n = 1, 2, 3, 4...$$

The spacing of the organo-clay which is the distance between the layers can be calculated from the d_{001} by subtrating from the d_{001} value the thickness of the silicate sheet, 9.6Å[3,75]:

$$c(Å) = d_{001} - 9.6 \qquad (4\text{-}2)$$

The thickness of the silicate sheet is the distance between the two repeat layers without the interlayer cations as shown in Figure 4.4[3,77].

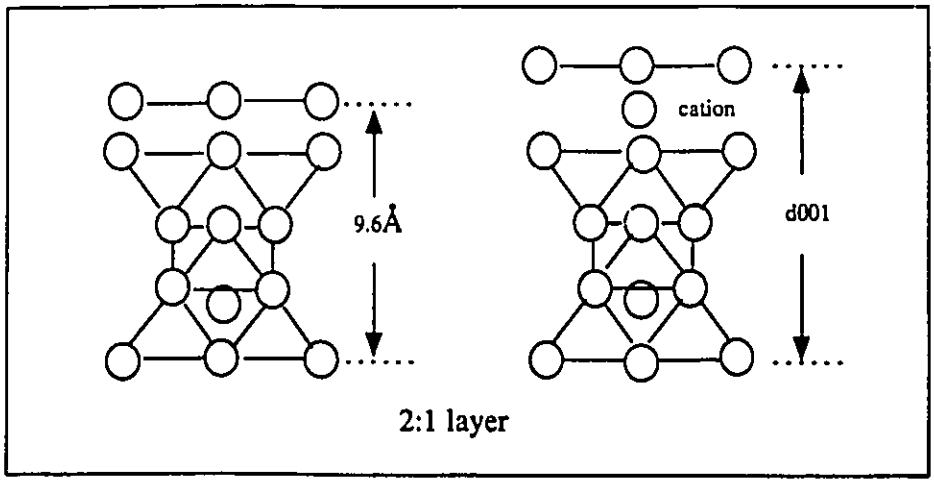

Figure 4.4 Diagrammatic sketch of smectite minerals.

4.2.2 X-ray diffraction patterns of organo-clay minerals

X-ray diffraction by clay minerals is used mostly as an analytical tool for the identification of minerals[3,68,78,79,80]. Oriented thin films of montmorillonite and hectorite exchanged with various organic cations were prepared as described in chapter 8 and their X-ray diffraction patterns were measured.

Figures 4.5 and 4.6 show the X-ray diffraction patterns of oriented films of Na^+-montmorillonite and Na^+-hectorite respectively. On these figures, the intensity of the diffracted X-rays is plotted on the vertical axis against the value of 2θ. In the spectra of Na^+-montmorillonite, two strong peaks, which are attributed to d_{001} and d_{004}, as well as two broad weak d_{002} and d_{003} peaks are observed. From these four d_{00l} peaks, a value of d_{001} = 12.1 Å is calculated. There are other small peaks at d = 1.99 Å, 2.82Å, 3.35Å and 4.27Å respectively. These peaks are attributed to the impurities quartz (d = 3.35, 4.27 Å) and NaCl (d = 1.99, 2.82 Å)[3]. The Na-hectorite gives a similar X-ray diffraction pattern except that relatively broader peaks are observed. In this case, the d_{001}, d_{002} and d_{003} are seen, from

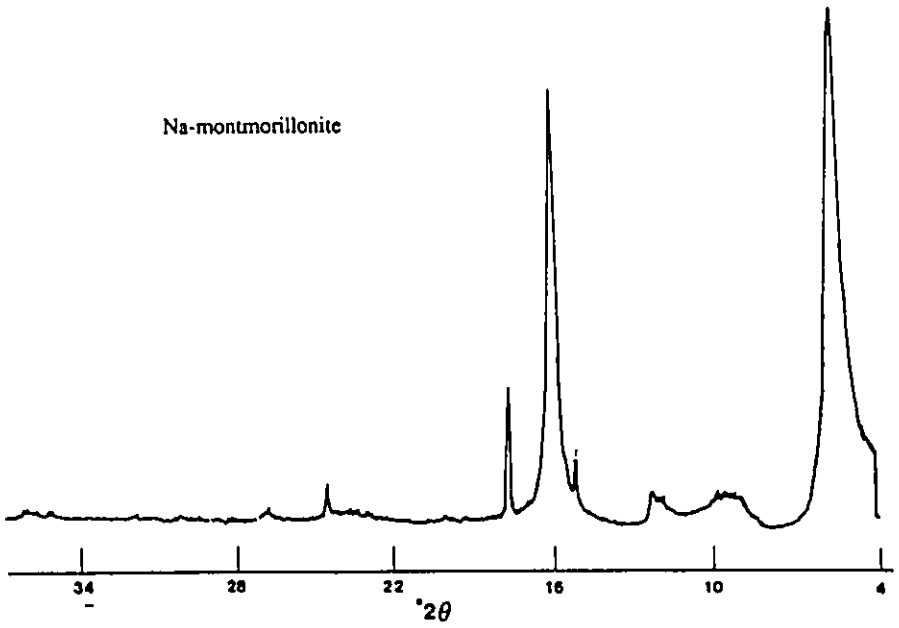

Figure 4.5 X-Ray diffraction spectrum of <0.2µm Na-montmorillonite

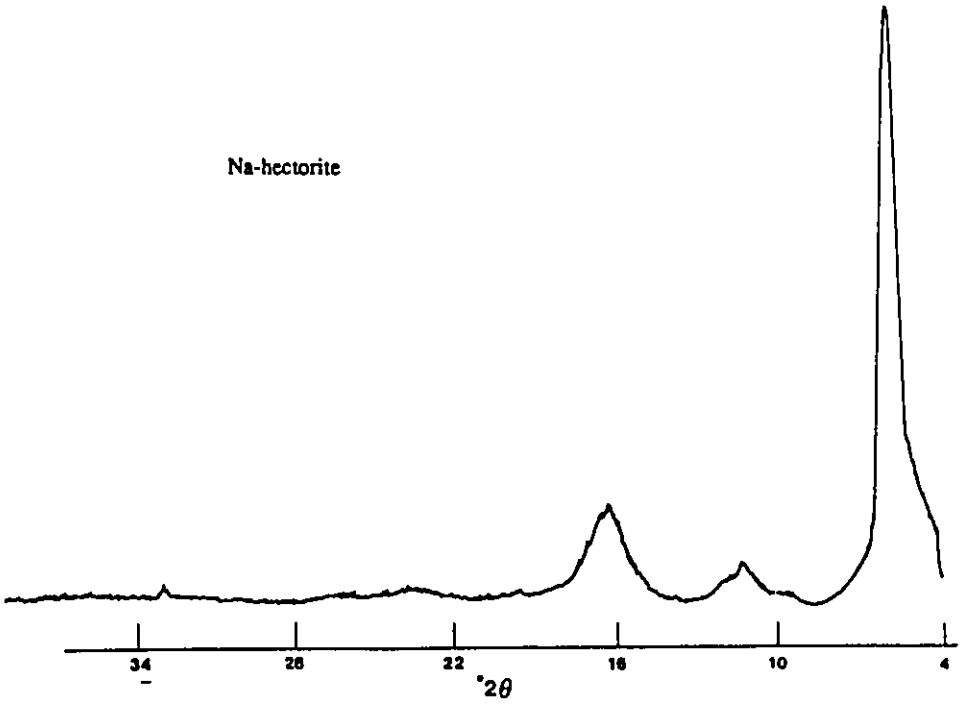

Figure 4.6 X-Ray diffraction spectrum of <2.0µm Na-hectorite

which a value of d_{001} = 13.6 Å is calculated.

Figure 4.7 and 4.8 show the X-ray diffraction patterns of oriented films of montmorillonite and hectorite exchanged with $MMDA^+$ cation. On these figures, the d_{001} values are seen to shift to higher values as compared to the Na-montmorillonite and Na-hectorite. In all the organo-montmorillonite and organo-hectorite samples, d_{001}, d_{003} and d_{004} are observed but d_{002} are very small. From the d_{00l} values, the d_{001} are calculated which are shown in Table 4.2. The quartz peaks are also found in those X-ray diffraction patterns of organo-clays. Another weak peak is seen in all the organo-clay samples at about 1.5 Å which is attributed to the d_{060} reflection[3]. The 060 reflections allow the distinction between dioctahedral and trioctahedral types because the b cell dimension is more sensitive to the size of the cations and to site occupancy in the octahedral sheet than are the a or c dimensions. The d(060) values depend on the composition of the octahedral sheet, the amount of Al in tetrahedral coordination and the degree of tetrahedral tilt[75]. Montmorillonite is a dioctahedral smectite whereas hectorite is a trioctahedral one. In all the organo-montmorillonite samples, the d(060) reflections are seen at 1.50Å and in the cases of organo-hectorite samples, the d(060) reflections are found at 1.52Å.

All the basal spacings (d_{001}) and the interlayer spacings of the organo-montmorillonite and the organo-hectorite are shown in Table 4.2 and 4.3. The spacings are calculated from equation 4-2. The basal spacings depend upon the size and the orientation of the alkylammonium derivative cations in the interlamellar space of the clays.

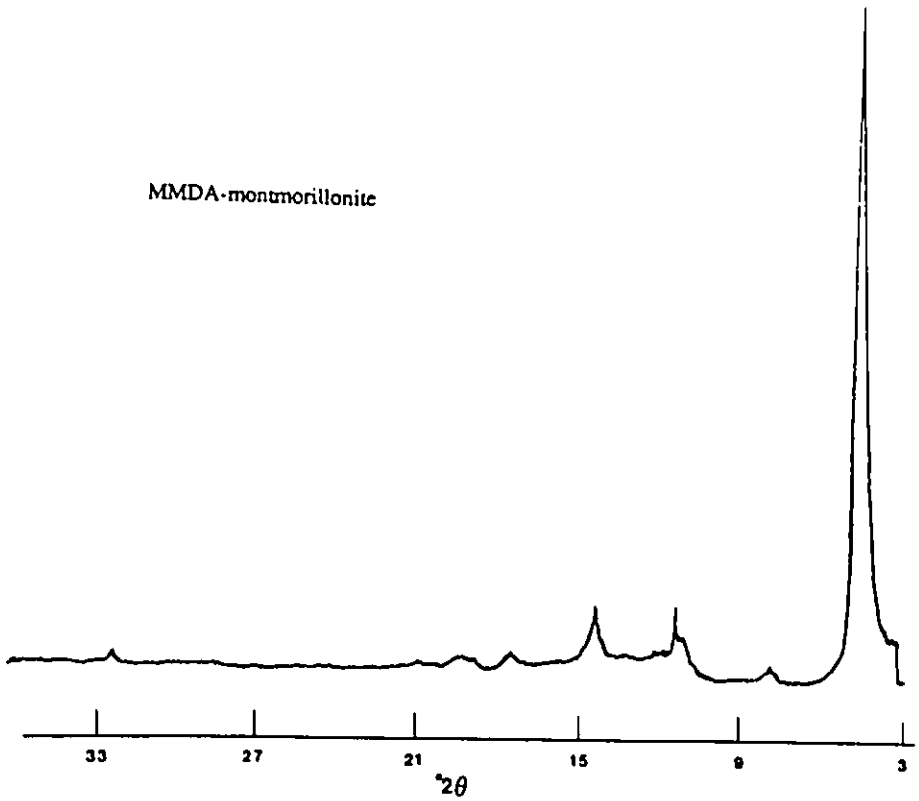

Figure 4.7 X-Ray diffraction spectrum of MMDA-montmorillonite

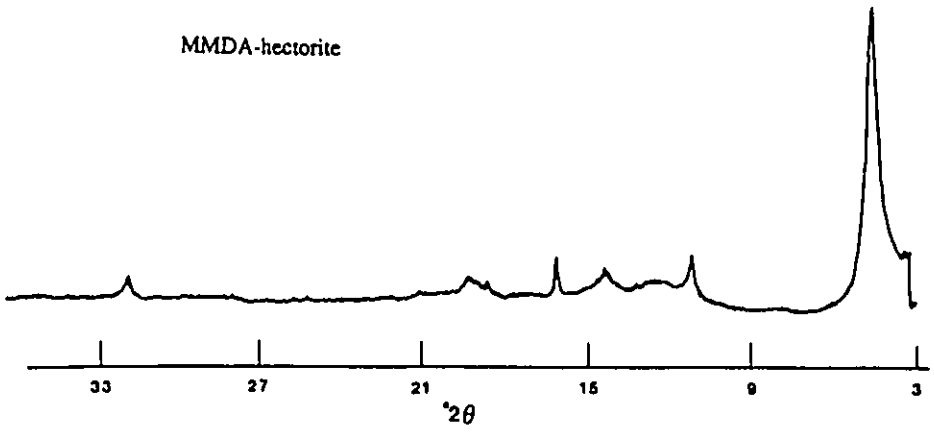

Figure 4.8 X-Ray diffraction spectrum of MMDA-hectorite

Table 4.2 Basal spacings and interlayer spacings of organo-montmorillonite

Sample	d_{001} (Å)	c (Å) = d_{001} - 9.6
Na-M	12.4	2.8
GLY-Et-M	13.6	4.0
TMA-M	13.9	4.3
LYS-Me-M	14.2	4.6
ORN-Me-M	14.0	4.4
MMDA-M	13.9	4.3
MEDA-M	14.0	4.4
MTETA-M	14.6	5.1
TPP-M	18.8	9.2

Table 4.3 basal spacings and interlayer spacings of organo-hectorite

Sample	d_{001} (Å)	C (Å) = d_{001} - 9.6
Na-Hectorite	13.4	3.8
TMA-H	14.2	4.6
LYS-Me-H	14.6	5.0
ORN-Me-H	14.4	4.8
MMDA-H	14.3	4.7
MEDA-H	14.5	4.9
MTETA-H	14.6	5.0
TPP-H	18.7	9.1

As can be seen in Tables 4.2 and 4.3, the interlayer spacings for Na-montmorillonite and Na-hectorite are 2.8Å and 3.8Å respectively. In these two purified clays, the clay sheets are held apart from each other by Na^+ cations and associated water molecules. In the expendable clays, the interlayer cations are attracted more to water than to the relatively small layer charge. It has been shown that a continuous variation of d_{001} with available water or relative humidity[3,81]. The change in apparent d_{001} results from an ordered interstratification of continuously changing proportions of successive hydrates, i.e., as relative humidity is increased from 1 to 100%, Na-smectite has discrete thicknesses of 9.6, 12.4, 15.2 and 18 Å. The value 2.8 Å corresponds to the thickness of one layer of water[3].

The spacings in most of the organo-clays are in the range 4-5Å which are larger than those of the parent clays. The orientation of the cations in the interlamellar spaces are strongly dependent on the charge density of the clay and the size of the cations. Figure 4.9 shows three different orientations of the alkylammonium cations[82]. As the charge density of the clay increases, the intercalated cations have to adopt a more perpendicular orientation with respect to the clay layers. In the extreme case, a completely perpendicular cation orientation is obtained. If the size of the cation exceeded the available area of the clay as in the case of tetraoctyl ammonium cation, there would be a jump from a monolayer to a double layer[32]. Since the cross-sectional surfaces of the organic cations in our cases are all smaller than the unit clay surface available, the interlamellar distances are independent upon the charge density of the clays. Therefore, the interlamellar distances depend only on the size of the cations intercalated. The interlamellar distances of these organo-clays (4-5Å) are corresponded to the height of the tri-methylated ammonium group, showing that the tri-methyl ammonium group determines the interlamellar distance, with the side chains of the organic derivatives lying parallel to the clay surfaces. For example, the optimum orientation of LYS-Me^{2+} is shown in Figure 4.10 where the dimensions, a and b, and the height of the molecule, are indicated. The length of the molecule, 11.5Å, is much larger

than the spacing measured from the X-ray diffraction such that a perpendicular orientation in the interlamellar space is impossible. The molecule takes a stable parallel orientation in the interlamellar space, producing a 4.6Å basal spacing. The height of the molecule, 5.6Å is slightly larger than the interlayer spacing, 4.6Å. This is attributed to the fact that the molecule can key into the vacancy of the silicate layers[83]. In the cases of TPP-M and TPP-H, the interlamellar distances increased to 9.1 and 9.2Å, respectively.

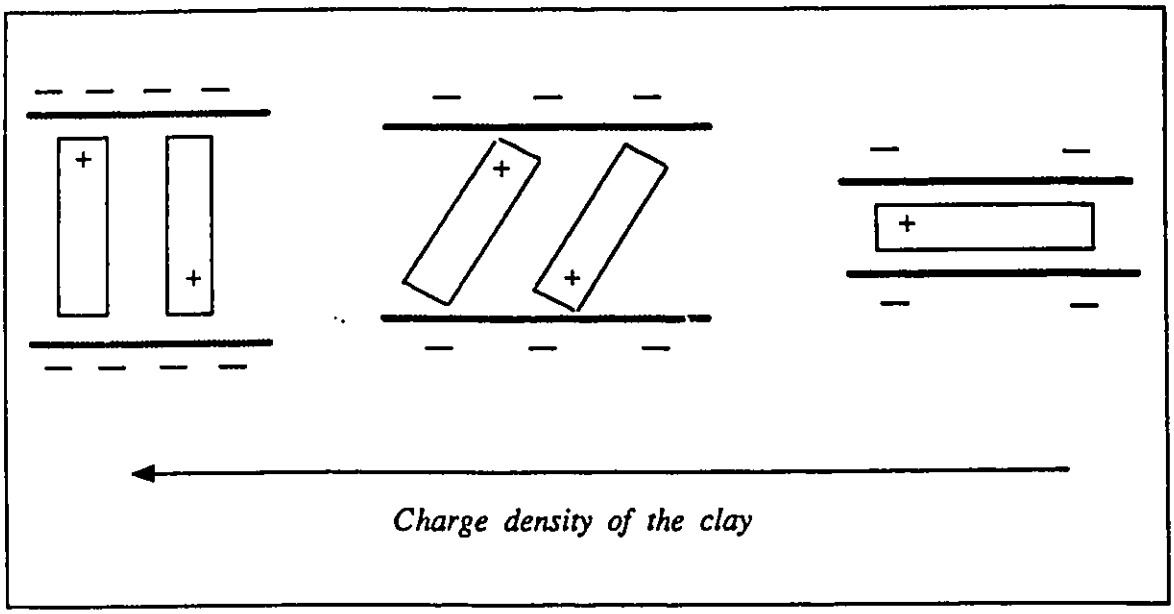

Figure 4.9 Dependence of charge density of the clay in the orientation of cations

In addition, the interlayer spacings for the organo-hectorites are larger than that for the corresponding organo-montmorillonites. The difference in the interlayer spacings between the two organo-smectites might be due to the different composition of the tetrahedral and octahedral sheets in these two clays. The organic cations could key further into the clay sheets in the montmorillonite than in the hectorite.

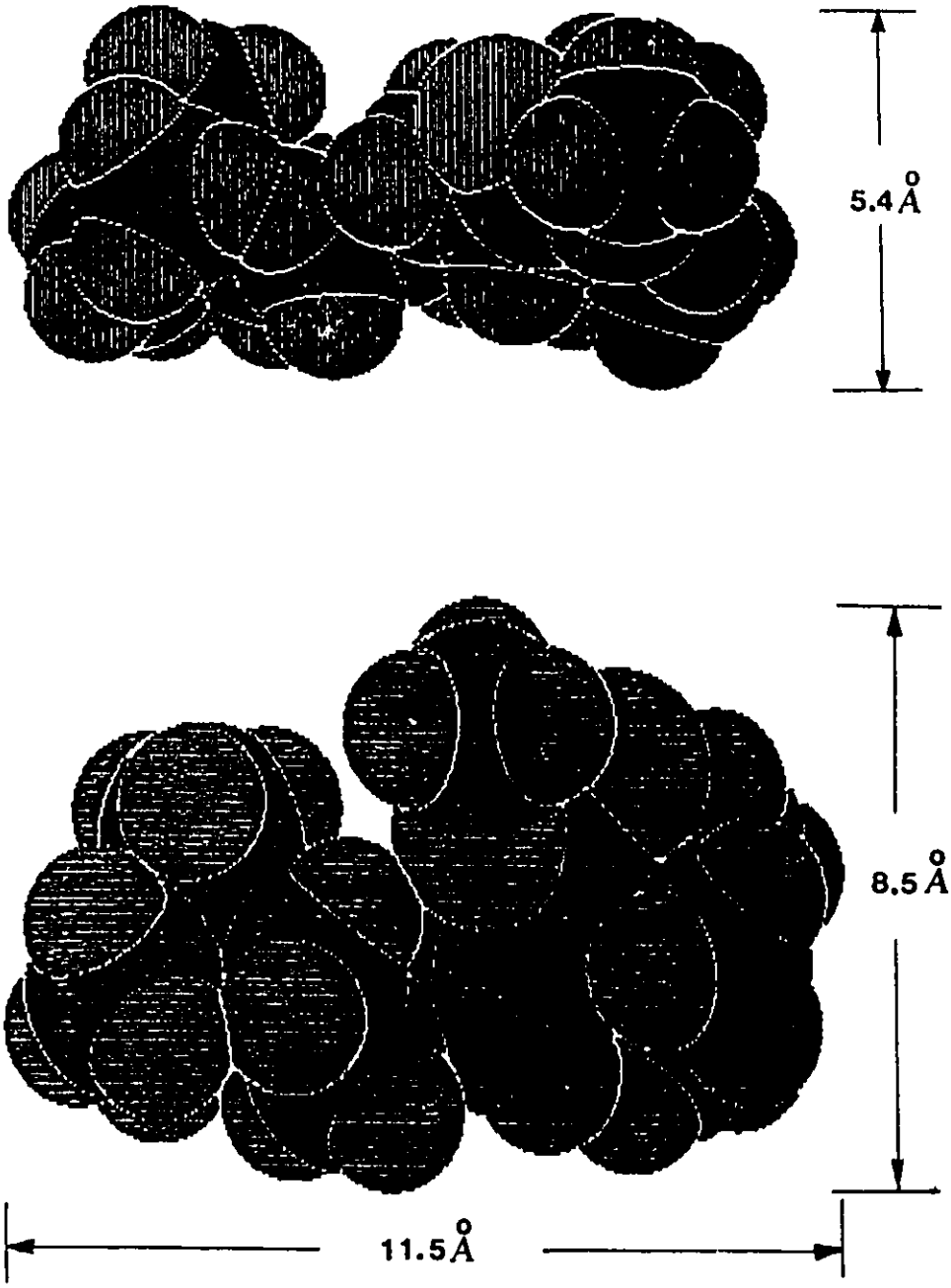

Figure 4.10 Size of a LYS-Me^{2+} cation and its orientation in the interlamellar space of the clay

4.3 Scanning electron microscopy of clay minerals

4.3.1 Scanning electron microscopy of clay minerals

In recent years, scanning electron microscopy (SEM) has proven to be a powerful tool for mineralogy study because it can produce photomicrographs with an apparent three dimensional quality[74]. In clay mineralogy, scanning electron microscopy is used either as an analytical tool for the identification of a given clay or to look at the morphology of clay minerals[84]. The characterization of clay minerals by SEM such as kaolin, chlorite and smectites has been well established[85,86]. In the study of clay morphology, SEM can give some information on a variety of characteristics and texture of the clays. For example, a sample made up of the two clays chlorite and smectite have different morphology but the same X-ray diffraction pattern[87]. SEM has been used to look at the configuration of clay particles such as size and shape[84]. Smectites are characterized by their crinkly, ridged, honeycomb-like texture[84,87]. SEM can also be used for the studies of the aggregation features, interlocking and interpenetration of the clay particles. For example, SEM showed that the aggregation of the Li-montmorillonite platelets are face-to-face arrangements[88]. In recent years, SEM has been used for the studies of aggregation stacking of pillared clays[83,89]. Scanning electron microscopy can be used to look at the way in which clay minerals are formed in nature. SEM has been used to look at such processes as the smectite to illite conversion series, the formation of kaolinite and the formation of montmorillonite[90,91,92]. In all these studies the change in the morphology of the clays was monitored by SEM. Finally, SEM has been well used for the studies of the surface characteristics of membranes and the pore structures of membranes[93,94].

4.3.2 SEM of organo-clay minerals

All the SEM were taken from the dried organo-clay samples. Figure 4.11 shows the layer structure of homoionic <0.2 μm Na^+-montmorillonite. It shows a typical morphology of very thin layer structure. The particle aggregation depends on the physico-chemical conditions of a sedimentation process[95]. Usually, there are three types of aggregates, including edge-edge-type aggregates, edge-face-aggregates and face-face-aggregates. Replacement of the Na^+ ions by TPP^+, LYS-Me^+ and $MMDA^{2+}$ organic cations has an effect on the configuration of the particles. The SEM micrographs of montmorillonite exchanged with these organic cations are shown in Figures 4.12-4.14. When the larger organic cations are intercalated into the interlamellar space of the Na-montmorillonite, the aggregation of the particles of the organo-clay will be different from the Na^+-montmorillonite. In general, all the organo-clays give similar platelets as seen in Figures 4.12(a)-4.14(a). In the cases of MMDA-M and LYS-Me-M, the higher magnification in Figures 4.12(b) and 4.13(b) show that these organo-clay platelets have very smooth surface shapes. In the case of TPP-M as shown in Figure 4.14(b), however, the particles appear as glassy shards as compared to the samples in Figures 4.12(b)-4.13(b). It has been shown that the surface properties of the particles of pillared clays are related to the layer aggregation[96]. It is possible to form delaminated layers for the pillared clays which result from the preparation procedures[96,97]. The delaminated structure of pillared clays results in the formation of very sharp edged particles[87]. The porosity studies (chapter 6) have shown that the TPP-M sample has a larger amount of mesopores and macropores. The mesopores and the macropores may be formed partly from the delamination of the layers once the larger cations are intercalated into the interlamellar space of the clay[96,97].

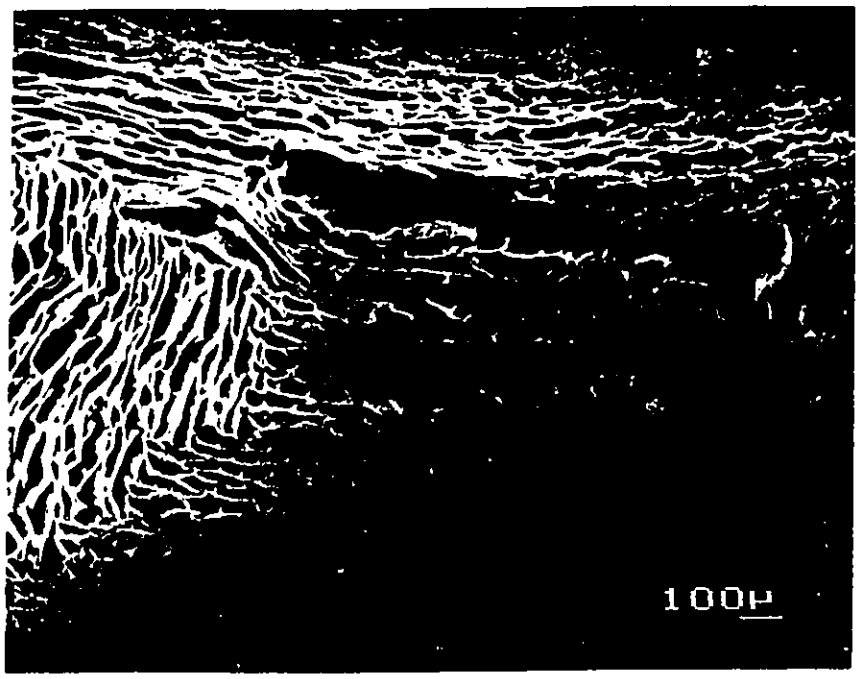

(a)

(b)

Figure 4.11 SEM photographs of <0.2μm Na-montmorillonite

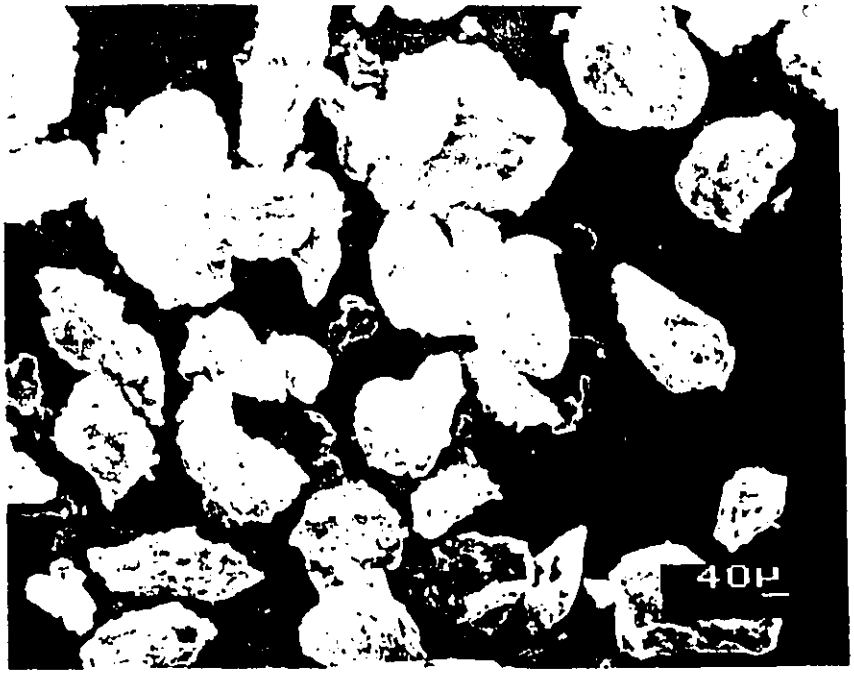

(a)

(b)

Figure 4.12 SEM photographs of MMDA-montmorillonite

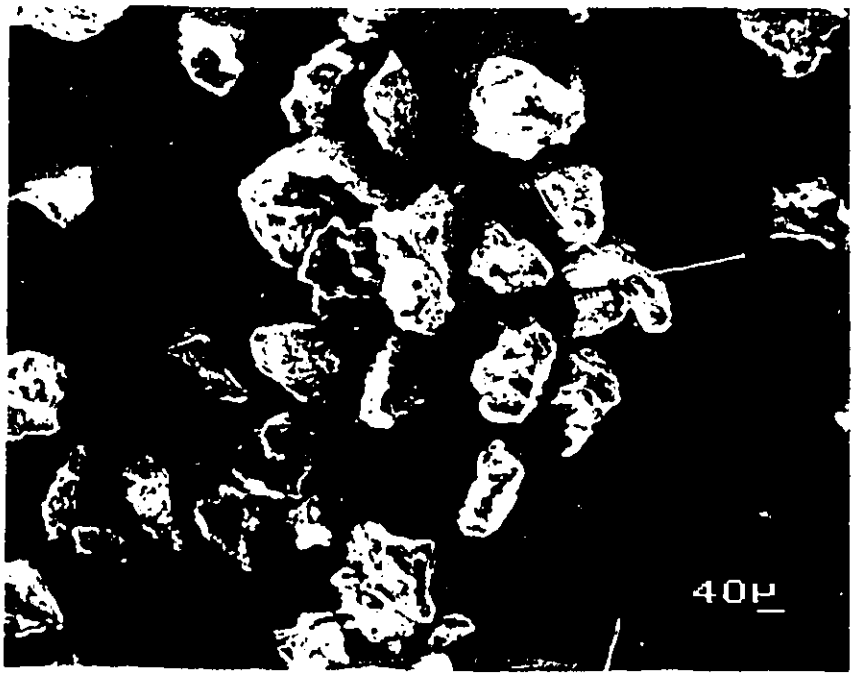

(a)

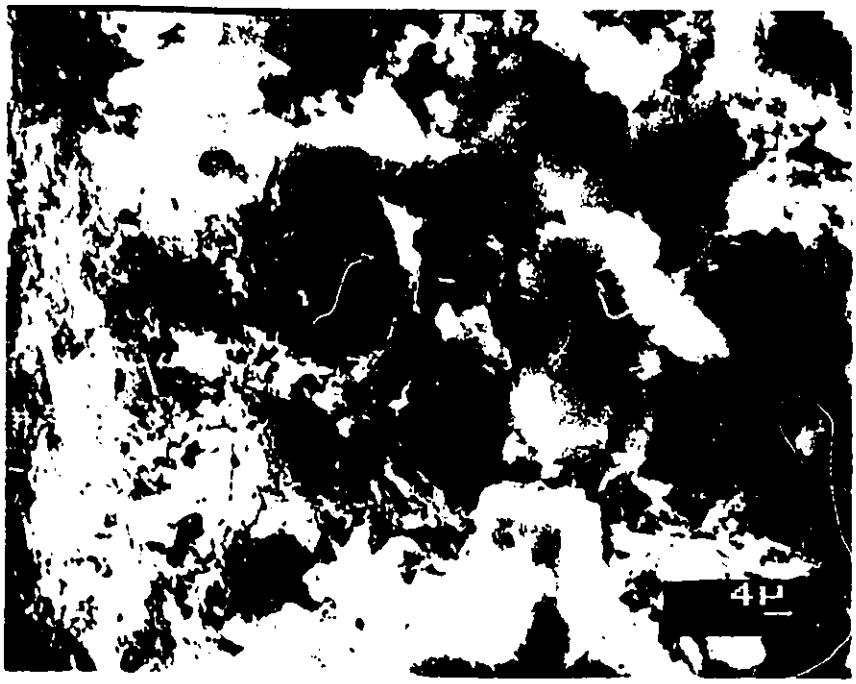

(b)

Figure 4.13 SEM photographs of LYS-Me-montmorillonite

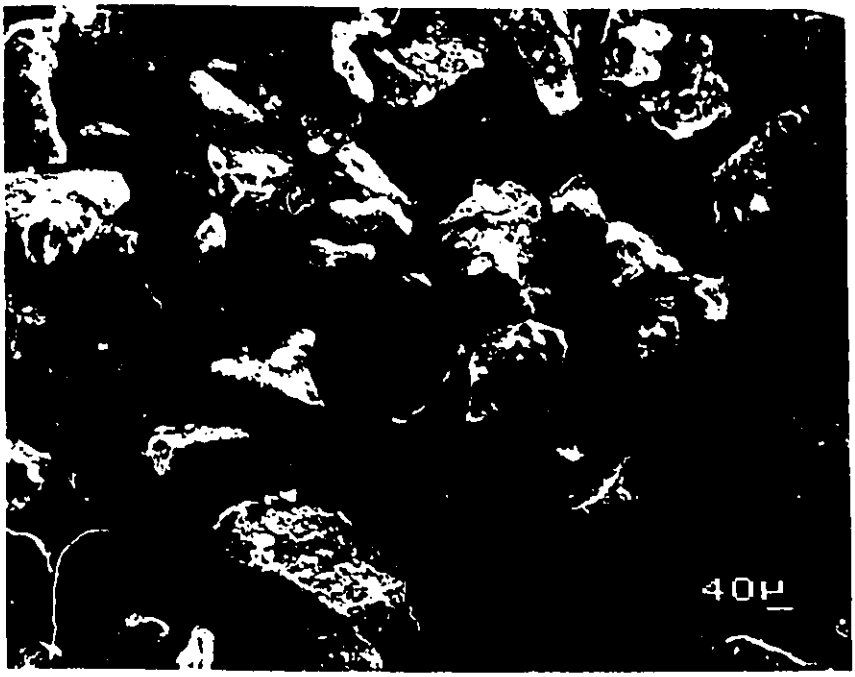

(a)

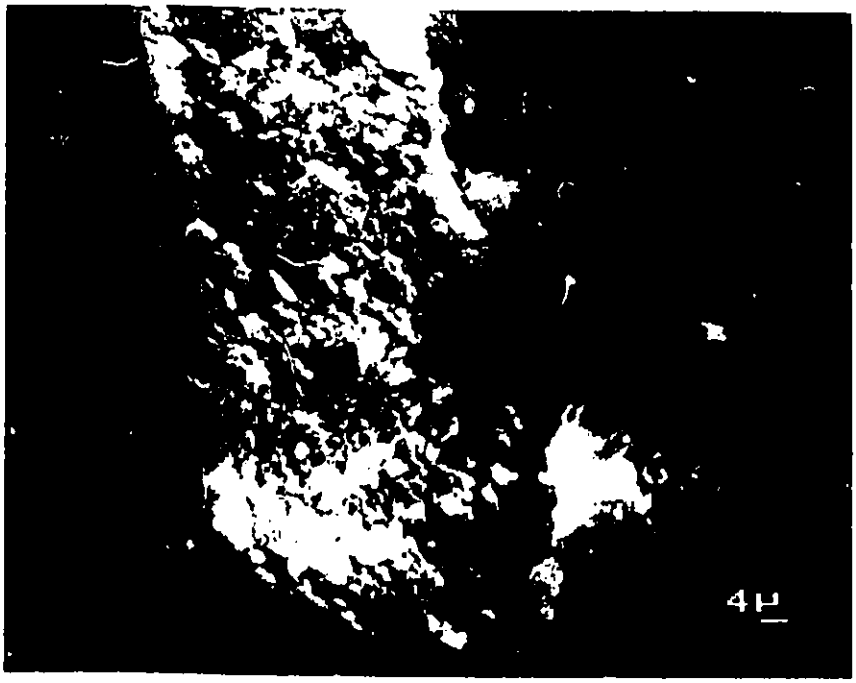

(b)

Figure 4.14 SEM photographs of TPP-montmorillonite

4.4 Conclusions

X-ray powder diffraction was used to study the changes of the basal spacing of the clay minerals upon intercalation of the quaternarized ammonium cations. SEM also gave information about the morphology of the clays and the organo-clays.

Chapter 5

Microporosity of Organo-Clay Minerals

5.1 Introduction

It has been shown that when the natural interlamellar inorganic cations of montmorillonite and hectorite were replaced by small alkylammonium organic cations, permanent microporosity was created, and sorption of gases and of organic molecules was very favored[10]. Figure 5.1 describes the intercalation of organic cations into the interlamellar space of the clay where d_1 is the distance between the layers and d_3 represents the distance between the cations.

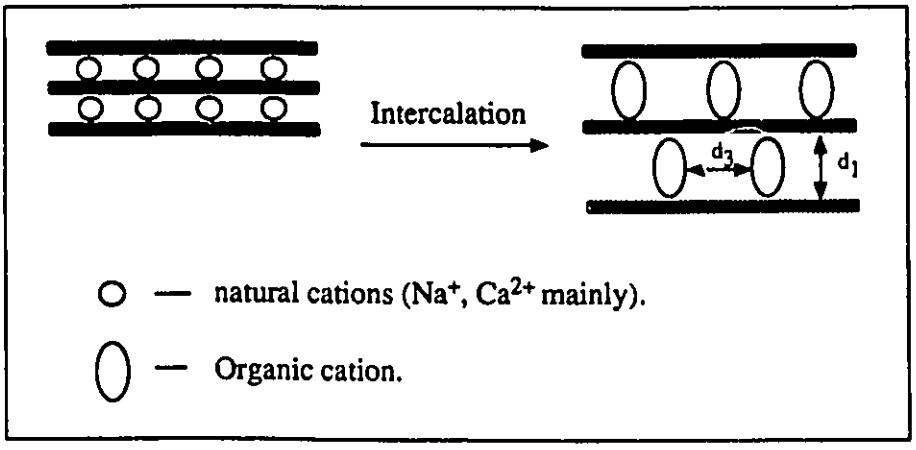

Figure 5.1 Schematic representation of intercalation of organic cation into the interlamellar space of clay

Such expanded clay minerals may function as molecular sieves, intercalating many permanent gases and non-polar hydrocarbons which are not intercalated by the parent Na-montmorillonite. These pillared clays behave like two-dimensional molecular sieves. Pore height d_1 (controlled by the size of the interlayer cation) can be obtained directly from X-ray diffraction measurements. The width d_3 of the pore opening is controlled by the charge densities of both the interlayer cation and the smectite. Since the layer charge distribution in smectite clays is inhomogeneous, hence, nonuniform pillars distribution and pore widths are expected[82]. Moreover, if the interlayer cations (Na^+, Ca^{2+} mainly) are replaced by oligomeric cations of elements such as Al, Zr, Ti, Cr and Fe, the interlamellar space d_1 can increase to 16-20Å [98]. An example of such a cation is the Keggin ion:

$$[Al_{13}O_4(OH)_{24}(H_2O)_{12}]^{7+}$$

In these pillared clays, the free distances, d_3 between the adjacent pillars are, however, not well defined. Probably, in the process used in their synthesis, some pillars may fuse together, giving a range of values of d_3 so that the micropores will be more irregular than those in the organoclay molecular sieves and in zeolites. According to the IUPAC classification, the micropores are defined as pores with diameter less than 20Å and mesopores are those with pore diameter between 20-500Å. Macropores are defined for those pores larger than 500Å in diameter[99]. The micropores are further divided into supermicropores with pore diameter between 6Å and 16Å and ultramicropores with pore diameter less than 6Å.

The porous structures of solids can be characterized by ^{29}Si NMR, XRD and gas adsorption methods[100,101]. Gas adsorption is a classical technique to study the textural properties of porous solids and clay minerals. The most commonly used procedure for

determining surface area of a powder is to derive the amount of adsorbed nitrogen (or other inert gas) at monolayer coverage from a BET plot of adsorption isotherm data. Knowing the projected cross sectional area per molecule in a monolayer, the surface area is calculated from the monolayer coverage. Since inert gases in general do not penetrate between layers of a clay, only the total external surface area is determined for these minerals. The external surface areas of montmorillonite (SWy-1) and hectorite (SHCa-1) have been reported to be 31 m^2/g and 58 m^2/g respectively using nitrogen adsorption method[102]. In order to determine the internal surface area of the clays, methods based on the adsorption of polar molecules such as water, glycol and glycerol have been reported[102]. The polar molecules which are able to penetrate between the layers of clays yield data for the total internal and external surface areas. For example, in the case of the sepiolite, a clay characterized by a chemical structure similar to zeolites, the micropore distribution and the effective size of the channels were measured by such a combination of incorporation and BET methods[103]. Before the BET measurement, the samples were treated under a water vapour atmosphere at various pressures to fill progressively the sepiolite micropores with water. The total surface area was then measured and the outer surface area was estimated by comparison of the surface area of the vacuum-dried sepiolite with that filled with adsorbed water. The effective size of the channels was estimated from the number of various molecules of different sizes sorbed by the sepiolite.

The classical BET technique for the measurement of surface area and pore volume is limited in certain circumstances, especially in the case of microporous solids. To overcome this intrinsic limitation, "continuous" adsorption techniques have been recently developed[104,105,106]. In those techniques, a low pressure sorption instrument is used to simplify the analysis of microporous solids and the adsorbate is admitted to the sample at a slow flow rate. The low relative pressure (10^{-7}-10^{-6} torr) permits previously unattainable insights into micropore structures down to 3Å. Moreover, the high resolution allows for

pore size distribution analysis of porous organo-clays. The continuous N_2 adsorption method has been used for the studies of the pore structure and surface area of organo-clay samples whose preparation was described in chapter 8.

5.2 *Nitrogen adsorption and desorption studies on microporous organo-clay minerals*

5.2.1 *Principles of nitrogen adsorption and desorption on porous solids*

When a solid is exposed in a closed space to a gas or vapour at some definite pressure, the solid adsorbs the gas. The quantity of gas taken up by a sample of solid is proportional to the mass m of the sample, and depends also on the temperature T, the pressure p of the vapour and the nature of both the solid and the gas[107]. The quantity (n) of gas adsorbed by the solid can be expressed in moles per gram of solid:

$$n = f(p, T, gas, solid) \qquad (5\text{-}1)$$

For a given gas and temperature, the equation 5-1 can be rewritten as:

$$n = f(p/p_0)_{T,\, gas,\, solid} \qquad (5\text{-}2)$$

p/p_0: relative pressure of gas

where p is the vapour pressure and p_0 is the saturated vapour pressure. Plotting n against the relative pressure p/p_0 results in an isotherm. Five types of isotherms (Types I-V) are usually obtained, as shown in Figure 5.2[107]. Types I and IV isotherms are typical isotherms for solids containing microporosity and mesoporosity respectively. Types III and V isotherms,

in which Type III is given by a non-porous or macroporous solid and Type V is given by a mesoporous or microporous solid, are characteristic of weak gas-solid interactions. The stepped isotherm Type VI is rare in practice. Type II is characteristic of non-porous solids.

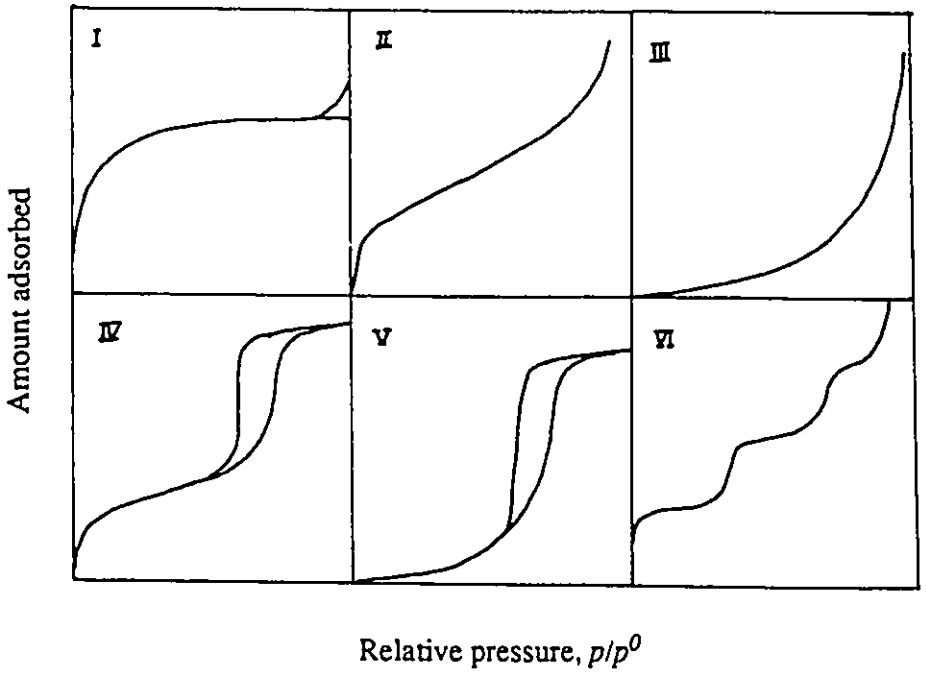

Figure 5.2 Five Types of adsorption isotherms, together with a stepped isotherm Type VI

Microporous solids are characterized by Type I isotherms as shown in Figure 5.3[107]. At lower pressure, there is an enhancement in gas-surface interaction energy and therefore the pore is filled for very low relative pressures (0.01 or less) so that the isotherm rises steeply from the origin. The enhancement of adsorption energy and the steepness of the isotherm are dependent on the nature of the adsorbent-adsorbate interaction and the polarizability of the adsorbate. At higher region of relative pressure (0.1-0.2), the interaction energy increases only slightly and the increased adsorption which is observed is the result of a cooperative effect. This will give rise to a rounded knee to the isotherm. As

the relative pressure is approaching unity, the isotherm shows a plateau which is nearly horizontal. This limit exists because the pores are so narrow that they cannot accommodate more than a single molecular layer on their walls. Thus a purely microporous solid will give rise to a Type I isotherm, having a very steep initial branch succeeded by a more gradual approach to the plateau. Xerogels of silica, titania, alumina and stannic oxide give Type I adsorption isotherms[107]. Particularly well defined Type I isotherm is typical of zeolites. If the isotherm is of Type I with a sharp knee and a plateau which is horizontal, the uptake n_s at a point close to saturation p/p_0, is then a measure of the micropore volume. When it is converted to a liquid volume, it may be taken as actually equal to the micropore volume as shown in Figure 5.3. For example, in the adsorption isotherm of TMA-M, a nearly Type I isotherm can be seen in the region of 0.006-0.1 p/p_0 (Figure 5.6, page 76). The micropore volume can be estimated by multiplying the volume adsorbed by the sample by the ratio of gas and liquid density of N_2, 0.00156.

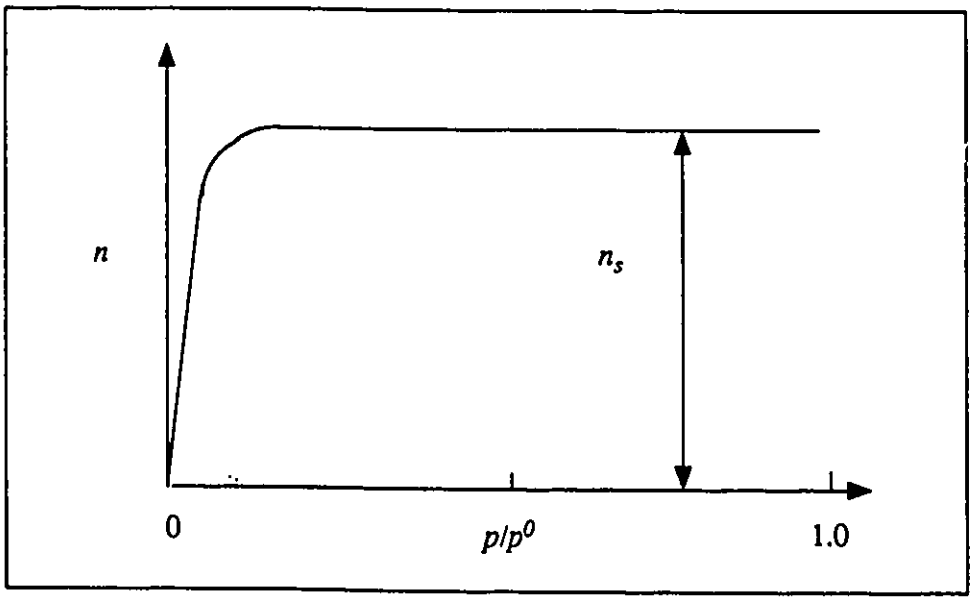

Figure 5.3 A Type I isotherm

Generally, the microporosity is associated with an appreciable external surface (mesoporosity or macroporosity). The mesoporous solids are characterized by Type IV adsorption isotherms. In micropores, the adsorption of gas occurs by micropore filling while the adsorption of gas in mesopores is thought to be processed by layer-by-layer coverage and capillary condensation. A characteristic feature of a Type IV isotherm is its hysteresis loop where the isotherms for adsorption branch and desorption branch do not coincide[107]. The exact shape of the loop varies from one adsorption system to another. It is also possible to relate the hysteresis loop to the morphology of the adsorbent. According to the IUPAC classification, a Type IV hysteresis loop can be divided into four types designated H1, H2, H3 and H4 as shown in Figure 5.4[107]. H1 and H4 represent extreme types, and, H2 and H3 may be regarded as intermediates between the two extremes. An hysteresis loop is normally associated with capillary condensation. The formation of a liquid phase from the vapour at any pressure below saturation cannot occur in the absence of a solid surface which serves to nucleate the process. Within a pore, however, the adsorbed film acts as a nucleus upon which condensation can take place at a pressure below the saturation pressure governed by the Kelvin equation (equation 5-3). In the initial part of the isotherm, adsorption is restricted to a thin layer on the walls until at a certain point capillary condensation commences in the finest pores. As the pressure is progressively increased, wider and wider pores are filled until the entire system is full of condensate at the saturation pressure. In the converse process of evaporation, the problem of nucleation does not arise. The liquid phase is already present and evaporation can occur spontaneously from the meniscus as soon as the pressure is low enough. It is because the processes of condensation and evaporation do not necessarily take place as exact reverses of each other that hysteresis can arise[107].

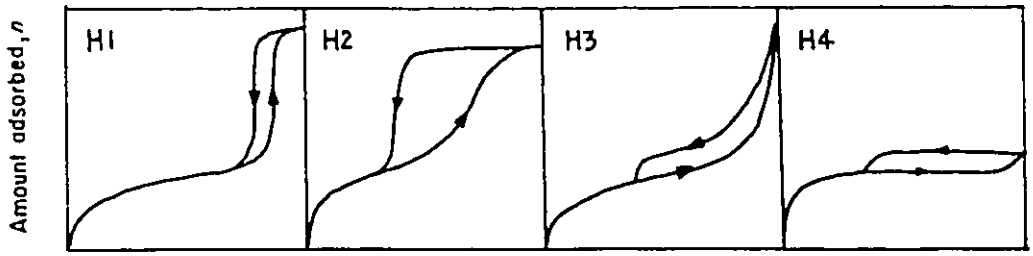

Figure 5.4 Four types of hysteresis loops

The shape of the hysteresis loops in Type IV isotherms depends on the structures of pores present in the solids. As mentioned above, a vapour is able to condense in the pores of a solid even when its relative pressure is less than unity. The vapour pressure for which a capillary condensation occurs is governed by the Kelvin equation[107]:

$$RT\ln p/p_0 = -2\gamma V_L/r_m \qquad (5\text{-}3)$$

where p/p_0 is the relative pressure of vapour in equilibrium with a meniscus having a radius of curvature r_m, R is the gas constant, T is the normal boiling point of nitrogen (77.3K) and γ *and* V_L are the surface tension (8.855 mN/m) and molar volume of the liquid nitrogen (34.6 cm^3 mol), respectively. In cylindrical pores with one closed end, capillary condensation commences at that end to form a hemispherical meniscus and evaporation can commence at this hemispherical meniscus at the same relative pressure. As a result, there is no hysteresis observed in this case. However, if the cylinder is open at both ends, the capillary condensation has to take place on the film of the walls. On the other hand, evaporation from the full pore can take place from the hemispherical meniscus at each end. Condensation and evaporation occur at different relative pressure and therefore a hysteresis

loop results. In the case of slit-shaped pores where the sides of the slit are truly planar and parallel, the capillary condensation cannot occur at any pressure below saturation since the mean radius of curvature of a plane is infinite (equation 5.3). The adsorbed films on opposite walls will increase in thickness and the pore becomes full of adsorbate when the films meet each other as shown in Figure 5.5. If the width of the pore exceeds a few molecular diameters, the state of the adsorbate is the same as its liquid. Thus, evaporation can commence at the cylindrical menisci at a certain relative pressure which is governed by the Kelvin equation. This process continues at that same pressure until the core is completely empty. Thus the mechanisms of filling and emptying are completely different. Multilayer formation on one hand and capillary evaporation on the other. In actual solids, not only will there be a distribution of slit widths, but the sides will rarely be exactly parallel or truly plannar and some plates will touch each other so as to produce wedge-shaped pores. Also, the adsorbent is frequently nonrigid, so that the slit-width increases during adsorption and decreases during desorption. Therefore, a hysteresis loop results in these slit-shaped pores. The hysteresis loops encountered in practice have the general form of Type H3 as to be seen in all the isotherms of organo-smectites which contain layered structure. Furthermore, numerous porous solids are made up of spherical particles, each in contact with two or more of its neighbours. Capillary condensation can be nucleated by the adsorbed film in the cavities between the particles at the pressure below the saturation pressure of the vapour. As the pressure increases, the liquid film extends inwards until the adjacent tori touch each other. At this point, a spherical cavity is formed and will then suddenly be filled up. Therefore the adsorption curve in this type will be given as a nearly vertical in shape at a certain relative pressure depending on the the radius of the cavity. Evaporation can commence at a hemispherical meniscus in the window of the cavities. Since the radius of the window is always larger than that of the cavity, the evaporation from the window will give a jump at a lower relative pressure. As a result, a

hysteresis is present and has a form of H1 (Figure 5.4). The type H2 loops are often found in some corpuscular systems such as silica gels where the distribution of pore size and shape is not well defined and type H4 is typical for Type I isotherm, indicative of microporosity[107].

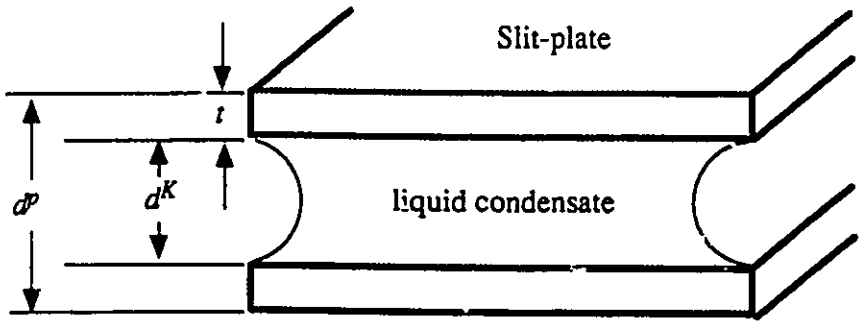

Figure 5.5 Slit-shaped pore of width d^P, showing adsorbed film with thickness t and core of width d^K.

5.2.2 *Adsorption isotherms and desorption isotherms of microporous organo-smectite*

In a continuous adsorption method which is based on volumetric analysis, the total volume of gas delivered or withdrawn from the sample is calculated by multiplying the flow rate by the total experimental time. The raw data obtained with these analysis are pressure-time data. The volume adsorbed by the sample is calculated by subtracting the "dead space" volume, that is, the volume of the mainfold, holder and sample from the total adsorbed volume. The calibration experiment consists simply of running an adsorption and desorption experiment with an empty holder with He, then the parameters obtained are corrected for the dead volume. Knowing the saturation pressure (p_0) and the volume adsorbed by the sample (V) at different pressures (p), an adsorption isotherm is obtained by plotting V as a function of the partial pressure of nitrogen, or relative pressure p/p_0. To

determine the volume of gas desorbed from the sample, the volume of gas not desorbed is subtracted from the total volume removed from the system. The volume not desorbed from the sample is calculated from the helium calibration. The desorption isotherm is then constructed by plotting the volume desorbed per gram of sample against the relative pressure, p_i/p_0. Before the N_2 adsorption and desorption measurements, the samples were outgassed at 150°C and 10^{-4}-10^{-5}torr in order to remove eventual traces of water. Table 5.1 shows that there was no significant change in weight before and after the heating treatment indicating that there were not any moisture in the samples treated by the normal drying procedure of the organo-clay (see chapter 8).

Table 5.1 Experimental data for organo-clay samples before and after heating treatment

Sample	Weight before heating	Weight after heating
TMA-M	0.0931	0.0930
LYS-Me-M	0.1276	0.1272
MMDA-M	0.0861	0.0840
TPP-M	0.1065	0.1060
GLY-Et-M	0.0992	0.0991
MMDA-H	0.0950	0.0943

The adsorption and desorption isotherms of organo-clays (TMA-M, MMDA-M, MMDA-H, LYS-Me-M, GLY-Et-M and TPP-M) are shown in Figures 5.6-5.8. Those adsorption isotherms are combination of Type I and Type IV adsorption isotherms indicating that there are micropores and mesopores in these organo-clays. Figure 5.9 shows the adsorption isotherms for all the organo-montmorillonite. From this figure, one can note that TMA-M and MMDA-M give relatively stronger micropore adsorption compared to that of GLY-Et-M, LYS-Me-M and TPP-M. In the latter cases, LYS-Me-M shows a stronger adsorption than GLY-Et-M and TPP-M. The shape of the adsorption and desorption isotherms can be qualitatively related to the pore structure and surface area contribution of the organo-clays. The shape of adsorption/desorption isotherms for the samples of TMA-M, MMDA-M and LYS-Me-M are very similar except that LYS-Me-M has lower adsorption in the lower p/p_0 region. This demonstrates that the pore structures in these three samples are very similar. In contrast, the isotherms for the samples of TPP-M, GLY-Et-M and MMDA-H are different. Especially in the case of TPP-M and GLY-Et-M, there is a very strong adsorption in the region of 0.9-1.0 p/p_0. As discussed above, the strong adsorption in the higher relative pressure indicates that there are relatively larger mesopore volumes in these two samples as compared to the others. The difference in the adsorption amounts at higher relative pressure region between the isotherms of MMDA-M and MMDA-H is attributed to the difference in the external/internal surface ratio. MMDA-H has a higher external surface area than MMDA-M.

Type H3 hysteresis loops are seen in all the isotherms of the organo-smectites of this study. The characteristic of type H3 hysteresis loop in these organo-clay samples indicates that the mesopores in the samples are slit-shaped pores. However, as seen in Figure 5.6-5.8, the hysteresis loops in the samples of MMDA-M, TMA-M and LYS-Me-M are different from the samples of GLY-Et-M, MMDA-H and TPP-M. In the latter cases, the desorption isotherms show larger hysteresis loops than the former cases. This is because

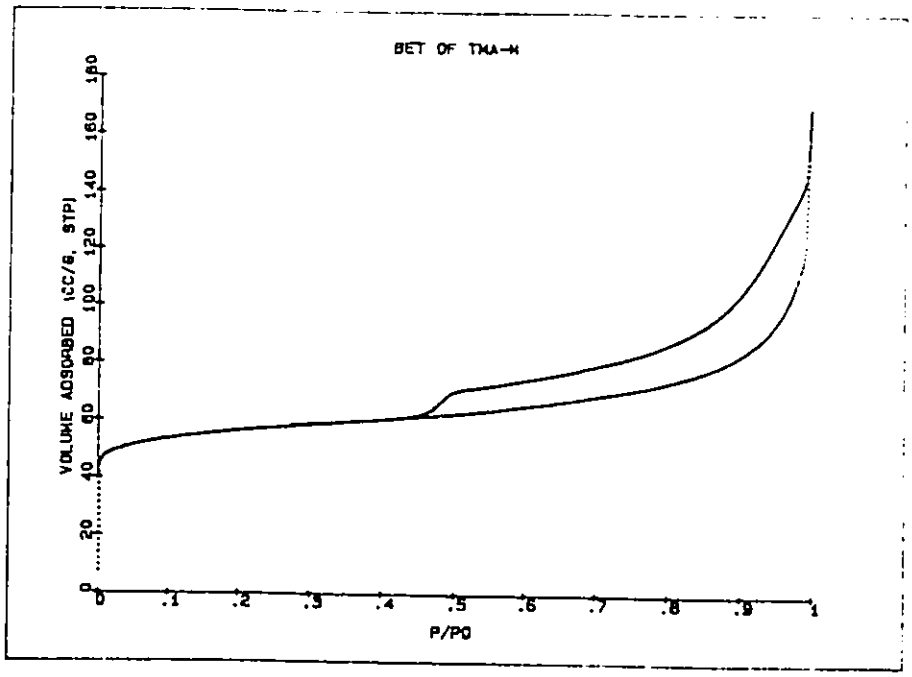

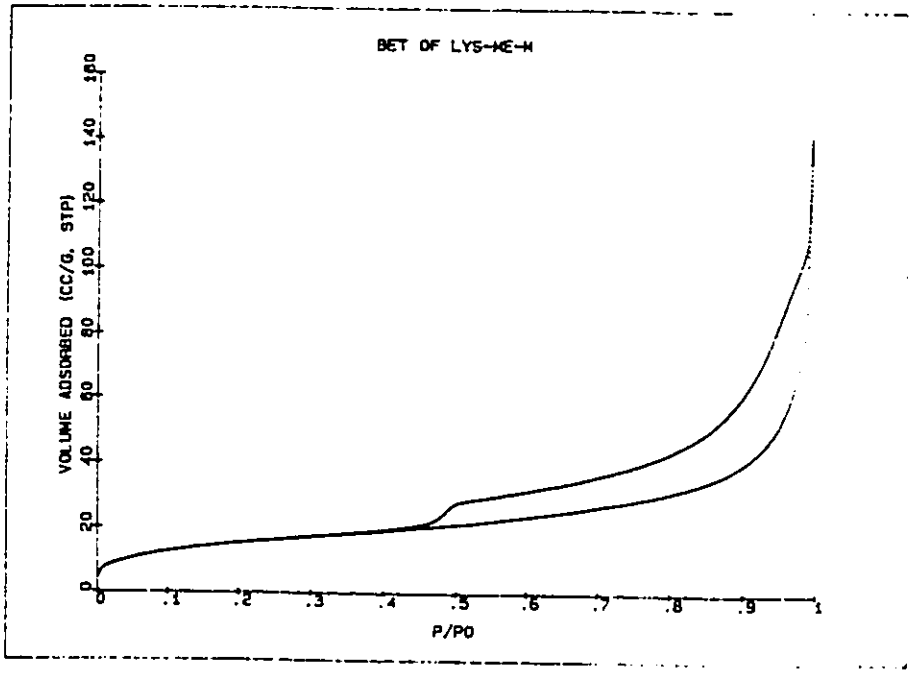

Figure 5.6 N_2 adsorption and desorption isotherms of TMA-montmorillonite and LYS-Me-montmorillonite

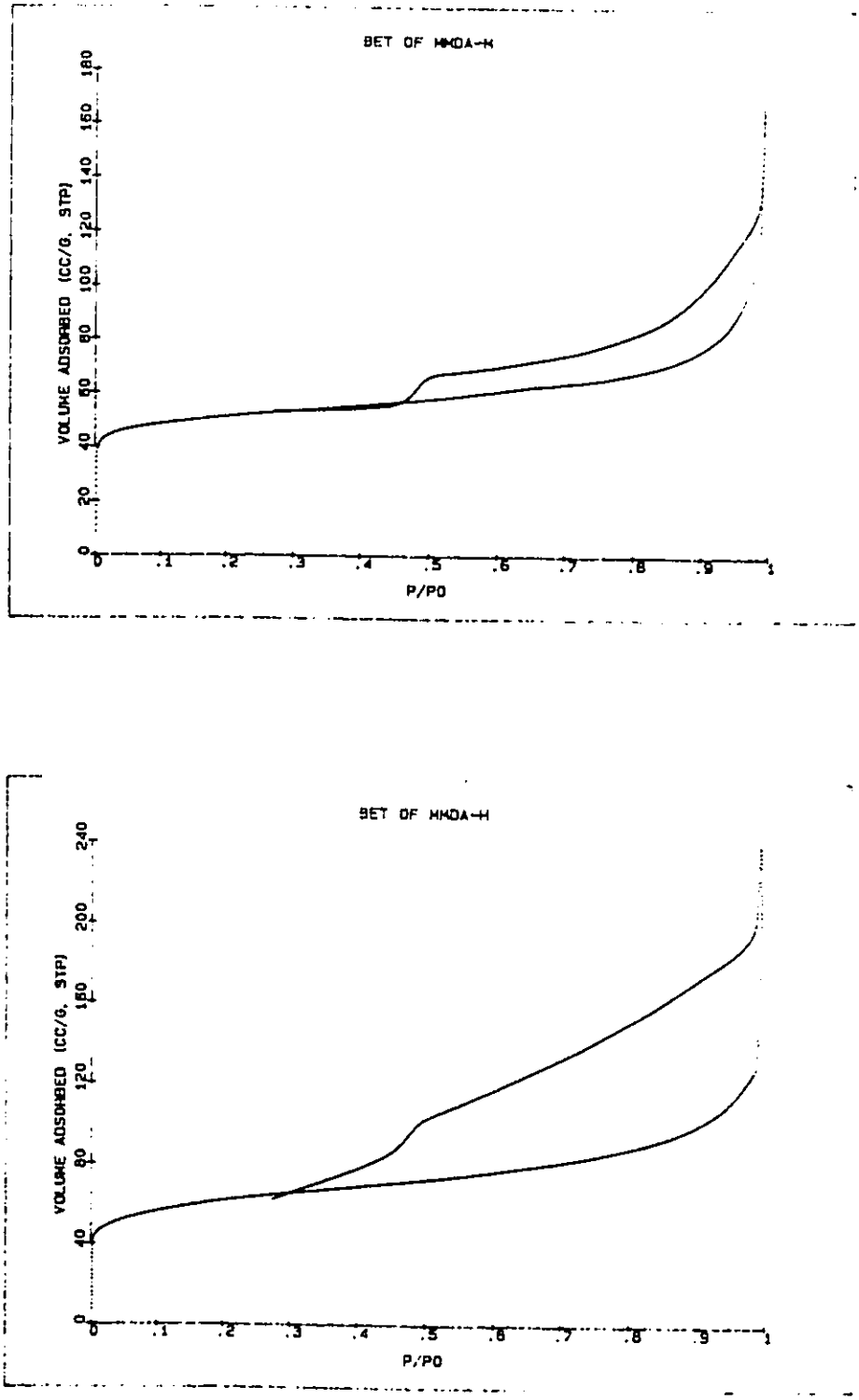

Figure 5.7 N_2 adsorption and desorption isotherms of MMDA-montmorillonite and MMDA-hectorite

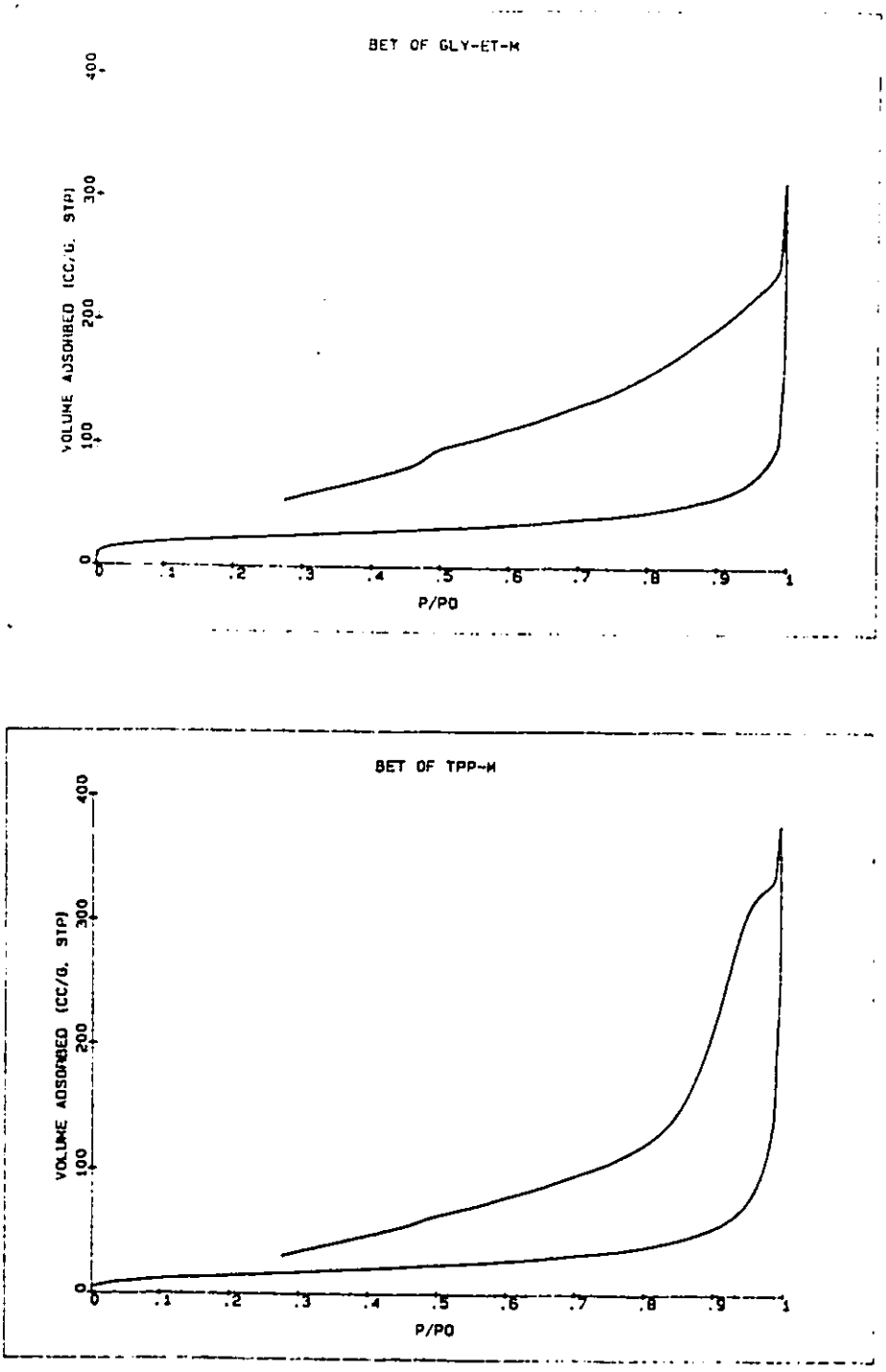

Figure 5.8 N_2 adsorption and desorption isotherms of GLY-Et-montmorillonite and TPP-Me-montmorillonite

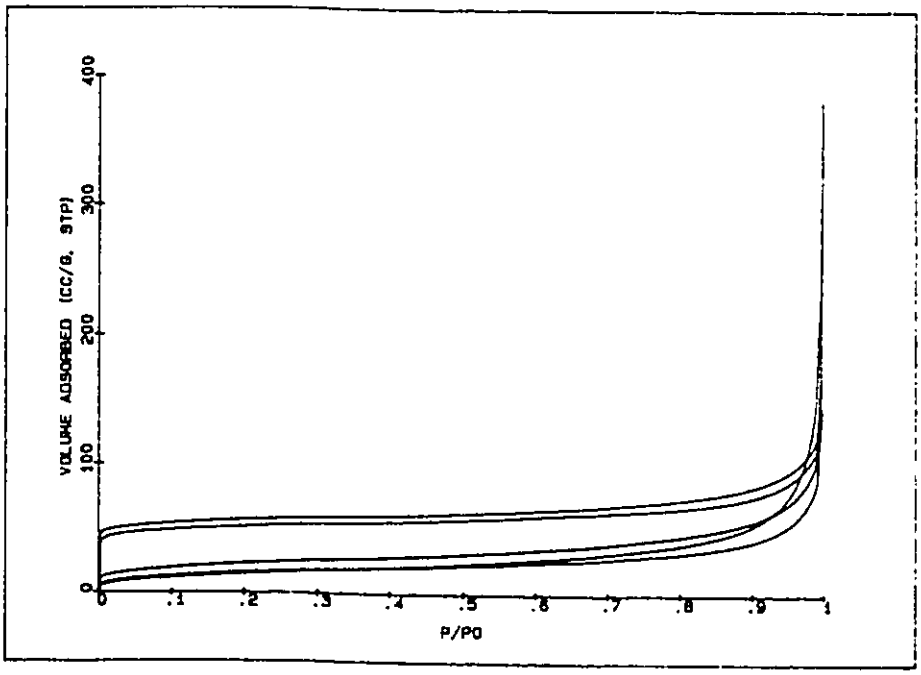

Figure 5.9 N_2 adsorption isotherms of organo-montmorillonite

there exist larger amount of mesopores in the latter samples as will be shown in the mesoporosity analysis (section 5.3.2). In the case of TPP-M, there is an enhanced desorption in the relative pressure region of 0.85-0.95, probably due to the larger mesopores in this sample. Moreover, for these samples, the desorption data could not be obtained at relative pressures of 0-0.3 p/p_0. In this region, the amount of sorbate leaving the solid becomes so low that the outlet valve is unable to maintain the set flow.

5.2.3 BET equation and BET surface areas of organo-clays

The BET model is derived from the non-porous solids which give rise to Type II isotherms[107]. From the Type II isotherm of a given gas on a particular solid it is possible to derive a value of the monolayer capacity of the solid which then can be used to calculate its specific surface[108]. The monolayer capacity is defined as the amount of adsorbate which can be accommodated in a completely filled, single molecular layer. The surface area per gram of the solid is given as:

$$S_A = V_m \cdot a_m \cdot N \qquad (5\text{-}4)$$

where S_A is the specific surface area, a_m is the average area occupied by a molecule of adsorbate in the monolayer , N is the Avogadro's constant and V_m is the monolayer capacity in moles of adsorbate per gram of adsorbent. The BET treatment is based on a kinetic model of the adsorption process in which the surface of the solid is regarded as an array of adsorption sites. The rate at which molecules arrive from the gas phase and condense on the bare sites is equal to the rate at which molecules evaporate from occupied sites. The total surface area of the sample can be calculated from the adsorption isotherm and the linearized BET equation, which is given below (equation 5-5):

$$p/[V(p_0-p)]=1/V_mc + [(c-1)/V_mc](p/p_0) \quad (5\text{-}5)$$

where V is the amount of adsorbate adsorbed in moles per gram of adsorbent and c is the BET constant which is related to the enthalpy of adsorption. Plotting the left side of the equation versus p/p_0 (the relative pressure of adsorbate) results in a straight line. V_m and c can then be obtained from the slope and the y-intercept of the linear regression.

$$S(\text{slope}) = (c-1)/V_mc \quad (5\text{-}6)$$

$$I(\text{intercept}) = 1/V_mc \quad (5\text{-}7)$$

The parameters c and V_m are obtained as $c = S/I + 1$ and $V_m = 1/(S + I)$. Therefore the BET surface area S_A can be calculated using equation (5-4). For nitrogen, a value of 16.2 $Å^2$ for a_m will be used and after applying the appropriate conversion factors, S_A (m^2/g) can be expressed as:

$$S_A = 4.35 \, . \, V_m \quad (5\text{-}8)$$

The total surface area in the solids containing micropores and mesopores can be readily estimated from the BET equation. The BET equations of various organo-clays which are calculated from the adsorption data of Figures 5.6-5.8 are given in Figures 5.10-5.12. In all the cases, the BET equations give curvature. The changes in slope can be attributed to the variation in the isosteric heat of sorption due to variable microporosity resulting from inhomogenities in pillars distribution and in clay platelets stacking[82]. The BET equations give straight lines only for p_i/p_0 values between 0.006 and 0.1. The BET surface area were calculated from this straight line region and are given in Table 5.2. The external surface area, calculated from the t-plots (section-5.3.3) are also given in Table 5.2.

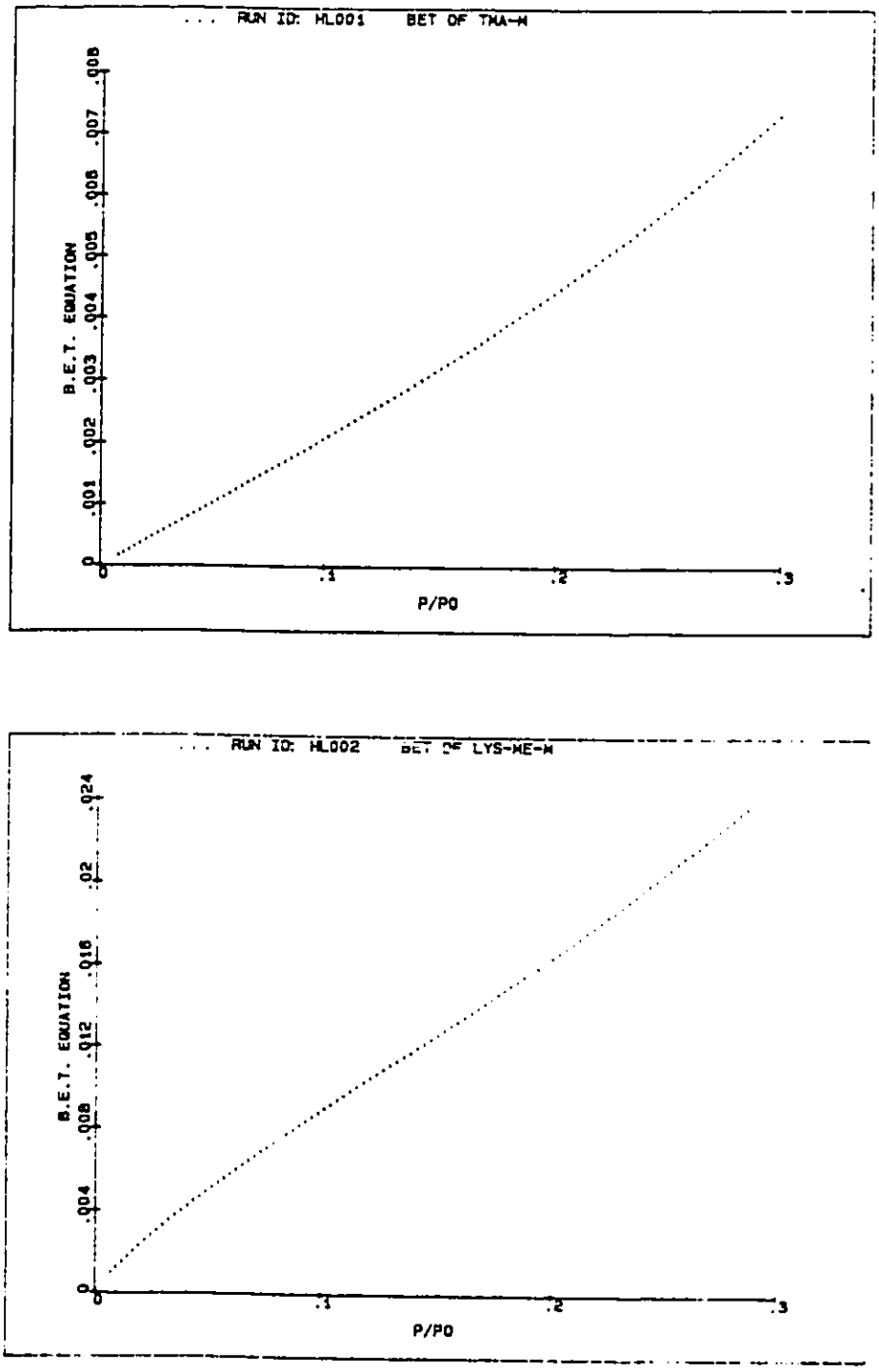

Figrue 5.10 BET equations of TMA-montmorillonite and LYS-Me-montmorillonite

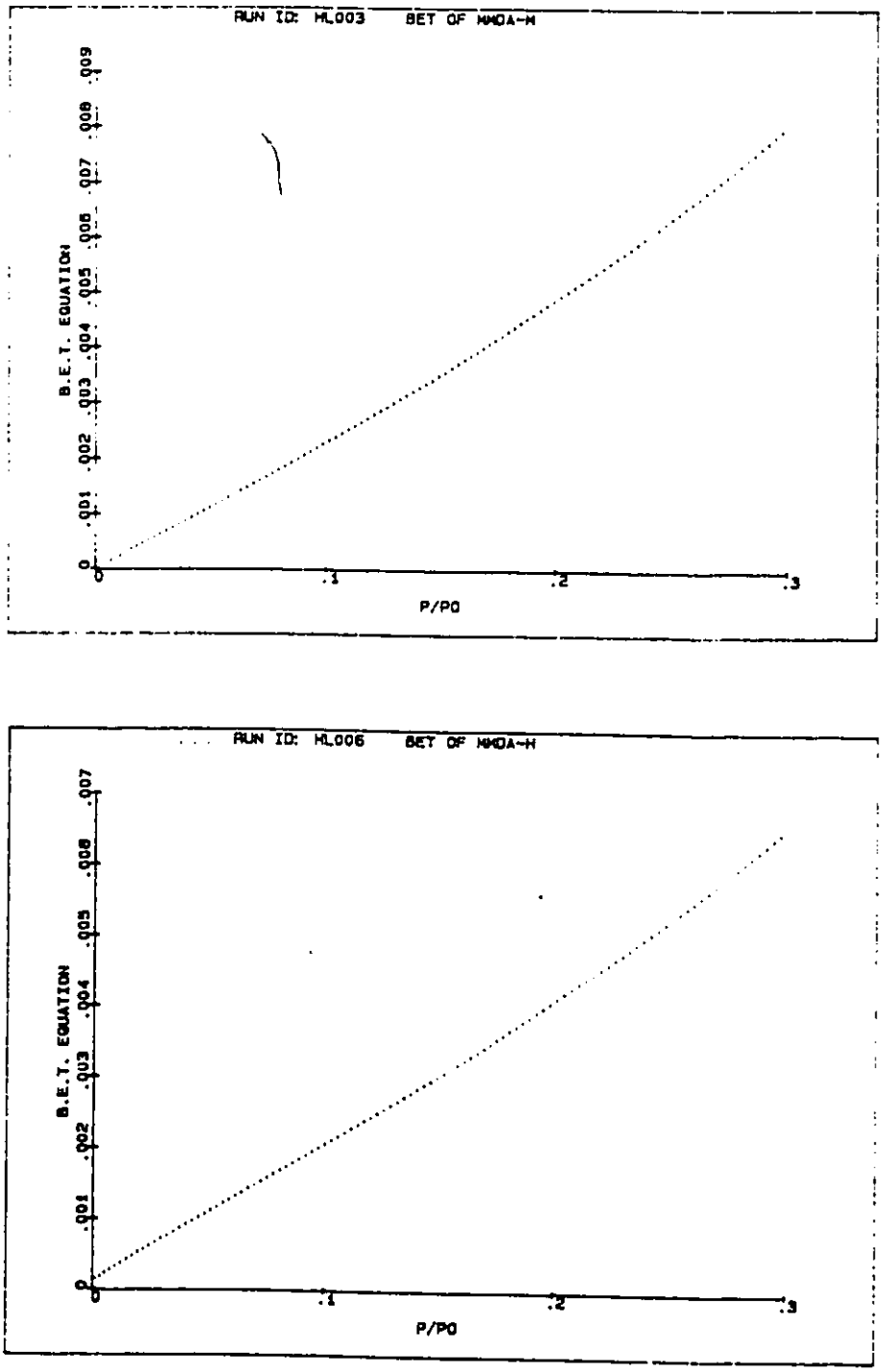

Figure 5.11 BET equations of MMDA-montmorillonite and MMDA-hectorite

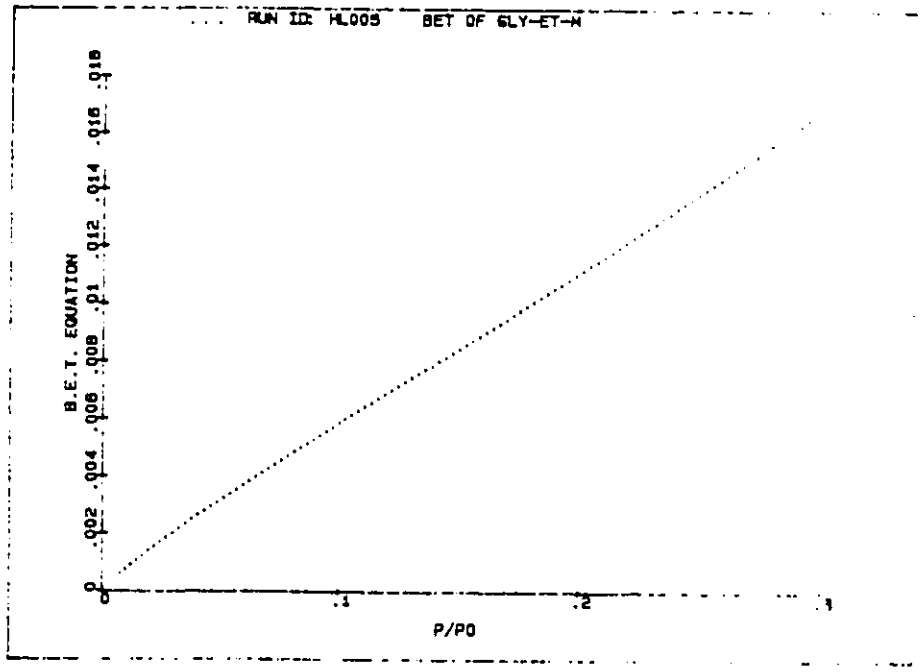

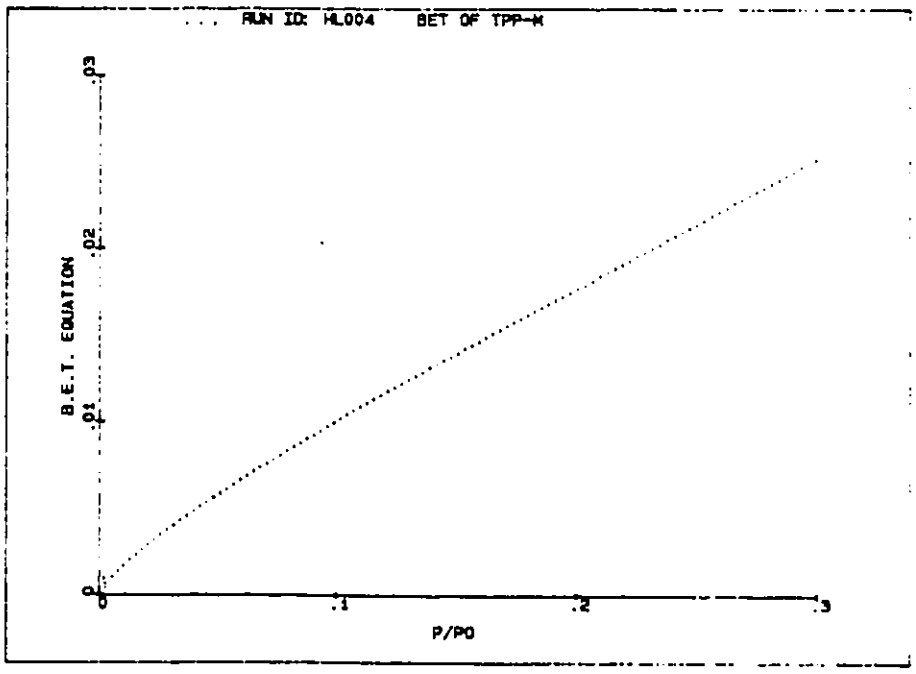

Figure 5.12 BET equations of GLY-Et-montmorillonite and TPP-montmorillonite

Since the height of the micropores in the organo-clays is in the range 4-5Å, only a single nitrogen layer can be adsorbed in the interlamellar spaces. Due to the bilayer characteristic of the clay structure, the difference between the BET surface area and the external surface area represents only the mono-interlayer surface area (surfaces for one layer in the micropore cavities). Therefore, the total interlamellar surface area would be twice as much as the mono-interlayer surface area. The total and mono-interlayer surface areas as well as the monolayer/BET surface ratio (microporosity) in percentage are also included in Table 5.2. TMA-M, MMDA-M and MMDA-H give 66-78% microporosity compared with 7-27% for LYS-Me-M and GLY-Et-M. The larger amounts of microporosity in the samples of TMA-M, MMDA-M and MMDA-H are attributed to the smaller size of these cations (higher cation charge density). These BET results demonstrate that the free interlayer surface area of the organo-smectites can be controlled by changing the size of the intercalated cations. The BET surface can be further increased to (300-496 m^2/g) if pillars such as $Zr_6(OH)_{18}^{3+}$ and $Al_{13}(OH)_{24}^{7+}$ are intercalated into the interlamellar space of the clay[82].

5.2.4 T-plot analysis and micropore volumes

The t-plot analysis method was developed by Lippens and deBoer as a way to differentiate between the adsorption mechanism in micropores and that occuring in mesopores and macropores[107]. The t-plot method may be used to arrive at a value of the micropore volume. A t-plot is obtained by plotting the adsorption isotherm in terms of the volume of gas adsorbed versus the statistical film thickness (t). The thickness (t) is defined as the thickness of the adsorbate gas molecule on the walls of the pores. It is equal to the product of the number of statistical molecular layers in the film (V/V_m) and the thickness of a single molecular layer (δ):

$$t = (V/V_m)\,\delta \qquad (5\text{-}9)$$

Table 5.2 BET surface area, external surface area and interlayer surface area of organo-clays

Organo-clay	BET surface area (m^2/g)	External surface area (m^2/g)	Mono-interl. surf. (m^2/g)	Total interl. surf. (m^2/g)	Microporosity (%)
TMA-M	210.3	45.4	164.9	329.8	78
MMDA-M	194.1	44.0	150.2	300.4	77
MMDA-H	219.2	76.5	143.7	287.4	66
LSY-Me-M	56.6	41.4	15.2	30.4	27
GLY-Et-M	77.3	72.0	5.3	10.6	7
TPP-M	55.9	58.7	0.0	0.0	0.0

$$V = (V_m/\delta)\, t = b_t\, t \qquad (5\text{-}10)$$

where V is the molar amount of adsorbate adsorbed by the adsorbent, V_m is the monolayer capacity known from BET and b_t is the slope of the t-curve. If N_2 is used as adsorbate, δ is then 3.54Å on the assumption that the arrangement of molecules in the film is hexagonal close packing. A t-plot is obtained by plotting the amount adsorbed against the statistical thickness t. In mesoporous and macroporous solids, the adsorption of gases take place in a layer-by-layer fashion. However, the mechanism of adsorption in micropores, on the other hand, does not follow this process and it is believed that adsorption in micropores occurs by pore filling or capillary condensation which is analogous to filling a glass with water. If the surface of the solid has standard properties, the t-plot corresponding to the isotherm of the nonporous powder will be a straight line passing through the origin and having a slope proportional to the specific surface of the powder. For the microporous powder, the t-plot will show an upward derivation curve and two linear regions are obtained which are separated by a transition region as seen in Figure 5.13-5.15[110]. The first region represents both micropore filling and surface coverage of large pores. The second linear region give the layer-by-layer adsorption taking place in meso and macropores but not in micropores. From these two regions, the micropore volume and the meso(macro)-pore surface area (external surface) can be calculated. Therefore, the volume occupied by the micropores is then obtained by extrapolating the second linear region to the y-axis. The y-axis intercept multiplied by the ratio of the gas and liquid densities of the adsorbate (0.00156 for N_2) will provide the micropore volume in cm^3 per gram of solid. The micropore volume and the mesopore volume will be discussed later. Since the surface area of porous solids have been defined (equation 5-4), the surface areas of mesopores and macropores are given as:

$$A_m = a_m \delta\, N\, b_t \qquad (5\text{-}11)$$

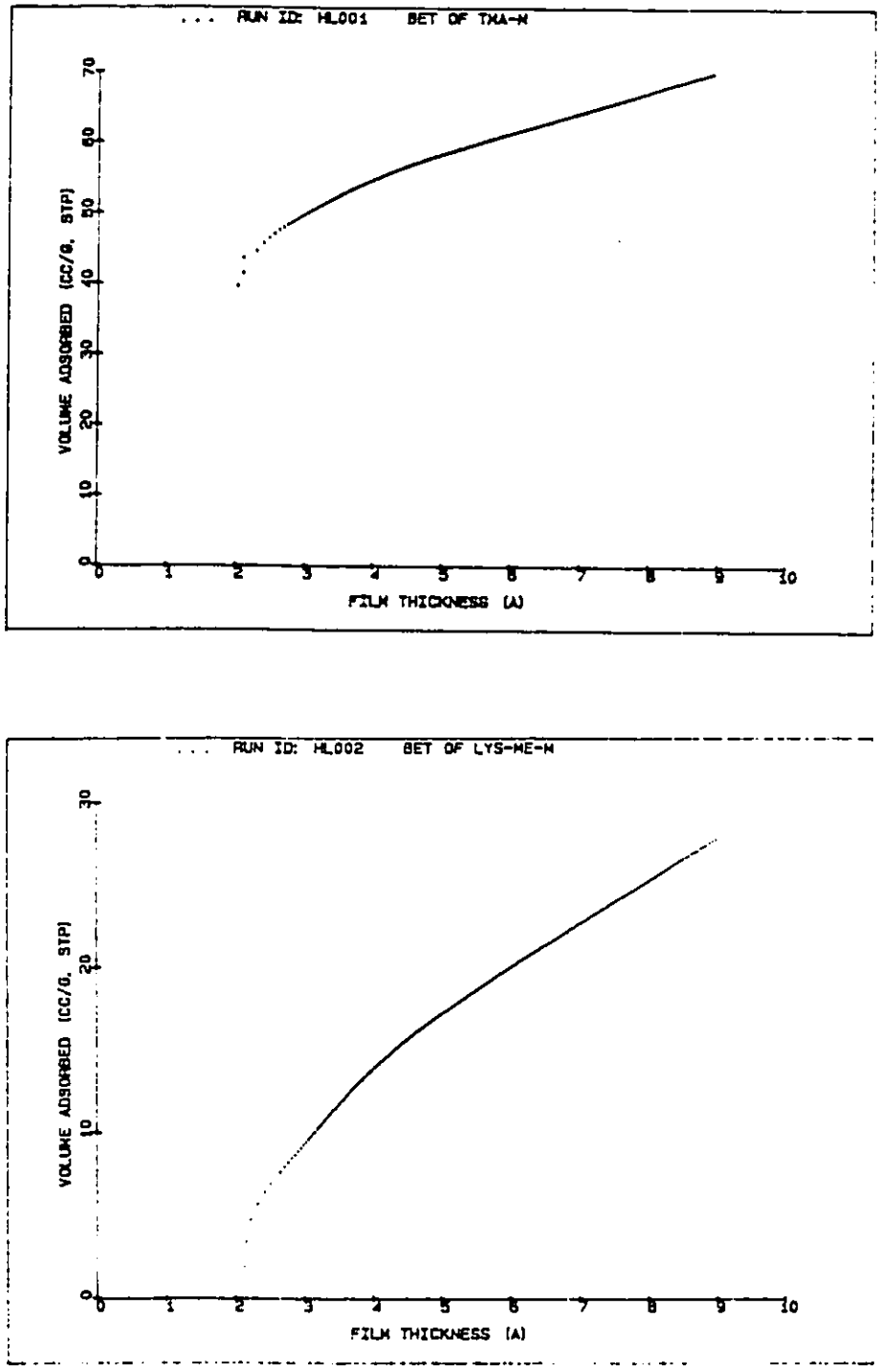

Figure 5.13 t-Plots of TMA-montmorillonite and LYS-Me-montmorillonite

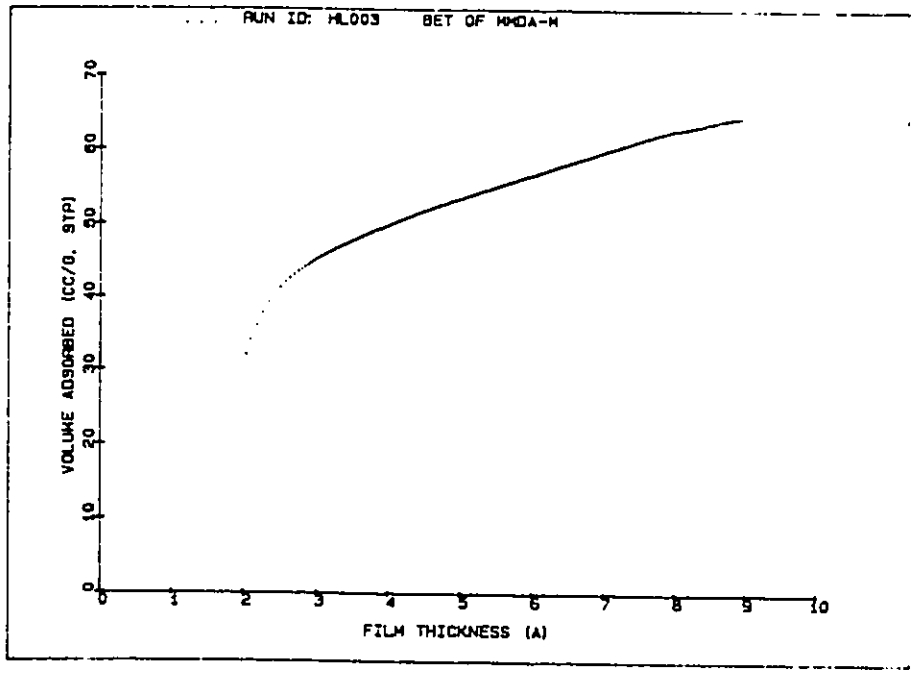

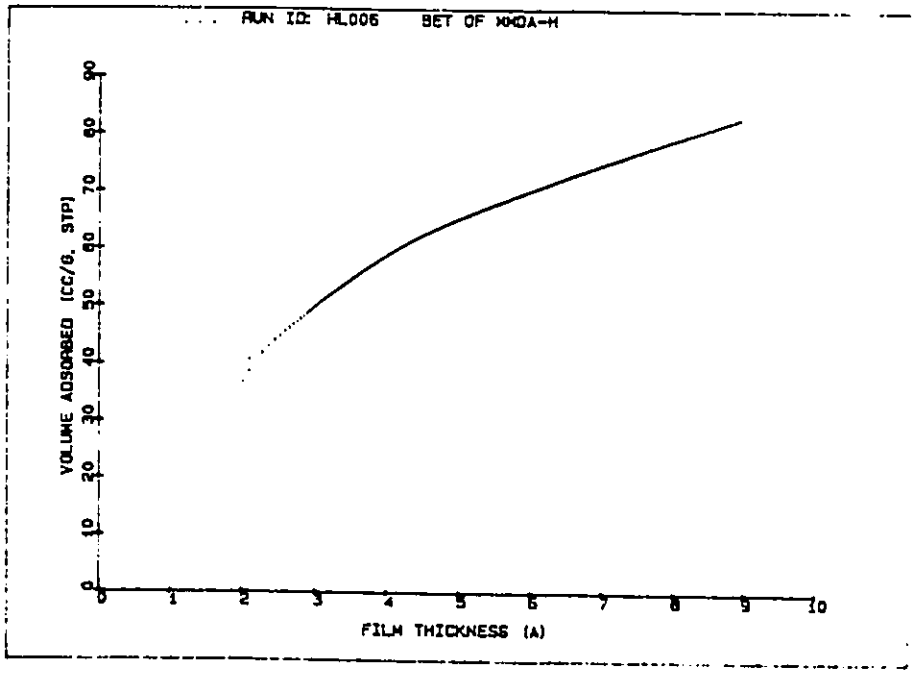

Figure 5.14 t-Plots of MMDA-montmorillonite and MMDA-hectorite

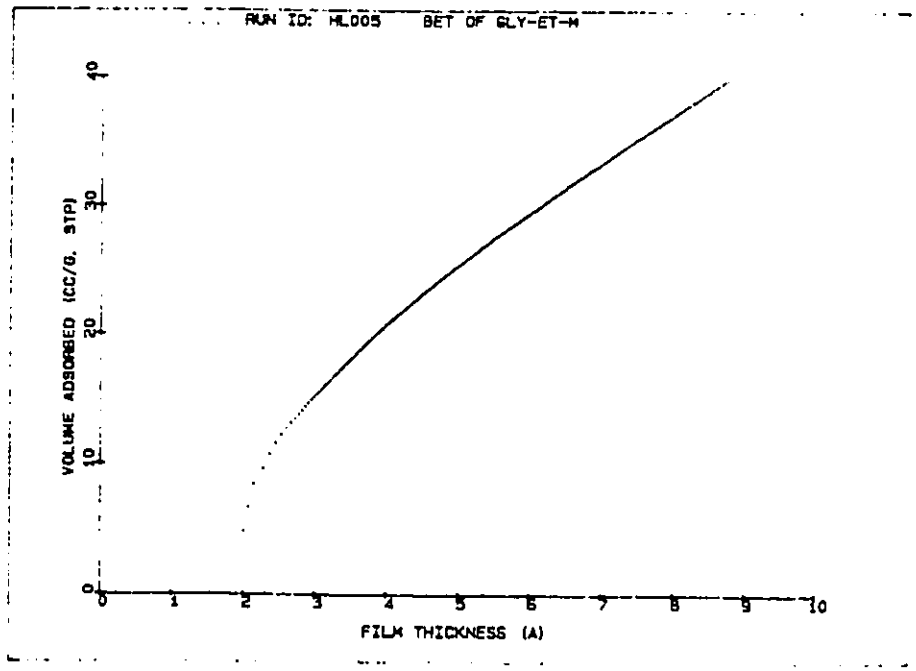

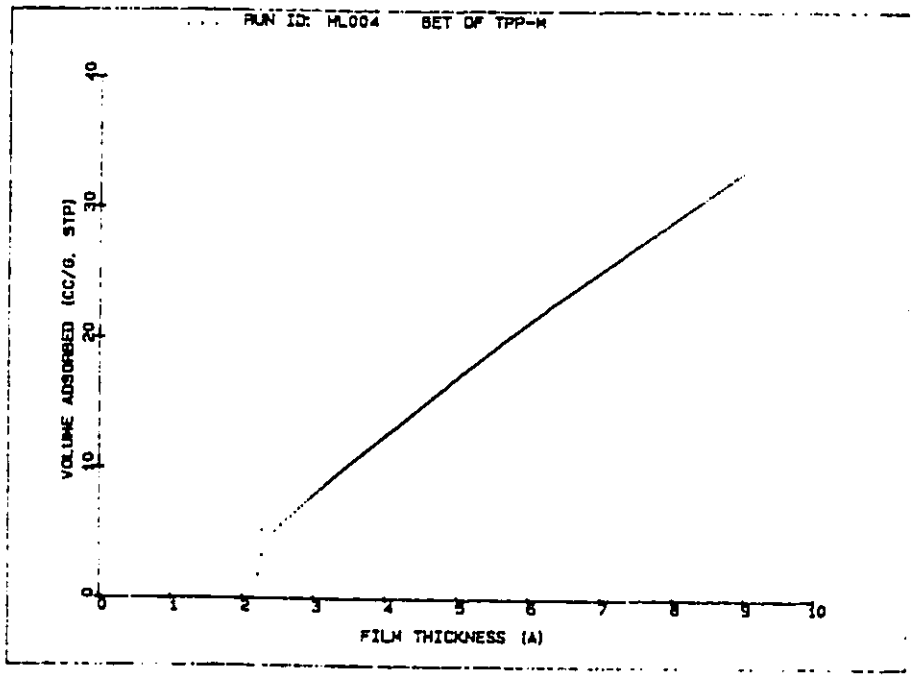

Figure 5.15 t-Plots of GLY-Et-montmorillonite and TPP-montmorillonite

The surface area of meso and macropores (external surface area), provided by pores with radii larger than 10Å will be given by the slope (b_t) of the second linear region once it is multiplied by 15.7 in order to convert to the appropriate units of square meters per gram of solid. The external surface area of organo-clay samples are shown in Table 5.2. It is noted that the external surface area in organo-montmorillonite are almost the same except in the case of GLY-Et-M which gives a relative larger external surface area. The larger external surface area is also found in the sample of MMDA-hectorite due to the larger external surface area of the hectorite as compared to the montmorillonite. From the external surface area as well as the BET surface area of organo-clays which are measured from the BET equations, the free interlamellar surface area available can be calculated.

5.2.5 Calculation of free interlamellar surface areas

The interlamellar free surface area which was measured experimentally can also be calculated from the total surface area of the clay and the cross-sectional surface area of the cation[111,112]. The formulae for Na-montmorillonite and Na-hectorite are[113]:

Na-montmorillonite:

$(Si_{7.84}Al_{0.16})(Fe^{+3}_{0.26}Al_{3.22}Mg_{0.40}Fe^{+2}_{0.12})O_{20}(OH)_4X^{+}_{0.68}$

Na-hectorite:

$(Si_{8.00})(Al_{0.04}Mg_{5.30}Li_{0.66})O_{20}(OH)_4X^{+}_{0.66}$

where X represents the inorganic cation in the interlamellar space of the clay.

The unit cell weight and total surface area can be calculated from the unit cell formulae and unit cell dimensions[68]. The external surface area of the clay is obtained from

the experimental measurement. The unit cell weight, total surface area and external surface area of the smectite clays are given in Table 5.3. The total interlamellar monolayer surface area can then be calculated. Because of the bilayer characteristic of the interlayer structure, the monolayer interlamellar surface area is half as much as the difference of the total surface area and the external surface area. The calculations are shown as follows:

SWy-1: $S_{T.I.M} = (740-31)/2 = 355 m^2/g$

SHCa-1: $S_{T.I.M} = (725-58)/2 = 332\ m^2/g$

where $S_{T.I.M.}$ is the total interlamellar monolayer surface area.

The calculated total interlamellar monolayer surface area of the organo-smectites are shown in Table 5.3.

Table 5.3 Unit-cell weight, total surface area, external surface area and interlamellar monolayer surface area of clays

Sample	Unit cell weight (g)	Total surface area (m^2/g)	External surface area (m^2/g)	Interlamellar monolayer area (m^2/g)
SWy-1	746.3	740	31	355
SHCa-1	762.6	725	58	332

Therefore, the free interlamellar monolayer surface area of organo-clays can be calculated by subtracting from the surface area covered by various interlamellar cations the total interlamellar monolayer surface area. The calculation must allow for the fractions of

the total cations which are located upon external surfaces of the crystallites. These fractions are estimated as 4% for montmorillonite and 11% for hectorite[111]. Since the X-ray diffraction results have demonstrated that the organic cations in the interlamellar space in all the cases are oriented nearly parallel to the sheets of the clay, the clay surface area occupied by the organic cation will be considered to be the cross-sectional surface area of the cation molecule. The cross-sectional area of molecule can be estimated from the projection on the a and b planes of the molecules[114,115]. On the basis of the molecular dimensions of the CPK models, the cross-sectional surface area of the cations was estimated. For example, the cross-sectional surface area of Me_4N^+ cation is 36 $Å^2$/ion and the interlamellar monolayer surface area occupied by the ions is :

$$S_{ion} = (0.68 \times 6.02 \times 10^{23} \times 36 \times 10^{-20})/746.3 \times 96\% = 190 m^2/g$$

Then the free interlamellar monolayer surface area of TMA-M is given by:

$$S_{FI} = 355\ m^2/g - 153\ m^2/g = 202\ m^2/g$$

These calculations allow the estimation of the interlamellar monolayer free surface area and the comparison with the experimental results. The cross-sectional surface area of the interlayer cations and the calculated free interlamellar monolayer area as well as the experimental free interlamellar monolayer surface area are given in Table 5.4.

Table 5.4 Calculated interlamellar free areas and experimental free surface areas of organo-clay

Organo-clay	Area of cation ($Å^2$/ion)	Area occupied by ion (m^2/g)	Calculated free interl. area (m^2/g)	Experimental free interl. area (m^2/g)
TMA-M	29	153	202	165
MMDA-M	47	124	231	150
MMDA-H	47	109	223	144
LYS-Me-M	93	245	110	15.2
GLY-Et-M	60	316	40	5.3
TPP-M	106	367	0	0

It is noted that the smaller cations, TMA^+ and $MMDA^{2+}$, occupy much less interlamellar space than the larger cations LYS-Me^{2+} and GLY-Et^+. Therefore the free interlayer surface area in the samples of TMA-M, MMDA-M and MMDA-H are much larger than that in the samples of LYS-Me-M and GLY-Et-M. The free interlamellar surface in LYS-Me-M is larger than that in GLY-Et-M. In the case of TPP-M, the large size cation (area 106$Å^2$/ion) is larger than the clay surface area available per unit charge (70$Å^2$ per monolayer clay sheet). However, the special C_3 orientation of TPP^+ cation can force the cations to adopt a compact packing inside the interlamellar space of the clay. The cations completely occupy all the interlamellar surface of the clay by head-to-end stackings and no microporosity is obtained in this sample. This consideration is in agreement with the experimental data which gave nearly zero micropore volume. As compared the surface area of MMDA-M with MMDA-H, one finds that the hectorite give larger external surface area than the montmorillonite while montmorillonite has larger interlamellar surface area than hectorite. It is also noted that the calculated free surface area are larger than the

experimental values. In the calculation, it is implicitely assumed that the distribution of organic cations in the clay is homogeneous and, as a result, that the organo-clays have an homogeneous pore size distribution. However, the organo-clays may contain different sizes of pores and therefore some very fine pores can exist in the samples, which are not accessible to nitrogen molecules. Also, it has been shown in the cation adsorption studies (chapter 3) that the amounts of cations adsorbed by the clays exceed the CEC values of the smectites. Since the calculation of the surface area occupied by the cations is based on the average CEC value, the actual surface area occupied by the interlayer cations are higher than the calculated value. Thus the experimental free interlamellar surface areas are lower than the calculated value. From the results presented above, one concludes that the larger is the size of the intercalated cation, the smaller is the free interlamellar surface available in the silicate sheets of the clay.

5.3 Micropore and mesopore size distribution analysis

5.3.1 Micropore size distribution

The analysis of nitrogen adsorption isotherms is a standard method for the detemination of the pore size distribution (PSD) of porous solids. Several analysis methods have been developed to calculate the pore size distribution, starting from the Kelvin equation which relates the size of a pore to the pressure at which capillary condensation occurs for the fluid whithin it[116,117,118]. These methods also require a description of the adsorbed layers which form on the pore walls prior to condensation. This is determined from an isotherm measured on a non-porous solid with a smililar chemical nature. The Kelvin equation is derived from thermodynamic considerations and is hence exact in the limit of large pores, but it becomes progressively less accurate as the pore size decreases

and breaks down completely when the pore becomes so small that the molecular structure of the fluid becomes significant[119,120]. Therefore these methods will fail for pore sizes in the micropore range. It has been shown that the lower limit of applicability of analysis methods based on Kelvin equation is about 90 Å[121]. The analysis of the micropore size distribution is even more problematical because these sizes are too small for thermodynamic techniques to be applicable. Recently a new analysis method has been developed which is based on a molecular model for nitrogen adsorption in a pore[121,122]. The development of this technique allows the calculation over both the mesopore and micropores size ranges using a single analysis method. The model gives a realistic representation of the phase behaviour of nitrogen in pores of all sizes, whilst reproducing the Kelvin equation in the limit of large pores.

Another simple quantitative model for the calculation of micropore sizes was proposed by Horvath and Kawazoe, who developed it for adsorption in active carbon[123]. This method (H-K) is based on statistical thermodynamics of the adsorbed gas molecules on surfaces. The free energy of a sorbed gas molecule was related to the distance between the gas molecule and the solid surface. The smallest pore size is constrained by the diameter of the sorbent molecule (e.g., for nitrogen: 3.65 Å). The interaction between the adsorbent and the adsorbate can be expressed as:

$$RT\ln(p/p_0) = U_0 + P_a \qquad (5\text{-}12)$$

where U_0 is the expression of the adsorbent-adsorbate interactions and P_a is an implicit function of the adsorbate-adsorbate-adsorbent interactions. In this method, the micropores are considered to be slits between two layer planes. The potential function over a surface (interaction energy between a gas molecule and an infinite layer) is given:

$$\Phi = 3.06\,\Phi^*[-(\sigma/r)^4 + (\sigma/r)^{10}] \tag{5-13}$$

$$\Phi^* = (N_a A_a)/(3.06)(2\sigma^4) \tag{5-14}$$

where σ is the distance between a gas atom and the surface at zero interaction energy, r is the distance from the surface, N_a is the number of atoms per unit area of surface, A_a is a constant.

The potential function between two parallel layers in the case of one adsorbate molecule is therefore given by:

$$\Phi = [(N_a A_a)/(2\sigma^4)][-(\sigma/r)^4 + (\sigma/r)^{10} - \{\sigma/(l-r)\}^4 + \{\sigma/(l-r)\}^{10}] \tag{5-15}$$

where l is the distance between the nuclei of the two layers. The potential function between the two layers filled with adsorbates is:

$$\Phi = (N_a A_a + N_A A_A)/2\sigma^4 \{ -(\sigma/r)^4 + (\sigma/r)^{10} - [\sigma/(l-r)]^4 + [\sigma/(l-r)]^{10}\} \tag{5-16}$$

where N_A is the number of molecules per unit area of the adsorbate and

$$A_A = (6mc^2\alpha_a\alpha_A)/[(\alpha_a/\chi_a) + (\alpha_A/\chi_A)] \tag{5-17}$$

$$A_A = (3mc^2\alpha_A\chi_A)/2 \tag{5-18}$$

where m is the mass of an electron, c is the velocity of light, α_a is the polarizability and χ_a is the magnetic susceptibility of an adsorbent atom, α_A and χ_A are the polarizability and magnetic susceptibility of an adsorbate molecule.

Equation (5-16) consists of two parts. The first part, $N_a A_a/2\delta^4$ multiplied by the expression in parentheses, corresponds to K^{-1}. U_0 (equation 5-12), and the second part corresponds to K^{-1} . P_a (equation 5-12). Having taken into account equation 5-12, an average potential value that depends on the absolute values of distances between the two layers can be calculated as:

$$RT\ln(p/p_0) = K(N_a A_a + N_A A_A)/2\sigma^4(l-d)\int_{d/2}^{l} [-(\sigma/r)^4 + (\sigma/r)^{10} - \{\sigma/(l-r)\}^4 + \{\sigma/(l-r)\}^{10}]\}dr \qquad (5\text{-}19)$$

where K is Avogadro's number and

$$d = d_a + d_A \qquad (5\text{-}20)$$

d_a is the diameter of an adsorbent atom and d_A is the diameter of the adsorbate molecule. Integration of equation 5-19 gives the following result:

$$RT\ln(p/p_0) = K(N_a A_a + N_A A_A)/\sigma^4(l-d) \times [\sigma^4/3(l-d/2)^3 - \sigma^{10}/9(l-d/2)^9 - \sigma^4/3(d/2)^3 + \sigma^{10}/9(d/2)^9] \qquad (5\text{-}21)$$

We now have a function of p with respect to l. Having used the data of a nitrogen isotherm at liquid nitrogen temperature, the expression can be obtained:

$$w/w_\infty = f(l-d_a) \qquad (5\text{-}22)$$

where w is the mass of the nitrogen adsorbed into pores, w_∞ is the maximum amount of nitrogen adsorbed into the pores and $l-d_a$ is the effective pore size. , the maximum amount

of nitrogen adsorbed into the pores (w_∞) can be determined at p/p_0 =0.9. The calculation of pore size distribution can be carried out by substituting different (l-d_a) valus in the range of 0.35-1.4nm into equation 5-21. Using the data of the adsorption isotherms, the w values corresponding to the chosen (l-d_a) pore sizes can be calculated. By plotting w/w_∞ against (l-d_a), the pore size distribution is obtained. The micropore size distribution of organo-clays are shown in Figure 5.16-5.18. The effective micropore size of these organo-clays are given in Table 5.5. It is noted that TMA-M, MMDA-M and MMDA-H yield very sharp micropore size distribution and show effective pore size at 5 Å. These compare with a size determined by XRD of 4.3, 4.3, 4.8Å respectively. The LYS-Me-M, GLY-Et-M and TPP-M have broad size distribution with pore sizes between 8-18Å. The broad micropore size distribution is attributed to the lower microporosity in these samples. The micropore volumes which are determined from t-plot are also presented in Table 5.5. It is found that those pillared smectites with smaller cations such as TMA^+ and $MMDA^{2+}$ give large micropore volume (about 0.06 cm^3/g) while those pillared smectites with larger cations such as LYS-Me^{2+}, GYL-Et^+ and TPP^+ give small or even no micropore volume (0-0.006 cm^3/g).

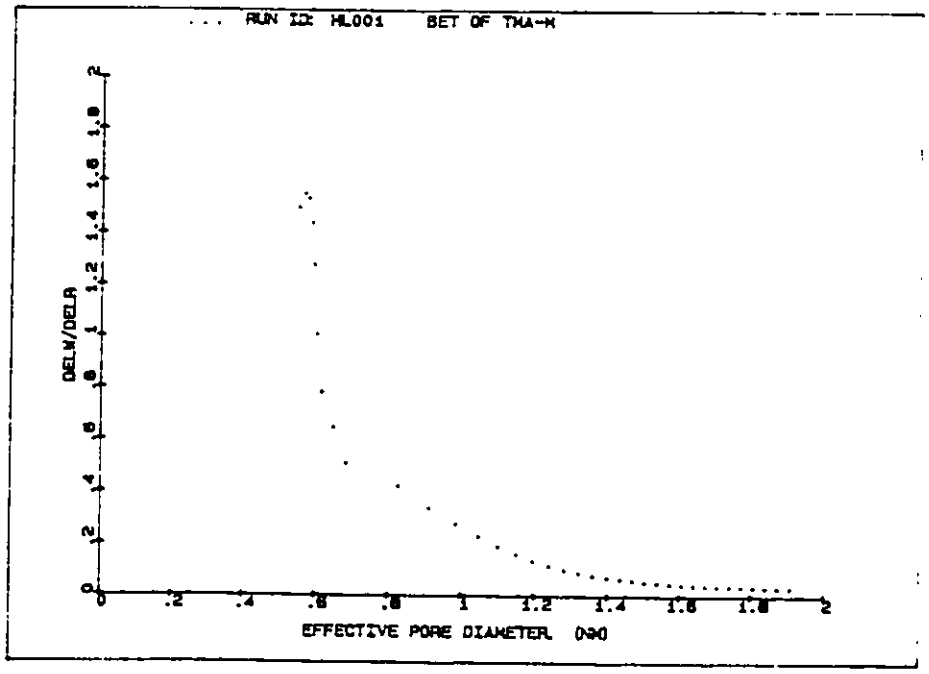

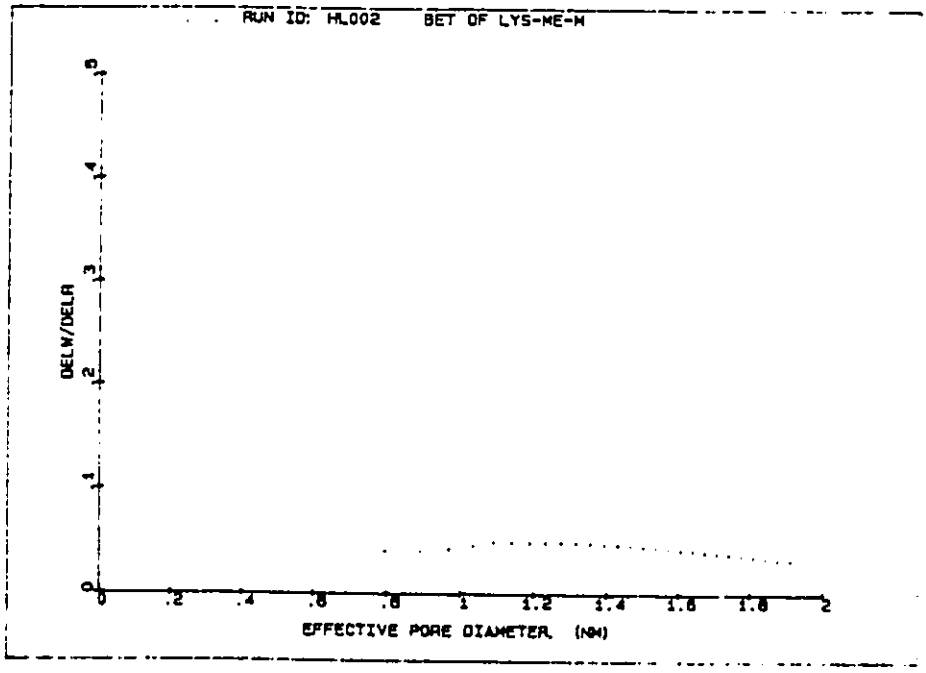

Figure 5.16 Micropore size distribution of TMA-montmorillonite and LYS-Me-montmorillonite

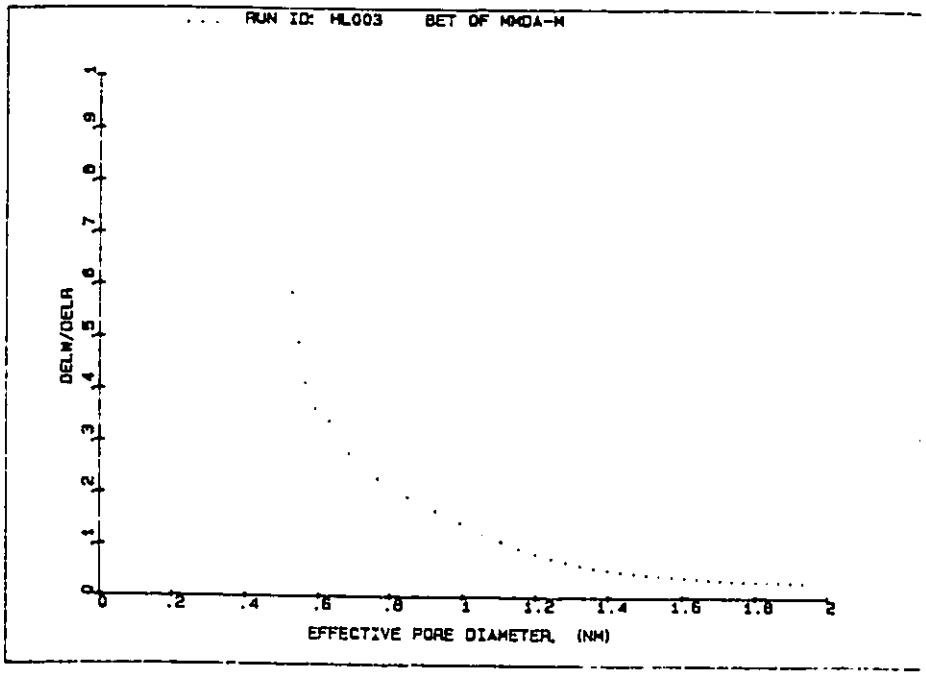

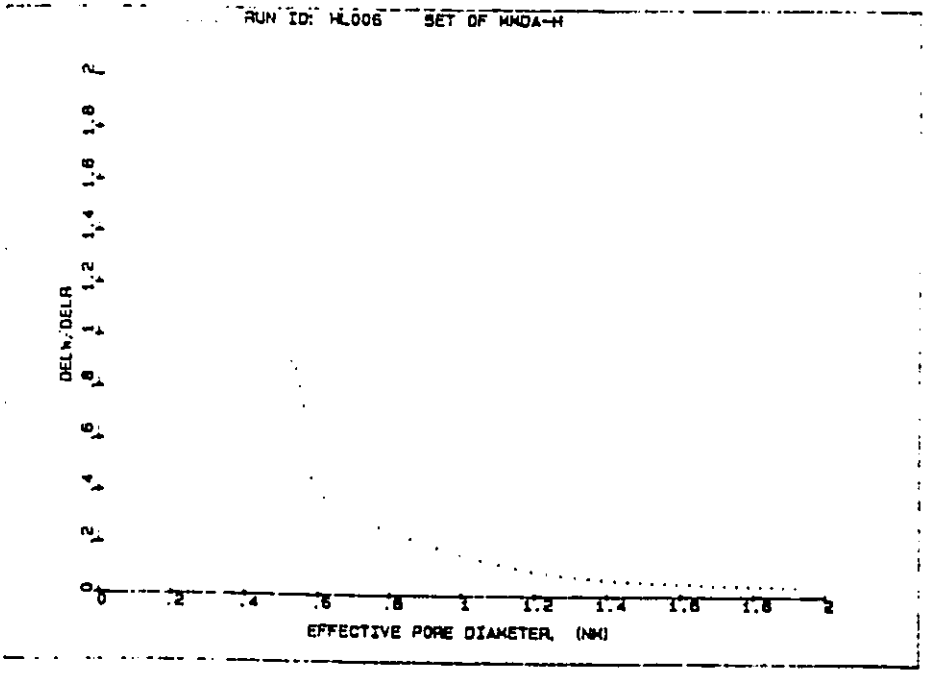

Figure 5.17 Micropore size distribution of MMDA-montmorillonite and MMDA-hectorite

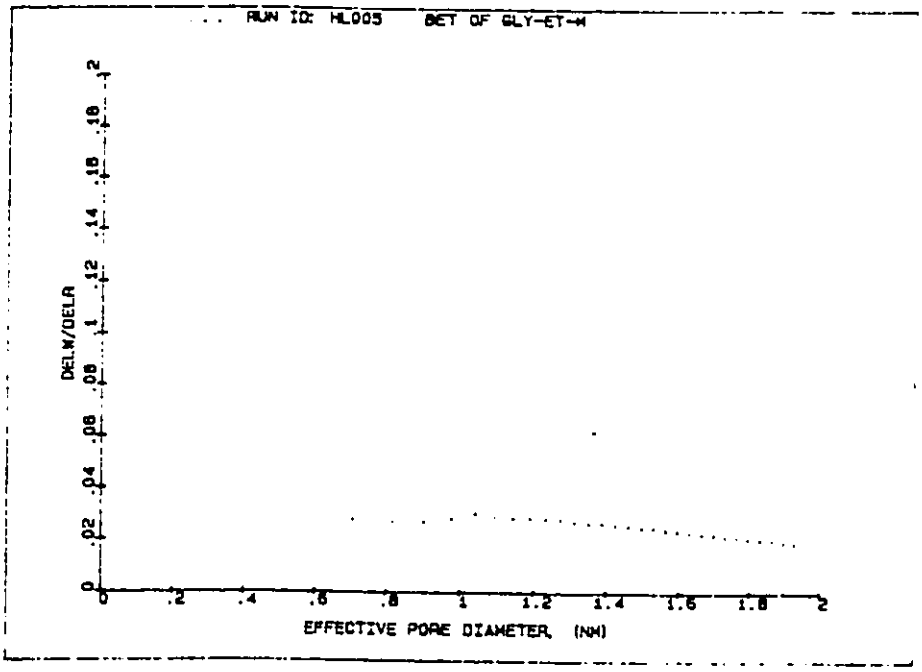

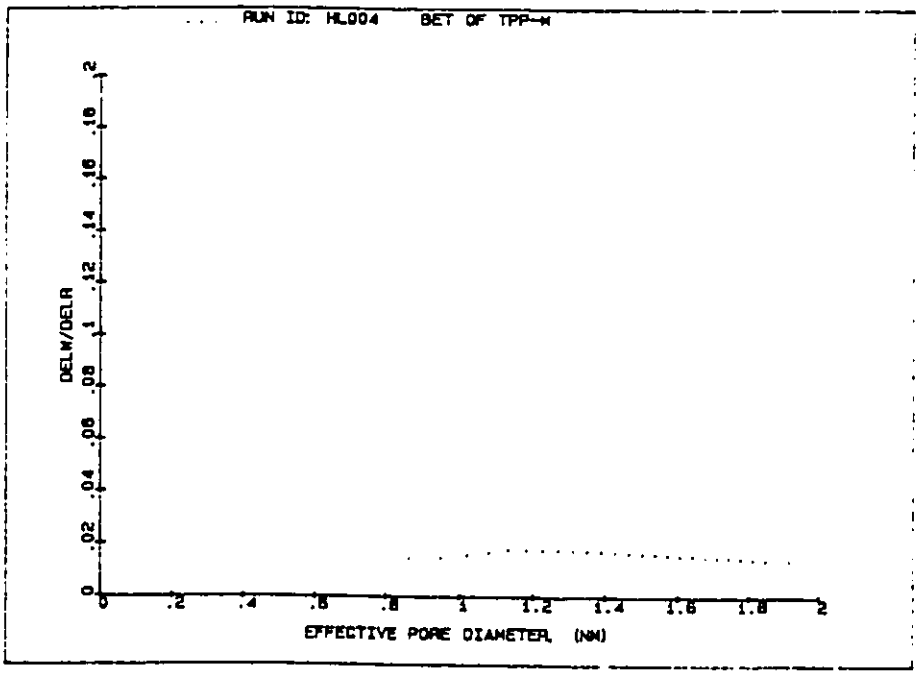

Figure 5.18 Micropore size distribution of GLY-Et-montmorillonite and TPP-montmorillonite

Table 5.5 Effective micropore pore size and micropore volume organo-smectite clays

Organo-clay	Effective micro-pore size (diam. Å)	Micropore volume (cm^3/g)
TMA-M	5-6	0.068
MMDA-M	5-6	0.061
MMDA-H	5-6	0.063
LYS-Me-M	8-18	0.006
GLY-Et-M	8-18	0.003
TPP-M	---	0

5.3.2 Mesopore size distribution

The possibility of calculating the pore size distribution of a porous solid from the capillary condensation region of its Type IV isotherm has long been recognized[107]. A relative pressure 0.95 is adopted as starting point with isotherms. The pore size distribution can be obtained by analysis of the desorption isotherm. The method used is based on the BET method which involves the area of the pore walls and uses the Kelvin equation to correlate the partial pressure of nitrogen in equilibrium with the porous solid to the size of the pores where capillary condensation takes place[116].The volumes desorbed from the sample at different pressures are converted to liquid volume by multiplying by 0.00156. As described in section 5.2.1, when capillary condensation takes place during the course of the isotherm determination, the pore walls are already covered with an adsorbed film having a thickness t. Thus capillary condensation occurs not directly in the pore itself but rather in

the inner core. Consequently the Kelvin equation (5-3) leads to values of the core size rather than to the pore size. Substituting the constants into the equation 5-3, the core radius r_m can be resolved:

$$r_m = 4.14 / \log(p_i/p_0) \qquad (5\text{-}23)$$

The thickness of the nitrogen film adsorbed on the walls of the pore at a given relative pressure is given[116]:

$$t(A) = 3.5 \times [5/2.302\log(p_i/p_0)]^{1/3} \qquad (5\text{-}24)$$

The radius of the pore r_p is given by adding to the Kelvin radius r_m the value of the film thickness t, that is:

$$r_p = r_m + t \qquad (5\text{-}25)$$

In calculation of the pore volume, it is necessary to correct for the core volume. The volume desorbed (δV_i) for a given group of pore at each interval of p_i/p_0 is calculated from the desorption isotherm and converted to a liquid volume. Then the core volume δV_i^K emptied during the stage i is given by:

$$\delta V_i^K = \delta V_i - \delta V_i^f \qquad (5\text{-}26)$$

The volume of the multilayer film on the walls of all the pores δV_i^f is obtained from the thinning of the nitrogen film:

$$\delta V_i^f = 0.064 \times \Delta t \times \Sigma (\delta A_p) \qquad (5\text{-}27)$$

where Δt is the difference between film thickness of the pore at two different pressures and δA_p is the surface area for a given group of pores.

Therefore the corresponding pore volume is given by:

$$\delta V_i^P = Q_i (\delta V_i - \delta V_i^f) \qquad (5\text{-}28)$$

where Q_i is the conversion factor.

Q_i is a function of both pore shape and film thickness:

$$Q_i = [r_p/(r_m + \Delta t)]^2 \qquad (5\text{-}29)$$

where r_p and r_m are the pore radius and core radius between pressures p_i and p_{i+1} and Δt is the difference between the film thickness of the pore at these two pressures. Since at values of the Kelvin radius above 30Å, the Δt is very small, then equation 5-29 becomes:

$$Q = (r_p/r_m)^2 \qquad (5\text{-}30)$$

The final volume ΔV_i^P will correspond to the volume desorbed from pores with average radius r_p. The pore size distribution is obtained by plotting the $\delta V_i^P/\delta r^P$ against δr^P.

Table 5.6 Effective mesopore size, mesopore volume and total pore volumes of organo-smectite clays.

Organo-clay	Effective mesopore size (diam. Å)	Mesopore volume (cm^3/g)	Total pore volume (>20Å, cm^3/g)
TMA-M	40	0.048	0.213
MMDA-M	40	0.051	0.215
MMDA-H	40	0.074	0.244
LYS-Me-M	40	0.018	0.215
GLY-Et-M	40	0.049	0.316
TPP-M	40 200	0 467	0.467

The mesopore size distribution analysis are shown in Figures 5.19-21. The effective meso(macro)-pore size and the total pore volumes (diameter >20Å) which are calculated from the mesopore size distribution analysis, together with the mesopore volumes are given in Table 5.6. As can be seen, all the organo-clays have mesopores with an effective size at 40Å in diameter except for TPP-M. The mesopores in the organo-smectites may contribute to the pores formed between the plate-like particles[78,97]. The total pore volume in TMA-M, MMDA-M, MMDA-H and LYS-Me-M are almost the same due to the same preparation procedure. In the case of TPP-M, there are two types of mesopores with sizes at 40Å and 200Å in diameter, respectively. The larger mesopore in the TPP-M sample may be attributed to the greater layer delamination occuring after the clay layers are greatly expended[89,96]. The delaminated layer structure is illustrated in Figure

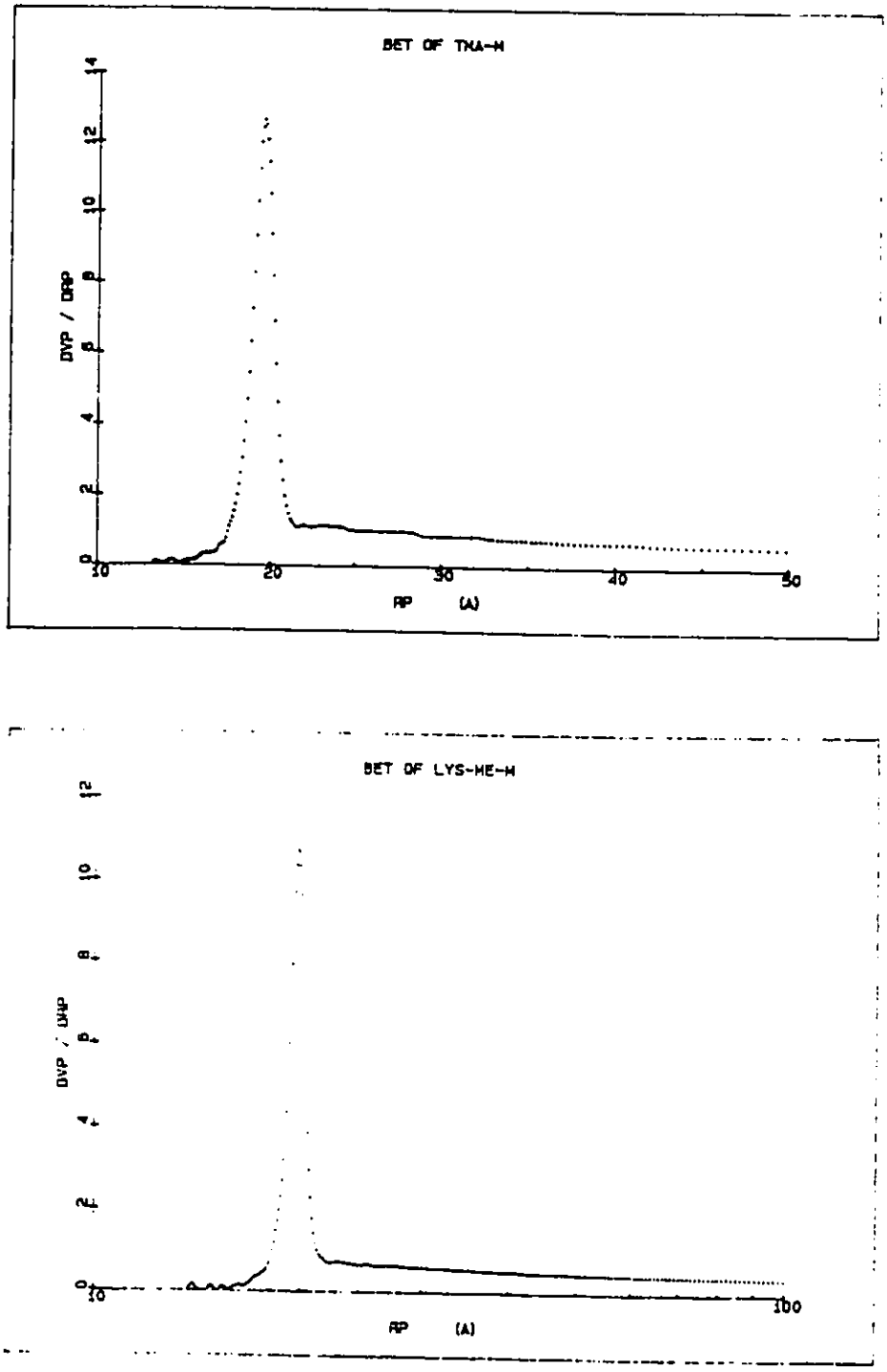

Figure 5.19 Mesopore size distribution of TMA-montmorillonite and LYS-Me-montmorillonite

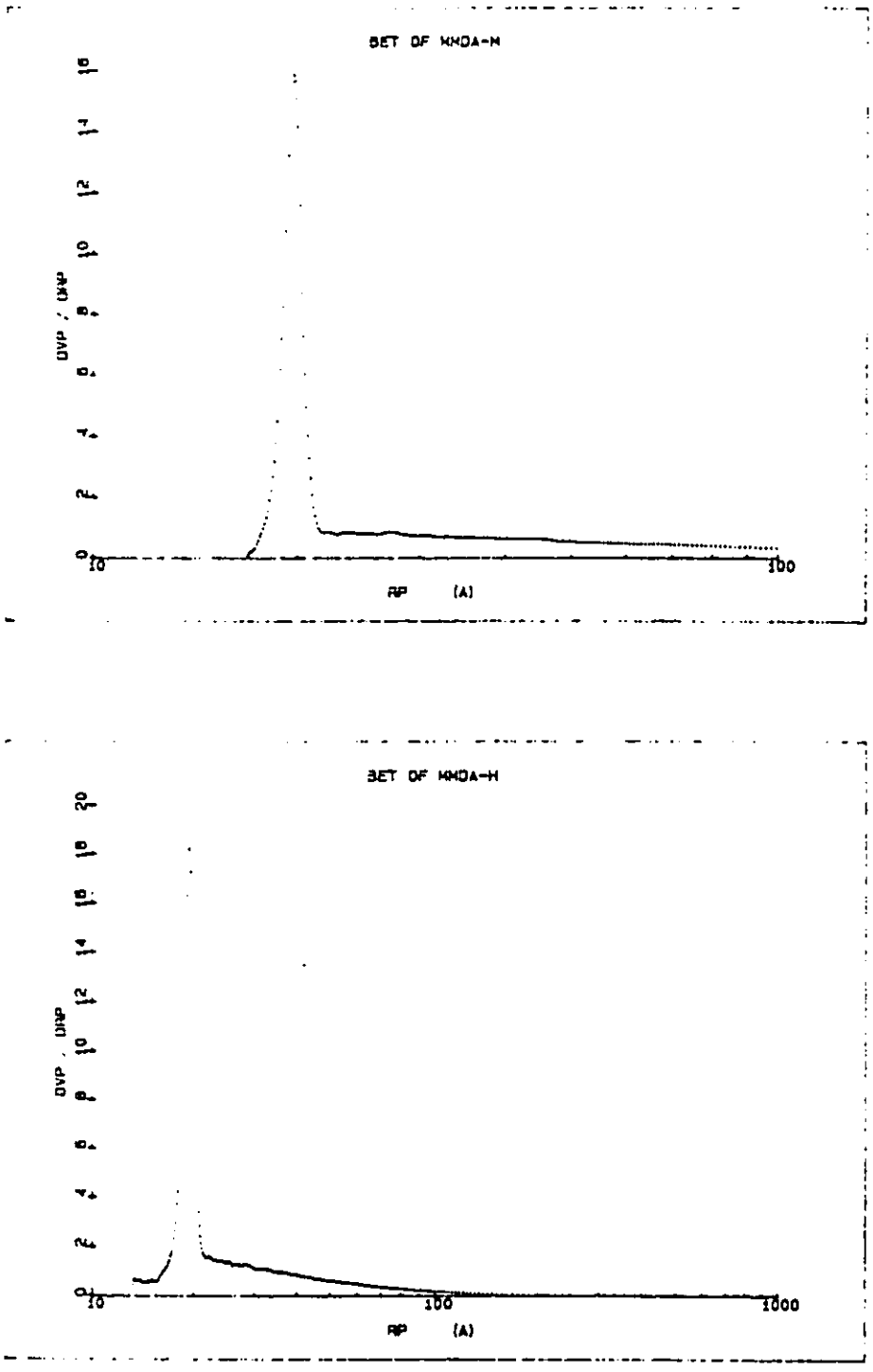

Figure 5.20 Mesopore size distribution of MMDA-montmorillonite and MMDA-hectorite

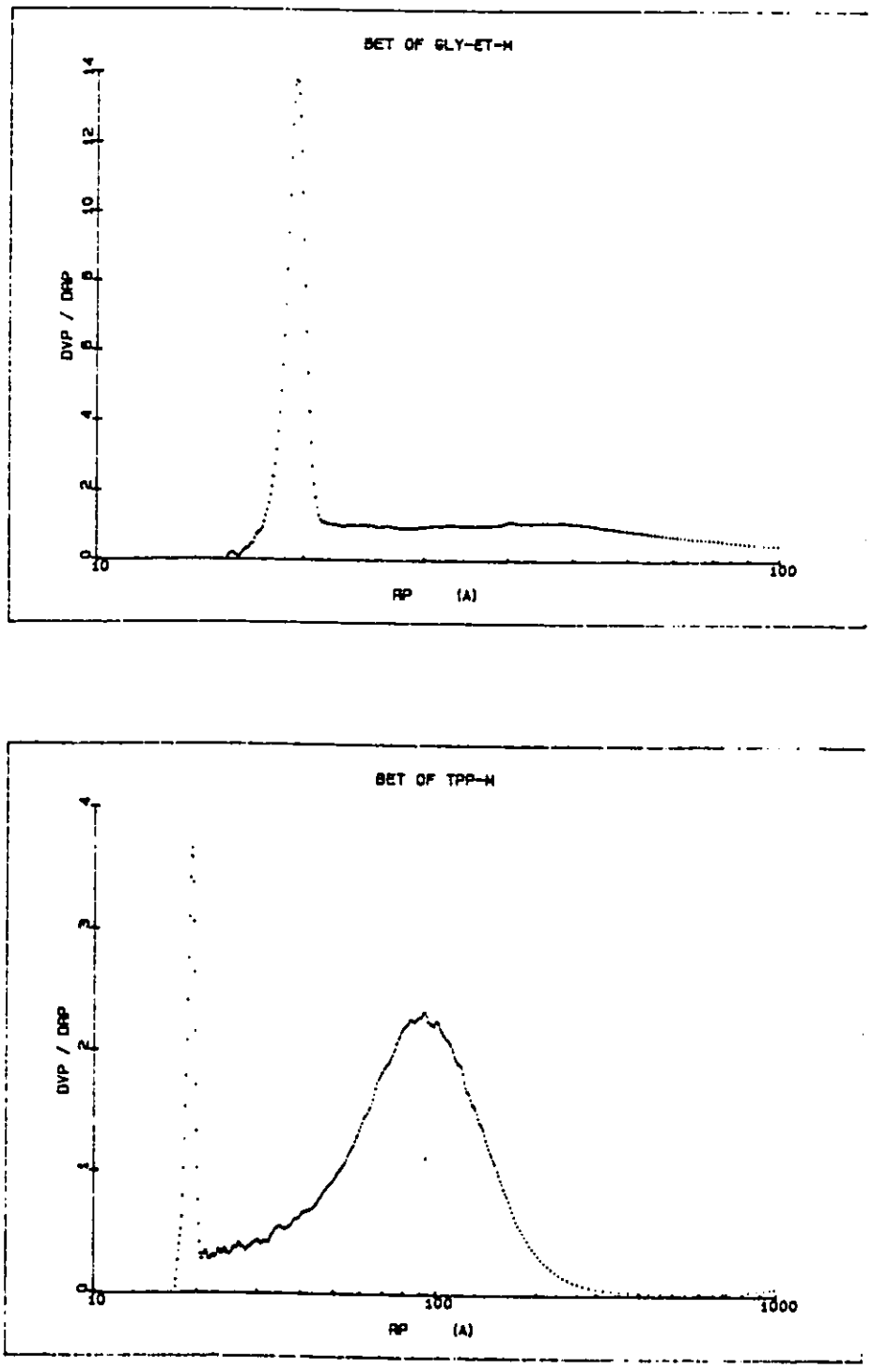

Figure 5.21 Mesopore size distribution of GLY-Et-montmorillonite and TPP-montmorillonite

5.22. For comparison, the micropore volume, mesopore volume and the calculated micropore volumes which are calculated by multiplying the interlamellar surface areas by the basal spacings of the organo-clays are shown in Table 5.7. The calculated micropore volumes agree with the experimental values in all the cases.

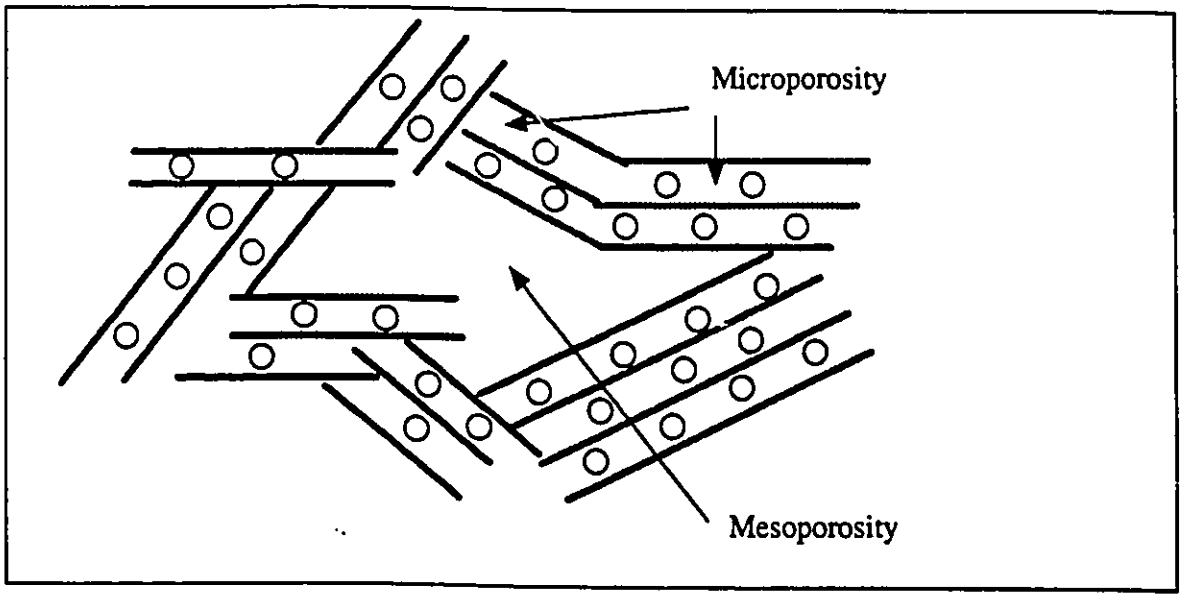

Figure 5.22 microporosity and mesoporosity in the pillared clays

Table 5.7 micropore volume and mesopore volume of organo-clays

Organo-clay	Free Interl. Surf. Area (m^2/g)	d_1 (Å)	Calculated Micropore Vol. (cm^3/g)	Micropore Volume (cm^3/g)	Mesopore Volume (cm^3/g)
TMA-M	165	4.3	0.071	0.068	0.048
MMDA-M	150	4.3	0.065	0.061	0.051
MMDA-H	144	4.7	0.068	0.063	0.074
LYS-Me-M	15	4.6	0.007	0.006	0.018
GLY-Et-M	5.3	4.0	0.002	0.003	0.049
TPP-M	0	9.2	0	0	0.467

5.4 Conclusions

The microporosity and the mesoporosity of the organo-smectites were studied by using a continuous nitrogen adsorption method. The BET surface studies gave both the external surface area and the interlayer surface area of the organo-smectites. The studies indicated that the interlamellar surface area of the organo-smectites can be controlled by changing the size and the charge density of the organic cation. Furthermore, the micropore and mesopore size distribution analysis allowed the estimation of the shape and size of the micropores and mesopores in the samples. The studies strongly proved that these microporous organo-smectite clays have the potential for the separation applications due to their microporosity.

Chapter 6

Chromatographic application of organo-smectites in gas separations

6.1 Introduction

There is a great deal of interest in industrial gas separation systems. It is estimated that the entire gas separation market will be $1.5 billion by the year 1995[124]. Currently, the greatest need for gas separation is for nitrogen enrichment for inert blanketing. The second largest need is for the removal of carbon dioxide from natural gas and hydrogen sulfide from natural gas. Other separations which have high priority are hydrogen recovery in refinery streams and methane recovery in mines. The separation of CO_2 from natural gas in enhanced oil recovery operation (EOR) is an important industrial process. CO_2 is considered as a suitable, high molecular weight gas which can be injected into a depleting well in order to keep the pressure up (2,000 psig) and hence maintain oil production capacity. Therefore natural gas contains high contents of CO_2 and subsequent removal of CO_2 from the natural gas is necessary. A EOR process is schematically represented in Figure 6.1 where a membrane system is used to remove the CO_2 for the reinjection and at the same time used to remove the light hydrocarbons[125]. Landfill gas has received attention as a source of renewable energy because it contains 40-60% CH_4, which was to be enriched to over 90% as pipelinequality[126]. Currently, there are several commercial separation

processes including cryogenic separation, adsorption separation and membrane separation processes. Cryogenic separation process is a liquefaction followed by distillation process. It remains the most frequently used process for large-scale applications. However, this is an energy consuming process. Adsorption separation process is an alternate method which provides efficient separation. A major development in adsorption technology is the pressure swing adsorption (PSA) process. In PSA the sorbent is periodically regenerated by reducing the total pressure. The cycle time is short due to the possibility of rapid pressure reduction. Consequently large throughputs can be achieved and an increasing number of new separations using PSA are being commercialized[127]. The adsorptive separation can be achieved by three mechanisms: steric, kinetic or equilibrium effect. In the steric separation process, only small and properly shaped molecules can diffuse into the adsorbent, whereas other molecules are totally excluded. There are only two major steric separation processes used in industry: the drying process by 3A zeolite and the separation of normal paraffins from iso-paraffins and cyclic hydrocarbons using 5A zeolite. Kinetic separation is achieved by virtue of the difference in diffusion rates of different molecules into the sorbent. Equilibrium separation can be achieved by the difference in affinities of gas molecules on the adsorbent. Commercial separation processes using molecular sieve zeolites are mainly equilibrium processes. The only kinetic commercialized separation is air separation using molecular sieve carbon. The kinetic separation of air by 4A zeolite and the separation of CH_4/CO_2 mixture using molecular sieve carbon have recently been investigated[128,129,130]. Membrane separation is a new efficient separation process which is economically comparable with other separation processes. As mentioned in the previous chapters, the intercalation of pillaring cations into the interlamellar space of the smectite clays results in a microporous material whose structure is similar to zeolites. These microporous organo-smectites might be used for separation processes due to their micropore structure. Moreover, a large flexibility is offered by these kinds of materials because the size of

intercalates can be changed and therefore the pore size and volume can be controlled. The chromatographic application of these organo-smectite clays on the separations of CH_4/CO_2 and C_1-C_4 hydrocarbons was studied here in order to explore the potentials of these microporous organo-clays for adsorption separation processes[131]. Further application of these materials in membrane separation processes will be discussed in chapter 8.

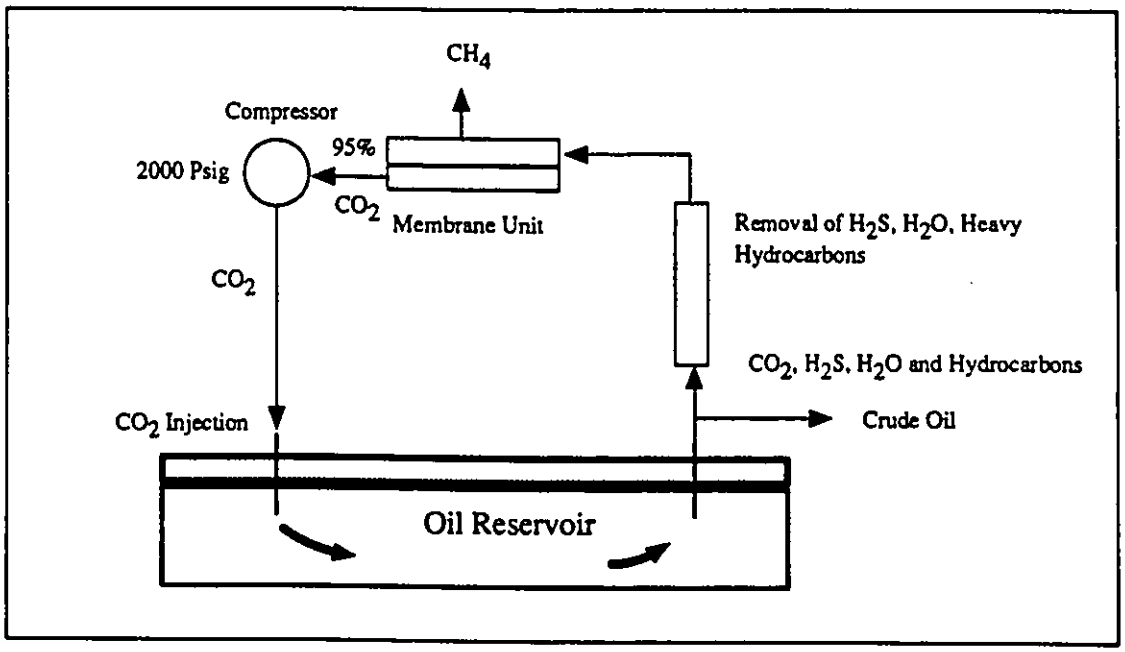

Figure 6.1 Schematic representation of a EOR process[125]

6.2 *Aspects of chromatographic applications of clay minerals*

The analysis of permanent gases (i.e. H_2, O_2, N_2, CO, CH_4 and CO_2) generally involves gas-solid chromatography. A wide variety of adsorbents have been used for this purpose. Zeolite A, X and ion-exchange modified zeolites give molecular sieve effects due to their homogeneous pore structures and pore sizes and they are useful for the analysis of many gases but irreversibly adsorb carbon dioxide at normal temperature[132]. Carbon molecular sieves do not separate oxygen and nitrogen as well as do zeolites; however, they elute carbon dioxide. Silica Gel and Aluminas are other adsorbents which can be used for the analysis of several gases and some of the lower hydrocarbons, but do not separate oxygen from nitrogen. Various porous polymers can also be used for the separation of gases. It has been shown that natural clay minerals such as attapulgite and sepiolite exhibit zeolite-like pore structures and these two clay minerals have been used as chromatographic adsorbents for the separations of inorganic gases and light hydrocarbons[133,134]. The concept of pillaring smectite clays was demonstrated more than 30 years ago by Barrer and MacLeod[135,12] and microporosity was first demonstrated in 1955 with Me_4N^+ and Et_4N^+ as the interlayer cations[10]. If layered silicates are exchanged with cations large enough to create an interlayer space, a notable range of shape-selective microporous sorbent can be obtained. The expanded clays freely intercalate many permanent gases and non-polar molecules that are not intercalated in the parent montmorillonite. As a result, the sorption capacity is greatly enhanced and, as with zeolites, intracrystalline sorption requires no threshold pressure. The selective uptakes of various gases, paraffins and aromatics on the modified organo-clays have been reviewed recently[10]. Dimethyldioctadecylammonium-montmorillonite (Bentone 34) was the first commercial chromatographic adsorbent in which cations swell a clay and fill all the interlayer spaces[136]. The long chains of the organic cations in this organo-clay are closely packed and are steeply

oriented to the clay surface. This organo-clay has been shown to permit the selective uptake of paraffins, aromatics and heterocycles[10,136]. In this case, the interlamellar distances played only a minor part in the separation of aromatic isomers, because the interlamellar surfaces of the clay were completely occupied by the cations. The Bentone 34 has also been modified as a liquid chromatographic phase by its mixture with a silicone oil and dispersion on Celite[137]. The utilization of organo-clays as chromatographic stationary phases has received much attention in that time. White[138] described the exchange of clays with several quaternary alkylammonium ions and these organo-clays displayed selective retention of aromatics relative to paraffins and naphthenes when they were used as stationary phase[138]. An organo-smectite exchanged with methylbenzyldioctadecylammonium and containing an amide additive has been shown to have selective adsorption for several organic compounds such as alcohols, esters, ketones and hydrocarbons[139]. However, only limited data on the application of organo-clays for gas separations can be found in the literature. Also possible applications of pillared clays as new adsorbents in separation processes remain largely unexplored. Thielmann and McAtee have studied the gas chromatographic behavior of montmorillonite exchanged with metal-*tris*-(EDA)(tri-(ethylene-diamine) chromium (III) cations in the separation of polarizable gas such as nitrous oxide and light hydrocarbons[140]. Several chloroalkylammoniums exchanged montmorillonites were also used for the separations of light hydrocarbons and oxides of nitrogen (NO, N_2O, N_2O_3 and N_2O_4)[141]. There is now renewed interest in intercalated clays, because it is realized that their pore sizes and shapes could afford larger flexibility than those of zeolites. The application of pillared organo-clays offer a new direction for separation processes. Our work on the application of various organo-smectites as chromatographic adsorbents for gas separations has been published recently[131]. At the same time, it was reported that separations of air, N_2/CH_4, C_6H_6/C_6H_{14}, CH_4/CO_2 and the C_8 aromatic isomers could be achieved in a pillared zirconyl-clay column[142,143]. The separation was considered to be accomplished by

equilibrium and/or kinetic separations.

If the height of the galleries network in the organo-clay is close to the kinetic diameter of the gases, one expects the diffusion of gas molecules in the interlamellar pores to be restricted. The diffusion restriction would allow the gas molecules to diffuse in different rates depending on their molecular size and the interactions with the interlamellar siliceous surface. The difference in diffusion rates of the gases contributes to the effective gas separation. It is known that pore size in the range 4-8Å is suitable for gas separation[144]. There are several ways to modify the micropore size of the organo-smectites: (1) varying the size and shape of the ionic interlayer props; (2) increasing the cation charge and therefore decreasing the number of the interlayer cations; and (3) altering the composition of the siliceous layers and therefore their anionic charge.

In this chapter, the application of microporous organo-clays as chromatographic adsorbents for gas separations will be explored and the effects of organic cation size, surface area, microporosity of the organo-clays and charge density of the clay on the retention parameters of N_2, O_2, CH_4, CO_2 and C_1-C_4 hydrocarbons will be studied.

6.3 Principles of gas chromatography

Generally, chromatographic separations are based on multiple partition of the compounds to be separated between phases during continuous, dynamic operation driven by the carrier gas flow. One of the two phases is stationary and the other is mobile, moving along the liquid or solid stationary phase. In gas chromatography the mobile phase is a gas and the stationary phase can be either a liquid (GLC = gas liquid chromatography) or a solid (GSC = gas solid chromatography)[145,146]. The carrier gas flows through the separation column and is the medium for the transportation of the components to be separated. The

individual components are temporarily dissolved in the stationary phase or adsorbed on the surface of the solid stationary phase, depending on the chemical properties of the solute and the stationary phase. The intensity of the intermolecular interaction between the solute and the stationary phase governs the vapor pressure or the concentration of a certain solute within the mobile phase. The partition equilibrium of a solute between the two phases is described thermodynamically by the partition coefficient. In GLC with a gaseous mobile and a liquid stationary phase, the partial pressure of the solute above the stationary phase at the equilibrium can be described by Henry's law if the concentration of the solute within the stationary phase is low. In GSC, a equilibrium between sorbate and sorbent is determined by the adsorption and desorption process.

The separation efficiency of chromatographic columns can be characterized by the theoretical plate numbers (N) and the height equivalent to a theoretical plate (HETP). The number of equivalent theoretical plates (N) , is given by the following equation:

$$N = t^2_R/b = 5.54\ (t_R/b)^2 \qquad (6\text{-}1)$$

where t_R is the total retention time measured in cm or minute and b is the peak width at half-height measured in cm or minute. In the plate theory, the column is thought to consist of a finite number of hypothetical stages and equilibrium is attained in each stage. The separation efficiency is indicated by the equivalent height of each stage which is given by the ratio of the theoretical plate number N and the column length L:

$$HETP = N / L \qquad (6\text{-}2)$$

A high separation efficiency is achieved by a small equivalent height. The equivalent height or height equivalent to a theoretical plate (HETP) is given by the van Deemter equation for

linear adsorption isotherms[3]:

$$HETP = A + B/\mu + C\mu \qquad (6\text{-}3)$$

where $A=2D_m/\tau$, $B=4R_p/Pe$ and $C=2\varepsilon/[kK(1-\varepsilon)]$

Here μ is the interstitial velocity, D_m is the molecular diffusivity, τ is the axial tortuosity, R_p is the particle radius, Pe is the Peclet number, ε is the interparticle void fraction, k is the mass transfer coefficient used in the linear driving force equation, and K is Henry's constant for the linear isotherm. The first term (A) in equation 6-3 accounts for the geometry of the packing. It is very difficult to have uniform particle size in the packing materials and the overall effect is that spaces along the column are not uniform. When a sample migrates down to the column each molecule follows different paths and each path is of a different length. In addition to these different path lengths there are variations in the velocities of the mobile phase. Therefore, irregular diffusion results from flow through randomly spaced particles in the column. The second term (B/μ) refers to the longitudinal diffusion in gas phase. The third term ($C\mu$) contributes to the resistance to mass transfer process.

The interstitial velocity μ plays a role in the contribution of the three terms on HETP equation. The dependence of HETP on μ is illustrated in Figure 6.2, showing the three contributions to the HETP. The optimum velocity which yields the minimum HETP is:

$$\mu_{opt} = (B/C)^{1/2} \qquad (6\text{-}4)$$

Below μ_{opt}, peaks are broadened mainly by molecular diffusion. Above μ_{opt}, the mass transfer resistance is the main cause for broadening. Equation 6-3 is the simplest form of the van Deemter equation. Many other effects can be taken into account leading to more complex equations[146].

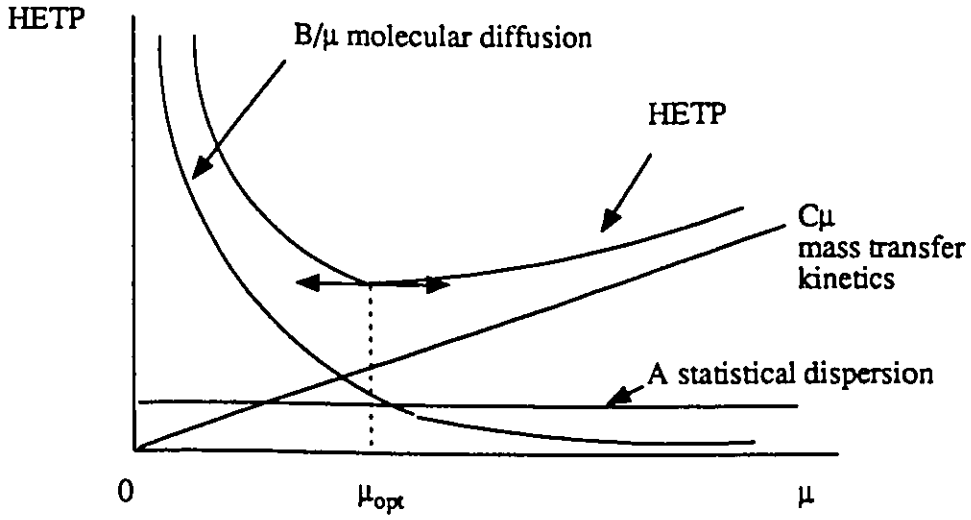

Figure 6.2 The dependence of HETP on the flow velocity[145]

A gas chromatogram is described by the retention value and effluent concentration as shown in Figure 6.3. The distance of a peak from the injection point I on the time coordinate is the total retention time t_R during which the solute is retained in the column[145]:

$$t_R = t_m + t_s \qquad (6\text{-}5)$$

where t_m is the time during which the solute is present in the mobile phase and t_s the time when it is in the stationary phase. The difference t_s is the so-called net retention time which is proportional to the partition coefficient K and increases as the latter increases. The capacity factor k'_i is given by the ratio of t_s and t_m:

$$k'_i = t_s / t_m \qquad (6\text{-}6)$$

The separation of the solute components can be evaluated by the selectivity coefficients or separation factors (α) which is given by the relative retention times of solute pairs:

$$\alpha = (t_s)_j/(t_s)_i = k'_j/k'_i \qquad (6\text{-}7)$$

The resolution between two Gaussian elution peaks is defined by the parameter:

$$R_{AB} = (t_{RA} - t_{RB})/4b_{AB} \qquad (6\text{-}8)$$

where $b_{AB} = (b_A + b_B)/2$, b_A and b_B are the half widths of peaks A and B, respectively.

Complete resolution requires $R_{AB} \geq 1.5$. The N needed to achieve the resolution R_{AB} for two Gaussian peaks is:

$$N = 4\, R^2_{AB}\, [(\alpha + 1)/(\alpha + 1)]^2 \qquad (6\text{-}9)$$

where α is the separation factor defined in equation 6-7. Thus the column height required for complete resolution is obtained directly as the product of HETP and N.

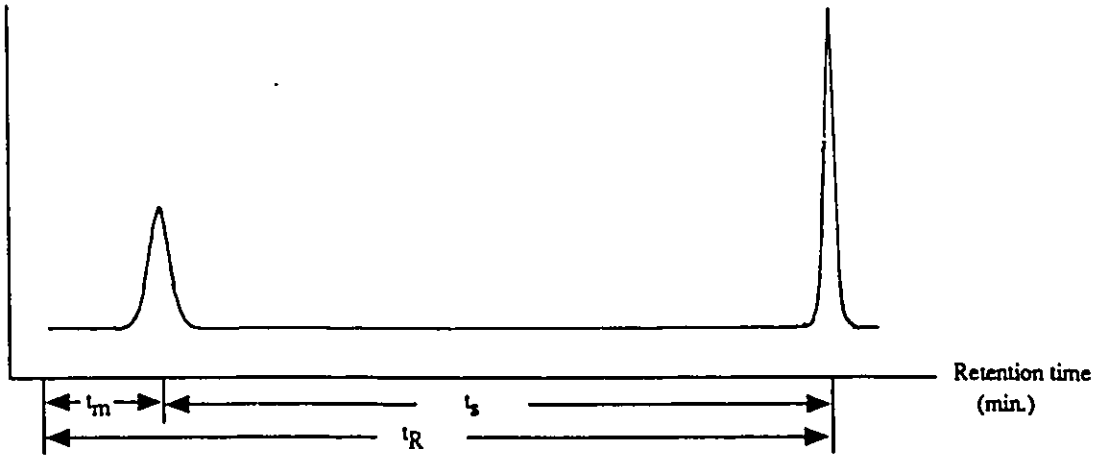

Figure 6.3 A gas chromatogram, showing the retention time and effluent concentration[145]

The above parameters are useful for the evaluation of the separation by gas-solid chromatographic methods. In the use of a solid adsorbent for GSC, the specific surface area, the chemical composition and the porous structure are very important factors affecting the performance of the chromatography. The greater the surface area the higher is the probability of sorption processes to occur. Retention of sorbate molecules on the adsorbent depends upon the chemical nature and geometric pore structure of the adsorbent, molecular weights of sorbate molecules, their geometric and electronic structure and the temperature of the column. The sorbate molecules may either diffuse toward sorbent surface and/or diffuse into the pores, depending on the size of the pores in the adsorbent and the gas molecules. The carrier gas may also have a significant effect on the separation process. Adsorbents with high surfaces may adsorb the carrier gas and thus decrease the number of the active sites, resulting in a change of component adsorption activity. A change in carrier gas from hydrogen or helium to nitrogen, for example, may produce sharper peaks because of the higher adsorption capacity for nitrogen[146].

6.4 *Separation of permanent gases by organo-clay smectites via chromatographic route*

6.4.1 Separation of carbon dioxide and methane by organo-smectite clays

It has been previously shown from the microporosity studies that the incorporation of organic cations into smectites can result in a microporous material with a network of cavities whose height and volume are controlled by the size and the shape of the organic cation. This is illustrated in Figure 6.4, showing three different types of organo-clays which are obtained by intercalation of different types of organic cations into the clay. Moreover, functionalities, such as ester groups, can be attached to the organic cation, so that one can easily synthesize a material with tortuous channels whose walls combine hexagonal arrays of silicate oxygens and organic functions. If the intercalated cations are large enough that the interlayer surfaces of the clay are covered completely by the cations (as in the first case of Figure 6.4), no microporosity can be obtained in the organo-clay. When the intercalated cation has the proper size, micropores are obtained. Therefore, the pore sizes can be controlled by both interlamellar distance (d_1) and inter-distance (d_3) as in the latter two cases of Figure 6.4. The X-ray diffraction results have already shown that the interlamellar distance in most of organo-smectite clays in our case are in the range 4.0-5.1Å. The height of galleries in these organo-clays is slightly larger than the kinetic diameter of gases such as N_2, O_2, CH_4 and CO_2. The kinetic (sieving) diameters (Å) of some permanent gases which are based on the sorption in zeolites are given as follows[147]:

N_2	O_2	CH_4	CO_2
3.64	3.46	3.8	3.3

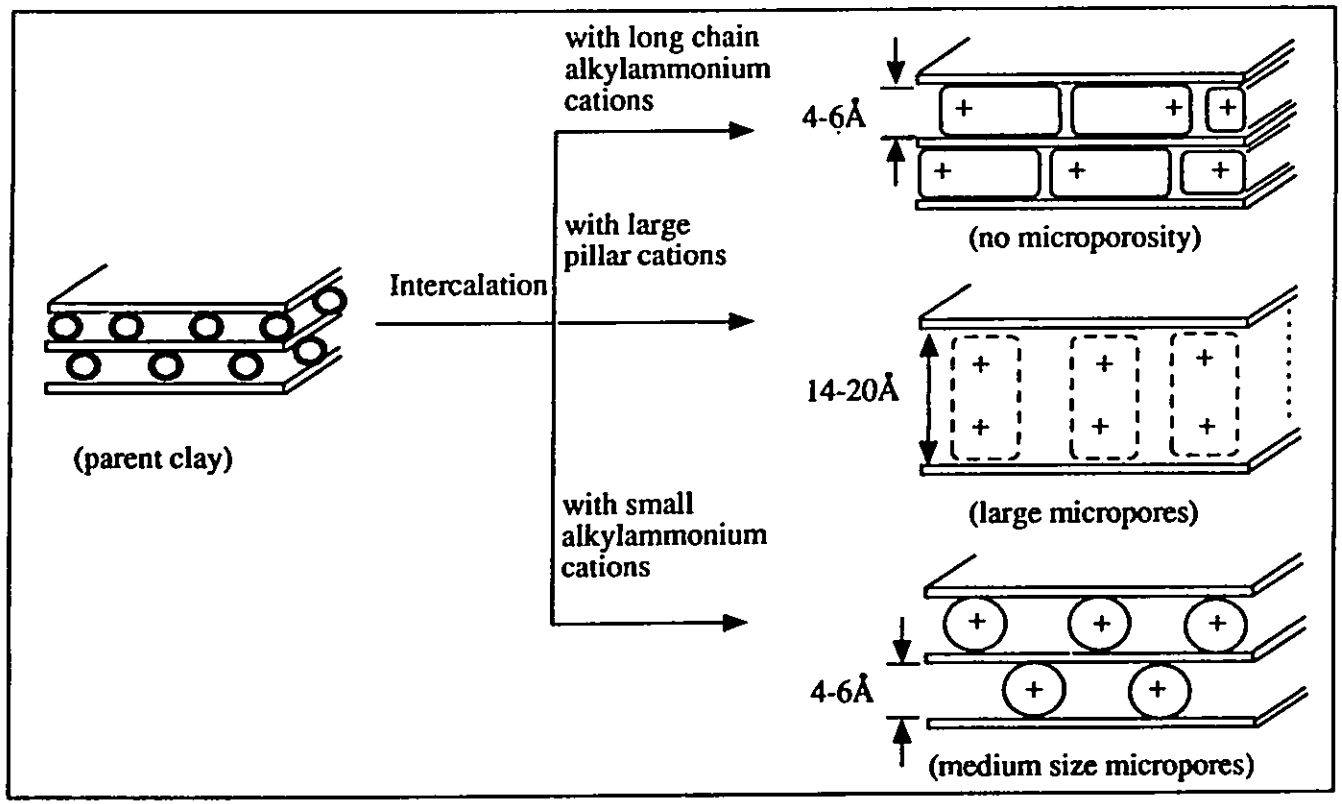

Figure 6.4 Three different organo-clays generated from natural clay by intercalation with cations

The chromatographic separations of gases by these organo-smectites were studied with focus on their ability in separating carbon dioxide-methane and C_1-C_4 hydrocarbons. All the quaternary alkylammonium derivatives were incorporated at full loading of the clay (100% of the CEC) and the particles of size 60-120 mesh were selected as packing material for chromatographic columns. The separation of gas mixture was accomplished in a 3ft x 1/8 in o.d. column. In all the cases, the flow rate (He) was controlled at 25 ml/min. The retention time was recorded as the time from the injection point to the point where the maximum response was obtained. In the calculation of the capacity factors, He gas was considered as a non-retained gas. Therefore, the time for He gas travelling through the column was the time of retention in a column (t_m) which was 0.14 minutes in all the cases. Thus, the net retention time could be calculated by subtracting the t_m(0.14 min) from the total retention time.Three different systems were examined:

(1) organo-smectites with quaternary phosphonium, quaternary ammonium or quaternary ammonium derivative cations (monocations, e.g. TMA^+, $GLY\text{-}Et^+$, TPP^+);

(2) organo-smectites with quaternary ammonium derivatives of amino acids bearing two amino-groups (dications, e.g. $LYS\text{-}Me^{2+}$, $ORN\text{-}Me^{2+}$);

(3) organo-smectites with quaternary ammonium cations (di- or polycations, e.g. $MMDA^{2+}$, $MDEA^{2+}$, $MTETA^{4+}$).

The gas chromatograms for the separation of air, CH_4 and CO_2 gas mixture by the three organo-montmorillonites in the first system are given in Figure 6.5 and the retention parameters as well as the separation factors for these systems are given in Table 6.1. For comparison, the chromatographic parameters for those gases on Na-montmorillonite column are also shown in the table.

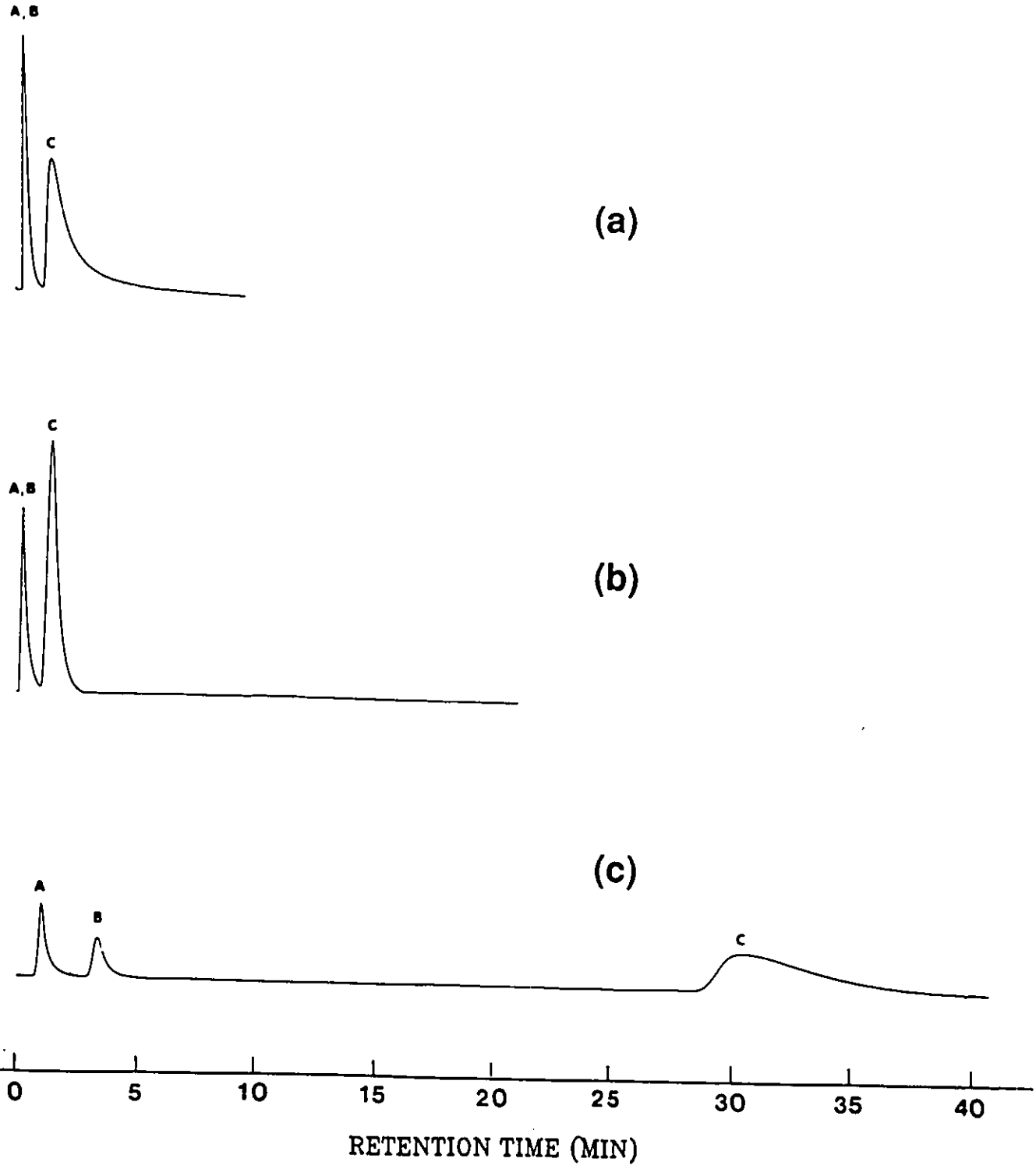

Figure 6.5 Chromatograms for the separation of air, CH_4 and CO_2 by organo-montmorillonites. Columns: 3ft x 1/8 in.o.d. Carrier gas: He at 25ml/min. Column temperature: 30°c. (a) TPP-montmorillonite; (b) GLY-Et-montmorillonite; (c) TMA-montmorillonite. Peak identification: A=air; B=methane; C=carbon dioxide.

Table 6.1 Retention parameters of air, CH_4, CO_2 on organo-smectites with mono-cations at 30^0c (He flow: 25 ml/min).

Column	t_R (air)	t_R (CH_4)	t_R (CO_2)	k'(CH_4)	k'(CO_2)	Sep. factor(α) (CO_2/CH_4)
GLY-Et-M	0.4	0.9	3.0	5.7	20.4	3.6
TPP-M	0.4	0.4	1.1	1.9	6.9	3.7
TMA-M	1.0	3.4	31.5	23.2	224	9.7
TMA-H	0.8	2.5	26.2	16.9	186	11.0
Na-M	0.2	0.2	0.3	0.4	1.1	2.0

While large separation of CH_4/CO_2 was observed for the column of TMA-M, relatively poor separations were observed for GLY-Et-M and TPP-M columns. No separation was observed for Na-montmorillonite. In the case of Na-M, the interlamellar distance (2.8Å) makes the interlamellar spaces inaccessible to the gas molecules with kinetic diameter larger than 2.8Å. The gas molecules have adsorption/desorption equilibrium only on the external surface. Therefore the differences in adsorption/desorption processes for air, CH_4 and CO_2 on the external surfaces are very similar such that no separation can be achieved in a short Na-montmorillonite column. The poor separation for CH_4/CO_2 in the case of TPP-M might be attributed to the large amounts of mesopores (pore size: 40Å, 200Å in diameter) in this sample as indicated in chapter 5. As a result, the gas molecules can be easier adsorbed into the mesopores and subsequently desorb from these pores. It is also noted that the retention times of CO_2 and CH_4 in TMA-M are higher than that in GLY-Et-M. In these two cases, the interlamellar distances (d_1) are in the range 4.0-5.0Å, but the size of the two intercalated cations are quite different, TMA^+ being smaller than GLY-Et^+. As a result,

TMA-M has much larger free siliceous surfaces than GLY-Et-M. These results indicate that the retention times of CH_4 and CO_2 are highly dependent upon the nature of the intercalated cations and thus the microporosity of the organo-clays. The cylindrical CO_2 molecule (dimensions 3.3Å by 5.3Å), constrained in a space of reduced dimensionality, is strongly interacting with the aluminosilicate surface, in strong contrast with the spherical, non-polar, CH_4 molecule (diameter 3.8Å).

The above results strongly suggest that the separation methane/carbon dioxide is principally controlled by interactions with the clay surfaces, not by the interactions with the polar alkylammonium chain. This means that organo-smectites with higher microporosity would provide better separation for CH_4/CO_2. Reducing the cation size is one way to increase the free interlayer surface area, thus the microporosity of the organo-smectites. Another approach to obtain a larger free interlayer surface area is to increase the charge density of the intercalated cation. The effects will be seen in the second system of organo-smectites with quaternary ammonium derivative dications. In this system, the interlamellar distances are also in the range 4.6-5.1Å, slightly larger than the kinetic diameter of CH_4 and CO_2. The retention times of air, CH_4 and CO_2 on these organo-smectites are given in Table 6.2. As noted, the CO_2 retention times decreased with an increase of the size of the cation intercalated. Separation factors 8.1 and 8.9 were achieved in the cases of LYS-Me-M and ORN-Me-M respectively. The effect of the charge density of the intercalated cation can be seen when comparing the quaternary ammonium derivatives of the amino esters LYS-Me^{2+} and ORN-Me^{2+} with the quaternary ammonium derivative of the amino ester GLY-Et^{+} given in Table 6.1. Although the size of GLY-Et^{+} and ORN-Me^{2+} are similar, the charge density of ORN-Me^{2+} is approximately twice as much as that of GLY-Et^{+}. ORN-Me-M provides more free interlayer surface area than GLY-Et-M and accordingly the separation of CH_4/CO_2 on ORN-Me-M is much better than on GLY-Et-M.

Table 6.2 Retention parameters of air, CH_4 and CO_2 on organo-smectite columns with di-cations at 30°c (He flow rate: 25ml/min).

Column	t_R(Air)	t_R (CH_4)	t_R (CO_2)	k'(CH_4)	k'(CO_2)	Sep. factor(α)
ORN-Me-M	0.7	2.1	16.1	14.0	114	8.1
LYS-Me-M	0.6	1.6	13.1	10.4	92.6	8.9
ORN-Me-H	0.6	1.5	13.2	9.7	93.3	9.6
LYS-Me-H	0.9	1.7	9.7	11.1	68.3	6.2

On the basis of the above results, it appears that the larger the free interlayer surface area is in the organo-smectite, the greater the separation of CH_4/CO_2 can be achieved. The free siliceous surface area plays a role in the separation of these gaseous mixtures. On the other hand, the functional groups in the intercalates play only a minor role in the separation mechanism. In addition, an optimum separation is obtained when the height of the galleries is slightly larger than the kinetic diameter of the gases. As further evidence supporting this conclusion, one should consider the results obtained for alumina-pillared montmorillonite. This Al_{13}^{7+}-pillared montmorillonite did not permit the separation of CH_4/CO_2 mixture. In this case, the height of the galleries network (7.4Å) is much larger than the kinetic diameter of the two gases and therefore the interaction of the CO_2 with the siliceous surface would be dramatically reduced.

In order to confirm the above interpretations, some other quaternary polyammonium cations with higher charge density were prepared including $MMDA^{2+}$, $MDEA^{2+}$ and

$MTETA^{4+}$. In some cases, the surface area per unit charge of cation is smaller than that for the cations in the first two systems and therefore the corresponding organo-smectites have relatively larger free interlamellar surface area. The retention parameters of air, CH_4 and CO_2 on these organo-smectites are shown in Table 6.3. The interlamellar distances of these organo-smectites are again in the range 4.3-5.1Å. Among these higher charged cations, $MMDA^{2+}$ has the smallest surface area per unit charge and the free interlamellar surface area in MMDA-M is the greatest. The retention times of CH_4 and CO_2 were found to be the largest in the MMDA-M column. This is a further indication that the siliceous surfaces of the organo-clays is a important factor for the separation of CH_4/CO_2.

Table 6.3 Retention parameters of air, CH_4 and CO_2 on organo-smectites with higher charge density cations at 30°c (He flow rate: 25ml/min).

Column	t_R(Air)	$t_R(CH_4)$	$t_R(CO_2)$	k'(CH_4)	k'(CO_2)	Sep. factor(α) (CO_2/CH_4)
MMDA-M	1.36	4.08	36.72	28.1	261.3	9.3
MDEA-M	0.81	2.03	25.63	13.3	181.9	13.7
MTETA-M	1.05	2.6	34.5	17.6	245.4	13.9
MMDA-H	1.01	2.97	27.34	20.2	194.3	9.6
MDEA-H	0.78	1.86	25.00	12.3	177.6	14.4
MTETA-H	0.55	1.48	25.70	9.6	182.6	19.1

Figure 6.6 shows typical chromatograms for the separation of air/CH_4/CO_2 by four different columns as discussed above. While no separation was observed for Na-montmorillonite, CO_2/CH_4 separation factors of 8.1 and 13.9 were obtained for

ORN-Me-M and MTETA-M, respectively. The retention times of CO_2 and CH_4 on these microporous organo-smectites can be correlated to the microporosity of the organo-smectite as compared the retention times of CH_4/CO_2 with the microporosity, as shown in Table 6.4. As noted, the retention times of CH_4 and CO_2 increase with an increase of the microporosity in the organo-smectites.

Table 6.4 Comparison of GC parameters of air, CH_4 and CO_2 on various organo-smectite columns with BET surface and microporosity

Organo-smectite	BET surface (m^2/g)	Microporosity (%)	$t_R(CH_4)$	$t_R(CO_2)$
GLY-Et-M	77.3	7	0.9	3.0
TPP-M	55.9	0	0.4	1.1
LYS-Me-M	56.6	27	1.6	13.1
TMA-M	210.3	78	3.4	31.5
MMDA-M	194.1	77	4.1	36.7

The charge density of the smectite clay can also affect the retention times of CH_4 and CO_2. Since the charge density is higher in hectorite than in montmorillonite, the organo-montmorillonite provides larger free surface area than the corresponding organo-hectorite. Also, the interlamellar distances in organo-hectorites are slightly larger than that in the corresponding organo-montmorillonites. These two effects are attributed to the relatively larger retention values for the organo-montmorillonites compared to the corresponding organo-hectorites (Tables 6.1-6.3).

To compare the gas chromatographic retention results systematically with the size of

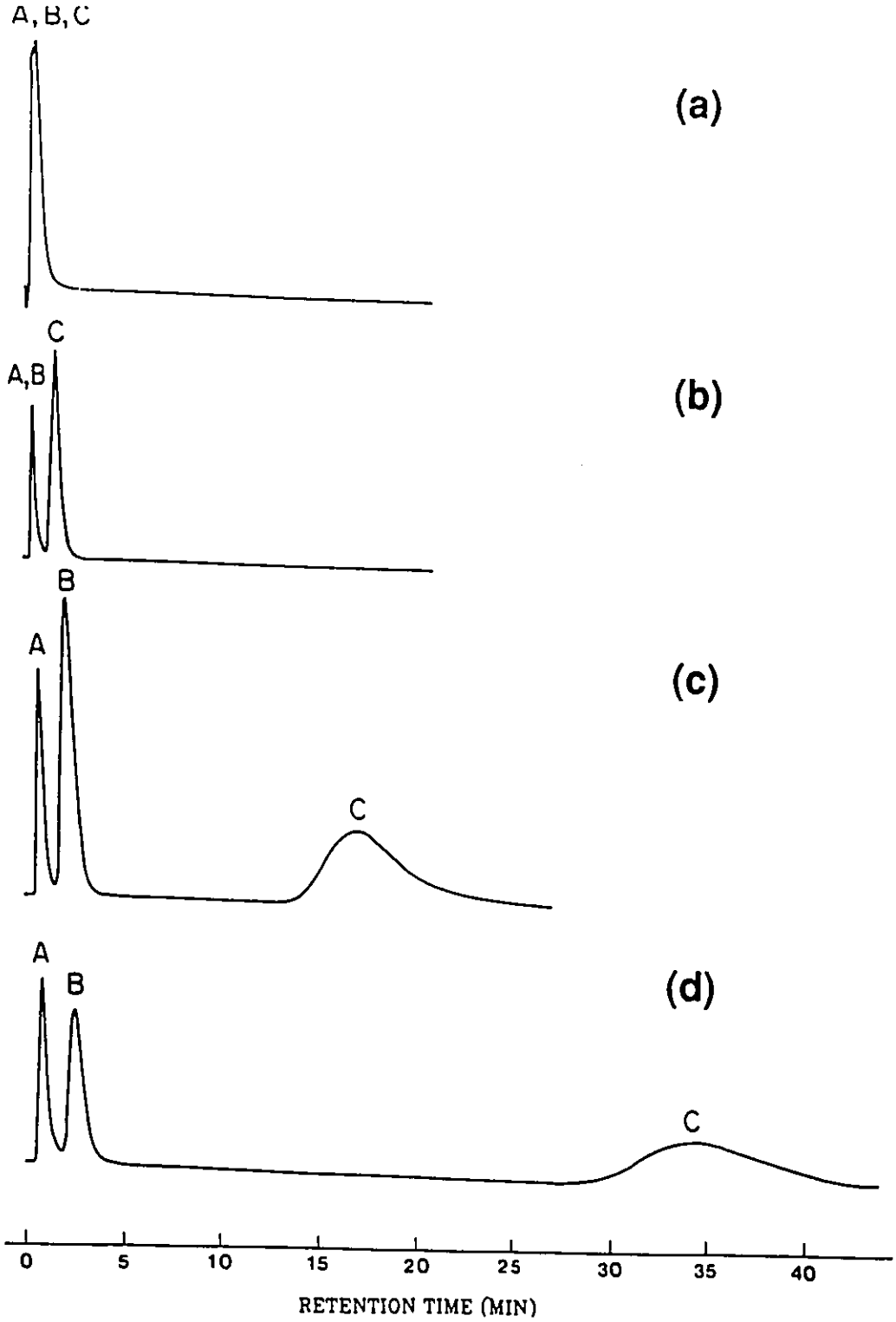

Figure 6.6 Chromatograms for the separation of air, CH_4 and CO_2 by organo-montmorillonites. Columns: 3ft x 1/8 in.o.d. Carrier gas: He at 25ml/min. Column temperature: 30°c. (a) Na-montmorillonite; (b) GLY-Et-montmorillonite; (c) ORN-Me-montmorillonite; (d) MTETA-montmorillonite. Peak identification: A=air; B=methane; C=carbon dioxide.

intercalates and subsequently the free interlayer surface area of the organo-smectites, a calculation for the free surface area of the organo-smectite is necessary.

6.4.2 Calculation of free interlayer surface area of organo-smectite clays

The total surface area of clays can be calculated from their CECs and the chemical formulas as described in chapter 5. The charge density (cd) of the smectite is derived from the CEC value and the total surface area of the clay[68]. The charge densities of SWy-1 and SHCa-1 are calculated as follows:

SWy-1:

$$cd = (740 \times 10^{20}\ \text{Å}^2/\text{g})/(6.023 \times 10^{23} \times 0.87 \times 10^{-3}\ \text{charge/g})$$

$$= 141\text{Å}^2/\text{charge}$$

SHCa-1:

$$cd = (725 \times 10^{20}\ \text{Å}^2/\text{g})/(6.023 \times 10^{23} \times 0.89 \times 10^{-3}\ \text{charge/g})$$

$$= 134\text{Å}^2/\text{charge}$$

The calculation shows that the surface area per unit charge in SWy-1 and SHCa-1 are 141Å^2 and 134Å^2, respectively. Because of the stacked structure of clays, the surface area per charge in each sheet of SWy-1 and SHCa-1 are 70Å^2 and 67Å^2, respectively. Figure 6.7 illustrates the unit surface area in the layered clay.

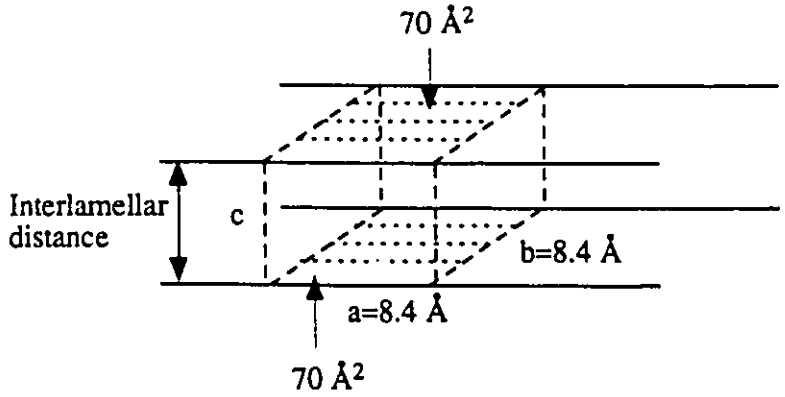

SWy-1: Charge density = 141 Å^2 / charge

Figure 6.7 Schematical representation of a unit squared surface of SWy-1

It is assumed that the charge distribution in the clays is homogeneous and therefore the unit surface is assumed to be squared. The dimensions of the unit square surface area in SWy-1 and SHCa-1 are thus $(8.4)^2$ and $(8.1)^2$Å^2, respectively. The X-ray diffraction studies of the organo-smectites have showed that the side chains of the organic derivatives must lie parallel to the clay surfaces. Therefore, the surface area occupied by the cation can be estimated from the cross-sectional surface area of the cation. The cross-sectional surface area of the cation can be calculated by measuring the projection surface area of its CPK molecular model with a flat orientation. The subtraction from 140Å^2 of twice the value of the cross-sectional area of the organic cation affords the free surface area per charge of the organo-clay. For example, the free interlayer surface area of GLY-Et-M is calculated from the unit charge density of montmorillonite and the cross-sectional surface area of the cation (60 Å^2/ion):

$$FSA_{GLY\text{-}Et\text{-}M} = 141 Å^2/ch - 2 \times 60 Å^2/ion = 21\ Å^2/ch$$

However, this calculation is only valid for the case of organic monocations. More generally, the free surface area per charge of this organo-clay (FSA, in $Å^2$) is given by the following equation[8]:

$$FSA = (n \times SAC - 2 \times CSA) / n \qquad (6\text{-}11)$$

where FSA is the free surface area of the organo-clay, SAC the surface area per unit charge of the clay, CSA the cross-sectional surface area of the cation and n the cation charge. The calculated free surface area of the organo-smectites and the gas chromatographic retention times of CH_4 and CO_2 on organo-montmorillonites and organo-hectorites are shown in Table 6.5 and 6.6.

By comparing the retention times of CH_4 and CO_2 with the calculated free surface area of the organo-smectites, it appears, in general, that both the retention times of CH_4 and CO_2 increase with the increase of free surface area of the organo-smectites. Figure 6.8 and 6.9 show the relationship between the retention times of CH_4 and CO_2 on various organo-smectite columns and the aluminosilicate surface area not covered by organic cations (free surface area).

Table 6.5 Gas retention parameters, interlamellar distances, and calculated free surface area of organo-montmorillonites.

Column	charge of cation	$t_R(CH_4)$	$t_R(CO_2)$	Interlayer spacing (Å)	CSA of cation (Å^2/ion)	FSA (Å^2/ch)
GLY-Et-M	+1	0.94	3.00	4.0	60	21
TPP-M	+1	0.40	1.10	9.2	102	---
TMA-M	+1	3.40	31.50	4.3	29	83
OP[illegible]-Me-M	+2	2.10	16.10	4.4	88	53
LYS-Me-M	+2	1.60	13.10	4.6	93	48
MMDA-M	+2	4.10	36.60	4.3	47	94
MDEA-M	+2	2.00	25.60	4.4	60	81
MTETA-M	+4	2.60	34.50	5.1	102	90
Na-M	+1	0.20	0.30	2.8	---	–

Table 6.6 Gas retention parameters, interlamellar distances, and calculated free surface area of organo-hectorites

Column	charge of cation	$t_R(CH_4)$	$t_R(CO_2)$	Interlayer spacing (Å)	CSA of cation (Å^2/ion)	FSA (Å^2/ch)
TMA-H	+1	2.50	26.20	4.6	29	76
ORN-Me-H	+2	1.50	13.20	4.8	88	47
LYS-Me-M	+2	1.70	9.70	5.0	93	42
MMDA-H	+2	2.97	27.34	4.7	47	87
MDEA-H	+2	1.86	25.00	4.9	60	74
MTETA-H	+4	1.50	25.70	5.0	102	83

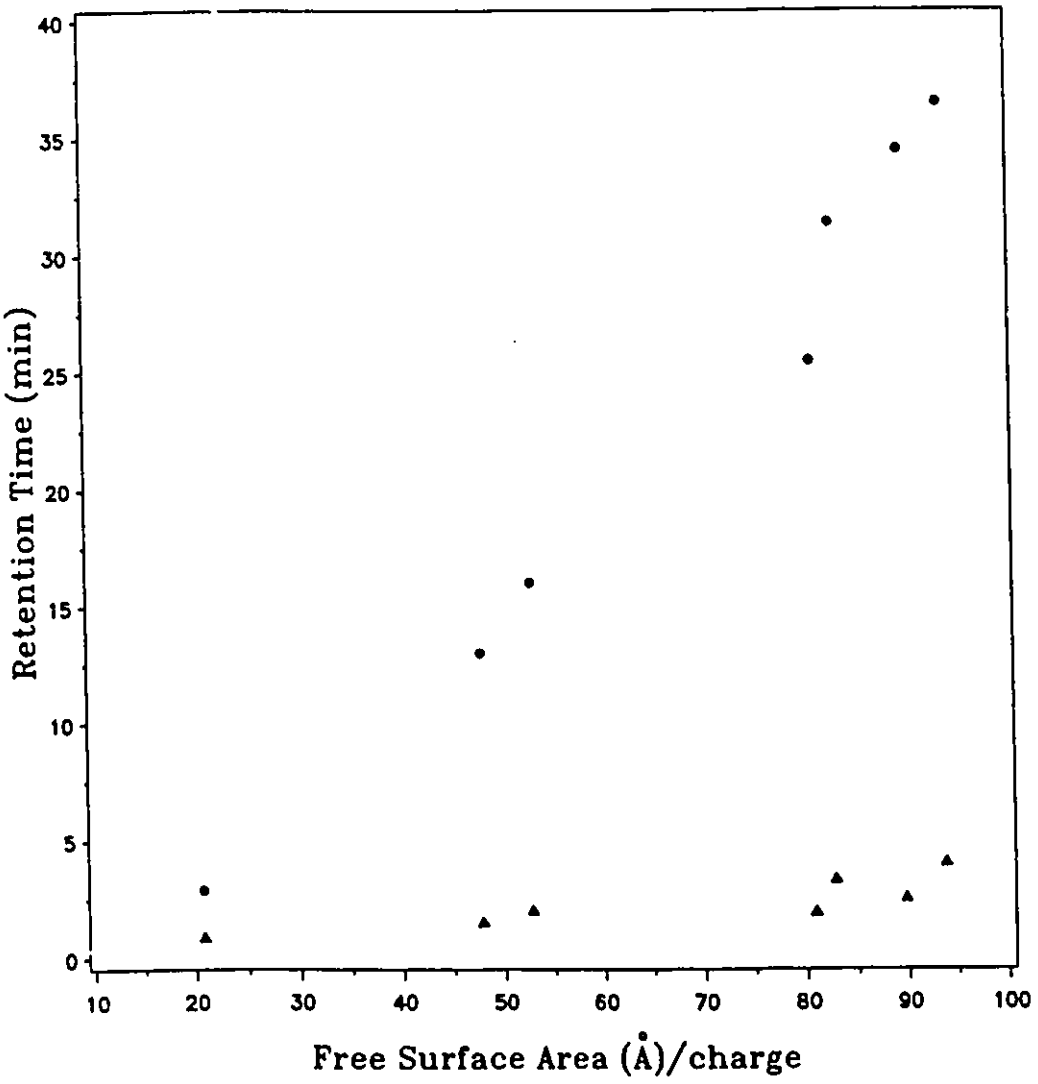

Figure 6.8 Retention time of methane (▲) and carbon dioxide (●) on a series of organo-montmorillonites as a function of the free surface area per charge of the organo-montmorillonite.

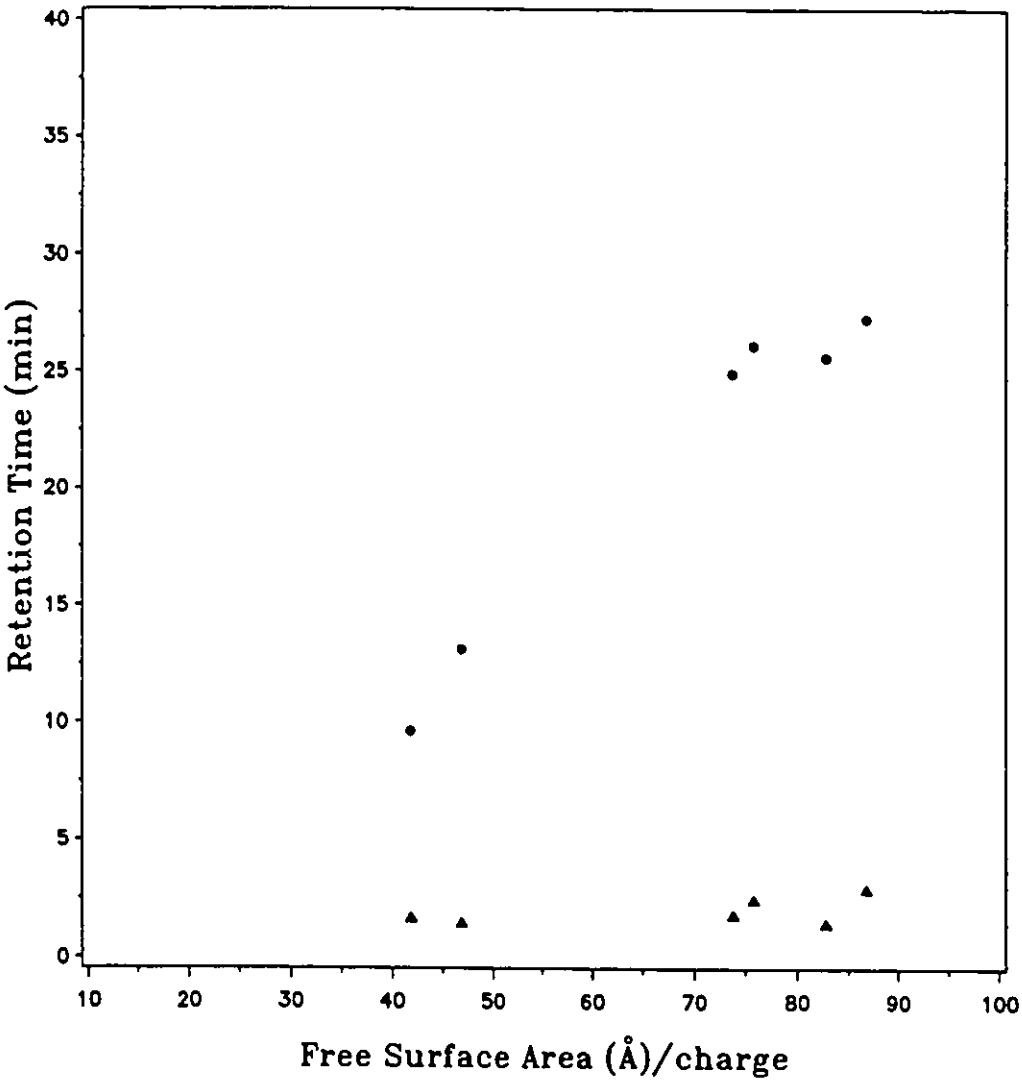

Figure 6.9 Retention time of methane (▲) and carbon dioxide (●) on a series of organo-hectorites as a function of the free surface area per charge of the organo-hectorite.

6.4.3 *Separation mechanisms for organo-smectites*

As mentioned in the beginning of the chapter, the adsorptive gas separation can be achieved by one of three mechanisms: steric, kinetic or equilibrium effects[126]. There are several possible chromatographic pathways for the separation of CH_4/CO_2 on the microporous organo-clays. Firstly, there might be an adsorption of gas molecules to the alkylammonium chains of the cations. It has already been pointed out that the retention times for CH_4 and CO_2 decrease with an increased size of the cation. This suggests that sorption on the intercalated cation is not the major pathway. Secondly, an alternate interpretation for the long retention times of CO_2 could be a chemical interaction with residual water molecules on the clay surface. This interpretation can be ruled out since very short retention times of CO_2 were observed when the samples were not, or imperfectly, dried, plausibly because of the decrease of microporosity. Also, the conditioning of the organo-smectite columns prior to use as chromatographic adsorbent removes the surface water. Table 6.7 shows the retention times of CO_2 on a MMDA-M column as a function of heating temperature and heating times used in the conditioning procedure. As noted, the retention times of CO_2 increased with the increase of the heating temperature and time, and finally the retention times remain constant. This experiment demonstrated that the heating treatment removed the water retained within the surface of the organo-smectite. Thirdly, separation of CH_4/CO_2 can occur on the basis of their dimensions or steric configurations (microsieve effect). However, the increasing sequences for the CH_4/CO_2 retention times are not in the same order as the increasing molecular diameter of the gases. The microsieve effects are not dominant in the case of CH_4/CO_2. Finally, the strong interaction of the CO_2 with the siliceous sheets could account for the separation of CH_4 and CO_2. Owing to the electronic structure of CO_2, carbonate could be transiently formed by binding of the carbon atom to the framework of oxygen or hydroxyl groups, as was shown, for example, for ion-exchanged zeolites[148] or for mica[149]. The larger the clay surfaces available in the

organo-clays the stronger is the interaction between the CO_2 and the clay surfaces. However, at this stage, we cannot distinguish between the physisorbed and chemisorbed CO_2.

Table 6.7 Retention times of air and CO_2 as a function of heating temperature and heating time on a MMDA-M column.

Heating temperature	30 °C	60 °C	90 °C	90 °C
Heating time	12 hr	3 hr	8 hr	8 hr
t_R (air)	0.56	0.86	1.34	1.36
t_R (CO_2)	13.50	18.58	36.52	36.72

In addition, the retention times of N_2 and O_2 were found to be smaller than that of CH_4 and no separation for N_2/O_2 was observed so far in the organo-clays columns (Tables 6.1-6.4). The microsieving effects can be seen as one compares the GC results with the molecular sizes of N_2, O_2 and CH_4. In these cases, the order of increasing retention time parallels the order of increasing kinetic diameter of the gases as shown below:

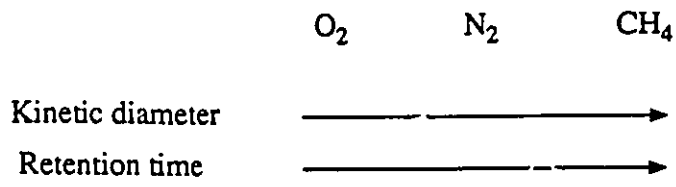

For N_2 and O_2, the adsorption/desorption equilibrium processes in the organo-clay are very similar because of their similar molecular sizes. Therefore, no separation could be achieved

in these organo-smectites which have a micropore size distribution.

Further evidences for the microsieving effects can be obtained from the retention values of carbon monoxide. The retention times of CO on various organo-smectites are given in Table 6.8. The CO retention times were smaller than that of CH_4, but larger than that of N_2 and O_2. It is also noted that the CO retention time increases slightly as the microporosity of the organo-clays increases. Since CO has a similar kinetic diameter as nitrogen and oxygen molecules, the retention of CO is close to that of N_2 and O_2. The relatively larger retention times of CO compared to N_2 and O_2 are attributed to the polar property of CO molecule. These results indicate that microsieving does occur, especially on the organo-clays with larger microporosity.

Table 6.8 Retention times (min) of CO and CO_2 on various organo-smectites at 30°C and He flow rate 25ml/min.

Column	$t_R(N_2, O_2)$	$t_R(CO)$	$t_R(CO_2)$
LYS-Me-M	0.44	0.56	13.10
LYS-Me-H	1.02	1.02	9.70
ORN-Me-M	0.62	0.62	16.10
ORN-Me-H	0.52	0.63	10.80
TMA-M	1.05	1.45	31.50
TMA-H	0.82	1.14	26.24
MMDA-M	1.36	1.84	36.60
MMDA-H	0.81	1.08	27.34
MDEA-M	1.13	1.64	25.60
MDEA-H	0.65	0.92	25.00
MTETA-M	1.05	1.30	34.50
MTETA-H	0.49	0.67	25.40

So far, it has been shown that the gases such as air, CO, CH_4 and CO_2 can be separated by using organo-smectite columns. Figure 6.10 gives a chromatogram showing

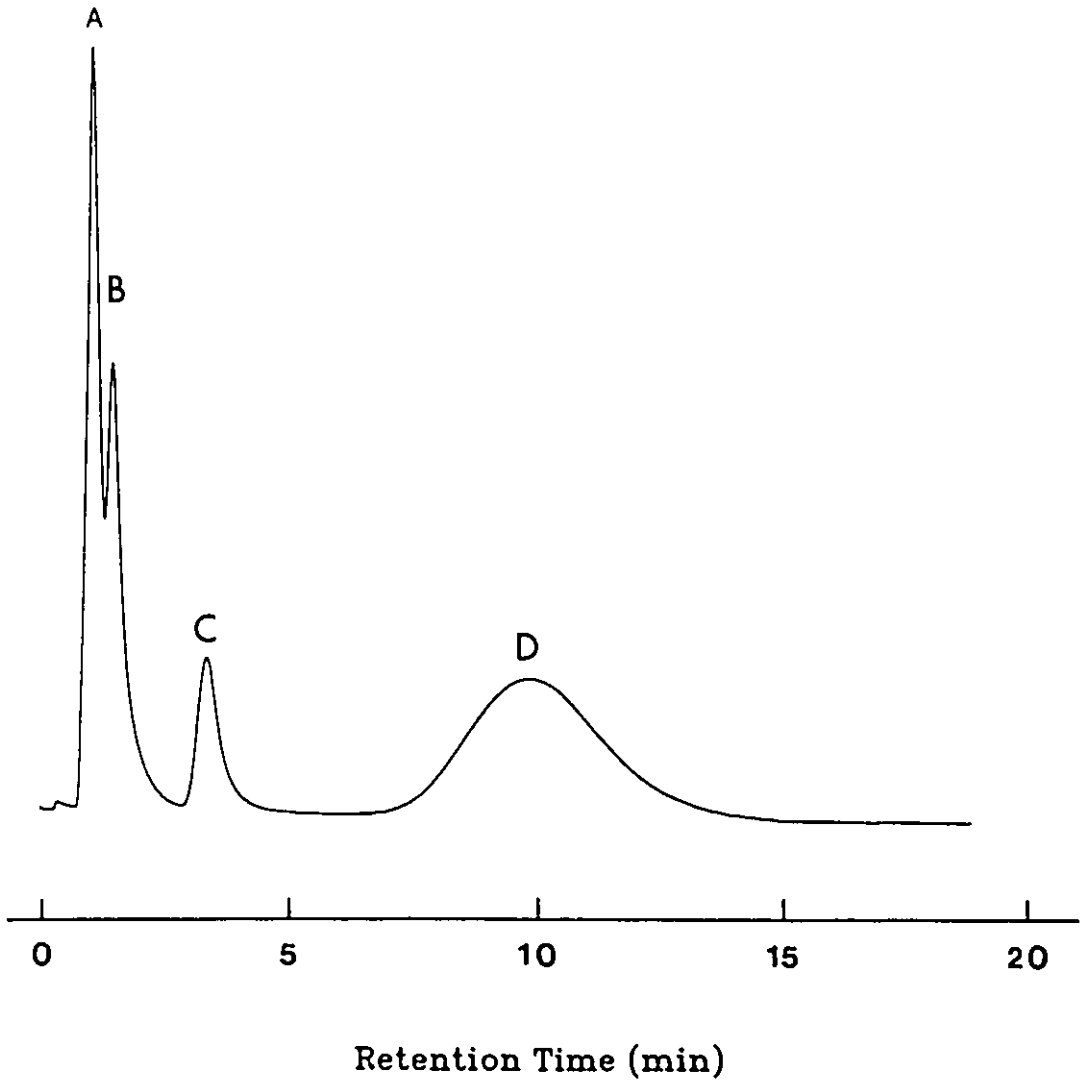

Figure 6.10 Chromatographic separation of air, CO, CH_4 and CO_2 by a MMDA-montmorillonite column. Columns: 3ft x 1/8 in.o.d. Carrier gas: He at 25ml/min. Column temperature: 30°C hold 4 min. then to 100°C at 10°C/min. Peak identification: A=air; B=carbon monoxide; C=methane; D=carbon dioxide.

complete separation of air, CO, CH_4 and CO_2 by a MMDA-M column where a temperature program was used. A good separation of various inorganic gases could be achieved in a short organo-clay column. Further chromatographic studies on these organo-smectites will be explored for the separation of C_1-C_4 and C_5-C_8 hydrocarbons.

6.4.4 Separation of C_1-C_4 and C_5-C_8 hydrocarbons by organo-smectites

Separation of C_1-C_4 is important for the petro-chemical industry. Consumption of energy in the cryogenic separation of the lower hydrocarbons which are formed in many processes is rather high. This leads to large investment in the processing of these gases by other technology[150]. Adsorption and membrane separation processes look quite promising for this purpose. The utilization of organo-clays as chromatographic adsorbents for the separation of C_1-C_4 hydrocarbons has been reported in the literature in which the retention times of C_1-C_4 hydrocarbons were related to the surface area and the interlamellar distance of the organo-clay.[133,134,137,138,140,141,151].

In order to determine the separation efficiency of organo-smectites for C_1-C_4 and C_5-C_8 hydrocarbons, several organo-smectites were used for this study. Usually, the chromatographic separation was performed in a 3ft x 1/8in. o.d. column. In some cases, a very short column, 9in x 1/8in o.d., was used to get a sharp separation for C_1-C_4 hydrocarbons. Due to the relatively higher molecular weight of hydrocarbons, higher temperature (140°C) and higher He flow rate (35 ml/min) than those used for CH_4/CO_2 separation were applied to reduce the retention time of hydrocarbons on these organo-smectites.

The retention times of C_1-C_4 hydrocarbons on various organo-smectites are shown in Table 6.9 and Table 6.10. The retention times of hydrocarbons on the organo-clay columns were observed to be larger than that on the Na-montmorillonite column. No measurable separation was observed for Na-M column. In contrast, complete separations of

C_1-C_4 hydrocarbons were observed in all the organo-smectite columns. In the case of Na-M column, the interlamellar spaces were inaccessible to the hydrocarbon molecules. As a result, the hydrocarbon molecules took the external paths and therefore the differences in the adsorption/desorption processes for various hydrocarbons were not enough to allow separation to occur. The longer retention times on the organo-clay columns are attributed to the fact that the hydrocarbons can be adsorbed in the micropores. The retention times of C_1-C_4 hydrocarbons are also seen to increase with the increase of carbon number of the hydrocarbons. This is illustrated in Figure 6.11, showing the relationship between the retention time of C_1-C_4 hydrocarbons on the organo-hectorites and the carbon number of hydrocarbons. This indicates that microsieving does occur in these organo-clay samples.

Table 6.9 Retention times of C_1-C_4 hydrocarbons on various organo-hectorites at 140°C and He flow 35 ml/min.

Column	Spacing(Å)	$t_R(C_1)$	$t_R(C_2)$	$t_R(C_3)$	$t_R(C_4)$
TMA-H	4.6	0.29	2.06	6.14	22.80
LYS-Me-H	5.0	0.47	2.24	8.38	34.19
ORN-Me-H	4.8	0.30	1.83	6.88	32.48
MMDA-H	4.7	0.29	1.94	5.87	21.82
MDEA-H	4.9	0.22	1.81	6.50	28.83
MTETA-H	5.0	0.17	1.14	4.46	20.38

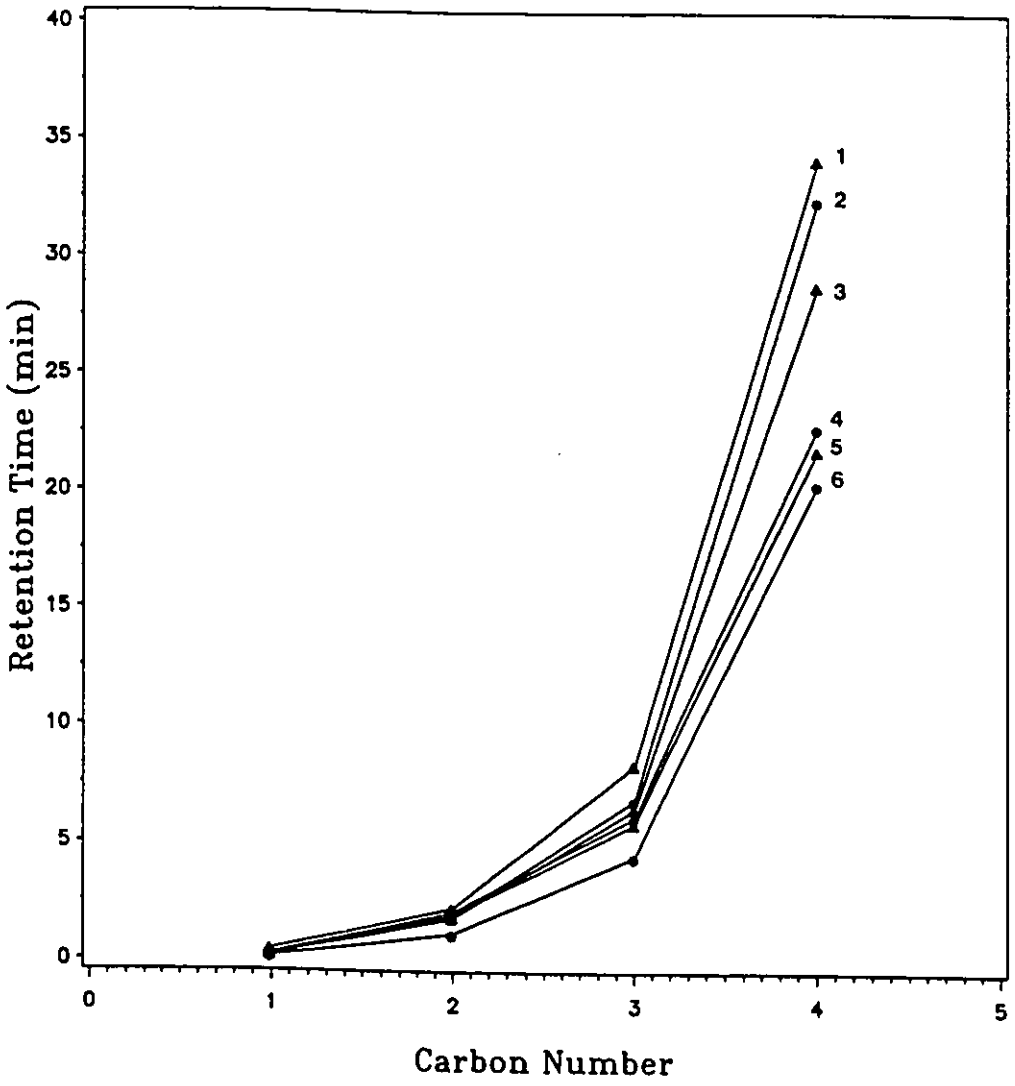

Figure 6.11 Retention time of C_1-C_4 hydrocarbons on various organo-hectorites vs. carbon number of the hydrocarbons. (1) LYS-Me-hectorite; (2) ORN-Me-hectorite; (3) MDEA-hectorite; (4) TMA-hectorite; (5) MMDA-hectorite; (6) MTETA-hectorite.

Table 6.10 Retention times of C_1-C_4 hydrocarbons on various organo-montmorillonites at 140°C and He flow 35 ml/min (*column temperature 30°C).

Column	Spacing(Å)	$t_R(C_1)$	$t_R(C_2)$	$t_R(C_3)$	$t_R(C_4)$
Na-M	2.8	0.10	0.10	0.10	0.10
TPP-M*	9.2	0.54	1.10	2.50	7.50
LYS-Me-M	4.6	0.66	2.63	8.30	32.08
ORN-Me-M	4.5	0.35	1.94	6.14	29.31
MMDA-M	4.3	0.33	2.35	6.54	24.94
MDEA-M	4.4	0.37	3.39	12.99	63.20
MTETA-M	5.1	0.28	1.58	5.23	24.30
TMA-M	4.3	1.64	5.15	---	---

In the case of TMA-M column, however, much longer retention times for C_1 and C_2 were measured, and the C_3 and C_4 hydrocarbons were totally adsorbed or trapped in the smectite The dimensions of the micropores in this sample and the cross-sectional dimensions of C_3 molecule are estimated as below:

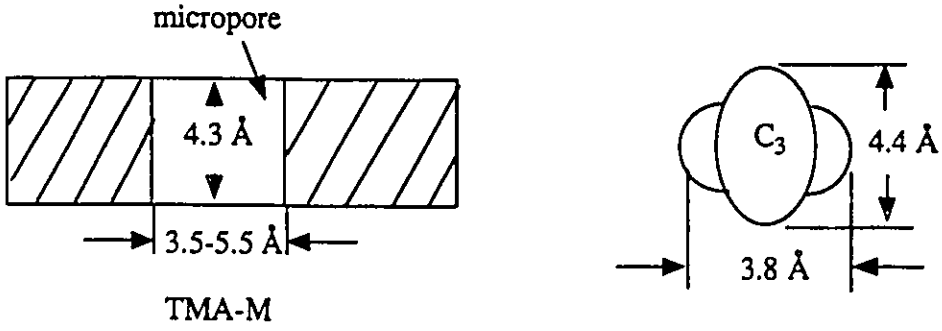

As can be seen, the smaller dimension of the C_3 molecule is larger than the lower limit of the micropore dimensions so that the C_3 molecule is totally trapped in the micropores. Similarly, C_4 molecule would be trapped in the micropores. Further evidences can be obtaind from the retention times of C_3/C_4 hydrocarbons on the MDEA-M column where larger retention times were recorded. Again, the dimensions of the micropores in this sample limit the adsorption/desorption process. This is a good indication of the microsieving effects for these organo-clays.

Contrary to the case of the CH_4/CO_2 separation, the retention times are smaller in the cases where a large free interlamella. surface was estimated. This suggests that the retention parameter of hydrocarbons are correlated to the micropore volume. The correlation between the retention times of hydrocarbons and the micropore volumes of are shown in Table 6.11. As can be seen, the retention times of C_3 and C_4 hydrocarbons decrease with an increase of the micropore volume. However, much smaller retention times of hydrocarbons were observed in TPP-M column in which large amounts of mesopores were found (Chapter 5). In this case, the C_1-C_4 separation could be achieved at room temperature as shown in Figure 6.12. This column could be used to separate higher hydrocarbons (C_5-C_8) due to the larger mesopores (Figure 4.13). Furthermore, a sharp separation of C_1-C_4 hydrocarbons could be achieved in a very short MMDA-hectorite column (9 in. x 1/8 in.o.d.) where a temperature program and higher flow rate were used as shown in Figure 6.14.

Table 6.11 Retention times of C_1-C_4 hydrocarbons on various organo-smectites and pore volumes of the corresponding organo-smectites at 140°C (He flow rate: 35 ml/min).

Column	Spacing (Å)	$t_R(C_1)$	$t_R(C_2)$	$t_R(C_3)$	$t_R(C_4)$	Pore Vol. (Å^3/ch)
LYS-Me-H	5.0	0.47	2.24	8.38	34.19	275
ORN-Me-H	4.8	0.30	1.83	6.88	32.48	283
MDEA-H	4.9	0.22	1.81	6.50	28.83	363
MMDA-H	4.7	0.29	1.94	5.87	21.82	409
MTETA-H	5.0	0.17	1.14	4.46	20.38	415

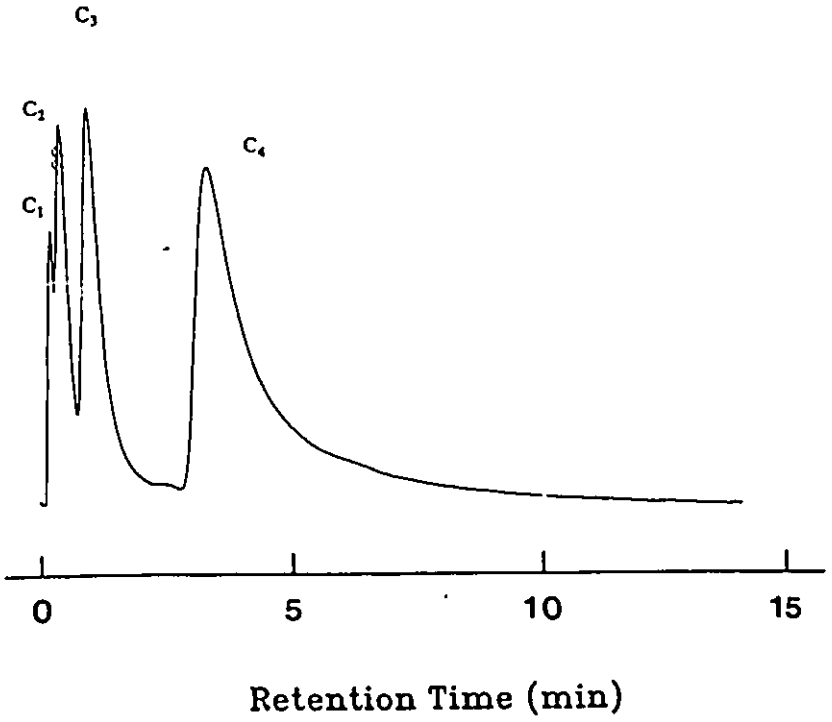

Figure 6.12 Chromatographic separation of C_1-C_4 hydrocarbons by a TPP-montmorillonite column. Columns: 3ft x 1/8 in.o.d. Carrier gas: He at 35ml/min. Column temperature: 30°C.

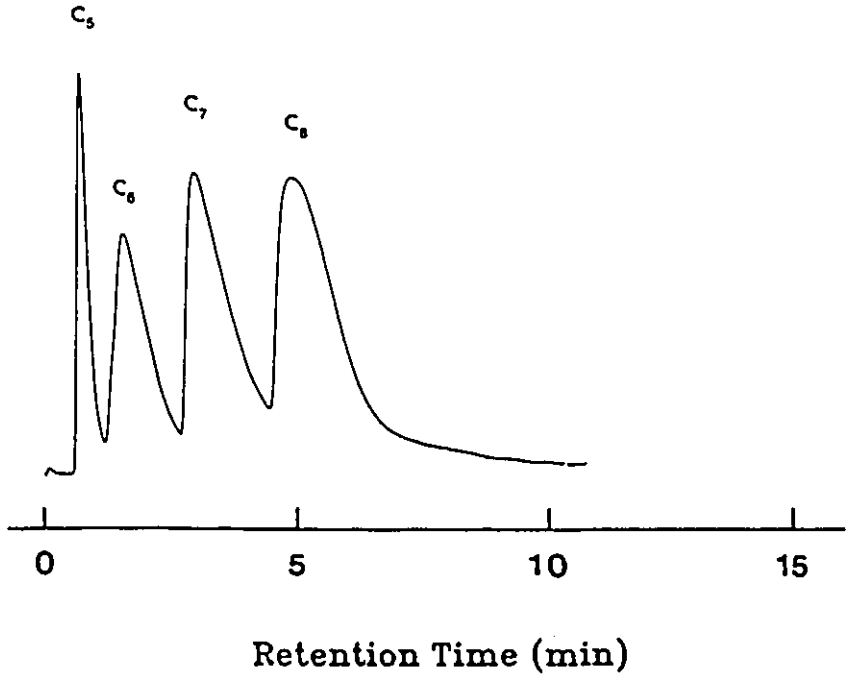

Figure 6.13 Chromatographic separation of C_5-C_8 hydrocarbons by a TPP-montmorillonite column. Columns: 3ft x 1/8 in.o.d. Carrier gas: He at 45ml/min. Column temperature: 90°C hold 1 min., then to 170°C at 20°C/min.

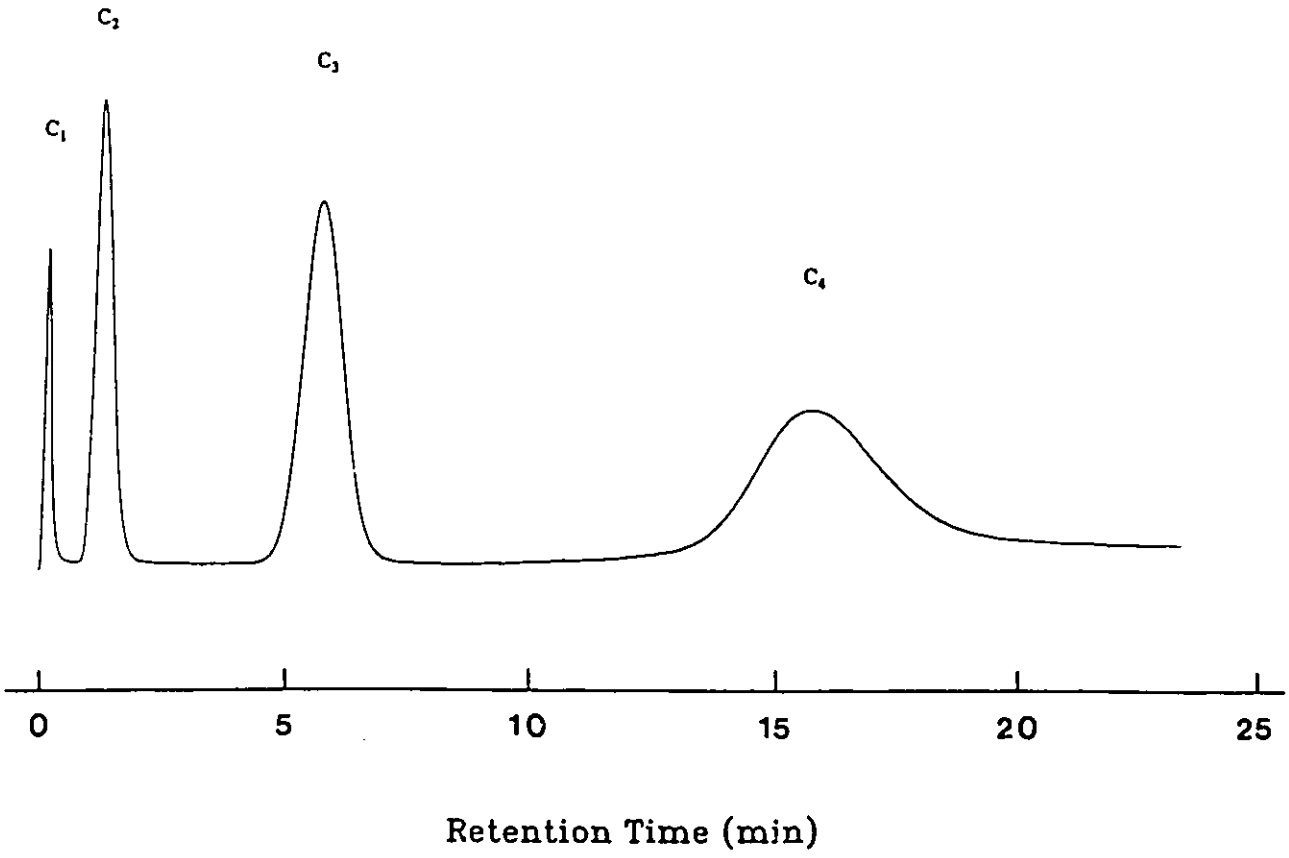

Figure 6.14 Chromatographic separation of C_1-C_4 hydrocarbons by a MMDA-montmorillonite column. Columns: 9 in. x 1/8 in.o.d. Carrier gas: He at 50 ml/min. Column temperature: 70°C hold 4min., then to 90°C at 10°C/min.

6.5 Conclusions

The gas chromatographic separation capacity of organo-smectites containing different quaternary ammonium cations and quaternary polyammonium cations were investigated. The microporous organo-smectites proved to be an effective gas-solid chromatographic adsorbent for gas separations. The separation CH_4/CO_2 is controlled by the molecular interactions with the clay surface, not by interactions with the polar substituents of the alkylammonium chain. The shape of the microporous cavities played a role in reducing the dimensionality of the chromatographic pathways. The height of the galleries (4.0-5.0Å) should be slightly higher than the kinetic diameter of the gases. The retention times of CH_4 and CO_2 on the organo-smectites were related to the microporosity of the organo-smectites. Microsieving effects were observed in the cases of N_2, O_2, CO and C_1-C_4 hydrocarbons, in which the increasing retention times were in the same order as the increasing molecular diameter of the gases. Moreover, it was shown that the retention times of C_1-C_4 hydrocarbons on the organo-smectites were controlled by the micropore volumes. More importantly, the GC results demonstrated that the organo-clays could provide large flexibility in controlling the pore size for the separation purposes.

Chapter 7

Gas Permeations in Organo-smectite-Polymeric Composite Membranes

7.1 Introduction

As described in chapter 6, gas separations are very important industrial processes which can be achieved by several approaches, including adsorption, cryogenic and membrane processes. Among these separation methods, membrane separation are viewed as a simplification of the present technology. Today, gas separation with membranes is widely accepted in the traditional chemical and petroleum refining industries[152]. A number of membrane plants are used for the separation of carbon dioxide from mixtures with hydrocarbons in OER processes[26]. Removal of hydrogen sulfide and carbon dioxide from natural gas is an ideal application for membranes since both H_2S and CO_2 permeate through the membrane much faster than methane[153]. Few membrane plants are used for the separation of nitrogen from air for the inerting process[26].

Membranes are microporous barriers of polymeric, ceramic or metallic materials, that can be used in separation processes[26]. The driving force for separation of a given component is provided by differences in hydrostatic pressure across the membrane. The membranes considered for gas separation are microporous materials or effectively nonporous materials. The concept of gas separation with a membrane involves taking a

mixture of gases (A + B) and passing it over a membrane and A (or B) is collected in the permeate stream while gas B (or A) passes over the membrane to be collected in the nonpermeate stream as shown in Figure 7.1[124].

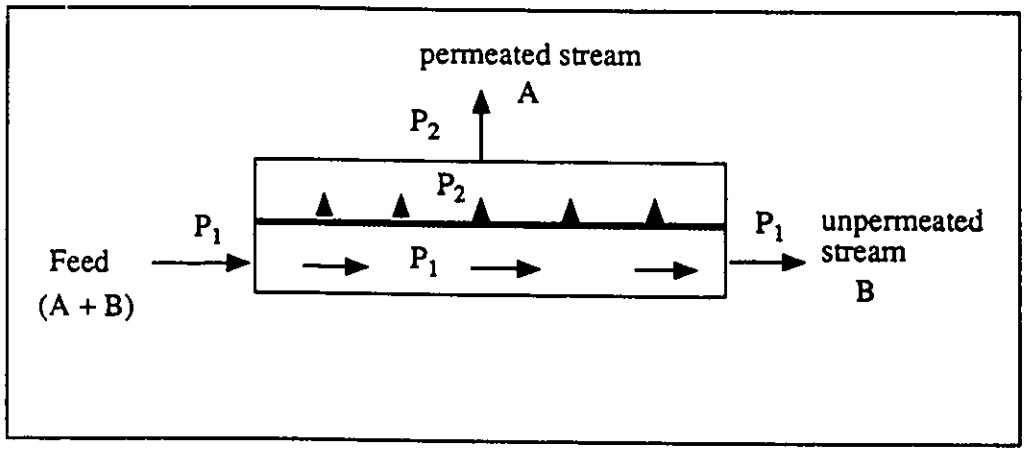

Figure 7.1 Schematic representation of a membrane separation system

Membranes may be classified according to their material, morphology and packaging geometry. There are many types of membrane materials available for the gas separations. Glassy polymers such as cellulose acetates, polysulfone, polyamides, polyimides and rubbery polymers such as silicone rubbers, nitrile rubbers are the most common polymeric materials. With respect to the economic standpoint, the membrane must exhibit high permeability, high selectivity, chemical inertness and mechanical stability. High permeability and selectivity are required in order to minimize the costs[26]. Polydimethylsiloxane (PDMS) is the most permeable of the polymeric materials to the gases, but shows very low selectivities[26,154]. In contrast, traditional glassy polymers have very high selectivities with permeation rates depending on the morphology of the membranes. Table 7.1 shows the gas selectivities for several different rubbery and glassy

polymers[25,26,155]. An asymmetric membrane which consists of a microporous layer (100-200μm thick) and a very thin (0.1-1.0μm) skin layer provides both high permeation rates and high selectivities[156,157]. The separation of gas mixtures through an asymmetric membrane occurs in its thin skin rather than in the porous layer such that high permeation rate and high selectivity result. A pure gas permeability ratio of 200 for CO_2/CH_4 could be achieved in an asymmetric cellulose acetate membrane[156]. Inorganic membranes have received much attention in recent years because they have advantages with respect to organic membranes due to their chemical and thermal stability and higher permeability[124,158,159]. The separation mechanism is controlled by Knudsen diffusion and surface diffusion. However, these separations have a relatively low selectivity. Recently, a separation factor of 65 for CO_2/CH_4 has been obtained in a modified microporous ceramic membrane[160]. It has been reported that zeolite-polymer membranes could be made by filling the zeolites into the polymer[161]. The filling of the zeolites caused very large increases in the diffusion time lag, but would have only minor effects on the steady-state permeation[162]. The separation of O_2/N_2 was increased from 2.99 to 4.06 by increasing the silicalite content of 25%[163]. Furthermore, the molecular sieve effect could be seen from the zeolite-polymer membranes for the separation of gas mixtures[161]. Recently, it was reported that filling of vermiculite and mica in polymer films resulted in a dramatical reduction of gas permeability[164].

It has been shown in chapter 6 that the microporous organo-clays are able to separate some gas mixtures via chromatographic route. In order to explore the possibility whether organo-clay materials can be used as membrane materials for continuous separation processes, some of the microporous organo-smectites were imbedded into rubbery polymers to make composite membranes. Furthermore, gas permeabilities of these organo-smectite-polymeric composite membranes were measured and the gas transport through the microporous organo-clay PDMS composite membranes was studied.

Table 7.1 Separation factors of rubbery and glassy polymers

Polymer	Ideal separation factor α(A/B)	
	O_2/N_2	CO_2/CH_4
	Rubbery polymers	
Polydimethylsiloxane	2.1	3.4
Natural Rubber	3.0	4.4
Butyl Rubber	3.9	6.6
	Glassy polymers	
Polysulfone	--	28
Cellulose acetate	--	31
Polyimide(6FDA-DAF)	--	51

7.2 Organo-smectite polymeric composite membranes

It has long been recognized that siloxane polymers, examplified by PDMS (polydimethylsiloxane), have much higher permeability to gases than most other polymer materials[154]. The uncross-linked polymers are widely used in the manufacture of cosmetics, food-processing materials, and medicinal preparations[165]. They are valued for their lubricity and their ability to lower surface tension and act as antifoam agents. The rigidity of the polymers depends on the molecular weight of the silicone. The siloxanes with lower molecular weight can be cross-linked to increase the molecular weights. Usually, four

processes are used to cure silicones[166]. In high-temperature vulcanizing (HTV) systems, polymers containing methyl or vinyl groups are cross-linked with peroxides. In room-temperature vulcanizing (RTV) systems, two cure methods are used[166]. In the older methods, silanols are condensed with a moisture-sensitive silane cross-linker, or a metal salt which catalyzes the reaction between silicon hydrides and silanols. The latter reaction liberates hydrogen which can be used to produce foamed products. The average polymer for heat cured rubber has aroud 7000 silicon units in the chain while the average RTV polymer has around 100 units in the chain. In addition to varying the molecular weight, important effects can be obtained by varying the structure of the polymer and the nature of the organic groups attached to the silicon atoms. A variety of groups including phenyl, vinyl and hydrogen can substitute for the methyl group in a silicone. For example, partial substitution of methyl with phenyl imparts improved high temperature oxidation resistance and also provides the greatest low temperature flexibility of any silicones, a property that is important in many low temperature applications, such as those encountered in the aerospace industry.

There is a wide variety of RTV systems commercially available. The most common type of RTV system is a one-package silanol condensation curing RTV system. The polymer in this system is usually a polydimethylsiloxane which is low in molecular weight and has hydroxyl end groups. A RTV system contains, a usual filler which is used to increase the strength and resistance to oxidation and hydrolysis, and a crosslinking system. The crosslinking system contains a trifunctional organosilane such as methyltriacetoxysilane, methyl-tris(ketoximino)silane, etc., and a catalyst such as dibutyltindilaurate. This combination of compounds is mixed by the manufacturer and is stable until it is exposed to the atmosphere. When exposed, the silane undergoes hydrolysis with atmospheric moisture and condenses with the polymer in a reaction catalyzed by the metal soap. Reaction of polymer at the three reactive positions of the silane thus develops

the crosslinked network needed for the attainment of physical properties approaching those of heat cured rubber. This type of product has many applications, mostly as sealants, adhesives and caulking compounds. A second type of RTV system is a two-package silanol condensation compound which uses a low molecular weight polysiloxane mixed with fillers. The usual cross-linking system is a polyfunctional silane such as ethyl orthosilicate or a hydrolyzed and condensed version of ethyl orthosilicate, along with a metal soap catalyst such as dibutyltindilaurate, stannous octoate, etc. In the two-package system, one package usually consists of polymer and filler mixed with the ethyl orthosilicate. In this case, the metal soap is the second package and is mixed in shortly before use. Alternatively, one package may consist of polymer and filler and the other of the orthosilicate and metal soap catalyst. A recent development is a one part addition cured system in which all the components are present but which require heat to trigger the reaction. Cure rates in all the systems are functions of the temperature and time of heating. The following scheme represents the cross-linking reaction between the silane and the metal salt:

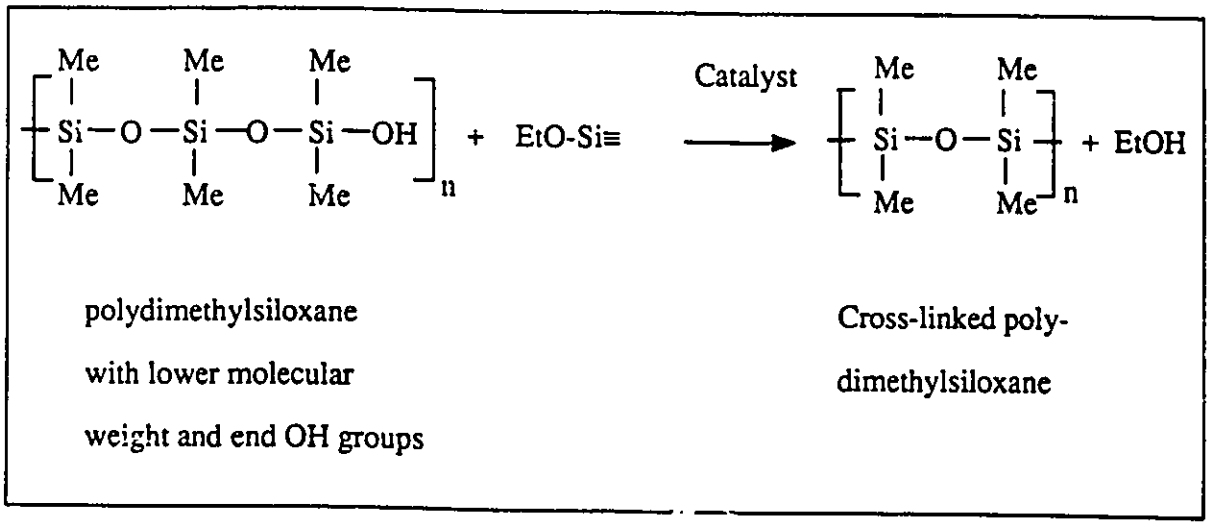

Figure 7.2 Silicone curing reaction

Siloxane polymers have much higher permeability to gases than most other polymer materials. Therefore, these polymers have long been of interest for gas separation membranes[26,154]. We have shown in the preceding chapters that microporous organo-smectites have the protential for gas separation. The questions immediately arise: (1) how can this organo-clay material be imbedded into the PDMS matrix to form a composite membrane? (2) how would the organo-clay affect the gas transport in the organo-clay PDMS composite membrane?

In this study, dried organo-clay materials with size less than 230 mesh were selected. The details for the preparation of organo-clay PDMS composite membranes are described in chapter 8. The membrane thickness and organo-clay content ranged from 110 to 140μm and from 20 to 45%(w/w), respectively. The space between the clay particles can be filled with the polymer material. The prepared composite membranes were used immediately for permeation experiments without further treatment.

7.3 Pure gas permeation in PDMS and Organo-clay-PDMS membranes

7.3.1 Resistance model through organo-clay PDMS composite membranes

Models describing gas transport through membranes depend on the morphology of the polymer materials. The solution-diffusion model is frequently used to describe the gas transport in a rubber polymer, e.g. polydimethylsiloxane (PDMS)[26,167,168]. This model postulates that permeation occurs by sorption of the penetrant gas in the membrane, molecular diffusion of the gas in and through the membrane, and desorption of the gas at the opposite interface. The permeation rate of the gas is a product of a mean diffusion coefficient and a solubility coefficient:

$$P = D\,S \tag{7-1}$$

where P is the permeability coefficient, D is the diffusion coefficient, S is the solubility coefficient. The diffusion coefficient D and solubility coefficient S are given by:

$$D = \left[\int_{c_1}^{c_2} D(c)\,dc\right] / (C_2 - C_1) \tag{7-2}$$

$$S = C_2 / p_2 \tag{7-3}$$

where C_2 and C_1 are the equilibrium concentrations of penetrant dissolved at the two membrane interfaces when the penetrant pressures at these interfaces are p_2 and p_1, respectively, and D(c) is the mutual diffusion coefficient for the penetrant/membrane system. This model assumes that the membrane contains no permanent pores through which gas flow can occur. Free volume model has been also developed to describe the gas transport in rubbery polymers[169,170]. It implies that the permeant diffuses by a cooperative movement of the permeant and the polymer segments, from one "hole" to the other within the polymer, the creation of a "hole" caused by fluctuations of local density.

Dual mode sorption model is commonly used in glassy polymers[171,172]. This model comprises a sorption isotherm consisting of a dissolved solubility which obeys Henry's law, and a "hole filling" solubility (molecules residing in microcavities) which obeys the non-linear Langmuir isotherm. Once again, an assumption that the membrane is essentially pore free, is made using this model. In contrast, in the case of porous membrane, the gas transport is described by adsorption on the surface of the pores and transportation due to the pressure difference through the pores to the permeate side[173,174,175]. The mechanism involves simultaneous Knudsen, slip, viscous, and surface flow through the porous

membranes. The permeation of a given gas mixture through the membrane is explained by defining an interaction parameter which is evaluated using experimental permeation data. The interaction parameter depends on the mixture components, their partial pressures and membrane for permeation of gases.

Another type of membrane is a composite membrane which is made by supporting a thin separating membrane on a porous substrate to achieve high fluxes[176]. In these membranes, the coating serves as the separating barrier and the substrate serves only as a physical support. A simple resistance model for gas transport through composite membranes was proposed by Henis and Tripodi[177,178]. A new resistance model called Wheatstone bridge model for the transport of gases through composite membranes that were prepared by laminating a silicone layer onto the top of a porous polyethersulfone sublayer was developed recently[179]. A resistance model has been also developed to describe the pervaporation flux and selectivity for the separation of ethanol/water mixtures with silicalite-filled silicone rubber[180]. However, there is not any report dealing with resistance model for gas transport through particle filled composite membranes.

In this study, a composite membrane is formed upon addition of microporous particles into the polymer matrix. Therefore the gas transport mechanism in these composite membranes should be different from that in the polymer itself. The resistance model which was developed by Henis and Tripodi[177,178] is employed here to describe the gas transport through the organo-clay polymer composite membranes, and the model is verified by the experimental permeation data. According to the resistance model, the gas permeation rate Q_i (cm^3/sec) is given by:

$$Q_i = P_i A \Delta p_i / l \qquad (7\text{-}4)$$

where P_i is the gas permeability in cm^3. cm/cm^2.sec.cmHg, A is the cross sectional surface

area of the membrane available for permeation, l is the thickness of the membrane through which the component permeates and Δp_i is the partial pressure difference across the membrane. An analogy is made between gas permeation and electrical flow, and the various portions of the composite membrane are described in terms of their resistance to gas permeation. The relationship describing the permeation of a gas through a membrane is equivalent to Ohm's law which describes the current flow through a resistor:

$$I = V / R \tag{7-5}$$

where I is the current, V is the voltage and R is the resistance. The permeation rate Q_i is equated to the current I and the partial pressure difference across the membrane Δp_i is analogous to the driving force for current flow V. Thus equation 7-4 can also be expressed as:

$$Q_i = \Delta p_i / R_i \tag{7-6}$$

in which the resistance to permeate flow R_i is equivalent to the electrical resistance R; combining 7-4 and 7-6, one obtain 7-7:

$$R_i = l / P_i A \tag{7-7}$$

The flux Q_i is a function of the pressure difference and the resistance of the membrane against gas transport. Since the transport can occur through both the rubber and the organo-clay particles, the membrane resistance R_i can be described by a combination of the resistance for both materials:

$$R_i = R_{PDMS} + R_{Org\text{-}clay} \tag{7-8}$$

In equation 7-8, R_{PDMS} and $R_{Org\text{-}clay}$ are in series. However, if the organo-clay particles are impermeable, there is still a transport route around the particles, and this leads to be taken into account as a third resistance, R_2 which is in parallel to the $R_{Org\text{-}clay}$ in equation 7-8. Therefore, the total resistance for organo-clay PDMS composite membrane is composed of three elements. The membrane resistance is a combination of resistances in series and in paralell. Therefore the total resistance of the composite membrane is defined as:

$$(R_t)_i = (R_1)_i + (R_2)_i.(R_3)_i/[(R_2)_i + (R_3)_i] = nR_{1,i} + [nR_{2,i}R_{3,i}/(R_{2,i} + R_{3,i})] \tag{7-9}$$

where n is the number of organo-clay particles along the transport path and $(R_1)_i$, $(R_2)_i$, $(R_3)_i$ are the resistances through polymer matrix, around the particle and through the particle, respectively. Figure 7.3 shows a schematic representation of the cross section of an organo-clay filled PDMS membrane and its electrical circuit analogue.

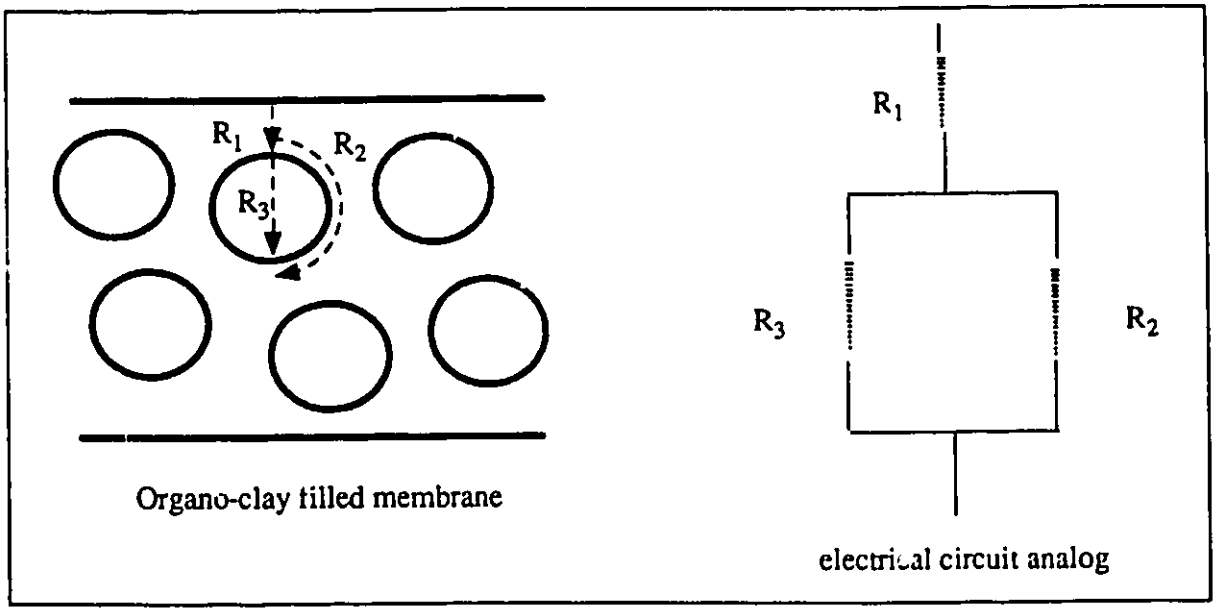

Figure 7.3 Schematic representation of the organo-clay filled PDMS composite membrane and its electric circuit analogue

The individual resistances of equation 7-9 can be determined from equation 7-7 where:

$$R_{1,i} = R_{PDMS,i} = l_1/P_{1,i} A_0 \quad (7\text{-}10)$$

$$R_{2,i} = R'_{PDMS,i} = l_2/P_{2,i} A_p \quad (7\text{-}11)$$

$$R_{3,i} = R_{Org\text{-}clay,i} = l_3/P_{3,i} A_c \quad (7\text{-}12)$$

In above equations, l_1 is the pathlength between the successive clay particles in the direction of transport, l_2 is the pathlength through the PDMS around the clay particles, and l_3 is the length of the clay particle. A_0 is the total membrane area, A_p is the area between the clay particles, and A_c is the area perpendicular to the flow as occupied by the clay in a cross section.

The l_1 and l_3 are related to the total thickness l as given below:

$$n\, l_1 + n\, l_3 = l \quad (7\text{-}13)$$

The pathlength around the clay particles is a function of the clay particle size, particle geometry and particle orientation. Since we assume that the clay particles are homogeneous and spherical, the following relation between l_2 and l_3 is made:

$$l_2 = \pi/2\, l_3 \quad (7\text{-}14)$$

The above relation is illustrated in Figure 7.4. By considering the clay particle content (ϕ_c) in the polymer matrix, the following relations can be made:

$$n\, l_1 = (1\text{-}\phi_c^{1/3})\, l \quad (7\text{-}15)$$

$$n\, l_3 = \phi_c^{1/3}\, l \tag{7-16}$$

where ϕ_c is the organo-clay content in the composite membrane[180,181].

The cross-sectional area, A_0, A_p and A_c can also be related to the organo-clay content ϕ_c:

$$A_p = A_0\,(1-\phi_c) \tag{7-17}$$

$$A_c = A_o\phi_c \tag{7-18}$$

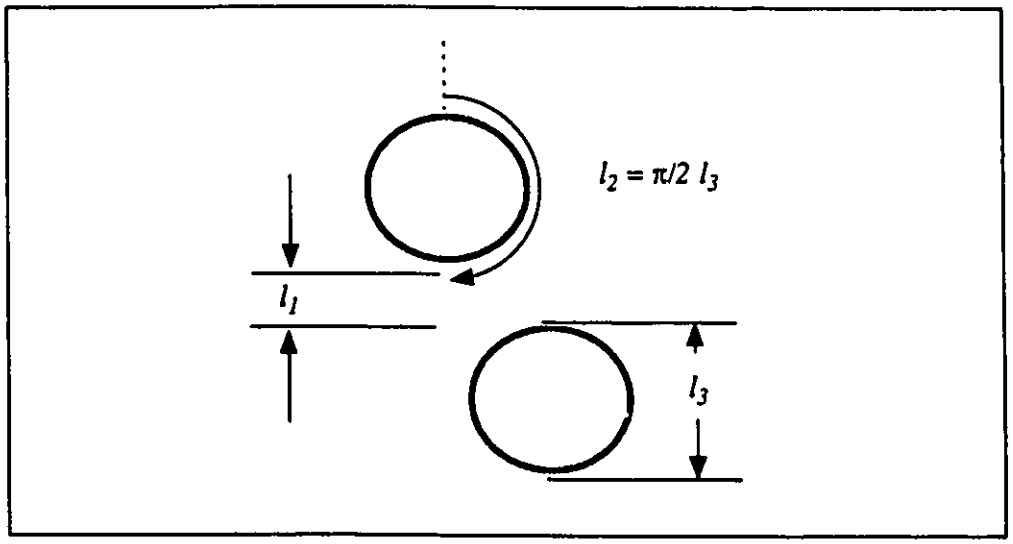

Figure 7.4 Schematic representation of organo-clay particles in the PDMS membrane and the pathlengths through and around the particles.

By combining all the above equations, the individual resistances and the total resistance across an organo-clay PDMS composite membrane can be expressed as:

$$(R_1)_i = n\, R_{1,i} = (1-\phi_c^{1/3})\, l\, /\, P_{PDMS,i}\, A_0 \tag{7-19}$$

$$(R_2)_i = n\,R_{2,i} = \pi/2\;\phi_c^{1/3}\;l\;/\;P_{PDMS,i}(1-\phi_c)A_0 \qquad (7\text{-}20)$$

$$(R_3)_i = n\,R_{3,i} = \phi_c^{1/3}\;l\;/\;P_{Org\text{-}clay,i}\,\phi_c\,A_0 \qquad (7\text{-}21)$$

$$(R_t)_i = (1\;/\;A_0)[(1-\phi_c^{1/3})l\;/\;P_{PDMS,i}+\pi/2\;\phi_c^{1/3}l\;/\;(P_{PDMS,i}\;(1-\phi_c)+\pi/2\;P_{Org\text{-}clay,i}\;\phi_c)] \qquad (7\text{-}22)$$

Therefore the component flux is given as a function of the organo-clay content of the membrane, membrane thickness, and the permeabilities of the membrane constituents:

$$(Q_t)_i = \Delta p_i A_0\;/\;[(1-\phi_c^{1/3})l\;/\;P_{PDMS,i}+\pi/2\;\phi_c^{1/3}l\;/\;(P_{PDMS,i}\;(1-\phi_c)+\pi/2\;P_{Org\text{-}clay,i}\;\phi_c)] \qquad (7\text{-}23)$$

From equation 7-4 and 7-22, the total permeability of the organo-clay PDMS composite membrane can be obtained:

$$(P_t)_i = 1\;/\;[(1-\phi_c^{1/3})\;/\;P_{PDMS,i}+\;\pi/2\;\phi_c^{1/3}\;/\;(P_{PDMS,i}\;(1-\phi_c)+\;\pi/2\;P_{Org\text{-}clay,i}\;\phi_c)] \qquad (7\text{-}24)$$

The permeabilities for polymer matrix $P_{PDMS,i}$ and organo-clay $P_{Org\text{-}clay,i}$ can be calculated by fitting the equation 7-24 on permeation data. It is reasonably assumed that both PDMS and clay permeabilities are independent of the organo-clay content of the membrane. Also both permeabilities are average values which can be measured only for the membrane as a whole. Both permeabilities may vary with the position of the particles inside the membrane. The model does not account for these variations.

Regarding to the overall resistance $(R_t)_i$, there are three contributions, $(R_1)_i$, $(R_2)_i$

and $(R_3)_i$, respectively. In the case of a composite membrane which contains impermeable particles, the overall resistance has only two components, $(R_1)_i$ and $(R_2)_i$ since $(R_3)_i$ is infinity. Therefore equation 7-9 becomes:

$$(R_t)_i = (R_1)_i + (R_2)_i = nR_{1,i} + nR_{2,i} \tag{7-25}$$

In the case of a composite membrane containing lower organo-clay content and medium microporosity in the organo-clay particles, the overall resistance is governed by three components $(R_1)_i$, $(R_2)_i$ and $(R_3)_i$. As the content and the microporosity of the organo-clay in the composite membrane increase, the resistance component through the organo-clay particles $(R_3)_i$ becomes smaller and most of the gas transports through the $(R_3)_i$ side. As a result, the overall resistance through the highly microporous organo-clay PDMS composite membrane is governed by $(R_1)_i$ *and* $(R_3)_i$. Thus the total resistance through the highly microporous organo-clay PDMS composite membrane is only given by:

$$(R_t)_i = (R_1)_i + (R_3)_i = nR_{1,i} + nR_{3,i} \tag{7-26}$$

since the term $nR_{2,i}R_{3,i}/(R_{2,i} + R_{3,i})$ is approximately equal to $nR_{3,i}$, if $R_{3,i} \ll R_{2,i}$.

Therefore the permeability of the organo-clay PDMS composite membrane is a function of organo-clay content and the microporosity of the organo-clay. From the experimental permeation data and the calculated permeabilities for both the polymer matrix and the organo-clay, the total and the individual resistances of the organo-clay filled PDMS composite membranes can be calculated:

The gas permeability (cm^3-cm/cm^2-sec-cmHg) is determined by the following equation:

$$P_i = Q_i l / \Delta p_i A_0 \quad (7\text{-}26)$$

where the parameters are defined as before.

The ideal selectivity, α, is defined as the ratio of the pure component permeabilities or the ratio of the component resistances:

$$(\alpha)_{i,j} = P_j / P_i = R_j / R_i \quad (7\text{-}27)$$

$$(\alpha_1)_{i,j} = (R_1)_j / (R_1)_i \quad (7\text{-}28)$$

$$(\alpha_2)_{i,j} = (R_2)_j / (R_2)_i \quad (7\text{-}29)$$

$$(\alpha_3)_{i,j} = (R_3)_j / (R_3)_i \quad (7\text{-}30)$$

where the parameters in the above equations are defined as before.

7.3.2 Pure gas permeation in PDMS and organo-clay-PDMS membranes

In order to examine the gas transport through the organo-clay PDMS composite membrane, six pure gases were used, including He, H_2, O_2, N_2, CH_4 and CO_2. The experimental details are described in chapter 8. The data collected for all the membranes were in terms of volume flow rate. This volume rate was corrected to STP and then converted to permeability using equation 7-26. During the experiments it was observed that at the beginning of permeation the gas permeabilities changed with time. The procedure in obtaining the volumetric flow rate consisted of setting the feed gas pressure to the desired pressure and then waiting 1/2 hour before taking the first flow rate measurement. A second flow rate measurement was taken 15 minutes later and compared with the first. If a significant difference arose a third flow rate measurement would be taken in another 15 minutes and again compared. This was repeated every 15 minutes until the flow rates were constant. For the gases, N_2, O_2, CH_4 and CO_2, the flow rates remained constant after 2

hours at a given pressure. However, in the cases of H_2 and He, more than 48 hours were needed for a constant flow rate to be established. Why He and H_2 gases take longer than other gases to reach steady state is not clear at this point.

In the beginning of the study, three organo-montmorillonites filled PDMS membranes with 20%(w/w) of filler, including TPP-montmorillonite, LYS-Me-montmorillonite, and MTETA-montmorillonite, as well as 20%(w/w) Na-montmorillonite filled PDMS membrane were prepared. For comparison purpose, the PDMS membrane was also prepared in the same way as organo-clay filled PDMS membranes. The thicknesses of all the organo-clay-PDMS membranes were kept approximatelly the same. The feed gas pressure was controlled at 110psig (758 KPag) and the permeation experiments were conducted at room temperature in all the measurements. All the pure gas permeabilities for Na-M-PDMS-20, TPP-M-PDMS-20, LYS-Me-M-PDMS-20 and MTETA-M-PDMS-20 membranes are shown in Table 7.2. The effect of the presence of organo-clay particles in the PDMS membranes are clearly seen. Decreases in gas permeabilities were observed in all the clay and the organo-clay filled PDMS composite membranes compared to the PDMS membrane. It is also noted that the permeabilities through organo-clay-PDMS membranes depend upon the nature of the gases and the organo-clays. The kinetic diameters of gases are shown in Table 7.3. With filling of organo-clay into the PDMS membranes, the permeabilities of "slow" gases (He, H_2, N_2) decreased greatly, whereas the permeabilities decreased only slightly for "fast" gases (O_2, CO_2, CH_4). Molecular sieving effects are not observed in these organo-clay PDMS composite membranes, since the decreases in permeabilities do not depend on the size of the gases. The gas permeability ratios of PDMS and various organo-clay PDMS composite membranes are shown in Table 7.4. Increases in the selectivities are observed in all the organo-clay PDMS composite membranes as compared to the PDMS membrane. The maximum permeability ratios achieved for O_2/N_2, CH_4/N_2, CO_2/N_2 and CO_2/CH_4 were 2.5,

Table 7.2 Pure gas permeabilities of PDMS and organo-clay-PDMS composite membranes at 758 KPag and 23°C.

Membrane	Thickness	Organo-clay % in membr.	Permeability x 10^{10}, cm^3-cm/cm^2-sec-cmHg					
			He	H_2	N_2	O_2	CH_4	CO_2
PDMS	125	0	192	337	292	665	951	3717
Na-M-PDMS-20	130	20			215	536	718	2875
TPP-M-PDMS-20	120	20			228	536	732	3118
LYS-Me-M-PDMS-20	120	20	117	164	202	505	711	2928
MTETA-M-PDMS-20	110	20			210	494	686	2868

3.5, 14.6 and 4.2, respectively.

Table 7.3 Kinetic (seiving) diameters of penetrants

Gas	He	H_2	O_2	N_2	CH_4	CO_2
Kinetic diam. (Å)	2.6	2.89	3.46	3.64	3.8	3.3

These results imply that for the low organo-clay content of the gas transport through the organo-clay PDMS composite membranes is governed mainly by the polymer matrix. The organo-clay in the composite membranes acts as a barrier to gas permeation. The addition of organo-clay in PDMS membrane changed the gas permeability as well as the permeability ratio. However, the gas selectivities in these organo-clay PDMS composite membranes are still low, presumably due to the low organo-clay content. The selectivity should be improved by increasing the organo-clay content in the composite membrane.

Table 7.4 Pure gas permeability ratios of PDMS and organo-clay embedded PDMS membranes at 758 KPag and 23°C.

Membrane	organo-clay (wt. %)	selectivity α			
		α (O_2/N_2)	α (CH_4/N_2)	α (CO_2/N_2)	α (CO_2/CH_4)
PDMS	0	2.3	3.3	12.7	3.9
Na-M-PDMS-20	20	2.5	3.3	13.4	4.0
TPP-M-PDMS-20	20	2.4	3.2	13.7	4.2
LYS-Me-M-PDMS-20	20	2.5	3.5	14.6	4.2
MTETA-M-PDMS-20	20	2.4	3.3	13.8	4.2

7.3.3 *Pure gas permeability dependence upon the organo-clay content in the LYS-Me-montmorillonite PDMS composite membranes*

An increase of the organo-clay content in the composite membrane should increase the resistance to the gas transport. Table 7.5 summarizes the permeabilities of Na-M-PDMS composite membranes and LYS-Me-M-PDMS composite membranes with different clay and organo-clay contents. As can be seen, the permeabilities decreased as the organo-clay content increased from 20% to 45% in the composite membranes. The decrease in gas permeabilities with the increase of the organo-clay content can be attributed to the lower permeability of the organo-clay compared to the PDMS. Using the resistance model and the permeability data of LYS-Me-M-PDMS membranes, the permeabillities of the polymer matrix $P_{PDMS,i}$ and of the organo-clay particles $P_{LYS\text{-}M,i}$ can be calculated from equation 7-24, since the data are known for several values of ϕ_c. Table 7.6 shows the calculated permeabilities of the polymer matrix and of the organo-clay LYS-Me-M for various gases. The calculated permeabilities of PDMS are in excellent agreement with the experimental values, determined in the case of a PDMS membrane. This is a good test of the pertinence of the model. Table 7.6 indicates that the permeabilities through the LYS-Me-M particles are lower than that through the polymer matrix. It is also noted that the permeabilities of the organo-clays for N_2 and CH_4 are about four times lower than the permeabilities of the PDMS polymer, while the permeabilities of organo-clay for O_2 and CO_2 are about two times lower than the permeabilities of the PDMS polymer. This indicates that the permeability through the LYS-Me-M is strongly dependent upon the size of the gases. From the calculated $P_{PDMS,i}$ and $P_{LYS\text{-}M,i}$ it is possible to calculate the overall resistance and various resistance components through the composite membranes using equations 7-9, 7-19, 7-20 and 7-21. Table 7.7-7.10 summarizes the calculated resistances to gases N_2, O_2, CH_4 and CO_2 for various LYS-Me-M-PDMS composite membranes.

Table 7.5 Pure gas permeabilities of organo-clay-PDMS membranes at 758 KPag and 23 °c.

Membrane	Thickness (μm)	Organo-clay content (%) in membr.	Permeability x 10^{10}, cm^3-cm/cm^2-sec-cmHg			
			N_2	O_2	CH_4	CO_2
Na-M-PDMS-20	130	20	215	536	718	2875
Na-M-PDMS-33	135	33	208	517	693	2772
LYS-Me-M-PDMS-20	120	20	207	518	711	2929
LYS-Me-M-PDMS-33	140	33	190	458	608	2644
LYS-Me-M-PDMS-44	130	45	146	398	473	2253

Table 7.6 Calculated permeabilities for PDMS matrix and LYS-Me-M in LYS-Me-M-PDMS membrane at 758KPag and 23°C.

Component, i	$P_{PDMS,i} \times 10^{10}$ (cm^3-cm/cm^2-s-cmHg)	$P_{PDMS,expt.} \times 10^{10}$ (cm^3-cm/cm^2-s-cmHg)	$P_{LYS\text{-}M,i} \times 10^{10}$ (cm^3-cm/cm^2-s-cmHg)
N_2	297	229	73
O_2	681	665	298
CH_4	987	951	216
CO_2	3821	3717	1792

Table 7.7 Total and individual resistances to N_2 permeation flow for LYS-Me-M PDMS composite membranes with different organo-clay content.

Resistance (sec-cmHg/cm^3)	Organo-clay PDMS composite membrane		
	LYS-Me-M-PDMS-20	LYS-Me-M-PDMS-33	LYS-Me-M-PDMS-45
R_1	1.74E+4	1.51E+4	1.06E+4
R_2	1.64E+4	3.79E+4	5.85E+4
R_3	49.93E+4	41.72E+4	31.50E+4
R_t	3.33E+4	4.98E+4	5.99E+4
$(R_t)_{exp}$	6.03E+4	7.66E+4	9.26E+4

Table 7.8 Total and individual resistances to O_2 permeation flow for LYS-Me-M-PDMS composite membranes with different organo-clay content.

Resistance (sec-cmHg/cm^3)	Organo-clay PDMS composite membrane		
	LYS-Me-M-PDMS-20	LYS-Me-M-PDMS-33	LYS-Me-M-PDMS-45
R_1	7.60E+3	6.60E+3	4.63E+3
R_2	7.18E+3	16.51E+3	25.46E+3
R_3	122.3E+3	102.2E+3	77.14E+3
R_t	14.38E+3	20.81E+3	23.77E+3
$(R_t)_{exp}$	24.08E+3	31.78E+3	33.95E+3

Table 7.9 Total and individual resistances to CH_4 permeation flow for LYS-Me-M-PDMS composite membranes with different organo-clay content.

Resistance (sec-cmHg/cm^3)	Organo-clay PDMS composite membrane		
	LYS-Me-M-PDMS-20	LYS-Me-M-PDMS-33	LYS-Me-M-PDMS-45
R_1	5.25E+3	4.56E+3	3.20E+3
R_2	4.96E+3	11.40E+3	17.58E+3
R_3	169.0E+3	141.2E+3	106.6E+3
R_t	10.07E+3	15.11E+3	18.29E+3
$(R_t)_{exp}$	17.51E+3	23.95E+3	28.57E+3

Table 7.10 Total and individual resistances to CO_2 permeation flow for LYS-Me-M-PDMS composite membranes with different organo-clay content.

Resistance (sec-cmHg/cm^3)	Organo-clay PDMS composite membrane		
	LYS-Me-M-PDMS-20	LYS-Me-M-PDMS-33	LYS-Me-M-PDMS-45
R_1	1.36E+3	1.18E+3	0.83E+3
R_2	1.28E+3	2.95E+3	4.54E+3
R_3	20.35E+3	17.00E+3	12.84E+3
R_t	2.56E+3	3.69E+3	4.18E+3
$(R_t)_{exp}$	4.26E+3	5.51E+3	5.99E+3

A closer inspection of these tables reveals the path taken by the permeating gas through the LYS-Me-M-PDMS membranes. The resistances through the LYS-Me-M material are much larger than the corresponding resistances through the polymer matrix. This is because the barrier in the pores of the organo-clay is much greater than that in the polymer matrix. The resistance components, R_1, R_2, R_3 are variable depending on the organo-clay content. As can be seen in the tables, R_1 and R_3 decrease while R_2 increases with an increasing content of the organo-clay. The decrease in R_1 is attributed to the progressive decrease of polymer content in the composite membrane. According to the resistance model, as the organo-clay content increases, the resistance R_2 increases while the resistance R_3 through the organo-clay decreases. Gas transport through the R_3 side is much preferable at higher organo-clay content than at lower organo-clay content. As a result, the contribution of organo-clay in the gas transport becomes greater at higher organo-clay

content. As can be seen, the overall resistance R_t increased with the increase of organo-clay content and the permeability through the composite membrane decreased with increasing organo-clay content. Figures 7.5-7.8 show the plots of various gas permeabilities of the composite membranes as a function of the organo-clay contents. The lines are calculated from the resistance model and the points are experimental data. These figures show that the resistance model fits well to the observed permeability results.

From the calculated resistance components, it is also possible to calculate the individual resistance ratios. Table 7.11 and 7.12 show various total and individual resistance ratios for the gas pairs: CO_2/CH_4 and O_2/N_2. The resistance ratios of LYS-Me-M for O_2/N_2 and CO_2/CH_4 are 4.1 and 8.3 as compared to 2.3 and 3.9 for PDMS membrane, respectively. However, the overall permeability ratios of LYS-Me-M-PDMS composite membrane are lower than that of the LYS-Me-M material because of the contribution of the PDMS matrix. The permeability ratio for CO_2/CH_4 are seen to increase with an increase of the organo-clay content. As shown previously in Tables 7-7-7.10, the resistance component R_3 for LYS-Me-M decreased as the organo-clay content increased and therefore the contribution of the LYS-Me-M becomes greater at higher organo-clay content. As a result, the differences between the total resistances for gas pair O_2/N_2 and CO_2/CH_4 increase since the selectivities for gases in LYS-Me-M are higher than in the PDMS polymer matrix.

Table 7.13 summarizes the separation factors for various LYS-Me-M-PDMS membranes. As the organo-clay content increases from 20% to 45%, the selectivity for the gas pairs O_2/N_2 and CO_2/CH_4 increases from 2.5 to 2.7 and from 4.1 to 4.8 respectively. In contrast, the increase of the clay content in Na-M-PDMS composite membranes does not result in a variation of the gas selectivities. Further evidence will be obtained from the permeation results in organo-clay PDMS composite membranes with high microporosity and high organo-clay contents.

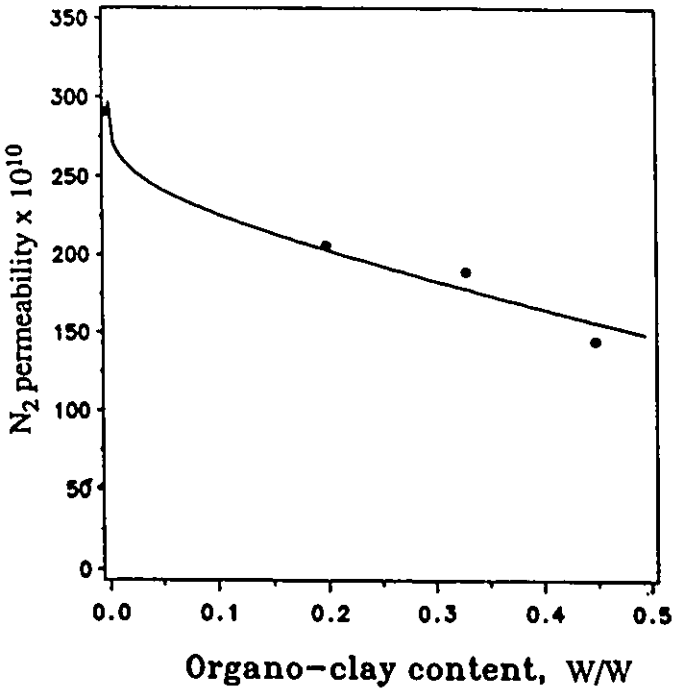

Figure 7.5 N_2 permeabilities of LYS-Me-M-PDMS composite membrane as a function of LYS-Me-M content.

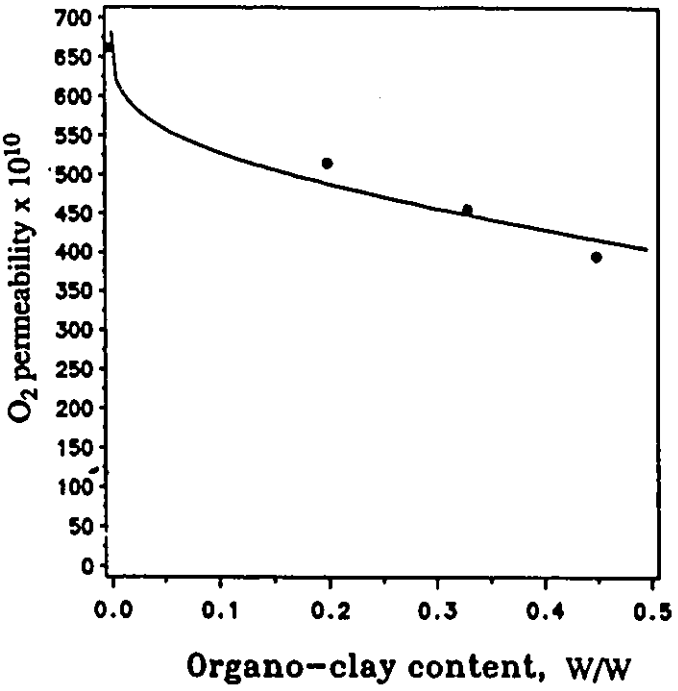

Figure 7.6 O_2 permeabilities of LYS-Me-M-PDMS composite membrane as a function of LYS-Me-M content.

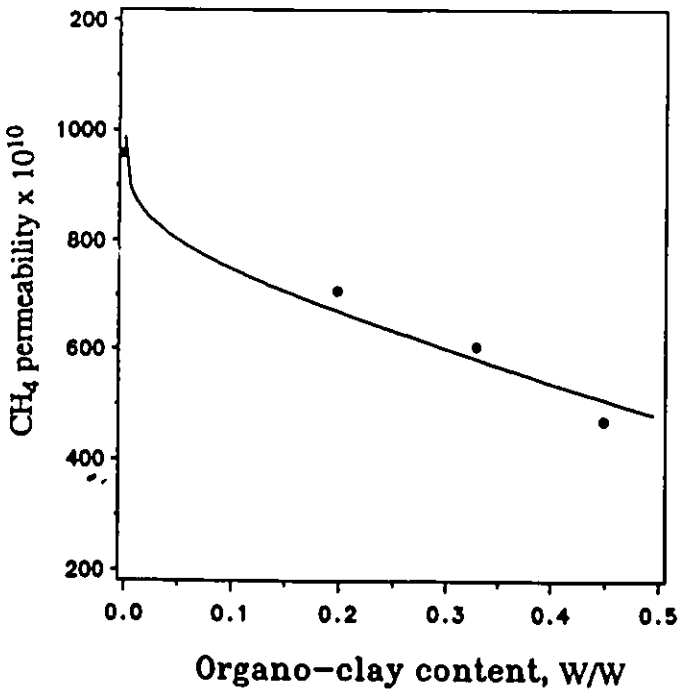

Figure 7.7 CH_4 permeabilities of LYS-Me-M-PDMS composite membrane as a function of LYS-Me-M content.

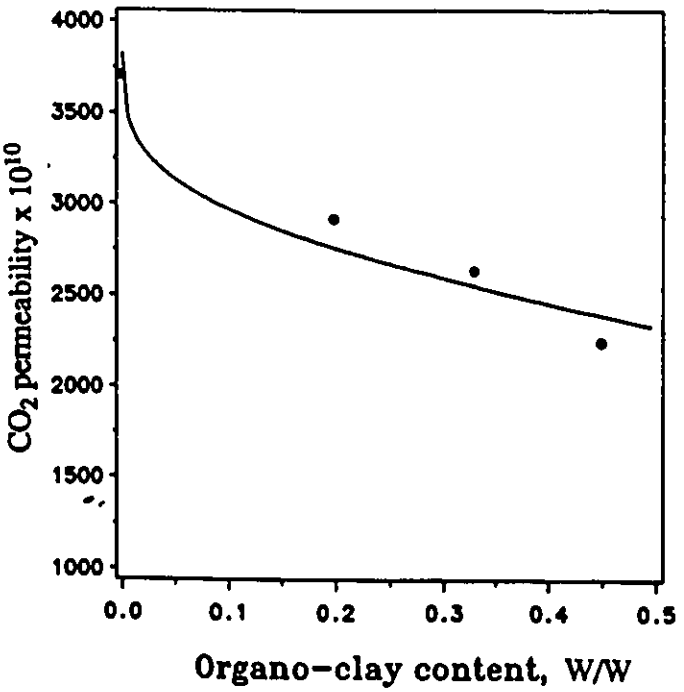

Figure 7.8 CO_2 permeabilities of LYS-Me-M-PDMS composite membrane as a function of LYS-Me-M content.

Table 7.11 Total and individual resistance ratios of LYS-Me-M-PDMS composite membranes for gas pair O_2/N_2 at 758KFag and 23°C.

Resistance ratio	Organo-clay PDMS composite membrane		
	LYS-Me-M-PDMS-20	LYS-Me-M-PDMS-33	LYS-Me-M-PDMS-45
α_1	2.3	2.3	2.3
α_2	2.3	2.3	2.3
α_3	4.1	4.1	4.1
α_t	2.3	2.4	2.5
$(\alpha_t)_{exp}$	2.5	2.4	2.7

Table 7.12 Total and individual resistance ratios of LYS-Me-M-PDMS composite membranes for gas pair CO_2/CH_4 at 758KPag and 23°C.

Resistance ratio	Organo-clay PDMS composite membrane		
	LYS-Me-M-PDMS-20	LYS-Me-M-PDMS-33	LYS-Me-M-PDMS-45
α_1	3.9	3.9	3.9
α_2	3.9	3.9	3.9
α_3	8.3	8.3	8.3
α_t	3.9	4.1	4.4
$(\alpha_t)_{exp}$	4.1	4.3	4.8

Table 7.13 Pure gas permeability ratios of organo-clay-PDMS membranes at 758 KPag and 23 °C.

Membrane	Thickness (μm)	Organo-clay content (%) in membr.	Selectivity, α			
			α (O_2/N_2)	α (CH_4/N_2)	α (CO_2/N_2)	α (CO_2/CH_4)
Na-M-PDMS-20	130	20	2.5	3.3	13.4	4.0
Na-M-PDMS-33	135	33	2.5	3.3	13.3	4.0
LYS-Me-M-PDMS-20	120	20	2.5	3.5	14.2	4.1
LYS-Me-M-PDMS-33	140	33	2.4	3.2	13.9	4.4
LYS-Me-M-PDMS-45	130	44	2.7	3.2	15.4	4.8

7.3.4 Pure gas permeation through higher microporous organo-clay PDMS composite membranes

As shown previously (chapter 5), TMA-montmorillonite and MMDA-montmorillonite are characterized by a high degree of microporosity. These two organo-clays were also imbedded into the PDMS polymer and the permeation through these composite membranes were studied here. The pure gas permeabilities of LYS-Me-M-PDMS-45, TMA-M-PDMS-45 and MMDA-M-PDMS-45 composite membranes are shown in Table 7.14. The gas permeabilities of the TMA-M-PDMS-45 and MMDA-M-PDMS-45 membranes are lower than that of the LYS-Me-M-PDMS-45 membrane. These results are a good indication that the microporosity of the organo-clay plays a role in the gas transport through the composite membranes.

As mentioned previously, the gas transport through the organo-clay composite membranes depends upon the microporosity of the organo-clay and the organo-clay content of the membrane. At higher organo-clay content and higher microporosity, the resistance through the organo-clay particles decreases and most of the gas transports through the polymer matrix and the organo-clay particles. In this case, the overall resistance is mainly controlled by the resistances R_1 and R_3(see p168). The total resistance is therefore the sum of the above two components. Since the organo-clay content in TMA-M-PDMS-45 and MMDA-M-PDMS-45 membranes are the same, the resistances R_1 can be calculated from equation 7-10 using the $P_{PDMS,i}$ values which were calculated from the permeability data of the LYS-Me-M-PDMS membranes of from the values obtained on the PDMS membrane (see Table 7.6). The overall resistances through TMA-M-PDMS-45 and MMDA-M-PDMS-45 are calculated from the permeability data. Thus the resistance R_3 through the highly microporous TMA-M and MMDA-M materials can be calculated by subtracting the resistance R_1 from the overall resistance R_t. Tables 7.15 and 7.16 summarize the calculated resistance components to various gases in TMA-M-PDMS-45 and

Table 7.14 Pure gas permeabilities of organo-clay-PDMS membranes at 758KPag and 23°C.

Membrane	Thickness	Organo-clay %	Permeability $x10^{10}$(cm^3.cm/cm^2-sec-cm Hg)			
			N_2	O_2	CH_4	CO_2
PDMS	125	0	292	665	951	3717
LYS-Me-M-PDMS-45	130	45	146	315	473	2263
TMA-M-PDMS-45	105	45	68	268	247	2019
MMDA-M-PDMS-45	115	45	107	296	222	1935

MMDA-M-PDMS-45 composite membranes.

Table 7.15 Resistances to various gases for TMA-M-PDMS-45 membrane.

Resistance (sec-cmHg/cm^3)	N_2	O_2	CH_4	CO_2
R_1	8.59E+3	3.74E+3	2.58E+3	0.67E+3
R_3	151.9E+3	36.99E+3	41.61E+3	4.74E+3
R_t	160.5E+3	40.73E+3	44.19E+3	5.41E+3

Table 7.16 Resistances to various gases for MMDA-M-PDMS-45 membrane.

Resistance (sec-cmHg/cm^3)	N_2	O_2	CH_4	CO_2
R_1	10.23E+3	4.45E+3	3.07E+3	0.79E+3
R_3	100.9E+3	35.90E+3	50.62E+3	5.39E+3
R_t	111.1E+3	40.35E+3	53.69E+3	6.18E+3

The resistances through the organo-clay particles are much greater than the corresponding values for the polymer matrix, indicating that the overall resistance through

the highly microporous organo-clay composite membrane is mainly controlled by the resistance of the organo-clay particles. In addition, the permeability sequence for O_2/CH_4 in the cases of TMA-M-PDMS-45 and MMDA-M-PDMS-45 are reverse as compared to the LYS-Me-M-PDMS-45 (see Table 7.14). This is a good indication that the gas transport in highly microporous organo-clay filled PDMS membranes is mainly controlled by the permeabilities of the organo-clays. From the resistance data, it is possible to calculate the permeabilities of the TMA-montmorillonite and MMDA-montmorillonite materials. Table 7.17 shows the calculated permeabilities of the three different organo-clay materials, LYS-Me-M, TMA-M and MMDA-M. As can be seen, the gas permeability of the organo-clay increases with an increase of the microporosity. The gas permeability sequency in those organo-clay materials is found to be:

$$CO_2 > O_2 > CH_4 > N_2$$

Due to the strong interaction of carbon dioxide with the siliceous surfaces of the organo-clay which has been shown in the chromatographic studies, CO_2 is the most permeable gas in these organo-clay materials. The smaller molecular size of O_2 accounts for its higher permeability while the larger molecular size of CH_4 accounts for the lower permeabilities. The lower permeability of N_2 in these highly microporous organo-clay filled PDMS membranes may be attributed to the relatively lower permeation through the polymer matrix.

Table 7.17 Permeabilities of PDMS, LYS-Me-M, TMA-M and MMDA-M.

Gas permeate	Permeability x 10^{10}, cm^3-cm/cm^2-sec-cmHg			
	PDMS	LYS-Me-M	TMA-M	MMDA-M
microporosity		7%	77%	78%
N_2	297	73	122	199
O_2	682	298	503	561
CH_4	987	216	447	399
CO_2	3821	1792	3921	3735

Table 7.18 Permeability ratios of CO_2/CH_4 and O_2/N_2 in organo-clay PDMS composite membranes at 758KPag and 23°C.

Permeability ratio	Organo-clay PDMS composite membrane		
	LYS-M-PDMS-45	TMA-M-PMDS-45	MMDA-M-PDMS-45
$\alpha_1 (CO_2/CH_4)$	3.9	3.9	3.9
$\alpha_1 (O_2/N_2)$	2.3	2.3	2.3
$\alpha_3 (CO_2/CH_4)$	8.3	8.9	9.4
$\alpha_3 (O_2/N_2)$	4.1	4.1	2.8
$\alpha_i (CO_2/CH_4)$	4.8	8.2	8.7
$\alpha_i (O_2/N_2)$	2.7	3.9	2.8
$\alpha_{expt} (CO_2/CH_4)$	4.8	8.2	8.7
$\alpha_{expt} (O_2/N_2)$	2.7	3.9	2.8

Various gas permeability ratios are calculated from the resistance components and are given in Table 7.18. MMDA-M has the highest permeability ratio for CO_2/CH_4 (9.36) and TMA-M has the highest permeability ratio for O_2/N_2(4.11). Although LYS-Me-M has a CO_2/CH_4 permeability ratio of 8.30, the overall CO_2/CH_4 permeability ratio in its PDMS composite membrane (LYS-Me-M-PDMS-45) is only 4.76. However, in the cases of TMA-M and MMDA-M, the permeability ratios (α_i) in their PDMS composite membranes are close to the (α_3) values. These results can be explained in terms of the different gas transport mechanisms within these three organo-clay PDMS composite membranes. In the LYS-Me-M-PDMS membrane, the gas transport is governed by both the polymer matrix and the organo-clay particles. In the cases of highly microporous TMA-M and MMDA filled PDMS membranes, the gas transport is controlled mainly by the organo-clays. The permeability ratio increases to a maximum level and this maximum level is approximately the α_3 value for the organo-clay material. If this maximum level is reached, any addition of organo-clay into the PDMS polymer actually deters from the gas permeability ratio. In contrast, if this maximum level is not reached as in the case of LYS-Me-M-PDMS composite membrane, the increase of organo-clay content enhances the gas permeability ratio.

The above study implies that the gas transport mechanism through the organo-clay PDMS composite membrane depends on the various resistance components within the composite membrane. In Na-montmorillonite PDMS membrane, the total resistance is the sum of R_1 and R_2. In the case of LYS-Me-M-PDMS membrane in which LYS-Me-M has a medium microporosity, the total resistance is a combination of three resistance components, R_1, R_2 and R_3. In the highly microporous TMA-M-PDMS and MMDA-M-PDMS membranes, the total resistance is the sum of R_1 and R_3.

It should be noted that all the above measurements and calculations are based on the pure gas permeation and if mixed gases were used the actual separation factors would be

lower[181]. The permeability of a "slow" gas will be reduced in the presence of a "fast" gas and vice versa. Taking into consideration the mixed gas effect, it appears that these simulations would lead to lower separation than actually predicted. Nevertheless, they still provide a means of designing a optimum composite membrane for a particular gas pair. Figure 7.9-7.12 show the gas permeability of the organo-clay PDMS composite membranes versus the organo-clay microporosity. Figure 7.13 shows the corresponding permeability ratio as a function of the microporosity of the organo-clay in the composite membrane.

7.4 Conclusions

Composite membranes with organo-clay material imbedded in cross-linked polydimethylsiloxane (PDMS) were prepared. The gas permeation results showed that the gas permeabilities of the organo-clay imbedded PDMS membranes decreased upon addition of the organo-clay. The pure gas permeability ratio of carbon dioxide and methane gases could be controlled by the organo-clay contents and the microporosity of the organo-clay in the membrane. A resistance model was used to describe the gas transport in these organo-clay PDMS composite membranes. The model permitted the calculation of permeabilities for both the polymer matrix and the suspended organo-clay particles. Various resistance components in the organo-clay PDMS composite membranes were also calculated using the same model. The contribution of each resistance components to the overall resistance was dependent upon the organo-clay content and the microporosity of the organo-clay. In the case of PDMS membranes filled with an organo-clay characterized by a low microporosity, the gas permeates through the polymer matrix, around the particles and through the microporous particles. In the cases of highly microporous organo-clay filled PDMS membranes, the gas transport permeates preferably through the organo-clay particles

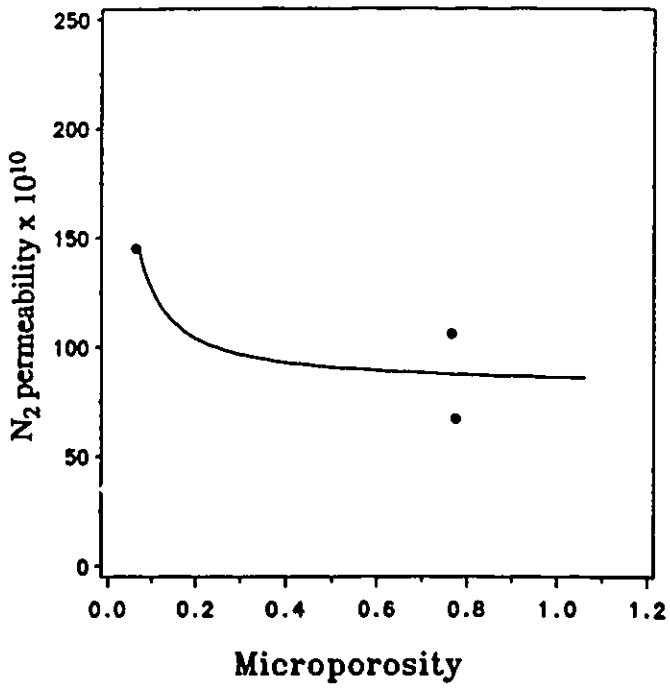

Figure 7.9 N_2 permeabilities of organo-clay PDMS composite membranes as a function of organo-clay microporosity.

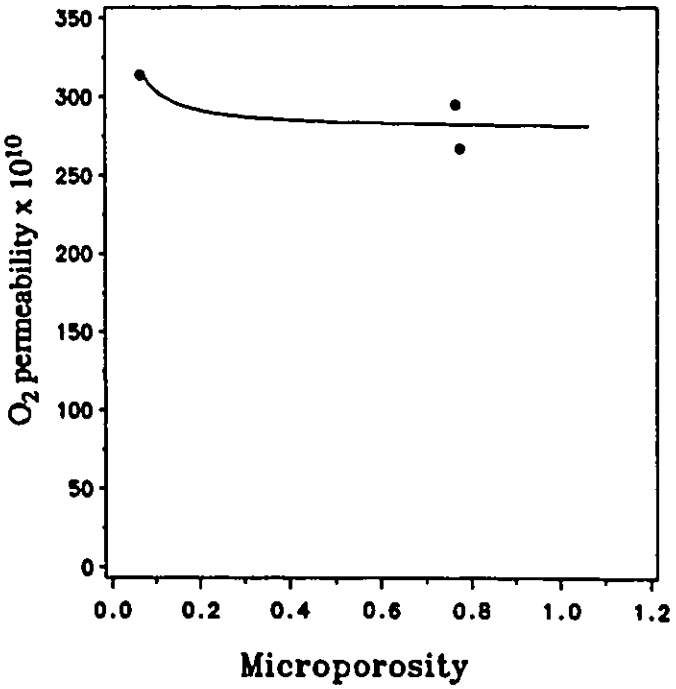

Figure 7.10 O_2 permeabilities of organo-clay PDMS composite membranes as a function of organo-clay microporosity.

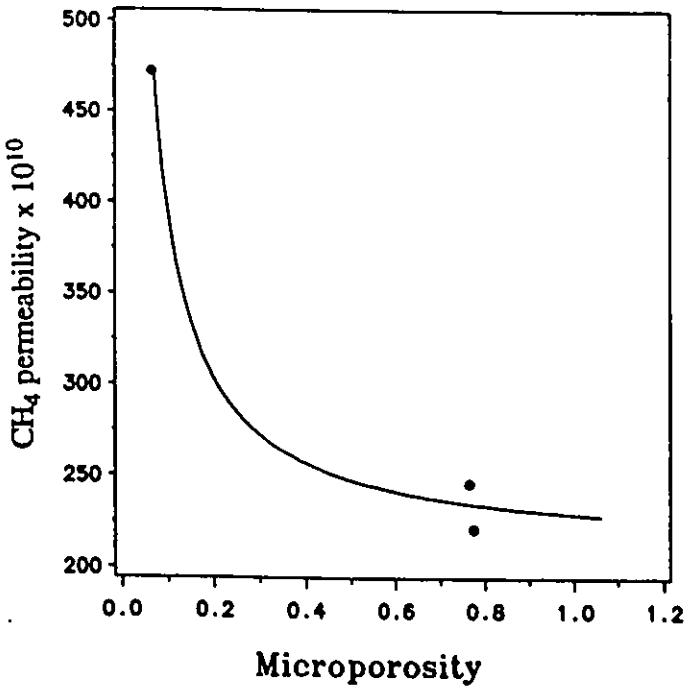

Figure 7.11 CH_4 permeabilities of organo-clay PDMS composite membranes as a function of organo-clay microporosity.

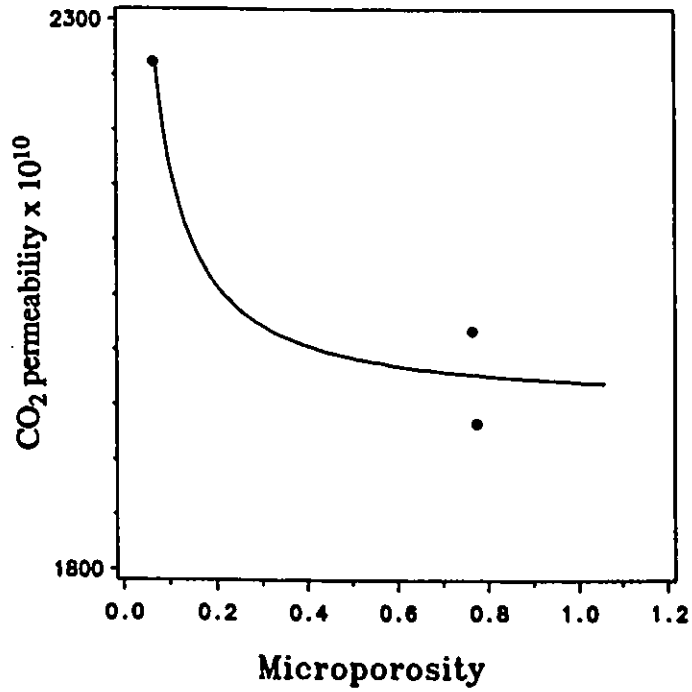

Figure 7.12 CO_2 permeabilities of organo-clay PDMS composite membranes as a function of organo-clay microporosity.

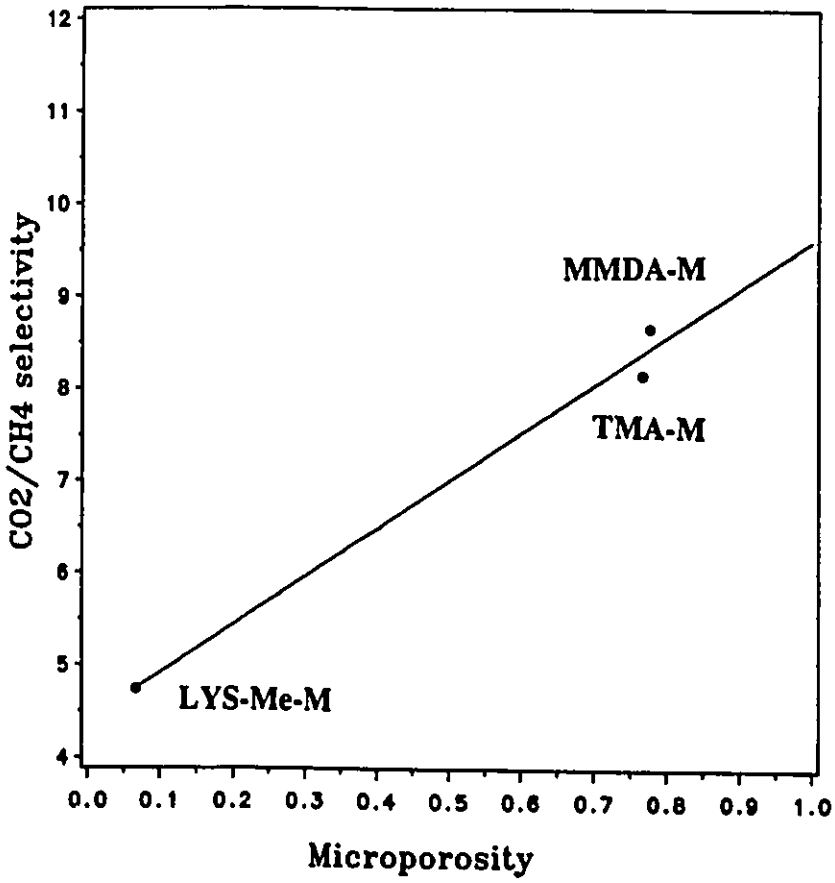

Figure 7.13 Permeability ratio of CH_4/CO_2 vs. organo-clay microporosity.

rather than around the particles. The overall resistance and permeability were shown to be functions of the content and of the microporosity of the organo-clay and of the size of the gases. The overall gas permeability of the composite membrane decreased and the selectivity increased with an increase of the organo-clay content. The higher selectivities for the gas pairs CO_2/CH_4 and O_2/N_2 in TMA-M-PDMS-45 and MMDA-M-PDMS-45 membranes were attributed to the greater contribution of the highly microporous organo-clay in the composite membranes. The maximum pure gas permeability ratios achieved for CO_2/CH_4 and O_2/N_2 were 8.7 and 4.1 in TMA-M-PDMS-45 and MMDA-M-PDMS-45 membranes as compared to 3.9 and 2.29 which were obtained for organo-clay free PDMS membranes.

Chapter 8

Experimental Methods

8.1 Purification of clays

8.1.1 Montmorillonite

The clay material was a source clay from Clay Spur Wyoming U.S.A.(SWy-1) obtained from the Clay Source Repository, University of Missouri.

Prior to use, the <0.2μm fraction was obtained according to the standard gravitation procedures described by Jackson et al[183] and by Mackenzie[184] for the purification of clay minerals. A suspension of 15g of the crude montmorillonite (SWy-1) in 200ml of water was prepared. To destroy the carbonates, 1N HCl was added until the pH was reduced to 3.5 and remained at or near that value for 10 minutes. The mixture was then centrifuged, the clear supernatant discarded and the sediment washed with HCl (pH 3.5) to remove soluble salts and exchangeable basic cations. After a second centrifugation, the sediment was redispersed in 200ml of water, the suspension pH was adjusted to 8.0 with 0.1N NaOH and the suspension was covered and allowed to stand overnight. It was then transferred to a 600ml beaker marked 10 cm from the inside bottom. Water was added to the mark. The suspension was sonified for 15 minutes and it was then stirred overnight.

The <0.2μm fraction of the clay was then separated by gravitation. After standing

undisturbed and free from vibrations overnight, the suspension above the sediment was siphoned off and poured into a large vessel. Water was added to the sediment up to the mark and the sediment was redispersed. The suspension temperature was taken and it was allowed to stand for the length of time needed for all particles larger than 0.2μm to deposit at the bottom of the beaker[183](6 hours in our case). The suspension above the sediment was then siphoned off and combined with the one siphoned off previously. This was repeated until the supernatant liquid became clear after the 6 hours waiting period. The siphoned suspension that contained all the <0.2μm clay was sonified for 15 minutes and then acidified to pH 3.5 with 1N HCl and 75 ml of a saturated NaCl solution was added to prepare the homoionic <0.2μm Na^+-montmorillonite. This caused the flocculation of the suspension. Most of the clear supernatant could then be siphoned off and discarded. The suspension was transferred into a dialysis tubing and it was placed in a large bath with deionized water (dialysis: membranes spectrapor, molecular weight cutoff=3500). The water was replaced regularly until a negative Cl^- ion test in the suspension was achieved (at least 1 week). The sediment was then freeze-dried for 3 days or was dried by direct heating. The freezed-dried samples were used for the adsorption experiments and the samples dried by heating was used for chromatographic experiments and membrane preparation.

8.1.2 Hectorite

The hectorite used was from San Bernardino country California U.S.A, HSCa-1 and was obtained from the Clay Source Repository, University of Missouri. The crude sample contained a large amount of carbonate impurities which could be removed by acidification with 1N HCl as described above. The <2.0μm homoionic Na^+-hectorite samples were prepared by the same conventional techniques using gravitations and saturated NaCl solutions of the cations as before (section 8.1.1).

8.1.3 Particle size analysis

The <0.2μm fraction of the homoionic Na^+-montmorillonite and <2.0μm Na^+-hectorite were checked by particle size analysis using a Sedigraph 5100 instrument. 2% suspension solution of the clay (2g/50ml of sodium metaphosphate 0.5%, temperature 34.5°C) was prepared and then transfered into a cell. The density of montmorillonite and hectorite were 2.54g/cm^3 and 2.81g/cm^3 respectively[185].

8.2 Synthesis of methyl quaternarized ammonium cations

8.2.1 Tetraalkyl ammonium and phosphonium cations

Tetramethyl ammonium iodide (TMA) and tetraphenyl phosphonium bromide (TPP) were obtained from Aldrich and were used in all the expereiments without further purification.

8.2.2 Preparation of methyl quaternarized amino methyl ester cations

8.2.2.1 Esterification of amino acids[38]

10g of amino acid (glycine, *L*-lysine, *L*-ornithine) was dissolved into a mixture containing 5 ml of $SOCl_2$ and 100 ml of MeOH at 10°C. The mixture was refluxed for 1.5 hours. The mixture was then cooled to room temperature and the product was isolated by crystallization after standing overnight. The crystals were filtered in suction and were dried under vacuum at 60°C for 6 hours. The product was recrystallized in a mixture of MeOH and diethyl ether (1:1) and 12.2g of methyl amino ester was obtained (total yield: 85%).

8.2.2.2 Quaternarization[43]

650mg of amino methyl ester and 3g of $NaHCO_3$ were added into a mixture of 8ml of MeI and 50 ml of MeOH. The mixture was stirred for 3 days and then 2ml of MeI was added. Stirring was continued for another 2 days. The reaction mixture was filtered into a flask and the excess MeI and the solvent were removed by vacuum rotary distillation. A solid was formed in the flask and the product was dissolved in 20 ml of MeOH again. The product was crystallized by adding 10 ml of diethyl ether into the mixture. Recrystallization in MeOH and diethyl ether (1:1) gave 620mg of the final methyl quaternarized amino methyl ester (total yield: >80%).

By this method, the trimethylated derivatives of glysine ethyl ester iodide (GLY-Et^+), *L*-lysine methyl ester diiodide (LYS-$Me^{2+}I_2^-$) and *L*-ornithine methyl ester (ORN-$Me^{2+}I_2^-$) diiodide were prepared.

Tri-methylated derivative of lysine methyl ester:

MP: 205-207°C;

^{1}H NMR, δppm (D_2O): 1.80(m, 2H, γ-C<u>H</u>$_2$), 2.3(m, 2H, δ-C<u>H</u>$_2$), 2.5(m, 2H, β-C<u>H</u>$_2$), 3.50(s, 9H, (C<u>H</u>$_3$)$_3$N(CH$_2$)$_4$-), 3.65(s, 9H, (C<u>H</u>$_3$)$_3$NCH-), 3.80(t, 2H, ϵ-C<u>H</u>$_2$), 4.30(s, 3H, COOC<u>H</u>$_3$), 4.70(m, 1H, α-C<u>H</u>);

^{13}C NMR, δppm (D_2O): 24.38(δ-CH_2), 24.62(γ-CH_2), 28.41(β-CH_2), 55.26(α-$(CH_3)_3N$), 55.80(ϵ-$(CH_3)_3N$), 57.0(-OCH_3), 68.44(ϵ-CH_2), 76.82(α-CH_2), 170.5(-COO);

IR(cm^{-1}): 3200-2900(s, CH, str.), 1750(s, C=O, ester, str.), 1250(m, C-N, str.);

MS analysis (m/e): 373.2(M^+-I^-, 46%), 245.3(M^+-2I^--1, 15.4), 314.1(M^+-I-$COOCH_3$, 10.5%), 185.1(M^+-2I^--$COOCH_3$-2H, 95.5).

Elemental analysis: $C_{13}H_{30}N_2O_2I_2$. Calculated: C 31.26%, H 6.06%, N 5.61% O 6.24%; Analysis: C 31.36%, H 6.04%, N 5.60%, O 7.37%.

8.2.3 *Preparation of methyl quaternarized polyammonium cations*[51]

8.2.3.1 *Preparation of methyl quaternarized methane diamine diiodide*

A solution of tetramethyl methane diamine (5g, 40mmol) and 30ml of EtOH was added slowly with MeI(13g, 92mmol) and the mixture was stirred for 1 hour. The mixture was then heated at 90°C for 3 hours and then the mixture was standed overnight. Solids formed in the solution and filtration gave 8.0g of methyl quaternarized methane diamine diiodide ($MMDA^{2+}I^{-}_2$) (yield: 78%).

^1H NMR, δppm (D_2O): 3.85(s, 18H, $2(CH_3)_3N^+$), 4.30(s, 2H, $-CH_2-$);

^{13}C NMR, δppm (D_2O): 58.0($(CH_3)_3N-$), 60.5(CH_2);

MS analysis, m/e (fragment, intensity%): 132.9(M^+-2I^-, 53.4), 327.2(M^+-Me_3N, 1.4).

8.2.3.2 *Preparation of methyl quaternarized ethylene diamine diiodide*

A solution of tetramethyl ethylene diamine (5g, 40mmol) and 30ml of EtOH was added slowly with MeI(13g, 92mmol) and was stirred for 1 hour. The mixture was then heated at 90°c for 3 hours and then the mixture was standed overnight. Solids formed in the solution and filtration gave 8.0g of methyl quaternarized ethylene diamine diiodide ($MEDA^{2+}I^{-}_2$) (yield: 80%).

^1H NMR, δppm (D_2O): 3.45(s, 18H, $2(CH_3)_3N^+-$), 4.08(t, 4H, $-CH_2CH_2-$);

^{13}C NMR, δppm (D_2O): 45.42($(CH_3)_3N-$), 57.20(CH_2CH_2).

8.2.3.3 *Preparation of N,N,N',N'-tetramethyl-N,N'-bis [2-N,N,N-trimethylamine ethyl]-1,2-ethanediaminet tetraiodide*

A mixture of tetraamine(4.8g, 21mmol), MeI(6.5g, 46mmol), and 30ml of EtOH was heated with stirring at 90°c for 3 hours and then allowed to stand overnight. Filtration gave 10.3g of yellow-white solid, which was partially quaternarized. A 4.6g (20mmol)

sample was combined with 14.2g(20mmol) of MeI in 30ml of EtOH and 50ml of distilled water was added. The solution was refluxed for 2 hours. 20 ml of EtOH was added and reflux was continued for another 3 hours. The mixture was allowed to stand overnight at 25°c. Filtration gave 7.8g of white powder, N,N,N',N'-tetramethyl-N,N'-bis [2-N,N,N-tri-methylamine ethyl]-1,2-ethane diamine tetraiodide ($MTETA^{4+}I_4^-$) (total yield:49%).

MP: 203-205°C (literature: 198°C);

^1H NMR, δppm (D_2O): 3.39(s, 18H, $(CH_3)_3N^+$-), 3.51(s, 12H, $(CH_3)_2N$=), 4.33(m, 12H, -CH_2CH_2-);

^{13}C NMR, δppm (D_2O): 55.30($(CH_3)_2N$=), 57.55($(CH_3)_3N^+$-), 60.60($Me_3N^+CH_2$-), 61.17(-$CH_2N^+Me_3$), 61.48(-$N^+Me_2CH_2CH_2N^+Me_2$-);

MS analysis (m/e): 671.0(M^+-I^-, 1.7), 544.2(M^+-$2I^-$, 0.2), 417.2(M^+-$3I^-$, 0.2), 289.1(M^+-$4I^-$, 1.7), 241.2(M^+-$4I^-$-$3CH_3$-2H, 59.7).

8.2.4 Preparation of organo-clay samples

The prepared quaternarized amino acid ester derivatives and the quaternarized polyamine derivatives as well as the tetraalkyl ammonium (phosphonium) cations were incorporated into the interlamellar spaces of Na-montmorillonite and Na-hectorite at full cationic exchange capacity (cec; 87±5 mequiv./100g of clay). The quaternarized derivatives and the tetraalkyl ammonium (phosphonium) (87 mequiv) were dissolved in distilled water and then 100g of clay was added into the solution. The mixture was stirred for overnight for complete exchange and the mixture was filtered. The resulted organo-clay was then dried under vacuum at 60°C overnight. Abbreviations used for the quaternarized and esterified amino acid derivatives and other quaternarized derivatives are shown in the following table.

8.3 *Adsorption measurements*

8.3.1 *Colorimetric method*[66]

8.3.1.1 *Preparation of standard methyl quaternarized ammonium cation solutions*

A series of standard solutions of LYS-Me^{2+}, ORN-Me^{2+}, TMA^{+}, $MMDA^{2+}$ and $MEDA^{2+}$ with different concentrations rangeing from $1.0x10^{-5}$m to $1.4x10^{-4}$M were prepared in distilled water.

5ml of each standard solution, 5ml of chloroform and 2ml of bromocresol green solution (10%, w/w in water) were mixed and the mixture was then shaked for 3 minutes in a closed separating funnel. The mixture was then allowed to stand for a few minutes and two layers were observed. The chloroform layer was separated and was transfered into a UV cell for absorbance measurement. By measuring the absorbance at 415.5nm of solutions with diffferent concentrations, the relation between the amount of cations and the absorbance was made.

8.3.1.2 *Determination of the amount of methyl quaternarized ammoium cations adsorbed by the clays*

In order to determine the amount of methyl quaternarized LYS-Me^{2+} cations adsorbed by <0.2μm Na^{+}-montmorillonite and <2.0μm Na^{+}hectorite, 50mg of clay was dispersed in 50ml of distilled water and 50ml of a solution of methyl quaternarized LYS-Me^{2+} cation (concentrations: from $1.0x10^{-4}$ to $2.0x10^{-3}$M) was added. The mixture was stirred overnight and then centrifuged for one hour. The solid was kept for further use. The supernatant solution was taken and was diluted 10 times with distilled water. 5ml of this diluted solution, 5ml of chloroform and 2ml of bromo-cresol green solution (10% in water) were mixed. The concentration of the cation remaining in the supernatant solution

was determined by measuring its absorbance at 415.5nm. The amount of cation adsorbed by the clay was determined from the difference of the concentration of the original solution and of the supernatant solution after adsorption by the clays.

The same precedure was used to determine the amounts of other cations (TMA^+, $ORN\text{-}Me^{2+}$, $MMDA^{2+}$ and $MDEA^{2+}$) adsorbed by the clays using their absorbances at 415.5nm after mixing with the standard bromo-cresol green solution (10% in water).

The instrument used for the UV-Vis spectroscopic measurements was a UVGILFORD model.

8.3.2 Sodium electrode method[39]

A series of standard solutions with different Na^+ concentration were prepared (from $1.0x10^{-4}M$ to $1.2x10^{-3}M$) and the voltages of these standard solutions were measured in a PH/ion meter Corning 155 using a sodium electrode (Corning 476210) and a reference electrode (Corning 476370). The relationship between the concentraion of the Na^+ and the voltage was obtained from the measurements of the standard solution.

The amount of Na^+ ions of the clay replaced by the methyl quaternarized ammonium (phosphonium) cations was determined by difference between the original solution and the supernatant solution of the clays exchanged with the cations. The adsorption amounts of TPP^+ and $MTETA^{4+}$ cations by the clays (Na^+montmorillonite and Na^+-hectorite) were measured by this method.

8.4 X-ray diffraction and Scanning electron microscopy

8.4.1 Preparation of samples

8.4.1.1 Na-montmorillonite and Na-hectorite

Oriented samples of clays were prepared as followed: A suspension of <0.2μm Na-montmorillonite or <2.0μm Na-hectorite was prepared (40mg in 2ml of distilled water). The dispersion solution was then pipetted onto a fine glass microscope slide. The dispersion was allowed to dry in atmosphere overnight.

8.4.1.2 Clays exchanged with methyl quaternarized ammonium (phosphonium) cations

The <230 mesh samples of organo-clay were selected by a mini-seive and the sample was dispersed in distilled water(40mg in 2ml of water). The suspension solution was sonified for 10 minutes and then pipetted onto a glass microscope slide. The dispersion was allowed to dry in atmosphere.

8.4.2 X-ray diffraction spectrum

The oriented films were recorded in a Philis PW 1050/81 Medel X-Ray diffractrometer using Cu *k*α x-radiation in Dr. Chao's laboratory at Carleton University. The x-ray diffraction patterns for different clays and clays exchanged with methyl quaternarized ammonium (phosphonium) cations were examined in order to measure the changes in d_{001} of the clays.

8.4.3 Scanning electron microscopy

The samples for SEM were prepared by deposition of clay particles on a support with carbon suspension to order to stick the clay particles and to assure the electron

conductivity.

The SEM measurement were taken on a Nanobabs 7 scanning electron microscopy in the department of chemistry of the university of Ottawa. The energy of the electron was 15kv.

8.5 Measurements of BET surface area, external surface area and pore size distribution

All the N_2 adsorption and desorption measurements were performed in OMNISORP 100 analyzer in the laboratory of Professor S. Kaliaguine, Department of Chemistry, Lava University. A schematic of the apparatus is presented in Figure 8.1. The instrument introduced the adsorbate gas continuously to the sample through a mass flow controller. The temperature of the sample is maintained at liquid nitrogen temperatures (77K) throughout the process. The rate of gas flow was maintained constant (better than 1%) throughout the adsorption and desorption experiments. The volume of gas adsorbed was calculated by intergrating the flow rate over time and subtracting the predetermined dead volume. Continuous precision measurements of p and p_0 were made and each p/p_0 isotherm data point was computed using an average of these readings. The continuous volumetric method provided a superior data base for surface area calculations, t-plot analysis, pore volume and pore size dsitribution information. TMA-M, LYS-Me-M, GLY-Et-M, MMDA-M, MMDA-H and TPP-M were used for microporosity studies and the particle size of the organo-clays were between 60-120 mesh. For the measurement of nitrogen adsorption isotherms, the samples were dried in an oven at 90°C overnight under vacuum. Before the adsorption and desorption measurement was conducted, the samples were outgassed for 3 hours at 150°C at 10^{-4}-10^{-5} torr. A dewar flask containing liquid

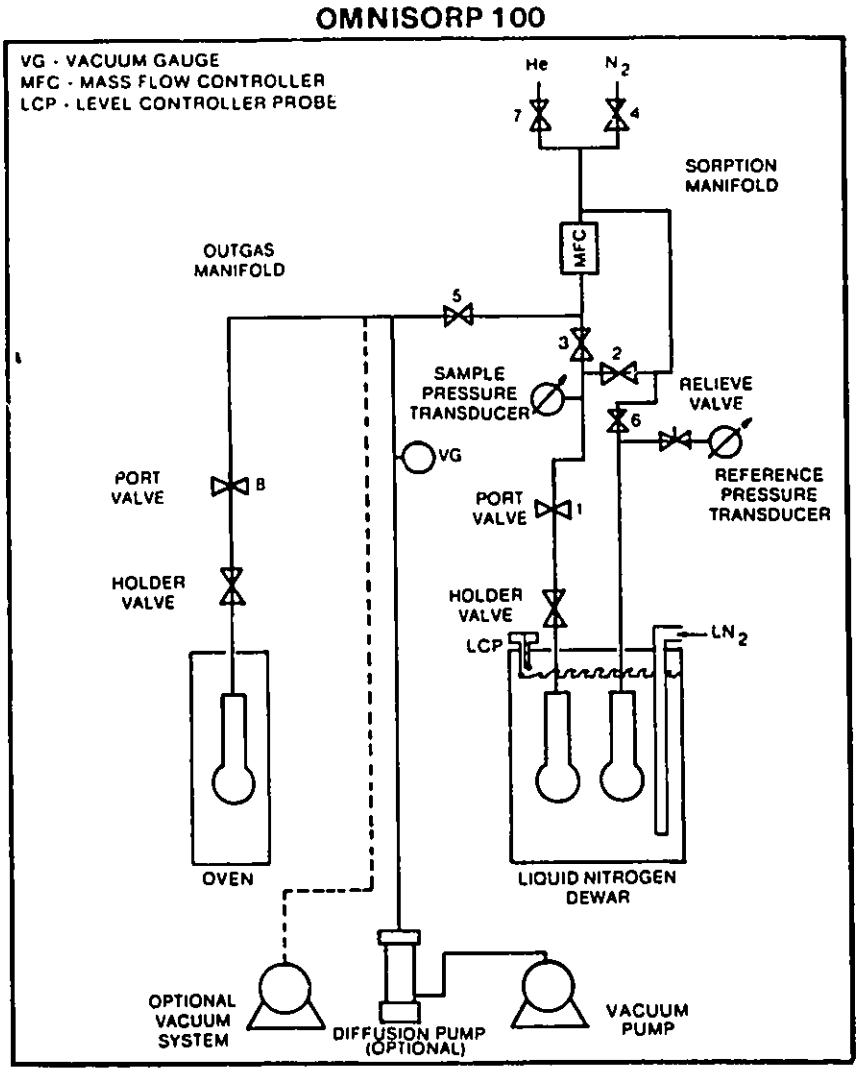

Figure 8.1 N_2 continuous adsorption apparatus (taken from the manual of OMINSORP 100)

nitrogen was placed around the sample tube; the level of nitrogen was kept constant by periodically replacing the liquid lost by evaporation.

The dead volume was determined by helium, the measurement was automatically conducted by the use of a computer. Helium was withdrawn from the apparatus, the sample was outgassed under vacuum until the vacuum was close to 10^{-5} torr. Then an nitrogen adsorption followed by desorption was performed. The volume adsorbed or desorbed by the sample and the relative pressures were recorded. The calculation from the adsorption and desorption data gave adsorption/desorption isotherms, BET surfaces, external surfaces, micropore volume, meso(macro)pore volume, micropore size distribution and meso(macro)pore size distribution (see chapter 5).

8.6 Gas chromatographic experiments

8.6.1 Column preparation

Several organo-clays were chosen as the packing materials for the gas chromatographic studies. They were TMA-M, TMA-H, TPP-M, GLY-Et-M, LYS-Me-M, LYS-Me-H, ORN-Me-M, ORN-Me-H, MMDA-M, MMDA-H, MEDA-M, MEDA-H, MTETA-M and MTETA-H. All the organo-clays samples were prepared on full loading (100% cec) of the clay as described in section 8.2.4.

The dried samples were grounded and size fractioned in a mini-sieve. The 60-120 mesh particles were chosen for column packing and were dried in an oven under vacuum at 90°C overnight. The columns were prepared from stainless steel tubing with outer diameter 1/8 in. The columns were packed with the prepared organo-clays (60-120 mesh) by pouring the organo-clays into the straight tubing while it was vibrated all the time. The filled columns were stopped with glass wool and were bent into coiling shape. The column

lengths were 3 ft. long in most the cases and 9 in. long in some cases.

8.6.2 Gas chromatographic experiments

8.6.2.1 Conditions of the gas chromatograph

The GC instrument used in this work was a GOW-MAC Model 69-550P with a thermal conductivity detector and a SP4270 chromatography integrator. Gas tight syringe was used for gas sampling. All the gases were supplied by Air Products with purity 99.8% or better.

The packed columns prepared as above were installed in the oven of the GC instrument and were conditioned at 90°C for 9 hours with carrier gas He at a flow rate 25 ml/min.

8.6.2.2 Separation of CH_4 and CO_2

Pure gases CH_4, CO_2, and, gas mixture of air, CH_4 and CO_2 were used in these experiments. The column temperature was controlled at 30°C and the injector temperature and the detector temperature were 35°C and 45°C respectively. He was used as carrier gas with a flow rate at 25 ml/min in all the cases.

8.6.2.3 Separation of gas mixture of H_2, N_2, O_2, CO, CH_4 and CO_2

The same conditions were used as described in section 8.6.2.2.

8.6.2.4 Separation of C_1-C_4 and C_5-C_8 hydrocarbons

Both column temperatures 30°C and 140°C were used. In some cases, a temperature program was also used in which the column temperature was initiated at 30°C and raised to 140°C with a rate of 10°C/min. The detector temperature and injector

temperature were 175°C and 160°C respectively. The flow rate of carrier gas was controlled at 35 ml/min in all cases.

8.7 Preparation of organo-clay-polymeric membranes and pure gas permeation experiments

8.7.1 Preparation of PDMS membranes[161]

The silicone rubber (polydimethylsiloxane, PDMS) membranes were prepared from RTV615B and RTV615 curing agent which were obtained from General Electric without further purification. 8.0g of RTV615B and 0.8g of RTV615B curing agent (10%) were mixed together. After stirring for 2 hours the mixture resulted in a paste. The paste was mechanically cast on a glass plate. The film was cured on the plate at 70°C for 16 hours and the thickness of the membrane was 110-120μm. The finished membranes were cut into a coupon in shape and were used immediately for pure gas permeation measurements.

8.7.2 Preparation of Organo-clay PDMS composite membranes

8.0g of RTV615B, 0.8g of curing agent and 2.2g (20% wt) of organo-clay powder (<230 mesh) were put together and were throughly mixed in a flask and stirred for 2 hr. Then the mixture was cast on a glass plate and the film was cured on the plate at 70°c for 16 hours to assure complete crosslinking. The membrane thickness was 100-140μm.

By this method, organo-clay-PDMS composite membranes were prepared with 33% and 45% organo-clay respectively. In the case of the 45% organo-clay-PDMS membranes, 1 ml of hexanes was added into the mixture of organo-clay and PDMS polymer in order to make a polymer solution.

8.7.3 Pure gas permeation experiments

A schematic diagram of the experimental apparatus of a single permeation cell are shown in Figure 8.2. Before placing the coupon into the permeation cell both the O-rings and surfaces that contacted with the membrace were cleaned using ethanol. The coupon was placed on top of a filter paper and both were attached with four small pieces of tape to the bottom flange of the cell. The membrane skin was left exposed to the gas feed, which entered from the top of the cell. The bottom flange was then fastened to the rest of the cell with six bolts. This porcedure was performed for all three cells. Helium gas was then passed through the apparatus at 100 psig and all fittings were checked for leaks using a solution of soap water. Flow rates were checked to ensure that none of the coupons were broken. A broken coupon exhibits very high permeation rates that were both measurable with the bubble meters.

The steady-state permeation rates at different operating pressures (recorded as psig, but converted to kPag) were measured at room temperature and pressure with a bubble flow meter. All gases were supplied by Air Products with a purity of 99.9% or better. The experimental data collected as volume flow rate for different gases was first corrected to standard temperature and pressure, and then converted to permeability data (cm^3cm/cm^2-sec-cmHg). The effective area of the membrane used for the permeation sudies was 9.62 cm^2. All membranes were tested with the gases in the following order: He, H_2, N_2, O_2, CH_4 and CO_2. After this sequence was completed the membrane was retested with He gas to ensure that membrane performance did not change significantly during the sequence. Once the experiments for one gas were completed, the membranes were left to relax for 24 hours, after which time another gas would be employed. The entire apparatus was flushed several times with this new gas. The operating pressure and the temperature were 110psi and 23°C for PDMS and PDMS-organo-clay membranes. In each experiment the membranes were kept under the operating pressure for at least 2 hours before the first

reading was taken. Atmospheric temperature and pressure were recorded daily while the experiment was in operation.

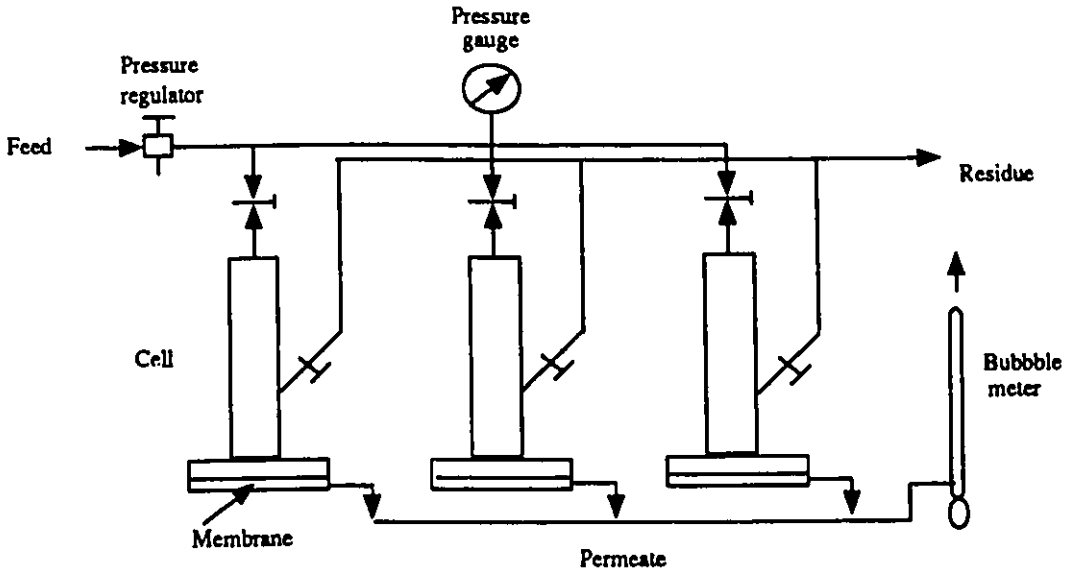

Figure 8.2 Schematic diagram of permeation apparatus.

References

(1) A.G. Cairns-Smith and H. Hartman, " Clay minerals and the origin of life ", Cambridge University Press, New York, 1986.

(2) H. van Olphen, " An Introduction to Clay Colloid Chemistry", 2nd Edition, John Wiley & Sons, New York, 1977.

(3) D.M. Moore and R.C. Reynolds, Jr., " X-Ray Diffraction and the Identification and Analysis of Clay Minerals ", Oxford University Press, 1989.

(4) H. Suquet, C. de la Calle and H. Pezerat, *Clays Clay Miner.*, (1975), **23**, 1.

(5) W.F. Jaynes and J.M. Bigham, *Clays Clay Miner.*, (1987), **35**, 440.

(6) T.J. Pinnavaia, *Science*, (1983), **220**, 365.

(7) G. Beson, A. Mifsud, C. Tchoubar and J. Mering, *Clays Clay Miner.*, (1974), **22**, 379.

(8) A.C.D. Newman, " Chemistry of Clays and Clay Minerals ", Mineralogical Society, 1987.

(9) V. Berkheiser and M.M. Mortland, *Clays Clay Miner.*, (1977), **25**, 105.

(10) (a) R. Barrer and D.M. MacLeod, *Trans. Faraday Soc.*, (1955), **51**, 1290. (b) R.M. Barrer and J.S.S. Reay, *Trans. Faraday Soc.*, (1957), **53**, 1253. (c) R.M. Barrer and G. Hampton, *Trans. Faraday Soc.*, (1957), **53**, 1462. (d) R.M. Barrer, *Pure Appl. Chem.*, (1989), **61**, 1903. (e) R.M. Barrer, *Clays Clay Miner.*, (1989), **37**, 386.

(11) P.M. Chapman, G.P. Romberg and C.A. Vigers, *J. Water Pollution Control Fed.*, (1982), **54**, 292.

(12) K.R. Srinivasan and H.S. Fogler, *Clays Clay Miner.*, (1990), **38**, 287.

(13) K.R. Srinivasan, H.S Fogler, E.G. Gulari, T.F. Nolan and J.S. Schuttz, *Environ. Progress*, (1985), **4**, 239.

(14) H.F. Fogler and K.R. Srinivasan, U.S. Patent 4,740,488, April 26, 1988.

(15) S.A Boyd, M.M. Mortland and C.T. Chiou, *Soil Sci. Soc. Amer. J.*, (1988), **52**, 652.

(16) J.F. Lee, M.M. Mortland, C.T. Chiou and S.A. Boyd, *J. Chem. Soc. Faraday Trans. I*, (1989), **85**, 2953.

(17) K.R. Srinivasan and S.H. Fogler, *Clays CLay Miner.*, (1990), **38**, 277.

(18) L.J. Michot and T.J. Pinnavaia, *Clays Clay Miner.*, (1991), **39**, 634.

(19) J.A. Ballantine, M. Davies, H. Purnell, M. Rayanakorn, J.M. Thomas and K.J. Williams, *J. Chem. Soc. Chem. Commun.*, (1981), 427.

(20) J.M. Adams, S.E. Davis and S.H. Graham, *J. Chem. Soc. Chem. Commun.*, (1978), 930.

(21) J.M. Adams, S.E. Davis and S.H. Graham, *J. Chem. Soc. Chem. Commun.*, (1979), 527.

(22) T.J. Pinnavaia, R. Raythatta, J.G.S. Lee, L.J. Halloran and J.F. Hoffman, *J. Amer. Chem. Soc.*, (1979), **101**, 6891.

(23) T.J. Pinnavaia, M.S. Tzou and S.D. Landou, *J. Amer. Chem. Soc.*, (1985), **107**, 4783.

(24) M.L. Occelli, " Studies in Surface Sceince and Catalysis ", (1988), **35**, 101.

(25) L.M. Robeson, *J. Membr. Sci.*, (1991), **62**, 165.

(26) S.A. Stern, " Synthetic Membranes ", M.B. Chenoweth, MMI press, 1986. p1-38.

(27) J. Haggin, C & EN, Chicago, 7, June, 1988.

(28) D. Li and S.T. Hwang, *J. Membr. Sci.*, (1991), **59**, 331.

(29) H.P. Hsieh, AIChE Symp. Ser., (1988), **84**, 1.

(30) H.L. Fleming, *Proc. 7th BCC Membrane Technology/Planning Conference*, Cambridge, Oct., 1989.

(31) A. Larbot, J.P. Febre, C. Guizard and L. Cot, *J. Membr. Sci.*, (1988), **39**, 203.

(32) L. Mercier, "*Intercalation of tetraalkylammonium cations into smectites*", B.Sc honours thesis, department of chemistry, University of Ottawa, 1991.

(33) R.C. Fuson, J. Corse and P.B. Welldon, *J. Amer. Chem. Soc.*, (1941), **63**, 2645.

(34) M.L. Bender and M.C. Chen, *J. Amer. Chem. Soc.*, (1963), **85**, 30.

(35) P.E. Pfeffer, T.A. Foglia, P.A. Barr, I. Schmeltz and L.S. Silbert, *Tetrahedron Lett.*, (1972), **40**, 4063.

(36) G.E. Ullyott, H.W. Taylor and N. Dawson, *J. Amer. Chem. Soc.*, (1948), **70**, 542.

(37) Su-Sun Wang, B.F. Gisin, D.P. Winter, R. Makofske, I.D. Kulesha, C. Tzougraki and J. Meienhofer, *J. Org. Chem.*, (1977), **42(8)**, 1286.

(38) R.A. Boisonnas, St.Guttmann, P.A. Jaquenoud and J.P. Waller, *Helv. Chim. Acta*, (1956), **39**, 1421.

(39) S. Latieule, "*Intercalation of amino acid derivatives into Na-montmorillonite*", Master's thesis, Department of Chemistry, University of Ottawa, 1991.

(40) W.G. Lloyd, *J. Org. Chem.*, (1967), **32**, 2816.

(41) T. Takemoto, K.Daigo and N. Takagi, *J. Pharm. Soc., Jpn*, (1964), **84**, 1180.

(42) G.J. Moore and N.L. Benoiton, *Can. J. Biochem.*, (1975), **53**, 1145.

(43) N.Leo Benoiton and F.M.F. Chen, *Peptide Proc., Eur. Pept. Symp.*, (1976), **14th**, 149.

(44) H. Kotsuki et al., *Bull. Chem. Soc. Jpn.*, (1988), **61**, 2684.

(45) A.J. De Koning, J. Boersma and G.J.M. Van der Kerk, *J. Organomet. Chem.*, (1980), **195**, 1.

(46) M.T. Pope, " *Heteropoly and Isopoly Oxametalates*", Springer Verlag: New York, 1983.

(47) R.G. Finke, M. Groege, J.R. Hutchinson and O.J. Gansow, *J. Amer. Chem. Soc.*, (1981), **103**, 1587.

(48) J.F.W. Keana, M.D. Ogan, Y. Lu, M. Beer and J. Varkey, *J. Amer. Chem. Soc.*,

(1985), **107**, 6714.

(49) J.F.W. Keana and M.D. Ogan, *J. Amer. Chem. Soc.*, (1986), **108**, 7951.

(50) J.F.W. Keana, M.D. Ogan, Y. Lu and M. Beer, *J. Amer. Chem. Soc.*, (1986), **108**, 7957.

(51) J.F.W. Keana, Y. Wu and G. Wu, *J. Org. Chem.*, (1987), **52**, 2571.

(52) G. Blunden, S.M. Gordon, T.A. Crabb, O.G. Roch, M.G. Rowan and B. Wood, *Magn. Res. Chem.*, (1986), **24**, 965.

(53) R. Greene-Kelly, *Trans. Faraday. Soc.*, (1955), **51**, 412.

(54) K.E. Clare, *Nature*, (1947), **160**, 828.

(55) R.V. Mikhalyuk and O.D. Kurilenko, *Khim. i Khim. Tekhnol.*, (1959), **2**, 74.

(56) W.W. Emmerson, *Nature, London*, (1960), **186**, 573.

(57) S.B. Hendricks, *J. Phys. Chem.*, (1941), **45**, 65.

(58) A. Weiss, *Clays Clay Miner.*, (1963), **10**, 191.

(59) B.K.J. Theng, D.J. Greenland and J.P. Quirk, *Clay Miner.*, (1968), **7**, 271.

(60) G. Lagaly, *Clay Miner.*, (1981), **16**, 1.

(61) D.A. Laird, A.D. Scott and T.E. Fenton, *Clays Clay Miner.*, (1989), **37**, 41.

(62) H. Favre and G. Lagaly, *Clay Miner.*, (1991), **26**, 19.

(63) A. Weiss, *Angew. Chem. Int. Ed. Engl.* (1963), **20**, 850.

(64) O.D. Bonner, F.L. Livingstone, *J. Phys. Chem.*, (1956), **60**, 530.

(65) A.S. Pearce, *Chem. Ind.*, 1961, 825.

(66) G.J. Chamberlin, "*Colorimetric chemical analytical methods*", 1980, 24.

(67) J. Koryta and K. Strilik, "Ion Selective Electrodes", 2nd Ed., Cambrigde University Press, 1983.

(68) G. Villemure, *Clays Clay Miner.*, (1990), **38**, 623.

(69) B.K.G. Theng, "The Chemistry of Clay-Organic Reactions", Adam Hilger Ltd., England, 1974.

(70) C.T. Cowan and D. White, *Trans. Faraday Soc.*, (1958), **54**, 691.

(71) D.J. Queenland and J.P. Quirk, *Clay Clay Miner.*, (1962), **9**, 484.

(72) R.M. Barrer and K. Brummer, *Trans Faraday Soc.*, (1963), **59**, 959.

(73) E.W. Nuffield, *"X-Ray Diffraction Methods"*, John Wiley and Sons, Inc., New York, (1966).

(74) T.A. Peters, *"Scanning Electron Microscopy"*, Part I, (1981), p603.

(75) M.J. Wilson, *"A Handbook of Determinative Methods in Clay Mineralogy"*, (1987).

(76) M.H.B. Hayes, M.E. Pick and B.A. Toms, *Residue Rev.*, 1975, **57**, 1.

(77) J.M. Serratosa, J.A. Rausell-Colom and J. Sanz, *J. Mole. Catal.*, (1984), **27**, 225.

(78) D. Carrol, *Geol. Soc. Amer.*, (1970), **126**, 1.

(79) T.J. Pinnavaia, M-S, Tzou, S.D. Landau and R.H. Raythatha, *J. Mol. Cata.*, (1984), **27**, 195.

(80) J. Sterte, *Clays Clay Miner.*, (1991), **39**, 167.

(81) D.M. Moore and J.Hower, *Clays Clay Miner.*, (1986), **34**, 379.

(82) E. Ruiz-Hitzky, *Mol. Crys. Liq. Inc. Nonlin. Opt.*, 1988, **161**, 433.

(83) M.L. Occelli, *Studies in Surface Science and Catalysis*, (1988), **35**, 101.

(84) B.F. Bohor and R.E. Huges, *Clays Clay Miner.*, (1971), **19**, 49.

(85) M.D. Wilson and E.D. Pittman, *J. Sediment. Petrology*, (1977), **47**, 3.

(86) R.E. Tompkins, *Clays Clay Miner.*,(1981), **29**, 23.

(87) W.D. Keller, *Clays Clay Miner.*, (1982), **30**, 150.

(88) D.J. Cebula, R.K. Thomas, S. Middleton, R.H. Otterwill and J.R. White, *Clays Clay Miner.*, (1979), **27**, 39.

(89) M.L. Occelli, S.D. Landau and T.J. Pinnavaia, *J. Catal.*, (1987), **104**, 331.

(90) W.D. Keller, R.C. Reynolds and A. Inoue, *Clays Clay Miner.*, (1986), **34**, 187.

(91) D.R. Peacor, V.E. Williams and G.E. Mustoe, *Clays Clay Miner.*, (1980), **28**, 241.

(92) H. Eswaran, *J. Soil Sci.*, (1979), **30**, 547.

(93) A. Bottino, G. Capannelli, P. Petit-Bon, N. Cao, M. Pegoraro and G. Zoia, *Separation Sci. Technol.*, (1991), **26**, 1315.

(94) A. Chahboun, R. Coratger, F. Ajustron, J. Beauvillain, P. Aimar and V. Scanchez, *J. Membr. Sci.*, (1992), **67**, 295.

(95) J. Stawiński, J. Wierzchoś and M.T. Garcia-Gonzaleez, *Clas Clay Miner.*, (1990), **38**, 617.

(96) M.L. Occelli, S.D. Landau and T.J. Pinnavaia, *J. Catal.*, (1984), **90**, 256.

(97) M.L. Occelli and D.H. Finseth, *J. Catal.*, (1986), **99**, 316.

(98) S. Yamanaka and M. Hattori, *Studies in surface science and catalysis*, (1991), **60**, 89.

(99) K.S.W. Sing, *Studies in surface science and catalysis*, (1991), **62**, 1.

(100) C. Fyfe, G. Kennedy, C. De Schutter and G. Kokotailo, *J. Chem. Soc. Chem. Comm.*, (1984), 54.

(101) W.C. Conner, P.Vincent, P. Man and J. Fraissard, *Catalysis Lett.*, (1990), **4**, 75.

(102) H. van Olphen and J.J. Fripiat, *"Data handbook for clay material and other non-metallic minerals"*, (1979), 209.

(103) S. Inagaki, Y. Fukushima, H. Doi and O. Kamigaito, *Clays Miner.* (1990), **25**, 99.

(104) K.R. Lange, *J. Colloid Sci.*, (1963), **18**, 65.

(105) P.S. Northrop, R.C. Flagan and G.R. Gavalas, *Langmuir*, (1987), **3**, 300.

(106) J. Rouquerol, F. Rouquerol, Y. Grillet and R.J. Ward, *Studies in Surface Science and Catalysis*, (1988), **39**, 67.

(107) S.J. Gregg and K.S.W. Sing, *"Adsorption, Surface Area and Porosity"*, Academic Press Inc., second edition, 1982.

(108) S. Brunauer, P.H. Emmett and E. Tellar, *J. Amer. Chem. Soc.*, (1938), **60**, 309.

(109) B.C. Lippens and J.H deBoer, *J. Catal.*, (1965), **4**, 319.

(110) K.S.W. Sing, *Chem. Ind.*, (1967), 829.

(111) R.M. Barrer and A.D. Millington, *J. Colloid Interf. Sci.*, (1967), **25**, 359.

(112) A.Y. Meyer, *J. Comput. Chem.*, (1986), **7**, 986.

(113) W.F. Jaynes and J.M. Bigham, *Clays Clay Miner.*, (1987), **35**, 440

(114) J.A. Rausell-Colom and C. Fornés, *Amer. Min.*, (1974), **59**, 790.

(115) J.M. Serratosa, J.A. Rausell-Colom and J. Sanz, *J. Mole. Catal.*, (1984), **27**, 225.

(116) E.P. Barrett, L.G. Joyner and P.H. Halenda, *J. Amer. Chem. Soc.*, (1951), **73**, 373.

(117) R.W. Cranston and F.A. Inkley, *Adv. Catal.*, (1957), **9**143.

(118) S. Brunauer, R.Sh. Mikhail and E.E. Bodor, *J. Colloid Interf. Sci.*, (1967), **24**, 451.

(119) R. Evans, U.M.B. Marconi and P. Tarazona, *J. Chem. Phys.*, (1986), **84**, 2376.

(120) J.P.R.B. Walton and N. Quirke, *Molec. Sim.*, (1989), **2**, 361.

(121) N.A. Seaton, J.P.R.B. Walton and N. Quirke, *Carbon*, (1989), **27**, 853.

(122) C.A. Jessop, S.M. Riddiford, N.A. Seaton, J.P.R.B. Walton and N. Quirke, *Studies in Surface Science and Catalysis*, (1991), **62**, 123.

(123) G. Horváth and K. Kawazoe, *J. Chem. Eng. Japan*, (1983), **16**, 470.

(124) L.C. Klein and N.Giszpenc, *Ceram. Bull.*, (1990), **69**, 1821.

(125) W.J. Koros and D.R. Paul, "Synthetic Membranes", M.B. Chenoweth ED., MMI Press Symposium Series, Hardwood Academic, New York, 1986, Vol. 5, pp155-189.

(126) R.T. Yang, "Gas Separation by Adsorption Processes", Butterworth, Boston, 1987.

(127) W.H. Isalski, "Separation of Gases", Oxford Science Publications, Oxford, 1989.

(128) H.S. Shin and K.S. Knaebel, *A.I.Ch.E. J.*, (1987), **33**, 654.

(129) Z.J. Pan, R.T. Yang and J.A. Riher, "New Directions in Sorption Technology", G.E. Keller Ed., Butterworth, Boston, 1989.

(130) A. Kapoor and R.T. Yang, *Chem. Eng. Sci.*, (1989), **44**, 1723.

(131) H. Lao, S. Latieule and C. Detellier, *Chem. Mat.*, (1991), **3**, 1009.

(132) T.G. Andronikashvili, O.S. Banakh and V.I. Rogovik, *Pure Appl. Chem.*, (1989),

61, 2061.

(133) G. Manara and M. Taramasso, *J. Chromatogr.*, (1972), **65**, 349.

(134) G. Manara and M. Taramasso, *J. Chromatogr.*, (1973), **77**, 109.

(135) R.M. Barrer and D.M. MacLeod, *Trans. Faraday Soc.*, (1954), **50**, 980.

(136) F.Vernon and A.N. Khakoo, *J. Chromatogr.*, (1978), **157**, 412.

(137) D.W. Grant, R.B. Meiris and M.C. Hollis, *J. Chromatogr.*, (1974), **99**, 721.

(138) D. White, *Nature*, (1957), **179**, 1075.

(139) C. Chukwnuenye and J.L. McAtee. Jr., *J. Chromatogr.*, (1987), **410**, 121.

(140) V.J. Thielmann and J.L. McAtee. Jr., *J. Chromatogr.*, (1978), **147**, 408.

(141) J.L. McAtee. Jr. and B.R. Harris, *Clay Clay Miner.*, (1977), **25**, 90.

(142) R.T. Yang and M.S.A. Baksh, *A.J.Ch.E. J.*, (1991), **37**, 679.

(143) M.S.A. Baksh and R.T. Yang, *Sep. Sci. Technol.*, (1991), **26**, 1377.

(144) R.L. Goldsmith, *J. Membr. Sci.*, (1988), **39**, 197.

(145) G. Schombury, "Gas Chromatography", VCH, Weinheim, 1990.

(146) R.L. Grob, "Modern Practice of Gas Chromatography", John Wiley & Son Inc., 1977.

(147) D.W. Breck, "Zeolite Molecular Sieves", John Wiley & Son, Inc., (1974), p636.

(148) H. Förster and M. Schumann, *J. Chem. Soc. Faraday Trans. I.*, (1989), **85**, 1149.

(149) K.G. Bhattacharyya, *Langmuir*, (1989), **5**, 1155.

(150) O.M. Ilinitch, G.L. Semin. M.V. Chertova and K.I. Zamaraev, *J. Membr. Sci.*, (1992), **66**, 1.

(151) G. Datar, P.S. Ramanathan and M.S. Das, *J. Chromatogr.*, (1975), **106**, 428.

(152) "Membrane Separation symposium", 41st Canadian Chemical Engineering Conference, Vancouver, B.C. October, 1991.

(153) W.J. Schell and C.D. Houston, "Industrial Gas Separation", Amer. Chem. Soc., ACS Symposium series, 1983, 223.

(154) J.E. Mark, "Silicon-Based Polymer Science", J.M. Zeigler and F.W.G. Fearon Ed., Amer. CHem. Soc., Washington, DC, 1990, p47-70.

(155) B.J. Story and W.J. Koros, *J. Membr. Sci.*, (1992), **67**, 191.

(156) B.S. Minhas, T. Matsuura and S. Sourirajan, *Ind. Eng. Chem. Res.*, (1987), **26**, 2344.

(157) A.E. Fouda, A. Lui and T. Matsuura, *Sep. Sci. Technol.*, (1988), **23**, 2175.

(158) R.C. Goldsmith, *J. Membr. Sci.*, (1988), **39**, 197.

(159) R.J.R. Uhlhorn, K. Keizer and A.J. Burggraaf, *J. Membr. Sci.*, (1992), **66**, 271.

(160) A.B. Schelekhin, E.J. Grosgogeat and S.T. Hwang, *J. Membr. Sci.*, (1991), **66**, 129.

(161) M. Jia, K-V. Peinemann and R-D Behling, *J. Membr. Sci.*, (1991), **57**, 289.

(162) D.R. Paul and D.R. Kemp, *J. Polym. Sci., Polym. Symp.*, (1973), **41**, 79.

(163) S. Kulprathipania, H. Estates, R.W. Neuzil, D. Grove, N.N. Li and A. Heights, *US Patent*, (1988), 4,740,219.

(164) W.J. Ward, G.L. Gaines, Jr., M.M. Alger and T.J. Stanley, *J. Membr. Sci.*, (1991), **55**, 173.

(165) B. Arkles, *ChemTech.*, Sept. (1983), 542.

(166) S.B. Hamilton, Jr., *Appl. Polym. Symposium, Silicone Technology*, P.F. Bruis Ed., John Wiley, New York, 1970.

(167) S.A. Stern and H.L. Frisch, *Ann. Re. Mater. Sci.*, (1981), **11**, 523.

(168) L. Matson, J. Loper and J.A. Quinn, *Chem. Eng. Sci.*, (1983), **38**, 503.

(169) J.S. Vrentas, J.L. Duda and H-C Ling, *J. Polym. Sci., Polym. Phys. Ed.*, (1985), **23**, 275.

(170) J.S. Vrentas, J.L. Duda and H-C Ling and A-C Hou, *J. Polym. Sci., Polym. Phys. Ed.*, (1985), **23**, 289.

(171) W.R. Vieth, J.M. Howell and J.H. Hsieh, *J. Membr. Sci.*, (1076), **1**, 177.

(172) W.R. Vieth and Y. Jiang, *J. Membr. Sci*, (1988), **38**, 1.

(173) S. Sourirajan and T. Matsuura, "Reverse Osmosis/Ultrafiltration Process Principles", National Research Council of Canada, (1985), Sept., p11.

(174) Y. Chen, A.E. Fouda and T. Matsuura, "Symposium on Advanced in Reverse Osmosis and Ultrafiltration", National Research Council of Canada, (1989), p259.

(175) M.A. Mazid, R. Rangarajan, T. Matsuura and S. Sourirajan, *Ind. Eng. Chem. Process Des. Dev.*, (1985), **24**, 907.

(176) J.M.S. Henis and M.K. Tripodi, *Sep. Sci. Technol.*, (1980), **15**, 1059.

(177) J.M.S. Henis and M.K. Tripodi, *J. Membr. Sci.*, (1981), **8**, 233.

(178) J.M.S. Henis and M.K. Tripodi, *Science*, (1983), **220**, 11.

(179) A. Fouda, Y. Chen, J. Bai and T. Matsuura, *J. Membr. Sci.*, (1991), **64**, 263.

(180) H.J.C. Te Hennepe, C.A. Smolders, D. Bargeman and M.H.V. Mulder, *Sep. Sci. Technol.*, (1991), **26**, 585.

(181) L.E. Nielsen, *J. Macromol. Sci.*, (1967), **A1**, 929.

(182) D.G. Pye, H.H. Hoehn and M. Panar, *J. Appl. Polym. Sci.*, (1976), **20**, 1921.

(183) M.L. Jackson, L.D. Wittig and R.P. Pennington, *Soil Sci. Amer. Proc.*, (1949), **14**, 77.

(184) R.C. Mackenzie, *Clay Min. Bull.*, (1956), **3**, 4.

(185) C.T. Deeds and H. Van Olphen, *Tenth National Conference on Clays and Clay Minerals*, (1976), 318-328.

PUBLICATIONS AND CONFERENCES

Publications:

1. "Molecular recognition in microporous organo-minerals. Shape specific interactions of carbon dioxide in functionalized organo-montmorillonite." Hongbai Lao, Sylvie Latieule and Christian Detellier, *Chem. Materials*, 3(6), 1009, **1991.**

2. "Preparation and physical properties of some C_{18} unsaturated fatty esters containing *L*-amino acid residues and methyl esters of N-stearylamino aicds." M.S.F. Lie Ken Jie, H.B. Lao and David W.Y. Leung, *Lipids*, 25(5), 260, **1990.**

3. "Synthesis and properties of amido fatty derivatives involving azido fatty esters and 1-phenyl-alkanols." M.S.F. Lie Ken Jie, W.L.K. Lam and H.B. Lao, *J. Chem. Soc., Perkin Trans. I*, 1, **1989.**

4. "^{13}C NMR studies of azido containing C_{18} fatty ester derivatives." M.S.F. Lie Ken Jie and H.B. Lao, *J. Chem. Soc. Perkin Trans. II*, 915, **1988.**

5. "Lipids in Chinese medicine. Characterization of all cis-5,11,14,17-eicosatetraenoic acid in Biota orientalis seed oil and a study of oxo/furanoic esters derived from Biota oil." M.S.F. Lie Ken Jie, H.B. Lao and Y.F. Zheng, *J. Am. Oil Chem. Soc.*, 65, 597, **1988.**

6. "Fatty acid, Part 31. The preparation and some physical properties of azido fatty acid esters." M.S.F. Lie Ken Jie and H.B. Lao, *Chem. Phys. Lipids*, 45, 65, **1987.**

Conference Presentations:

Poster: "Design of Organo-Clay Membranes.

Hongbai Lao, C. Detellier and S. Latiuele(University of Ottawa); T. Matsuura (National Research Council of Canada, Division of Chemistry, Ottawa, Ontario), in ICST(The Institute for Chemical Science and Technology) Technology Day, Mississauga, Toronto, Ontario, Canada, November 18, **1991.**

Poster: "Microporous Organo-Clay Materials In Gas Separation."

Hongbai Lao, S. Latiuele, J. Tunney and C. Detellier, in 74th Canadian Chemical Conference, Hamilton, Ontario, Canada, June 2-6, **1991.**

"Organo-Clay in Gas Separation Processes."

C. Detellier, Hongbai Lao, S. Latiuele, D. Carriere and J. Tunney, in ICST Technology Day, Toronto, Ontario, Canada, November 19, **1990.**

"Intercalation of Amino Acid Derivatives into Smectites and Separation of gazeous mixtures."

C. Detellier, Hongbai Lao, S. Latieule, J. Tunney (University of Ottawa) and J. Ripmeester (National Research Council of Canada, Institute of Environmental Sciences, Ottawa, Ontario), in an Industial Seminar, Kingston, Ontario, Canada, June, **1989.**